Covalently-Bound Organic Modifiers on ZnO: Effects on the Electronic and Chemical Surface Properties

A report submitted in partial fulfilment

of the requirements for the degree of

Doctor of Philosophy in Chemistry

in the

School of Physical and Chemical Sciences, Te Kura Matū

University of Canterbury, Te Whare Wānanga o Waitaha

by

Alexandra Rose McNeill

under the supervision of

Professor Alison Downard

and

Associate Professor Martin Allen

August 2018

Acknowledgements

Firstly, I wish to thank my supervisors, Professor Alison Downard and Associate Professor Martin Allen, for their incredible support, encouragement, patience, and wisdom, as well as for all the opportunities they have given me. I am extremely grateful to Professor Bob Hamers for hosting and helping me at the University of Wisconsin-Madison for a year. Thank you to the University of Canterbury, The MacDiarmid Institute, and Fulbright New Zealand for funding my research and allowing me to take so many wonderful opportunities.

The Downard Dream Team, past and present, has been a joy to work with. Anna, Kalib, Ting, Joel, and Liam: thank you for The Rapport. I must also thank the physicists and engineers who put up with my airy-fairy chemistry ways for so long: Alana, Rodrigo, Jonty, Adam, and Alex. Huge thanks to the Hamers Group for being so welcoming, friendly, and helpful during my time at UW (and after), especially Arielle, Laura, Liz, Margy, Lindy, Cat, Kelly, Sarah, and Tim.

I also wish to thank Dr Colin Doyle at the University of Auckland for the excellent XPS experiences, and Professor Roger Reeves and Dr Paula Brooksby for sound advice and support. We are very lucky at the University of Canterbury to have superb technicians – a huge thank you to Wayne, Nick, Oliver, Gill, and Laurie in Chemistry, and Helen and Gary in the Nanolab.

Finally, I thank my friends and whānau, especially my parents, for all their support.

Table of Contents

Abstract

This thesis describes the method development and characterisation of the chemical modification of polar and non-polar ZnO surfaces. Due to the native OH termination on ZnO, the material exhibits downwards band bending at the surface, and an accompanying surface electron accumulation layer. This gives the ZnO surface a conducting nature which is undesirable for the development of efficient transparent semiconductor devices. The use of covalently-bound organic modifiers to tune the work function and stability of ZnO surfaces has previously been investigated, but there is little systematic data on the changes in band bending produced by these modifiers on the three main crystal faces of ZnO: Zn-polar, O-polar, and m-plane ZnO. This work investigates the effects on band bending when phosphonic acids, thiols, and aryldiazonium ions are used to modify the surface of ZnO.

Three different phosphonic acid (PA) modifiers on ZnO were studied using synchrotron X-ray photoelectron spectroscopy. Octadecylphosphonic acid (ODPA) significantly increased the downwards band bending at the surface of all three ZnO faces. Surprisingly, a fluorinated analogue (1*H*,1*H*,2*H*,2*H*-perfluorooctyl phosphonic acid, F_{13}OPA) also increased the surface band bending despite the electron withdrawing properties of fluorine. This was attributed to X-ray-induced decomposition of the molecules and subsequent F-Zn interactions. A fluorinated aromatic PA, 2,3,4,5,6-pentafluorobenzyl phosphonic acid (PFBPA), was analysed using a lower X-ray flux, and was found to decrease the downwards band bending on ZnO. The PA modification layers were stable when stored in air and darkness, but UV light caused degradation of all three modifiers. Despite this, ODPA was able to prolong the effect of persistent photoconductivity on O-polar ZnO.

Polar and non-polar ZnO samples were also modified with alkane- and arylthiols. In contrast to some previous studies, the main binding mode of thiols on ZnO was determined to be via sulfonate bonds, which increased downwards band bending slightly. O-polar ZnO with unoxidised octadecanethiol (ODT) on the surface showed a decrease in surface band bending. Zn-polar and m-plane ZnO appeared to oxidise thiols more readily than the O-polar face, due to the relative differences in catalytic

reactivity. A large increase in downwards band bending was seen for all ZnO faces that had been modified with an isothiocyanate derivative (3,5-bis(trifluoromethyl)benzyl mercaptan), although the chemical nature of the bound modifier and its binding mode are unclear.

Aryl layers 1 – 8 nm thick were grafted to ZnO via electrochemical reduction of nitrobenzene diazonium ions. The electrochemical behaviour was similar to that on carbon substrates. The modification reduced the downwards band bending on all three ZnO faces, and the magnitude of the change appeared dependent on the thickness of the modification layer. Electrochemical reduction of nitro to amino groups was attempted on the nitrophenyl films but was only successful on the O-polar and m-plane faces, and the band bending did not significantly change relative to unreduced samples for any ZnO face. In contrast, large upwards band bending was observed when nitrophenyl films were treated with Na_2S in attempt to chemically reduce the nitrophenyl groups. This is a very interesting phenomenon that is tentatively attributed to Na adsorption on ZnO and possible incorporation into the lattice.

Sb-doped ZnO thin films (MBE-ZnO) with high charge carrier concentrations were electrochemically modified with nitrophenyl and trifluoromethyl layers from the corresponding aryldiazonium salts, giving good reproducibility across samples and removing the downwards band bending of ZnO as shown with synchrotron XPS. These changes were attributed to the electron withdrawing nature of the modifiers, however when synchrotron XPS was used to reduce the nitrophenyl groups to aminophenyl moieties, upwards surface band bending became more pronounced despite amino groups being electron donating. This was attributed to ZnO valence band electrons participating in the reduction mechanism and leaving an electron-depleted surface. Both modifiers were stable when stored in the dark but desorbed from the surface when exposed to UV light.

Overall, this thesis work shows that ZnO remains a promising transparent conducting oxide for electronic applications because of the ability to tune the surface band bending over a range of ~1 eV with relatively stable covalently-bound surface modifiers.

Abbreviations and Symbols

ζ	Energetic separation of the valence band maximum and the Fermi level
ξ	Energetic separation of the conduction band minimum and the Fermi level
2DEG	2-Dimensional electron gas
4TFMBM	4-Trifluoromethylbenzyl mercaptan
AFM	Atomic force microscopy
ASF	Atomic sensitivity factor (also known as 'relative sensitivity factor')
BE	Binding energy
CA	Contact angle
CV	Cyclic voltammogram
E_C	Conduction band minimum
E_F	Fermi level
E_V	Valence band maximum
F_{13}OPA	1*H*,1*H*,2*H*,2*H*-perfluorooctyl phosphonic acid
F_{13}OT	1*H*,1*H*,2*H*,2*H*-perfluorooctanethiol
IMFP	Inelastic mean free path
IPA	Isopropanol
ITC	3,5-Bis(trifluoromethyl)phenyl isothiocyanate
ITO	Tin-doped indium oxide
NBD	4-Nitrobenzenediazonium tetrafluoroborate

N_C	Conduction band effective density of states
NP	4-Nitrophenyl
ODPA	Octadecylphosphonic acid
ODT	Octadecanethiol
PA	Phosphonic acid
PFBPA	2,3,4,5,6-Pentafluorobenzylphosphonic acid
SCE	Saturated calomel electrode
SEAL	Surface electron accumulation layer
TFMBD	4-Trifluoromethylbenzenediazonium tetrafluoroborate
TFMP	4-Trifluoromethylphenyl
THF	Tetrahydrofuran
UPS	Ultraviolet photoelectron spectroscopy
VB	Valence band
V_{bb}	Valence band bending
ΔV_{bb}	Change in valence band bending
XPS	X-ray photoelectron spectroscopy

Publications

(1) McNeill, A. R.; Hyndman, A. R.; Reeves, R. J.; Downard, A. J.; Allen, M. W. Tuning the Band Bending and Controlling the Surface Reactivity at Polar and Nonpolar Surfaces of ZnO through Phosphonic Acid Binding. *ACS Appl. Mater. Interfaces* **2016**, *8* (45), 31392–31402.

(2) McNeill, A. R.; Bell, K. J.; Hyndman, A. R.; Gazoni, R. M.; Reeves, R. J.; Downard, A. J.; Allen, M. W. Synchrotron X-Ray Photoelectron Spectroscopy Study of Electronic Changes at the ZnO Surface Following Aryldiazonium Ion Grafting: A Metal-to-Insulator Transition. *J. Phys. Chem. C* **2018**, *122*, 12681–12693.

1 Introduction

Zinc oxide (ZnO) is an earth-abundant, non-toxic, transparent semiconductor that has the potential to provide a low-cost replacement for indium tin oxide (ITO) in electronic devices. ITO is a common component in touch screens, liquid crystal television screens, and solar cells due to its transparency and electrical conductivity.[1] However, there have been increasing concerns with the volatility of both the price and supply of indium, so alternatives to ITO are being sought.[2] Zinc is not only more abundant than indium, but its mineral extraction process is less difficult and less toxic.[1] The biocompatibility and wide range of high-surface-area nanostructures of ZnO also make it useful for biosensing devices.[3,4]

As an n-type semiconductor, ZnO has a wide direct band gap (3.37 eV at room temperature), which places it in the UVA region of the electromagnetic spectrum with potential for use in UVA sensors and light-emitting diodes.[5] ZnO also has a high thermal conductivity and strong piezoelectric properties, whereby mechanical stress can be converted to electricity due to its polar crystal.[6] However, the behaviour of ZnO in electronics can be difficult to control, reducing its efficiency in devices and presenting a challenge for industrial applications. This is attributed to the chemical instability of its surfaces, which drives reactions with atmospheric water to form a hydroxylated termination.[5] The variability of this OH termination can lead to a lack of reproducibility between devices.[7] It is known that replacing the OH layer by purposely attaching other chemical species in the form of self-assembled monolayers (SAM) can not only stabilise the chemical reactivity, but also change the work function of ZnO.[8] An example of an application of this is gas sensing for assessing the freshness of food, as the adsorption of trimethylamine, released by decomposing plants and animals, affects the electrical conductivity of ZnO.[5] By purposely adsorbing different types of molecules to the surface, the properties of ZnO can be tuned for particular electronic applications.[9] Additionally, these molecules may be functionalised further to selectively recognise particular analytes, and thus achieve a specific sensor system.

ZnO has several crystallographic faces, consisting of different arrangements of surface atoms, which have different chemical reactivities.[10] Although some aspects of ZnO surface chemistry have been examined, a full study of the chemistry of the various faces and the optimal approach for chemically modifying each face has not yet been undertaken. This thesis aims to compare the reactivity of ZnO faces to different covalently-bound modifiers. In addition, a range of modifiers will be compared to assess their ability to improve the electronic properties and stability of ZnO electronic devices.

1.1 Background

1.1.1 Structure and Preparation of ZnO

In its crystalline form, ZnO exists as hexagonal, Wurtzite-type crystals as seen in Figure 1.1.[11] Within the crystal, each Zn atom is tetrahedrally coordinated to four O atoms, and each O atom is tetrahedrally coordinated to four Zn atoms. Different crystal faces have different chemical makeup and therefore different reactivities. An example of this is their susceptibilities to dissolution in acid: the topography of the non-polar faces changes more than the polar faces on immersion in acidic dye solutions.[12] Also, gas-phase solvent molecules such as ethanol and acetone adsorb dissociatively on Zn-polar ZnO and non-dissociatively on O-polar ZnO due to the higher reactivity of the Zn-polar ZnO.[13]

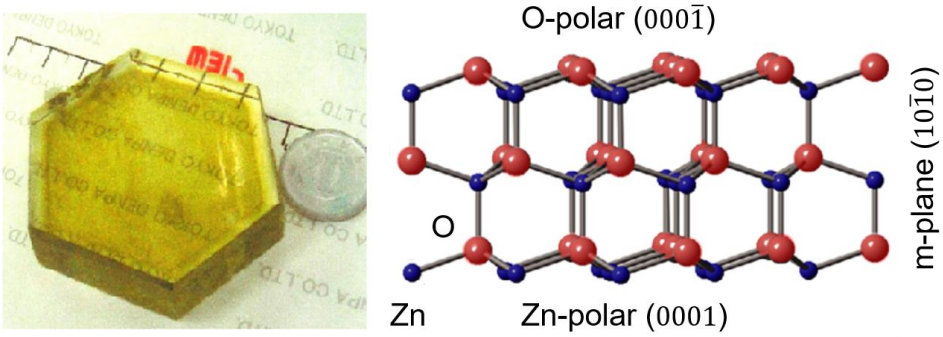

Figure 1.1: A hydrothermally-grown ZnO crystal (left) and a depiction of its Wurtzite crystal structure (right). Adapted from Janotti et al.[5]

1.1.1.1 Polar Faces of ZnO

A ZnO crystal has a Zn-polar (0001) surface on one side with a corresponding O-polar $(000\bar{1})$ face on the other (Figure 1.1 and Figure 1.2). On the Zn-polar surface, each Zn atom lacks the final oxygen atom necessary to complete its tetrahedral coordination; this leaves a Zn sp^3 'dangling bond'.[14] On the O-polar face, a similar effect occurs whereby each O atom has a dangling bond. This results in a localised charge imbalance at each of these surfaces. Despite this instability, polar ZnO faces are frequently found in nature, indicating the effect is somehow balanced. Evidence suggests that this is achieved via charge rearrangement, the formation of surface defects, and hydroxylation of the surface atoms, although due to the significant ionicity of Zn-O bonds, a spontaneous polarisation remains between the two faces. On both faces, water is chemisorbed to the surface to give an OH-terminated surface (Figure 1.2b). Each Zn on the Zn-polar face is attached to an OH group, while on the O-polar face, each O is attached to an H atom.[15] Several groups have confirmed through X-ray techniques that the hydroxyl termination on the polar faces is approximately a monolayer, corresponding to a surface concentration of 1.8×10^{-9} mol cm^{-2} for both Zn-polar and O-polar faces, calculated from the unit cell.[16–18] Additional water and oxygen molecules can physisorb to the hydroxylated layer, affecting the ability of ZnO to act as a semiconductor (see Section 1.1.3). At higher pH (~10), the OH groups are deprotonated to $-O^-$ on both faces.[19] The O-polar $(000\bar{1})$ ZnO face is more susceptible to attack by acid than Zn-polar (0001) ZnO due to the partial negative charge of the surface attracting the positive charge of hydronium ions (H_3O^+).[20] Conversely, the positively-charged Zn-polar face is affected more by basic solutions due to the attraction of negatively-charged hydroxide ions (OH^-) and the relative repulsion of H_3O^+. However, both faces may be etched faster if there are defects at the surface. Zn-polar ZnO is considered more catalytically active than O-polar ZnO: gaseous small alcohols and related compounds like water adsorb most strongly on the Zn-polar face, and least strongly on the O-polar face.[13,21] This is due to Zn ions being shielded by O ions on the O-polar face, and partially shielded on the m-plane face. This not only reduces the iconicity of the O-polar face but means that steric effects further reduce the ability of molecules to adsorb to Zn ions.

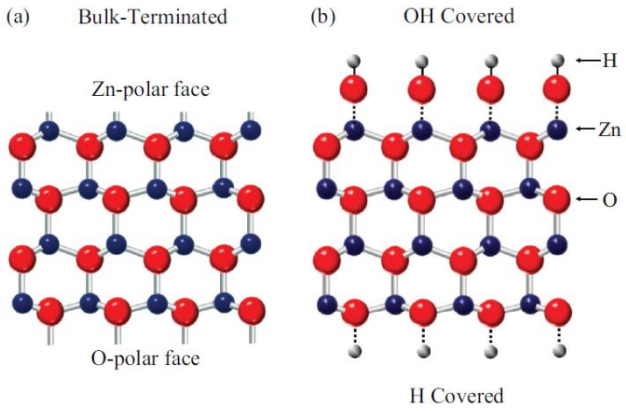

Figure 1.2: A 2-dimensional view of ZnO showing (a) the polarity of its opposite faces and (b) how OH and H groups bind to the Zn- and O-polar faces, respectively. Adapted from Heinhold et al.[10]

The polarisation effects on polar ZnO surfaces mean that electrons and holes are spatially separated, reducing their probability of recombination. This means that for devices which rely on the recombination of electrons and holes for light emission, polar faces are less efficient than non-polar faces.[22]

1.1.1.2 Non-Polar Faces of ZnO

The m-plane $(10\bar{1}0)$ face of a ZnO crystal is non-polar, and is the most stable and most abundant surface on many ZnO nanostructures, including nanowires.[23] Figure 1.3 shows that it is perpendicular to the polar faces. The m-plane surface consists of both Zn and O atoms, terminated by approximately a monolayer of H, OH, and H_2O.[24] This corresponds to a surface OH concentration of 2.2×10^{-9} mol cm^{-2}, calculated from the unit cell.[18] The non-polar a-plane $(11\bar{2}0)$ and semipolar r-plane $(10\bar{1}2)$ are similar, although they are less stable than m-plane ZnO and thus more difficult to grow.

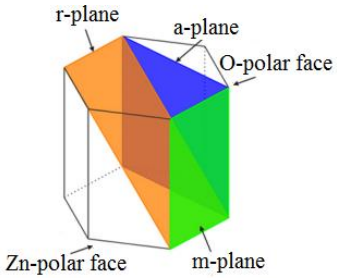

Figure 1.3: Non-polar and polar planes of Wurtzite ZnO. Adapted from Neiman.[25]

1.1.1.3 ZnO Growth Methods

Single-crystal ZnO can be grown via gas or vapour transport, hydrothermal growth, and pressurised melt growth.[5] These methods use combinations of heat, pressure, and other factors to produce crystals with a range of sizes and qualities. Polycrystalline films can be fabricated using methods such as electrochemical deposition, sol-gel synthesis, and through the oxidation of pure Zn films.[5] However, these films are not usually suitable for electronic applications due to the relatively high concentrations of defects and impurities. Instead, epitaxial films mainly containing a single crystal face are preferred.

One approach to growing good-quality, monocrystalline thin films is slowly depositing films atom by atom on a heated substrate, which allows them to find the most stable position within the lattice. When performed in this way, pulsed laser deposition (PLD) and molecular beam epitaxy (MBE) can both be used to obtain single crystalline ZnO.[26,27] In PLD, a laser vaporises a ZnO target in an oxygen atmosphere, and the vapour adsorbs onto the heated substrate. In MBE, separate beams of gaseous elements (O and sublimed Zn) are simultaneously introduced into a vacuum chamber, where they slowly deposit onto the substrate. The high level of control over the growth parameters allows a range of crystal orientations to be fabricated, with slow rates of deposition giving very precise surfaces.[18] The quality of the thin film is also affected by the choice of substrate: a common substrate for ZnO growth is sapphire because it is robust and transparent, although buffer layers such as MgO or ZnO itself can enhance the orientation of the deposited ZnO film through improved matching of the crystal lattice parameters.[28] Typically, PLD and MBE growth preferentially produce films with an O-polar face, but changing the orientation of the crystal face of the substrate allows for the growth of different ZnO faces.[5] For example, a novel method of growing semi-polar r-plane ZnO on a silicon substrate by PLD at high O_2 pressure was shown by Aggarwal et al. in 2010.[22] Here, a buffer layer of yttria-stabilised zirconia was used to match the lattice of r-plane ZnO, resulting in single-crystalline r-plane thin films.

In addition to thin films, ZnO forms a great variety of nanostructures including nanoparticles,[13,19,29–31] nanowires,[32–37] nanoribbons,[38] and nanorods.[39–44] Nanowires are of particular interest due to their

large surface to volume ratio, which makes them ideal for sensing purposes where adsorption of an analyte affects an electrical signal in the device. ZnO nanowires can be grown from the gaseous phase or by hydrothermal growth from seed crystals; the latter is most commonly used due to the simplicity of the setup and growth conditions.[45] Typically, the majority of the surface area of nanorods and nanowires comprises non-polar m-plane ZnO.[46]

1.1.2 ZnO as a Semiconductor

Semiconductors play a vital role in most of today's electronics such as computer chips and light emitting diodes (LEDs). They have an electrical conductivity between that of insulators and metallic conductors, and their conductivity increases with temperature.[47] This property arises from a band gap between the energy levels of the valence and conduction bands, in which the Fermi level (E_F) usually resides (Figure 1.4). As-grown ZnO is intrinsically n-type. This is thought to be due to natively-occurring oxygen and zinc vacancies and interstitials (interstitials are atoms present in typically unoccupied sites).[5] Even at low concentrations, impurities within the lattice such as Li or H can have a large impact on the electrical and optical properties of ZnO as a semiconductor.[48,49]

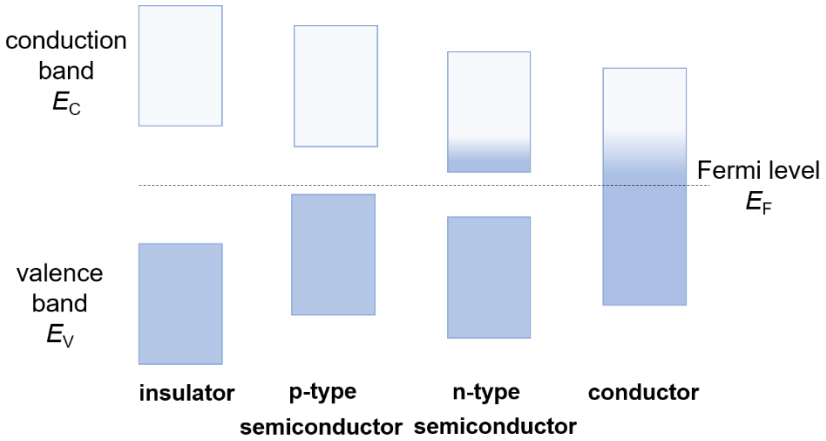

Figure 1.4: Band energy diagrams for intrinsic insulators, n- and p-type semiconductors, and conductors. The shaded areas represent the position of the electron density for each material.

It has proven difficult to dope ZnO to give reproducible and stable p-type conductivity, but its semiconductor properties can also be altered through the addition of molecules on the surface.[5] ZnO

can be doped with a metal containing more valence electrons than Zn, such as Al or Ga.[50] Antimony (Sb) may also be used. Typically, Sb-doping gives p-type conductivity because of the complex defects that it forms with ZnO.[51] However, at concentrations up to 1%, Sb increases the charge carrier concentration of ZnO while maintaining n-type conductivity.[52] Such doping can result in an increased band gap due to the Moss-Burstein effect, wherein the donor electrons occupy states at the bottom of the conduction band, preventing electrons from the valence band from being excited into these states due to the Pauli exclusion principle. Instead, with additional energy, these valence electrons can be excited to higher-energy states in the conduction band, resulting in a broadened energetic transition and thus a wider optical band gap.[53] A disadvantage of doping is that it increases crystal disorder which can lead to a decrease in transmittance, and thus limit the usability of the material in transparent devices.[54]

1.1.2.1 Work Function and Band Bending

Transparent metal oxides have applications in devices such as organic light-emitting diodes (OLEDs) and organic photovoltaic cells (OPVCs). A critical part of predicting the performance of a semiconductor in a particular application is understanding the semiconductor band structure.[18] Doping or the adsorption of molecules on the surface, for example hydroxylation of the ZnO surface, can affect the energies of its bands and result in changes in work function and band bending.[55] Table 1.1 shows some typical values for band gap, work function, and carrier concentration for different faces of ZnO.

Table 1.1. Literature values for work functions, band gaps, and carrier concentrations of intrinsic or deliberately doped Zn-polar, O-polar, and m-plane ZnO.

ZnO face	Dopant	Work function (eV)	Band gap (eV)	Carrier Concentration (cm^{-3})	Ref.
Zn-polar	-	3.7	-	-	[56]
	-	4.25	-	-	[57]
	-	5.5 – 5.6	-	-	[58]
	-	-	3.24	9.92×10^{16}	[52]
	-	-	-	$\sim 2 \times 10^{17}$	[10]
O-polar	-	4.96	-	-	[57]
	-	4.5	-	10^{17}–10^{18}	[56]
	-	-	-	$\sim 2 \times 10^{17}$	[10]
	-	-	3.3	-	[59]
m-plane	1 % Sb	-	3.26	3.57×10^{17}	[52]
	-	4.64	-	-	[57]
Polycrystalline	-	4.1	-	-	[7]
	-	-	-	$\geq 10^{16}$	[60]
	2 % Al	-	-	4.7×10^{20}	[61]
	2 % N	-	-	10^{13}	[60]

Work function (ϕ, measured in electron volts, eV) is a property relating to how easily an electron can be moved from the Fermi level (E_F) of a metal or semiconductor to the vacuum level. A lower work function indicates that electrons are less strongly bound to the surface. When two materials such as a metal and a semiconductor are brought together to create a metal-semiconductor junction, their difference in work function will affect the energy bands of the semiconductor. Electrons from the material with a lower work function will flow to the higher work function material until equilibrium is reached – that is, until the E_F of both materials are the same (Figure 1.5).[62] A Helmholtz double layer appears at the interface; for a situation where the metal has a higher work function than that of the semiconductor, the surface of the metal will be negatively charged due to excess electrons and the semiconductor surface will be positively charged. The layer of negative charge in the metal will now repel electrons in the semiconductor, which causes their potential energies to increase while also forming a near-surface electron depletion region. As a result, the bands of the semiconductor bend

upwards as seen in Figure 1.5c (left hand side). In the case where the metal work function is less than that of the semiconductor, the semiconductor bands will bend downwards (Figure 1.5c, right hand side).

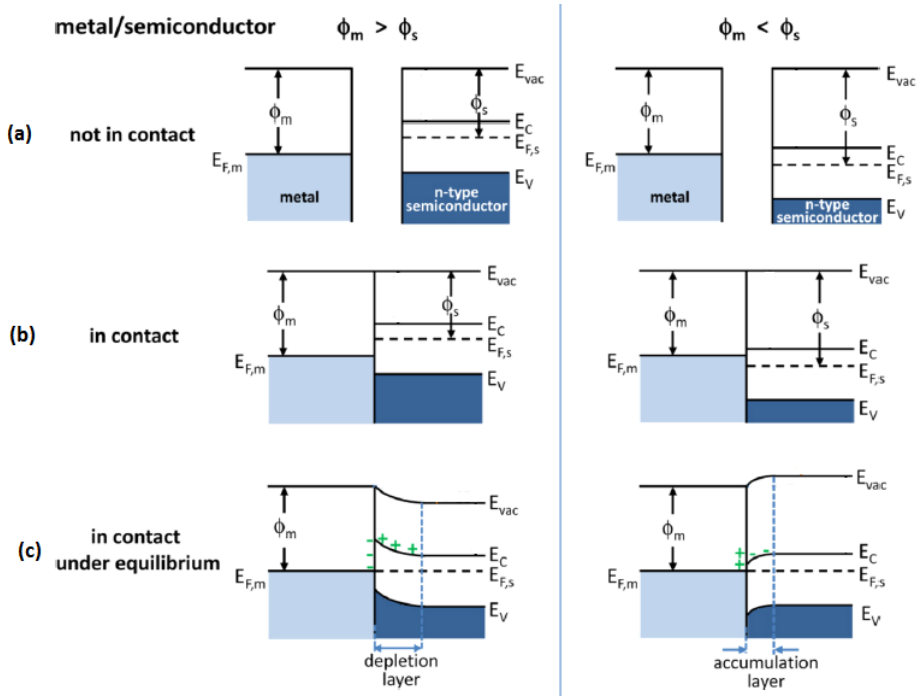

Figure 1.5: Band energy diagrams for a metal and n-type semiconductor coming into contact. The band energies are labelled as follows: E_{vac}, vacuum energy; E_C, conduction band energy; E_V, valence band energy; Φ_m, work function of metal; Φ_s, work function of semiconductor. $E_{F,s}$ and $E_{F,m}$ refer to the Fermi energy levels of the semiconductor and the metal, respectively. Adapted from Zhang et al.[62]

In OLEDs, transparent metal oxides such as ITO are used as the anode, which injects holes into the organic layer.[63] A typical ITO work function of ~4.6 eV does not allow efficient hole injection into the HOMO of organic hole transport materials, which typically have HOMO at higher energies (e.g. 5.4 eV). ITO surface treatments such as oxygen plasma or attachment of conducting polymers or other organic modifiers can increase the ITO work function and decrease the energetic barrier height for hole injection from ITO to the hole transport material. Furthermore, organic surface modifiers can convert the ITO surface from hydrophilic to hydrophobic and thus increase the surface energy

compatibility between ITO and the hole transport layer.[64] These factors can improve the efficiency and brightness of OLEDs.

The principles of Figure 1.5 can be applied to the behaviour of a semiconductor electrode in electrolyte solution for an electrochemical experiment.[65] For the two components to be in equilibrium, their electrochemical potential must be equal. The electrochemical potential of the solution is like a work function in that it relates to the tendency of the chemical species to gain or lose electrons. It is governed by the potential of the redox species in solution. Similarly, the electrochemical potential of the semiconductor is determined by its work function. A typical n-type semiconductor at open circuit will have its E_F energetically higher than the redox potential of the solution species, so the same process as Figure 1.5(a – c) occurs, giving a depletion layer and upwards band bending at the semiconductor near-surface region. Varying the applied potential on the semiconductor electrode shifts the E_F and bulk band energies, but not the surface band energies, meaning that the band bending can be tuned. The flat band potential is where the electrode E_F is the same as the redox potential of the solution species, so no transfer of charge occurs and thus there is no band bending. If the applied potential is more positive than the flat band potential, an n-type semiconductor will have upwards band bending and an electron depletion region. Likewise, applied potential more negative than the flat band potential will cause an accumulation of electrons at an n-type electrode surface, causing downwards band bending.

ZnO is one of several unusual n-type metal oxides which possess native downwards surface band bending in air: In_2O_3,[66] SnO_2,[67] CdO,[68] and InN[69,70] also have this property. The direction of the band bending means that electrons accumulate on the surface to give ZnO a metallic nature; this is known as a surface electron accumulation layer (SEAL)[17,71,72] or 2D electron gas (2DEG).[5,73,74] This is shown in Figure 1.6, a schematic of the energy level diagram for ZnO where ζ is the energetic separation between the valence band maximum and the Fermi level ($E_F - E_V$), ξ is the energetic separation between E_F and the conduction band, and the typical band gaps for ZnO range from 3.3 to 3.44 eV.[5]

The 2DEG can be influenced by adsorbates such as O_2, NO_2, and H_2O,[72,75,76] which change the surface conductivity and allow ZnO to be used for gas sensing applications.

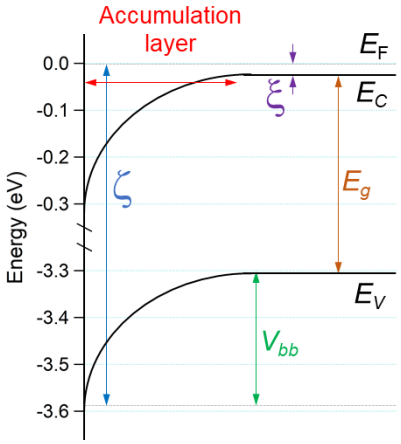

Figure 1.6. Schematic energy level diagram of bare ZnO surface, where V_{bb} is the surface band bending, E_C is the conduction band, E_V is the valence band, E_F is the Fermi level, E_g is the band gap (~3.37 eV for ZnO), ζ is the difference between E_V and E_F, and ξ is the difference between E_C and E_F.

This downward band bending on ZnO is attributed to donor-like surface species such as hydroxyl groups.[24] Heinhold et al. showed that surface H could be removed from O-polar ZnO upon heating to high temperatures (750 °C) in ultrahigh vacuum (UHV), leaving ~0.5 of a hydroxyl monolayer on the surface.[10] On m-plane and a-plane ZnO, this effect was heightened and all surface OH and H was removed under the same conditions.[24] The difference in reactivity was attributed to the polarity of the faces: the O-polar face requires hydroxyl termination in order to stabilise the charge imbalance, while nonpolar faces do not. Importantly, the removal of surface OH groups resulted in upward band bending on O-polar, m-plane, and a-plane ZnO, converting the surface from a metallic to insulating nature (Figure 1.7b) and confirming the role of hydroxyl groups in downwards band bending. However, once the samples were exposed to atmosphere, the surfaces were immediately re-hydroxylated, and the surface regained its downwards band bending and metallic nature, so this is not a practical method for obtaining 'clean' ZnO for electronic applications. Moreover, the Zn-polar face could not be manipulated in this way, as its terminating OH layer was largely resistant to heating.

Although some hydroxyl groups were removed and the downwards band bending decreased, heat treatment was not able to significantly change the electronic nature at the surface (Figure 1.7d).

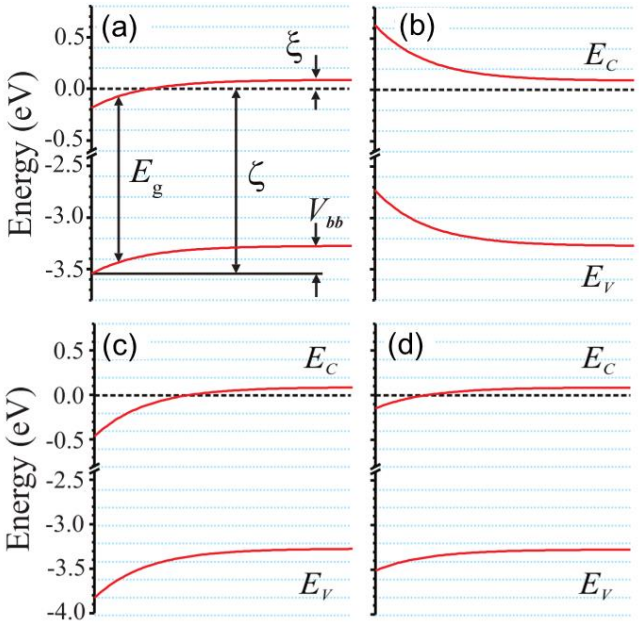

Figure 1.7. Schematic band bending diagrams of O-polar ZnO (a) before and (b) after annealing at 750 °C in UHV, and Zn-polar ZnO (c) before and (d) after the same. E_C and E_V are the conduction and valence bands, respectively; E_F is the Fermi level; E_g is the band gap of ZnO; V_{bb} is the band bending; ζ is the energetic separation of E_V and E_F, and ξ is the separation of E_C and E_F. Adapted from Heinhold et al.[10]

Deliberate modification of semiconductor surfaces with selected molecules can tune the work function and allow optimisation of charge transfer and band bending at the surface.[58,77–79] The work function and band bending of a modified surface can depend on the strength of the molecular dipoles, the uniformity and angle at which the molecules are arranged, and how the surface charge redistributes itself in response to these.[80] It is possible to predict the effect of a molecular monolayer through computational methods such as density functional theory (DFT).[81] These theoretical studies can give good starting points for choosing a molecule for its ability to modify the work function of a surface.

1.1.2.2 Determining Band Bending from Experiment

There are several methods for determining the band bending at a semiconductor surface, including Mott-Schottky analysis, scanning Kelvin Probe Force Microscopy (KPFM), and X-ray and ultraviolet photoelectron spectroscopy (XPS and UPS, respectively).

Electrochemical Mott-Schottky plots of a semiconductor in an electrolyte can be made by determining its capacitance as a function of applied potential and frequency.[23] A linear extrapolation allows the calculation of the flat-band potential, which is related to the degree of band bending relative to the redox species in the electrolyte.[82] However, capacitance measurements of metal oxide semiconductors are known to be easily affected by surface states; they are also heavily dependent on the sample preparation.[39] This makes results difficult to reproduce.

Scanning KPFM is an atomic force microscope (AFM) method with very high spatial resolution. It can be carried out in ambient conditions to measure the contact potential (V_{cp}) difference between a semiconductor surface and a metal tip, often gold.[83,84] This can be related to band bending, V_{bb}, by the equation:

$$V_{\mathrm{bb}} = \phi_{\mathrm{M}} - qV_{\mathrm{cp}} + \phi_{\mathrm{off}} - \chi + E_{\mathrm{F}} \qquad (1.1)$$

where ϕ_M is the work function of the tip, q is the electronic charge, ϕ_{off} is a measured voltage offset found via a calibration sample (gold), χ is the electron affinity of the semiconductor, and E_F is the Fermi level relative to the conduction band minimum.[83] Because it is a highly surface-sensitive technique, UHV should be used to remove contaminants which may disturb the surface during scanning.[85] Additionally, the work function of the probe needs to be measured on a sample with well-defined work function in order to obtain absolute values. Switching between the calibration and analysis samples decreases the accuracy of work function measurements.[85]

X-ray photoelectron spectroscopy (XPS) is a popular technique for chemically characterising material surfaces and can also be used to characterise the valence band density of states. In UHV conditions,

soft X-rays eject photoelectrons from the sample, the kinetic energies of which are recorded (E_{kinetic}) and related to their original binding energy (BE) in the sample:[86]

$$BE = h\nu - E_{\text{kinetic}} + \phi \qquad (1.2)$$

where ϕ is the work function of the XPS analyser and $h\nu$ is the energy of the X-ray photons. The latter is a key factor, as the photon energy determines how surface sensitive the XPS analysis is. For typical fixed-energy laboratory instruments with an Al X-ray source, $h\nu$ = 1486.6 eV, whereas tuneable synchrotron photon sources can provide energies as low as $h\nu$ = 50 eV.[87,88] While X-rays typically penetrate relatively long distances (several µm) into a sample, it is the photon energy which determines the kinetic energy of the ejected photoelectrons and therefore how far these electrons can travel before being inelastically scattered, which is in the order of nm.[86] Thus, the higher the photon energy, the greater the depth that the photoelectrons can escape from the sample, and therefore the less surface-sensitive the measurement. Figure 1.8 shows an XPS valence band (VB) region spectrum for ZnO.

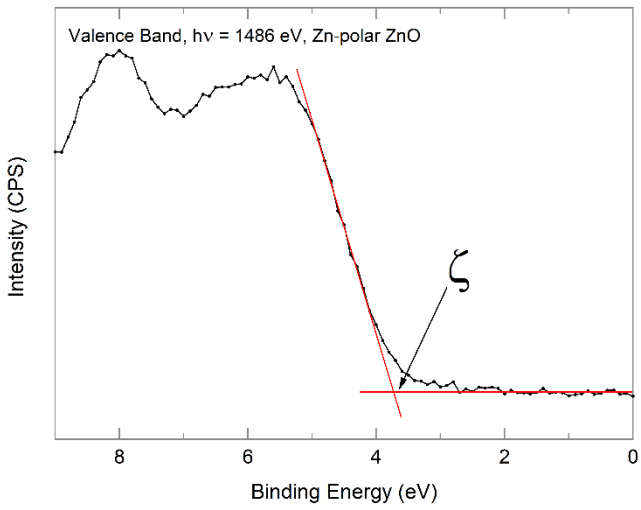

Figure 1.8. Typical fixed-energy XPS valence band spectrum for Zn-polar ZnO, showing how ζ is determined from the linear extrapolation of the VB edge to the instrument background. This work.

Linear extrapolation of the low BE edge of the VB spectrum to the instrument background gives the value of ζ, which can be related to V_{bb} as shown in Figure 1.6 and detailed in Chapter 2. However, it is

important to note that calculated values of V_{bb} are dependent on how far into the sample the VB spectrum was been measured, i.e. the photon energy used for measurements.

UPS is very similar to XPS, though a much lower photon energy (20 – 50 eV) is used.[89] This makes the technique much more surface sensitive and allows easier deconvolution of molecular orbitals.[78] However, this sensitivity can be problematic as it means that very small variations in surface conditions (e.g. carbon contamination) between or across samples can greatly affect the spectra and the extracted V_{bb}.

Photoelectron spectroscopy can also be used to calculate work function. On the UPS or XPS spectrum, photoelectrons from the sample and from the analyser overlap. Biasing the sample with a negative potential increases the kinetic energy of the sample photoelectrons but not the photoelectrons arising from the analyser. This separates the two sets of photoelectrons and allows the work function of the sample to be determined. In all cases, a reference sample such as Au or Pt must be used to calibrate the Fermi level so that absolute values of work function and ζ can be found.

1.1.3 Photoconductivity of ZnO

ZnO is known to display persistent photoconductivity (PPC). This phenomenon occurs upon irradiation of ZnO with UV light, resulting in an increase in the surface conductivity. When the UV light is switched off, this conductivity is slow to return to its original value. The exact mechanisms for these effects are not completely certain, but Figure 1.9 shows a proposed mechanism. In ambient conditions, the hydroxylated, electron-dense, conductive surface of ZnO is susceptible to physisorption of atmospheric species such as O_2 and H_2O. These species take up electrons from the 2DEG and as a result, the surface of ZnO becomes more resistive due to fewer delocalised electrons available. UV irradiation generates electron-hole pairs throughout the sample. The holes move towards the surface where they recombine with the trapped electrons and release the physisorbed species into atmosphere. The conductive surface is now re-established and remains for as long as the surface is

exposed to UV light. When the light is turned off, atmospheric species slowly physisorb to the surface again, thus gradually returning the resistivity to its typical value.

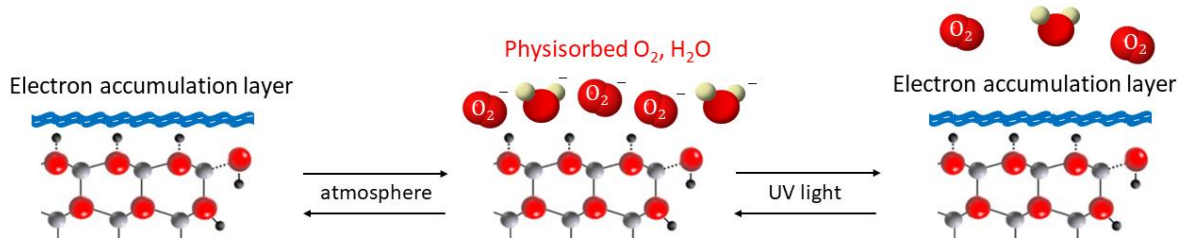

Figure 1.9. Proposed mechanism for photoinduced conductivity changes on O-polar ZnO. Adapted from work by Dr Alana Salkeld, University of Canterbury.

PPC presents a challenge for device applications based on ZnO, since UV light can change the conductivity of the surface in unpredictable ways. For example, UV sensors require there to be a change in current on exposure to UV light, but ideally this current increase should be rapid and immediately reversed to the base current when the UV source is removed ('dark current'). The slow reversal of PPC introduces a varying background that must be subtracted to obtain useable data. A method of removing the PPC from ZnO is highly desired for this application.

It has been reported that UV irradiation increases hydroxylation on ZnO surfaces and can therefore enhance surface modification reactions which involve surface OH groups.[90] Photogenerated holes and electrons can also be responsible for the degradation of organic molecules such as dyes at ZnO surfaces via the formation of hydroxy radicals.[91] Thus, the stability of organic surface modifiers on UV-exposed ZnO is of interest.

1.1.4 Deliberate Surface Modification of ZnO

ZnO surfaces can be deliberately modified with molecules to improve their stability and functionality and mitigate some of the issues highlighted in the previous sections.

1.1.4.1 Gas Phase Methods

ZnO has been modified with various gas-phase reactants, ranging from single atoms to whole molecules. These reactions are carried out in vacuum, often after Ar^+ ion cleaning and/or annealing to obtain pristine, highly-reactive surfaces. Polydorou et al. used UPS to show that fluorine (SF_6) plasma treatment increased the downwards band bending at the surface of ZnO films, proposing through computational calculations that F atoms substitute O atoms and act as donors.[79]

Ozawa et al. showed that tetrathiafulvalene (TTF), evaporated over ZnO in a UHV chamber, adsorbed both molecularly and dissociatively to the surface Zn atoms.[14] As expected, the amount of TTF on the surface was higher on the Zn-polar face than on the O-polar and m-plane faces. On the Zn-polar face, the level of TTF dissociation was relatively low, and the adsorbed molecules acted as electron acceptors. On the O-polar and m-plane faces, a higher level of dissociation of TTF caused by neighbouring O led to significant atomic S on the surface, which acted as an electron donor. These differences resulted in upwards band bending on the Zn-polar face, and downwards band bending on the O-polar and m-plane faces. In more recent work, Ozawa et al. showed that acridine orange increases downwards band bending on all ZnO faces, with the largest effect seen on the O-polar face.[92] Schlesigner et al. used 2,3,4,6-tetrafluoro-7,7,8,8-tetracyanoquinodimethane to control the work function and band bending on polar ZnO surfaces.[56] On both O-polar and Zn-polar surfaces, the downwards band bending was replaced with upwards band bending.

Gao et al. exposed m-plane ZnO nanopowders to gas-phase propiolic acid under high vacuum and observed that the surface topography was maintained.[93] Using infrared (IR) spectroscopy, they determined that the molecules were bound to the ZnO surface via carboxylate linkages, leaving the alkyne available for a gas- or liquid-phase click reaction with benzyl azide. They cited this as an 'important method' for surface functionalisation, as it negated the need for wet chemistry and achieved strong carboxylate linkages without etching of the ZnO by the carboxylic acid.

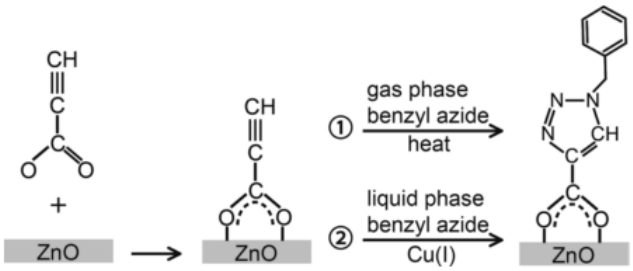

Figure 1.10. Reaction scheme for ZnO nanopowder modification with propiolic acid, followed by a click reaction with benzyl azide. From Gao et al.[93]

Although gas-phase surface modifications can be used on a wide range of ZnO structures, the stabilities of the surfaces upon removal from vacuum are often not investigated. Furthermore, the process of evaporation can be time-consuming, involving long pump-down times of > 16 h as well as specialised equipment.[93] There are also limitations on the size of substrate that can be modified. These factors limit the scalability and efficiency of gas-phase methods.

1.1.4.2 Wet Chemical Methods

Various functional groups have been shown to form covalent bonds with metal oxides through reaction with surface OH groups.[94] From silanes on glass to thiols on gold, self-assembled monolayers (SAMs) have been well-studied over the last 35 years.[95] During this time, different substrates and modifiers have been combined to achieve different outcomes and properties. The general principle of self-assembly relies on the affinity of the modifier for the surface; molecules spontaneously adsorb to the surface, forming bonds which reflect the strength of this affinity (Figure 1.11). A selection of molecules shown to self-assemble on ZnO are discussed below.

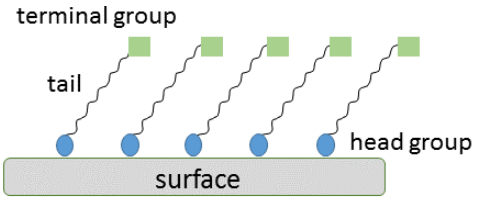

Figure 1.11: A general diagram of a self-assembled monolayer on a surface.

1.1.4.2.1 Phosphonic Acids

Phosphonic acids (PA) are a promising starting point for ZnO surface modification: fluorinated,[58,77] aliphatic,[58,77] and aromatic PAs[7,8,77] have been successfully attached to ZnO nanorods,[40,96] nanowires,[97] single crystals,[58,97,98] and sputtered surfaces.[6,23,99] This success has been attributed to the PA anchoring to the surface in either a bi- or tri-dentate fashion, as depicted in Figure 1.12.

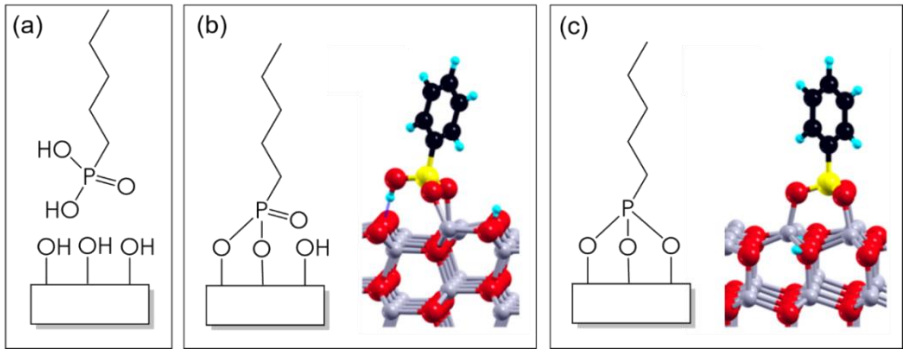

Figure 1.12: Interactions between phosphonic acids and ZnO: (a) unbound pentylPA; (b) pentylPA and phenylPA bound in a bidentate fashion (m-plane ZnO); (c) pentylPA and phenylPA bound in a tridentate fashion (Zn-polar ZnO). Adapted from Wood et al.[77] and Ostapenko et al.[100]

Some studies report that heating is required to obtain strong phosphonate covalent bonds on metal oxides[58,101] while others claim that the bonds form in ambient conditions.[99,102] Ford et al. hypothesised that annealing affects the binding mode of the PA, as heat may drive a different set of condensation reactions to those which occur at room temperature. Computational models have been used alongside high-resolution XPS to determine binding modes.[50,58,77] Timpel et al. calculated that each Zn-polar ZnO unit cell is capable of binding either one or two PA molecules, via tridentate or bidentate configurations, respectively.[58] As such, bidentate PAs have a unit-cell-limited, maximum theoretical surface concentration of 5.47 molecules nm^{-2} on ZnO, while tridentate PAs have a maximum theoretical coverage of 2.73 molecules nm^{-2}.

The change in ZnO work function after PA modification has been experimentally determined on the Zn-polar and O-polar faces,[58,98] while computational studies have also been carried out to provide

theoretical values for these studies.[103] Braid et al. used 2,6-difluorophenylvinylPA and 2,6-difluorophenylethylPA to decrease the work function of ZnO by 0.78 eV and 0.57 eV, respectively.[8] The difference was attributed to the former PA having a C=C bond between the phosphonate group and the aryl group, while the latter did not. In contrast, Sharma et al. modified ITO with octadecylphosphonic acid (ODPA) and 1*H*,1*H*,2*H*,2*H*-perfluorooctyl phosphonic acid (F_{13}OPA) to increase the workfunction,[63] while Wang et al. used long-chain fluorinated PAs of various chain lengths.[104] The former noted that the fluorinated chain increased the work function more than the non-fluorinated molecules, while Wang et al. observed that the longer-chain PAs gave larger increases in work function than shorter chains. Recently, Zheng et al. compared pentafluorobenzylPA (PFBPA) and a long-chain fluorinated PA on ITO.[64] The linear PA increased the work function more than the aromatic one. These results agree with those found by Paniagua et al., who investigated a variety of PAs on ITO.[105] A summary of these work function changes is shown in Table 1.2.

Table 1.2. Work function changes of PA-modified metal oxides relative to unmodified samples.

Substrate	Modifier	ΔΦ	Ref.
Polycrystalline ZnO	2,6-difluorophenylvinylphosphonic acid	−0.78	8
	2,6-difluorophenylethylphosphonic acid	−0.57	8
Zn-polar ZnO	4-trifluoromethylbenzyl phosphonic acid	> +1.5	7
	4-trifluoromethylbenzyl phosphonic acid	+1.35	58
	F_{13}OPA	+1.7	58
O-polar ZnO	4-trifluoromethylbenzyl phosphonic acid	> +1.5	7
	4-cyanophenyl phosphonic acid	−0.29	96
	4-methoxyphenyl phosphonic acid	+0.49	96
	Phenylphosphonic acid	−0.20	96
ITO	ODPA	+0.0	63
	F_{13}OPA	+0.7	63
	F_9OPA	+0.64	104
	F_{13}OPA	+0.70	104
	F_{21}OPA	+0.91	104
	F_{21}OPA	+0.99	64
	Pentafluorobenzylphosphonic acid	+0.38	64
	Pentafluorobenzylphosphonic acid	+0.31	106

Compared to work function studies, little work has been done on the effect of these PA modifications on the band bending of semiconductor materials. Wood et al. proposed from computational work that the binding mode of fluorinated benzyl PA determines the effect on band bending: bidentate binding results in electron density situated at the ZnO surface, while tridentate-bound molecules have electron density focussed at their tail group.[77] The former results in an increase in surface downwards band bending, while the latter can decrease downwards band bending. Using Mott-Schottky analysis, Chen et al. showed that modification of m-plane ZnO with alkyl chain PAs decreased the downwards band bending.[23] The values of ζ ($E_F - E_V$), extracted from the XPS VB spectra of ZnO modified with fluorinated PAs, appear to decrease in work presented by Timpel et al., which again indicate a reduction in downwards band bending.[58] These results make PAs a promising candidate for tuning the band bending of ZnO via stable organic layers.

1.1.4.2.2 Carboxylic Acids

The main appeal of carboxylic acids as surface modifiers is the availability and range of functionalised acids available, as well as the bidentate binding mode which is proposed to enhance their stability (Figure 1.13). However, it is hard to obtain uniform monolayers, the stability of the layers deteriorates over time, and etching of the ZnO surface has been observed.[107] Carboxylic acids have been used on ZnO and iron oxide, as well as on TiO_2 nanoparticles in dye-sensitised solar cells.[94] On ZnO, citrate was found to bind only to the Zn-polar face, not the O-polar face or m-plane.[46] Chen et al. noted from AFM measurements that modification of ZnO from an ethanol solution of carboxylic acid resulted in etching of the surface due to the acidic nature of the molecule, while little evidence of carboxylic acid attachment was seen.[23] Similarly, Gao et al. modified m-plane ZnO surfaces with liquid propiolic acid and observed from scanning electron microscopy (SEM) that the substrate was significantly etched.[93]

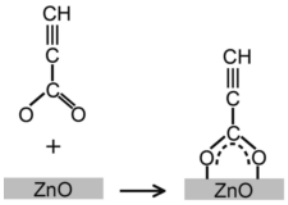

Figure 1.13. Carboxylic acid bound to ZnO in a bidentate fashion. From Gao et al.[93]

1.1.4.2.3 Alkanethiols

Alkanethiols have been used to form self-assembled monolayers (SAMs) for several decades, with gold being a popular substrate due to its strong affinity with sulfur (Figure 1.14).[108] As such, they are well-studied and there is a wealth of literature on the topic.[109–115] In contrast, alkanethiol-based SAMs on metal oxides are little studied. Alkanethiol SAMs have been reported on metal oxides including ZnO, although there are contradictory findings in the literature. A complicating factor is that thiols can be oxidised by mild oxidising agents to form disulfides; oxidation can also give sulfenic acid, which in turn can be oxidised into sulfonic acid.[116] Thiol oxidation over time has been seen for alkanethiol monolayers on gold, and is attributed to gradual reaction of the SAMs with atmospheric oxygen and UV exposure.[13]

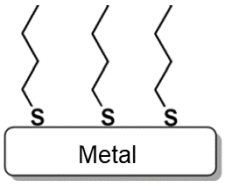

Figure 1.14. Alkanethiols on metal substrate. Adapted from Pujari et al.[94]

Work by Chen et al. showed that octadecanethiol forms strong and uniform SAMs on m-plane ZnO, and the authors argued that the monolayers were more uniform and stable than PA SAMs.[23] Perkins, however, modified polycrystalline ZnO with hexanethiol and hexylPA, and concluded the latter were more thermally stable than alkanethiol SAMs.[99] These differences may be due to different binding modes: Chen et al. observed a S-Zn binding via XPS, while Perkins observed an additional signal arising from sulfonate bonding. Sadik et al. reported sulfonate binding on O-polar ZnO and thiolate binding

on Zn-polar ZnO.[117] In contrast, Pesika et al. observed sulfonate binding on thiol-treated Zn-polar face and thiolate binding on O-polar ZnO.[13] Clearly questions remain concerning thiol binding to ZnO, and the reactions may be worth further investigation.

In their study of alkanethiol modification of m-plane ZnO, Chen et al. carried out electrochemical impedance measurements and determined that both octadecanethiol (ODT) and octadecylPA reduced the downwards band bending of m-plane ZnO.[23] No other reports of thiol-induced band bending changes were found.

1.1.4.2.4 Silanes

Strong covalent bonds have been observed between silanes and polycrystalline ZnO, as well as SnO_2 and ITO.[90,94,118,119] These bonds form in two steps (Figure 1.15). Firstly, water on the surface of the substrate hydrolyses the silane, removing leaving groups such as Cl or OC_2H_5 and forming silanol groups. These can then undergo condensation reactions with OH groups on the substrate, making a hydroxylated surface necessary.

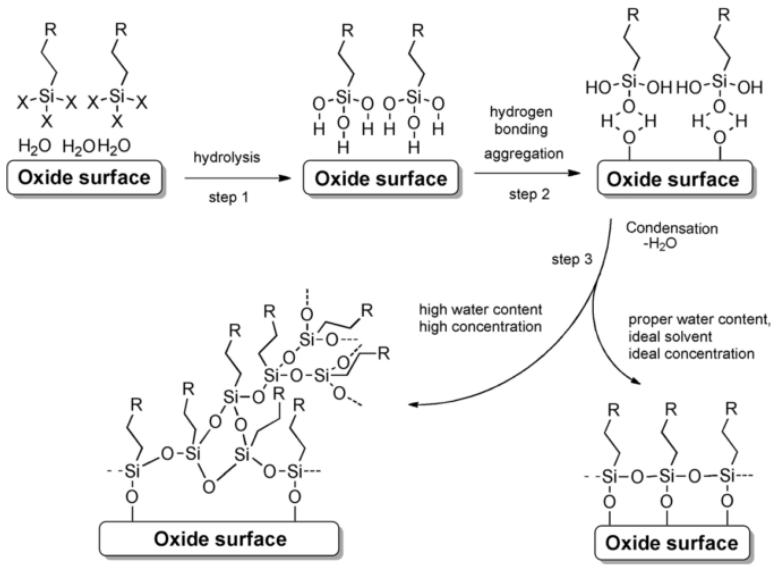

Figure 1.15. Silanes bound to a surface in both disordered and uniform structures, depending on the modification parameters. X = e.g. Cl, OH, H, OCH_3, OC_2H_5. From Pujari et al.[94]

Drawbacks of silanes as modifiers include lack of hydrolytic stability before and during modification, leading to polymerisation and irreproducible multilayers on the surface.[94] While anhydrous solutions have been shown to not form silane modification layers, too much water in solution favours polymerisation of the silanes.[120] Silanes can be used as capping molecules to stabilise nanoparticles in solution and prevent aggregation.[121] However, Allen et al. used triethoxysilane to modify planar polycrystalline ZnO, using a catalyst to enhance grafting, and observed sub-monolayer coverage of a disordered silane layer.[90] They noted that the percentage of moisture in both the catalyst and the silane greatly affected the coverage, making silanes a somewhat unreliable approach to surface modification.

1.1.4.2.5 Amines

ZnO nanoparticles are often capped with alkylamine ligands to help disperse them in solution.[122–124] Coppel et al. proposed that the strongest binding between alkylamines and ZnO nanoparticles is due to lone-pair electron interactions between nitrogen atoms in the amines and Zn atoms of ZnO, while weaker attachments arise from hydrogen bonds or van der Waals interactions.[125] The behaviour of ethylenediamine (en) at planar ZnO was investigated to determine its usefulness in directing the orientation of hydrothermally-grown ZnO during synthesis.[46] While en was observed by FTIR on m-plane ZnO during immersion in 10 mM en in D_2O, it was not observed on the Zn-polar face, indicating a lack of affinity or bonding. Even on the m-plane face, most of the ethylenediamine was removed by rinsing, suggesting it was not strongly bound. Chen et al. also determined from AFM and XPS that dodecylamine did not bind strongly to m-plane ZnO.[23] Amines are therefore not suitable for long-term surface modification of ZnO.

1.1.4.3 Photochemical Methods

Alkenes present a promising option for modifying the surface of ZnO as they can be photochemically grafted onto ZnO to give either mono- or multilayers, depending on the type of alkene.[39] They have also been bound to other metal oxides such as ITO,[126] and TiO_2.[127] Figure 1.16 shows a proposed

binding mechanism which begins when UV light emits photoelectrons from the substrate to the modifying solution. Consequently, the substrate become positively charged and becomes vulnerable to nucleophilic attack by the alkene, forming Zn-O-C bonds.

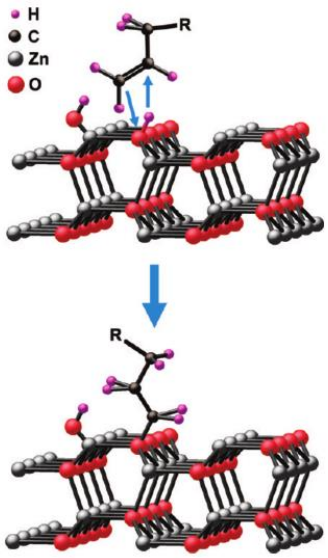

Figure 1.16. Schematic showing a possible pathway to Zn-O-C bonds from an alkene at m-plane ZnO under UV light. From Ruther et al.[39]

Ruther et al.[39] showed that alkene-derived monolayers on m-plane ZnO are very stable and dense, although multilayers can form if exposed to UV light for too long. The choice of tail group affects the grafting process, with better electron acceptors giving better grafting: alkylalkenes such as 1-dodecene underwent very inefficient grafting, while ester-terminated molecules were found to graft more efficiently to ZnO to form monolayers. An electron-accepting trifluoroacetamide tail group was shown to graft very efficiently to ZnO, giving multilayers. The same group also showed from Mott-Schottky measurements that alkene modification did not significantly change the band bending of ZnO.[39]

1.1.4.4 Electrochemical Methods

Organic molecules can also be bound to surfaces using electrochemistry. The relative ease of aryldiazonium salt synthesis and grafting makes aryldiazonium ions a popular reagent for surface

modification. Their value lies in the formation of an aryl radical upon the reduction of the diazonium ion which can then react with a substrate to form covalent bonds (Figure 1.17).[128] This reduction can be carried out by electrochemical means or by the addition of a chemical reducing agent such as iron or zinc powder.[129] Mirkhalaf et al. showed that sonication of nitrobenzenediazonium (NBD) ions can lead to radical formation and grafting on ITO.[130] 'Spontaneous' grafting, where the aryldiazonium ion is reduced by the substrate itself, can also occur at certain materials.[131–134] Additionally, it has been proposed that aryldiazonium cations can directly react with Au surfaces to form Au-N=N-R bonds, and that further grafting can occur via decomposition of the aryldiazonium ion.[135] Meanwhile, grafting via electrochemical reduction of aryldiazonium ions is a commonly-used approach for modifying carbon and metal surfaces, as well as metal oxides.[136–139]

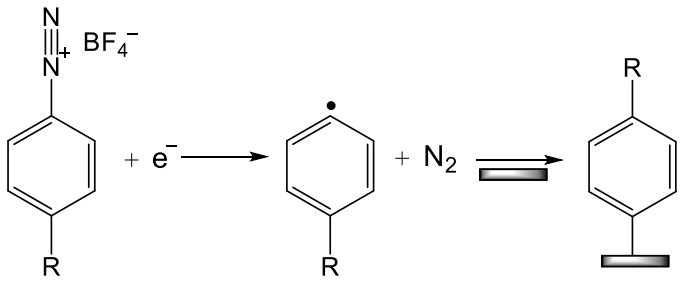

Figure 1.17: The reduction process for an aryl diazonium salt, the radical of which readily reacts with a substrate. Adapted from Bahr et al.[140]

Due to the reactive nature of aryl radicals, loose-packed multilayer formation on the substrate is typical unless steps are taken to prevent it.[129] The first radicals attach to the substrate, while subsequent radicals can also attach to the surface, or to the first layer of grafted aryl groups (Figure 1.18). Reaction with non-reduced aryldiazonium ions can give rise to azo (N=N) linkages within the film. In grafting processes which require electrons to come from the substrate, that is, spontaneous or electrochemical grafting, electron transfer must occur over an increasingly thick insulating layer as the film grows. Eventually the rate becomes negligible and film growth stops, typically at a film thickness of a few nm.[141]

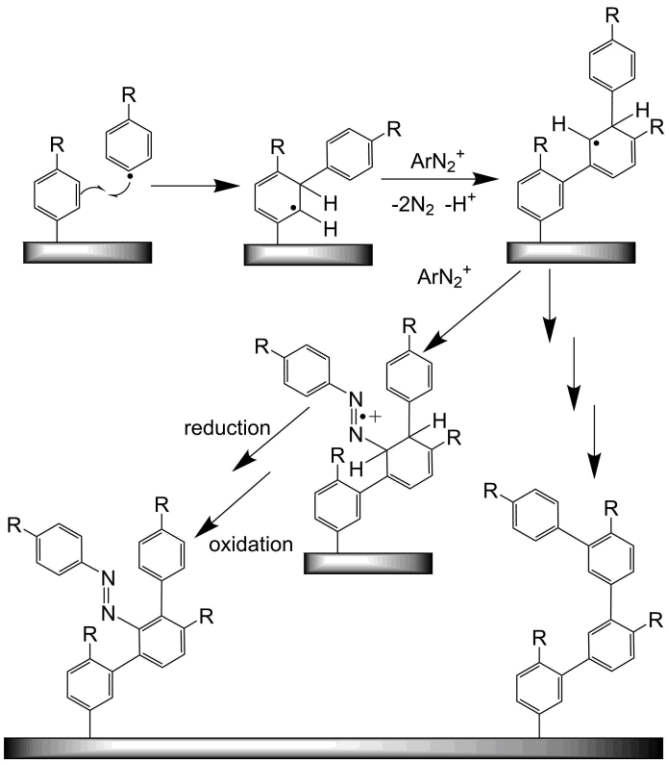

Figure 1.18. Proposed mechanisms for the formation of polyaryl multilayers during the electrografting of aryl diazonium salts. Adapted from Doppelt et al.[142]

Chen et al. used a modifier with dual functionality, 4-aminophenylmethylPA, to probe the difference in stability between a modification layer formed via PA self-assembly on ITO, and a layer formed after in situ preparation of a diazonium ion and then electrochemical attachment via reduction.[143] A diagram of the binding modes is given in Figure 1.19. It was observed that the PA-attached monolayer had no electrochemical blocking properties compared to the multi-layer formed by the diazonium functionality. The electrochemically-modified surface is less well-defined than the PA-modified surface due to the variable grafting mechanisms and multilayer formation. The authors noted their surprise that 10.54% of the electrochemical layer was due to phosphonate binding, given that the grafting took place over 5 minutes whereas traditional PA binding has required immersion times in the order of hours (Section 1.1.4.2.1). However, the samples were not sonicated after modification, which may account for this result.

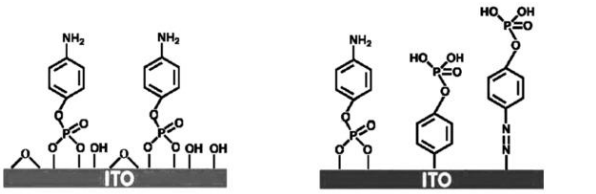

Self-assembled layers Electrochemical reduced layers

Figure 1.19. Binding modes for 4-aminophenylmethylphosphonic acid-modified ITO, modified either through self-assembly or electrochemically. Adapted from Chen et al.[143]

Another approach for obtaining aryl layers was shown by English et al.[144] Hydroxylated TiO_2 was able to react with aryl iodides through nucleophilic substitution to give aryl layers on the surface. Koefoed et al. also used aryl iodides in electrochemical grafting, similar to that done with aryldiazonium ions.[145] They comment that the grafting efficiency is less than that for aryldiazonium ions but note that aryl iodide grafting is an option that gives greater control over film thickness and density.

Wang et al. have recently used aryldiazonium ion grafting to modify ZnO films for DNA sensing (see below),[146] and Bangle et al. used amperometry on a film of ZnO nanoparticles to modify them with a Ru-based dye for dye-sensitised solar cells (see below).[147] However, these application-based studies made no attempt to characterise the bonding of aryl groups to the ZnO surface or the effect on the band bending. Although Bangle et al. did not provide high resolution N 1s spectra, they claimed that no strong evidence for azo linkages within the modification layer was observed due to the binding energy overlap with azo and N=C bonds within the Ru complex, with large, bulky nature of the ligands expected to prevent multilayer formation.[147] To date, there has been no report on the effect on the band bending of ZnO upon modification via aryldiazonium ion chemistry, nor on the binding mode between aryl groups and ZnO.

Hunger et al. performed nitro-, bromo-, and methoxyphenyl grafting on Si(111).[78] They compared the UPS valence band spectra to those of the respective gas-phase benzene derivatives found by Chin et al. in 1992 (nitrobenzene)[148] and Fujisawa et al. in 1986 (all other derivatives).[149] The nitrobenzene film reduced the band bending at the surface from −0.49 eV to almost flat bands (−0.09 eV), and

increased the electron affinity. These observations were associated with the dipole moment of the grafted molecules (3.9 D) and it was suggested that only the first monolayer of adsorbates was responsible. Film thickness was determined by XPS as between 3 and 5 nm, matching the results on metal and carbon in the literature.[141]

1.1.4.5 Applications

Bare and surface-modified ZnO have both been used in devices. A recent review by Gao and Teplyakov outlines difficulties associated with modifying semiconductor surfaces:[150] examples include eliminating impurities such as water or oxygen from modification layers grown through wet chemistry, and creating modification layers which are stable to light, water, and heat. Other aspects to consider are maintaining transparency on an intrinsically-transparent substrate and the effect on the electronic properties of the substrate. Below are some existing applications for ZnO and similar metal oxides.

Field-Effect Transistors

Field-effect transistors (FET) are the basis for many devices, including sensors and screen displays, because they can use a change in electric field caused by adsorbates to induce a change in conductivity and electronic response. ZnO is an attractive material because of its transparency and the wide variety of ZnO nanostructures.[151] However, a native hydroxyl-terminated ZnO surface with downwards band bending cannot be used in a FET because its surface conductivity is too high. To remove the conductivity, ZnO can be annealed to high temperatures to decrease the native H doping and thus the number of charge carriers at the surface.[152,153] Alternatively, an additional dielectric layer can be added. Figure 1.20 shows the top-gate FET based on ZnO nanowires, fabricated by Kälblein et al.[152] It contains source and drain terminals (in this case, aluminium), between which a voltage is applied. The gate (Au) controls the electron flow between the source and drain terminals while the Si substrate enables the device to be additionally biased. An ODPA monolayer is used as the gate dielectric as its thinness is suitable for conformal coverage of individual ZnO nanowires whilst still being insulating. Compared to an identical set-up without ODPA, which relied solely on the formation of a charge

depletion region in the semiconductor at the semiconductor-gate interface to control the source-drain current (Section 1.1.2.1), the FET format shown in Figure 1.20 had 3 orders of magnitude lower gate leakage current.[152]

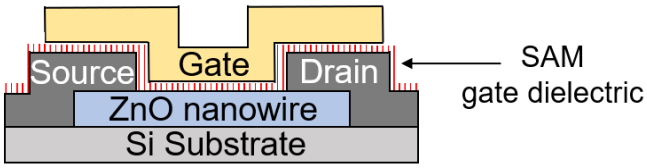

Figure 1.20. Schematic of top-gated ZnO FET with PA SAM indicated by red and white stripes. Adapted from Kälblein et al.[152]

Another popular dielectric material is parylene, which is a biocompatible polymer. Zong et al. used parylene-protected ZnO nanowires in a FET to measure the forces involved in cell growth, making use of the piezoelectric properties of ZnO.[154] Silane-based self-assembled dielectrics have also been used, although the positive charge of the dielectric decreased the performance of the FET.[151] Thin dielectric layers which do not require high-temperature heat treatment are useful for flexible devices based on plastic substrates, provided they function as a good gate-insulator.

Sensors

The surface reactivity of ZnO to gases makes it a useful component in sensing devices for species such as H_2,[155,156] ethanol,[157] ammonia,[9] NO_2,[158] and water.[159] Challenges include increasing the analyte sensitivity and decreasing the detection limit at room temperature, as well as lowering the power consumption and response and recovery time of the sensors.[156] Nanowires and rods are a popular choice for sensing due to their large surface area:volume ratio,[9] and their selectivity and sensitivity have been further enhanced by incorporating surface modifiers. Wang et al. showed in 2005 that coating ZnO nanorods with Pd clusters increased both these parameters for H_2 sensing due to the catalytic reaction of H_2 with Pd,[156] an approach previously used on other semiconductor materials. Recently, Choo et al. showed that increasing the operating voltage of bare ZnO nanorod H_2 sensors

more than halved the response time compared to previous ZnO and metal oxide-based sensors, coupled with a relatively short recovery time.[155] However, their sensors were not as sensitive as others, and thus less suited to quantitative H_2 sensing.

Wan et al. made a simple ethanol-sensing device based on bare ZnO nanowires.[157] As explained in Section 1.1.3, O_2 molecules in ambient conditions adsorb onto ZnO, trapping electrons from the conduction band to form O_2^-. This results in a high surface resistance, but gaseous ethanol can react with these adsorbed species to release the electrons and decrease this resistance. Although this is a surface effect, the thinness of the nanowires means that the increase in conductivity can be seen in the bulk measurements as well. However, the sensitivity of the device proposed by Wan et al. was greatest at 300 °C, which is not a practical temperature. In a different study, Wan et al. were able to use Cd-doped ZnO to sense humidity by taking advantage of defects on the nanowire surface, which have a high local charge density in dry conditions and promote the dissociation of water, allowing protons to act as charge carriers. In high humidity, water condenses on the surface and forms conduction paths between the nanowires. The change in resistance in a humid environment compared to dry air was more than 3 orders of magnitude greater than that for non-doped ZnO.

Waclawik et al. sought to increase the sensitivity of ZnO nanowire sensors towards nitrogen-containing species by attaching tris(hydroxymethyl)aminomethane (tris) or dodecanethiol to the surface.[158] With or without tris attachment, ZnO was capable of detecting NO_2 to low (2 ppm) concentrations. Tris-modified ZnO giving a slightly enhanced response, while the thiol failed to give a stable surface layer and did not enhance the sensing capabilities. Kuo et al. used an organic semiconductor poly(3-hexylthiophene) (P3HT), to enhance ammonia sensing at ZnO nanowires.[9] Spin-coating P3HT gave thick layers of several hundred nm, and a detection limit of < 0.1 ppm for ammonia. Importantly, they also showed that the maximum detectable concentration was 3 orders of magnitude greater than that reported for other ZnO-based ammonia sensors. The sensor was used to test ammonia in the breath of those suspected to have liver disease.

ZnO-based biosensors have also been developed for aqueous conditions. Ahmad et al. recently created a phosphate-sensing bio-FET incorporating ZnO nanowires, shown in Figure 1.21, for pollutant detection in water.[160] The enzyme pyruvate oxidase was immobilised on the ZnO via an immersion process, and protected with a Nafion® coating. Upon exposure to phosphate, H_2O_2 is formed by the enzyme. The H_2O_2 is then oxidised by the ZnO, increasing the signal current between the source and drain terminals. The resulting sensor had a lower detection limit and a wider detection range than those without the ZnO nanowires, or those previously reported using carbon or cobalt electrodes. The authors attributed this to the large surface area and fast electron transfer at the nanowires. No characterisation of the enzyme immobilisation was carried out.

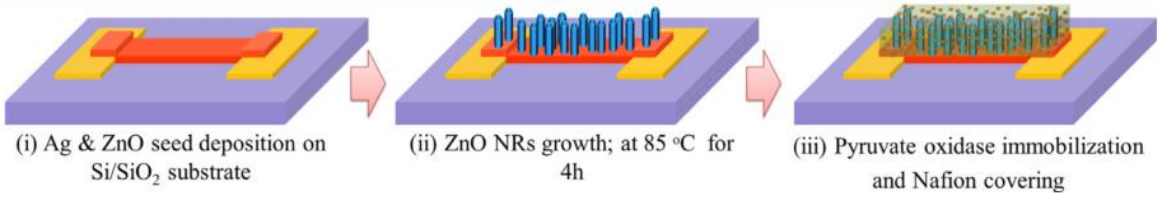

Figure 1.21. Schematic of bio-FET fabrication for phosphate sensing, based on ZnO nanorods (NR). From Ahmad et al.[160]

In terms of physiological sensors, such as those used in blood analysis, Shanmugam et al.[3] used ZnO nanowire arrays for detecting the cardiac biomarker cTnI. The nanowires were modified with thiol or PA molecules, the tail groups of which were functionalised with the cTnI antibody. The antibody binds with cTnI, changing the capacitance and impedance at the surface/electrolyte interface, which is measured by the sensor. The authors observed that the thiol modification provided a more sensitive response to cTnI, because the PAs gave multilayers on the nanowire surface while the thiols gave a monolayer coverage.

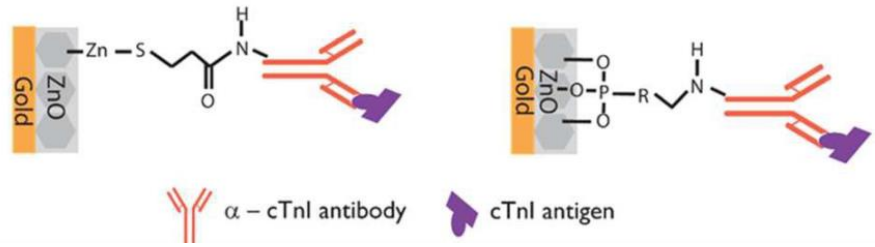

Figure 1.22. Diagram of ZnO nanowire arrays functionalised with thiol- and phosphonic acid-based linkers with cardiac biomarker cTnI antibody tail groups. From Shanmugam et al.[3]

Another example of a ZnO-based bio-FET is that designed by Hagen et al. for the detection of riboflavin (vitamin B2) in aqueous solution.[161] Nanostructured ZnO with a large surface area, deposited by PLD at room temperature, was modified with silanes which were then coupled with a single-stranded riboflavin aptamer. When bound to riboflavin, the aptamer undergoes a structural change (Figure 1.23). Due to the negative charge on its backbone, this produces a decrease in current flowing between the source and drain terminals of the device. If the aptamer is tagged with a ferrocene moiety, this injects electrons into the ZnO and the sensing signal becomes an increase in current. The latter arrangement allows for greater signal response and thus sensitivity.

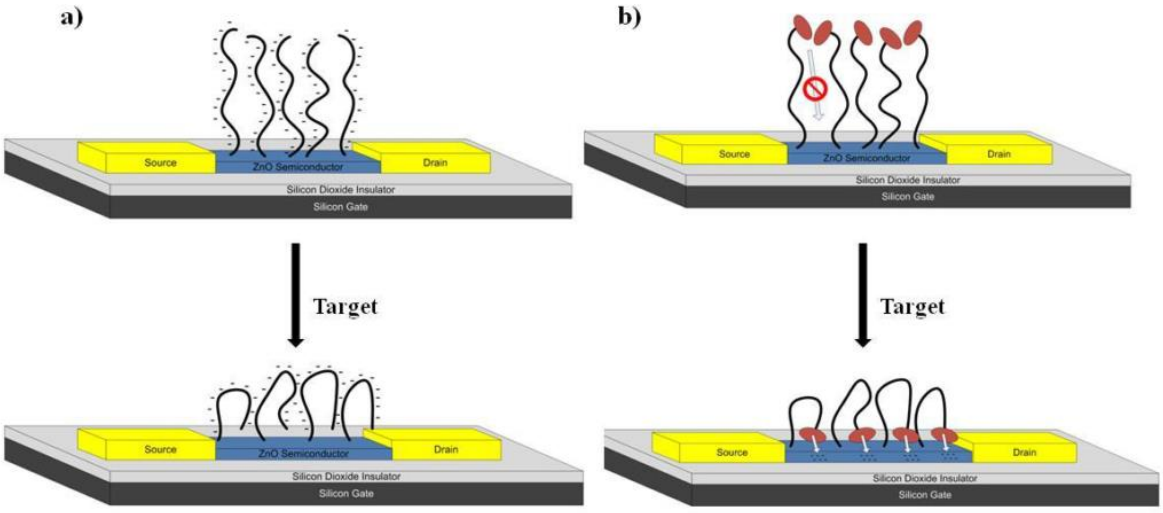

Figure 1.23. Schematic of ZnO-based riboflavin bio-FET, with (a) aptamers and (b) ferrocene-terminated aptamers. From Hagen et al.[161]

Sensors can also be electrochemical: Baek et al. electrostatically immobilised gold clusters (Au_{25}) on ZnO nanorods to sense alkaline phosphatase (ALP), a biomarker for liver and bone disease.[4] The sensing mechanism is outlined in Figure 1.24: ALP oxidises *p*-aminophenylphosphate (APP) to *p*-aminophenol (AP) in solution. The Au_{25} clusters are oxidised via an applied electrode potential, and the oxidised clusters then catalytically oxidise the AP to QI. The reduced clusters are then re-oxidised at an electrode, giving an increase in current as the signal. This approach gives a sensitivity > 100 times those previously reported, which is attributed to the dense packing of gold clusters on the nanorods giving high electrocatalytic activity. In this example, the ZnO nanorods function as a high-surface-area conductive support for the clusters.

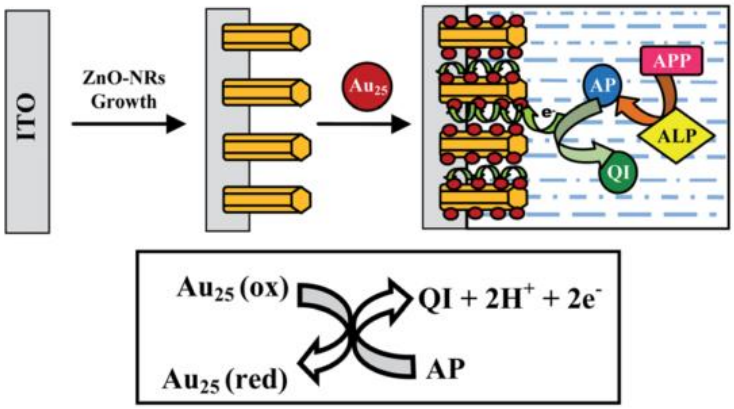

Figure 1.24. Schematic of electrochemical biosensor for ALP based on Au-cluster-functionalised ZnO nanorods on ITO. Adapted from Baek et al.

Wang et al.[146] have recently used aryldiazonium ion grafting to modify nanocrystalline ZnO films for DNA biosensing via fluorescence. After electrochemically forming a nitro-terminated aryl film, the nitro groups were reduced to NH_2 species, which were then coupled to single-strand probe DNA. After immersion in the analyte, fluorescence microscopy was used to quantitatively determine the amount of target DNA that had been fluorescently tagged. The selectivity of this setup was high: for strands that differed to the target DNA by only one base, fluorescence was observed at only 30% of that seen with fully-matched DNA.

Photovoltaics

PA-modified metal oxides have found application in photovoltaic devices, where the modification layer acts to improve the surface energy compatibility between a transparent electrode and the organic transport or donor layers of the device.[64,162] The PA buffer layer can also increase the electrode work function and thus lower the electron injection barrier between the electrode and the organic layer. ZnO is a promising photoanode material for solar cells as it has excellent bulk electron transport, especially when compared to TiO_2.[163] However, it does not make efficient dye-sensitised solar cells (DSSC) due to its sensitive surface chemistry. In DSSCs, dye is excited by photons and injects electrons into the conduction band of a wide band gap semiconductor such as ZnO. A redox couple in the electrolyte solution transfers an electron to the excited oxidised dye, returning it to its ground state. A range of dyes has been trialled based on their ability to absorb light and efficiently eject electrons. However, they are typically acidic and dissolve ZnO, while TiO_2 is more robust to a broader range of dyes.[163] Palacios-Lidón et al. saw that this chemical reactivity at ZnO is face-dependent: upon attachment of DSSC dye to single-crystal ZnO, the O-polar face morphology was unchanged, while the m-plane face was significantly etched.[12] This suggests that ZnO nanorods, which are primarily m-plane, are unsuitable for DSSCs.

Lund et al. were interested in reducing the anode leakage of DSSCs having sintered fluorine-doped tin oxide (FTO) and TiO_2 surfaces as photoanodes.[164] Without modification, the open circuit voltage (maximum voltage available from the solar cell) was 0 V for the FTO | TiO_2 electrodes, indicating poor performance. It was expected that an insulating organic layer would help. FTO and TiO_2 were modified with nitrophenyl groups from nitrobenzenediazonium salt solution, resulting in a multi-layered modification film which was macroscopically inert to both acidic and basic, aqueous and non-aqueous, solutions. The insulating effect was investigated by examining the effect of the layer on electron transfer from ferrocene to the surface. Samples treated to 450 °C, despite having lost FTIR evidence for the presence of nitro groups and having a smaller amount of organic material on the surface, still

blocked the ferrocene redox reaction. Modification layers reduced current leakage and improved the open circuit voltage.

A similar application to photovoltaics is metal oxide-based dye-sensitised photoelectrosynthesis solar cells (DSPEC). Recently, Bangle et al. grafted organic layers from Ru-aryldiazonium ions on an array of metal oxides to improve the stability of DSPECs (Figure 1.25).[147]

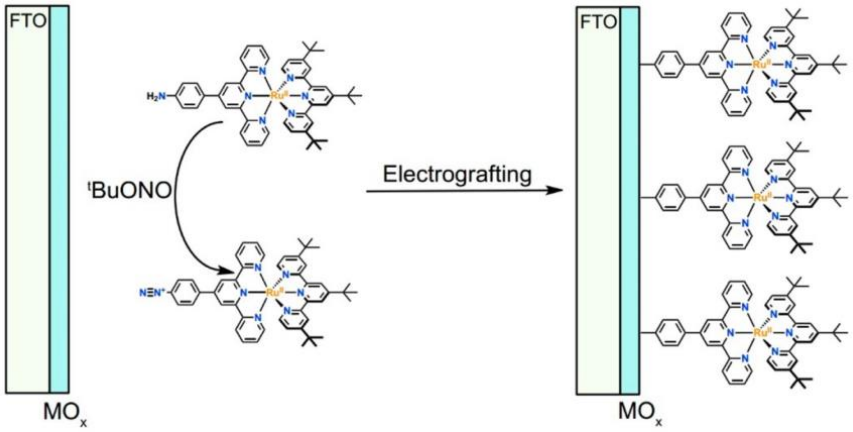

Figure 1.25. Schematic of electrochemical grafting of in situ-formed aryldiazonium ions to metal oxide nanoparticle films (MO_x) on fluorine-doped tin oxide (FTO) for use in DSPEC. Adapted from Bangle et al.

Like DSSCs, a photosensitiser is anchored to the photoanode and ejects electrons into the anode when photoexcited. Specifically, the redox process to regenerate the sensitiser involves the oxidation of water to O_2 (Eq 1.3), aided by a catalyst. Protons formed in the reaction diffuse through a proton-exchange membrane and are reduced to H_2 at a photocathode (Eq 1.4). Water oxidation is fastest in basic conditions, and thus the photosensitisers need to be stable in alkaline solution.

$$2H_2O \rightarrow O_2 + 4e^- + 4H^+ \qquad (1.3)$$

$$4H^+ + 4e^- \rightarrow 2H_2 \qquad (1.4)$$

While it does not appear that Bangle et al. tested the stability of the aryldiazonium ion-derived layers on ZnO, the same layers were stable from pH 5 to ~12 on SnO_2 and TiO_2. Similar experiments showed

that PA and carboxylic acid modifications were only stable to pH 7 and pH 4, respectively. The films grafted from diazonium ions were also stable in ambient light conditions for several months.

1.2 Aims

The aim of this work is to investigate a range of methods for attaching organic modifying layers to the surface of ZnO with the goal of removing the downwards band bending at the ZnO surface. Formation of layers that protect the ZnO surface from environmental instability is also important, and the chemical reactivity differences between the three main faces after modification will also be explored.

This thesis is organised as follows:

Chapter 2: *Experimental Methods*: describes general experimental methods, chemicals, substrates, and equipment used in this work.

Chapter 3: *Phosphonic Acid Modification of Single Crystal ZnO*: describes the surface modification of thin-film and single-crystal ZnO with a variety of phosphonic acids, their stability, and their effect on band bending.

Chapter 4: *Thiol Modification of Single Crystal ZnO*: describes the surface modification of single-crystal ZnO with thiol derivatives and characterises the resulting layers.

Chapter 5: *Aryldiazonium Ion Chemistry at Single-Crystal ZnO*: describes the use of aryldiazonium ions and electrochemistry to modify single-crystal ZnO with disordered, multi-layered aryl layers, and investigates the effect on band bending.

Chapter 6: *Aryldiazonium Ion Chemistry at MBE-Grown ZnO Thin Films*: describes the electrografting of aryldiazonium ions at thin-film ZnO surfaces and characterises the binding mode, stability, and band bending.

Chapter 7: *Conclusions*.

1.3 References

(1) Virolainen, S.; Ibana, D.; Paatero, E. Recovery of Indium from Indium Tin Oxide by Solvent Extraction. *Hydrometallurgy* **2011**, *107* (1–2), 56–61.

(2) U.S. Geological Survey. Mineral Commodity Summaries 2015: Indium http://minerals.usgs.gov/minerals/pubs/mcs/2015/mcs2015.pdf (accessed Jul 29, 2015).

(3) Shanmugam, N. R.; Muthukumar, S.; Prasad, S. Surface Modification of ZnO Nanostructured Electrodes with Thiol and Phosphonic Acid Moieties for Biosensing Applications. *Anal. Methods* **2017**, *9*, 5525–5533.

(4) Baek, G.; Pandurangan, P.; Ko, E.; Mo, Y.; Lee, D. Redox-Active Gold Nanoclusters Immobilized ZnO Nanorod Electrodes for Electrochemical Sensing Applications. *RSC Adv.* **2014**, *4*, 10766.

(5) Janotti, A.; Van de Walle, C. G. Fundamentals of Zinc Oxide as a Semiconductor. *Reports Prog. Phys.* **2009**, *72* (12), 126501.

(6) Hotchkiss, P. J.; Malicki, M.; Giordano, A. J.; Armstrong, N. R.; Marder, S. R. Characterization of Phosphonic Acid Binding to Zinc Oxide. *J. Mater. Chem.* **2011**, *21* (9), 3107–3112.

(7) Lange, I.; Reiter, S.; Kniepert, J.; Piersimoni, F.; Pätzel, M.; Hildebrandt, J.; Brenner, T.; Hecht, S.; Neher, D. Zinc Oxide Modified with Benzylphosphonic Acids as Transparent Electrodes in Regular and Inverted Organic Solar Cell Structures. *Appl. Phys. Lett.* **2015**, *106* (11), 113302.

(8) Braid, J. L.; Koldemir, U.; Sellinger, A.; Collins, R. T.; Furtak, T. E.; Olson, D. C. Conjugated Phosphonic Acid Modified Zinc Oxide Electron Transport Layers for Improved Performance in Organic Solar Cells. *ACS Appl. Mater. Interfaces* **2014**, *6* (21), 19229–19234.

(9) Kuo, C.; Chen, J.; Chao, Y.; Chen, P. Fabrication of a P3HT-ZnO Nanowires Gas Sensor Detecting Ammonia Gas. *Sensors* **2017**, *18* (1), 37.

(10) Heinhold, R.; Williams, G. T.; Cooil, S. P.; Evans, D. A.; Allen, M. W. Influence of Polarity and Hydroxyl Termination on the Band Bending at ZnO Surfaces. *Phys. Rev. B - Condens. Matter Mater. Phys.* **2013**, *88* (23), 235315.

(11) P.A.Cox. *The Surface Science of Metal Oxides*; Cambridge University Press: Cambridge; New York, 1994.

(12) Palacios-Lidón, E.; Pickup, D. F.; Johnson, P. S.; Ruther, R. E.; Tena-Zaera, R.; Hamers, R. J.; Colchero, J.; Himpsel, F. J.; Ortega, J. E.; Rogero, C. Face-Selective Etching of ZnO during Attachment of Dyes. *J. Phys. Chem. C* **2013**, *117* (36), 18414–18422.

(13) Pesika, N. S.; Hu, Z.; Stebe, K. J.; Searson, P. C. Quenching of Growth of ZnO Nanoparticles by Adsorption of Octanethiol. *J. Phys. Chem. B* **2002**, *106* (28), 6985–6990.

(14) Ozawa, K.; Munakata, S.; Edamoto, K.; Mase, K. Electron Donor Molecule on the Oxide Surface: Influence of Surface Termination of ZnO on Adsorption of Tetrathiafulvalene. *J. Phys. Chem. C* **2011**, *115* (44), 21843–21851.

(15) Allen, M. W.; Zemlyanov, D. Y.; Waterhouse, G. I. N.; Metson, J. B.; Veal, T. D.; McConville, C. F.; Durbin, S. M. Polarity Effects in the X-Ray Photoemission of ZnO and Other Wurtzite Semiconductors. *Appl. Phys. Lett.* **2011**, *98* (10), 2009–2012.

(16) Schlepütz, C. M.; Yang, Y.; Husseini, N. S.; Heinhold, R.; Kim, H. S.; Allen, M. W.; Durbin, S. M.; Clarke, R. The Presence of a (1×1) Oxygen Overlayer on ZnO(0001) Surfaces and at Schottky Interfaces. *J. Phys. Condens. Matter* **2012**, *24* (9), 1–4.

(17) Heinhold, R.; Allen, M. W. Polarity-Dependent Photoemission of In Situ Cleaved Zinc Oxide Single Crystals. *J. Mater. Res.* **2012**, *27* (17), 2214–2219.

(18) Morkoç, H.; Özgür, Ü. *Zinc Oxide: Fundamentals, Materials and Device Technology*; Wiley-VCH: Weinheim, 2009.

(19) Ma, L.; Liu, B.; Huang, P. J. J.; Zhang, X.; Liu, J. DNA Adsorption by ZnO Nanoparticles near Its Solubility Limit: Implications for DNA Fluorescence Quenching and DNAzyme Activity Assays. *Langmuir* **2016**, *32* (22), 5672–5680.

(20) Hüpkes, J.; Owen, J. I.; Pust, S. E.; Bunte , E. Chemical Etching of Zinc Oxide for Thin-Film Silicon Solar Cells. *ChemPhysChem* **2012**, *13* (1), 66–73.

(21) Akhter, S.; Lui, K.; Kung, H. H. Comparison of the Chemical Properties of the Zinc-Polar, the Oxygen-Polar, and the Nonpolar Surfaces of Zinc Oxide. *J. Phys. Chem.* **1985**, *89* (10), 1958–1964.

(22) Aggarwal, R.; Zhou, H.; Jin, C.; Narayan, J.; Narayan, R. J. Semipolar R-Plane ZnO Films on Si(100) Substrates: Thin Film Epitaxy and Optical Properties. *J. Appl. Phys.* **2010**, *107* (11), 1–6.

(23) Chen, J.; Ruther, R. E.; Tan, Y.; Bishop, L. M.; Hamers, R. J. Molecular Adsorption on ZnO$(10\bar{1}0)$ Single-Crystal Surfaces: Morphology and Charge Transfer. *Langmuir* **2012**, *28* (28), 10437–10445.

(24) Heinhold, R.; Cooil, S. P.; Evans, D. A.; Allen, M. W. Stability of the Surface Electron Accumulation Layers on the Nonpolar $(10\bar{1}0)$ and $(11\bar{2}0)$ Faces of ZnO. *J. Phys. Chem. C* **2014**, *118* (42), 24575–24582.

(25) Neiman, A. The Effect of Annealing on the Optical Properties of Zinc Oxide. M.Sc. Thesis [Online], University of Canterbury, Christchurch, New Zealand, 2014.

(26) Muth, J. F.; Kolbas, R. M.; Sharma, A. K.; Oktyabrsky, S.; Narayan, J. Excitonic Structure and Absorption Coefficient Measurements of ZnO Single Crystal Epitaxial Films Deposited by Pulsed Laser Deposition. *J. Appl. Phys.* **1999**, *85* (11), 7884–7887.

(27) Chen, Y. M.; Huang, T. H.; Yan, T.; Chang, L.; Chou, M. M. C.; Ploog, K. H.; Chiang, C. M. Epitaxial Growth of Nonpolar and Polar ZnO on γ-$LiAlO_2$(100) Substrate by Plasma-Assisted Molecular Beam Epitaxy. *J. Cryst. Growth* **2013**, *377*, 82–87.

(28) Cho, M. W.; Setiawan, A.; Ko, H. J.; Hong, S. K.; Yao, T. ZnO Epitaxial Layers Grown on C-Sapphire Substrate with MgO Buffer by Plasma-Assisted Molecular Beam Epitaxy (P-MBE). *Semicond. Sci. Technol.* **2005**, *20* (4), S13–S21.

(29) Quiñones, R.; Shoup, D.; Behnke, G.; Peck, C.; Agarwal, S.; Gupta, R.; Fagan, J.; Mueller, K.; Iuliucci, R.; Wang, Q. Study of Perfluorophosphonic Acid Surface Modifications on Zinc Oxide Nanoparticles. *Materials (Basel).* **2017**, *10* (12), 1363.

(30) Chang, J.; Waclawik, E. R. Experimental and Theoretical Investigation of Ligand Effects on the Synthesis of ZnO Nanoparticles. *J. Nanoparticle Res.* **2012**, *14* (8).

(31) Viñes, F.; Iglesias-Juez, A.; Illas, F.; Fernández-García, M. Hydroxyl Identification on ZnO by Infrared Spectroscopies: Theory and Experiments. *J. Phys. Chem. C* **2014**, *118* (3), 1492–1505.

(32) Mora-Seró, I.; Fabregat-Santiago, F.; Denier, B.; Bisquert, J.; Tena-Zaera, R.; Elias, J.; Lévy-Clément, C. Determination of Carrier Density of ZnO Nanowires by Electrochemical Techniques. *Appl. Phys. Lett.* **2006**, *89* (20).

(33) Li, Y.; Della Valle, F.; Simonnet, M.; Yamada, I.; Delaunay, J.-J. Competitive Surface Effects of

Oxygen and Water on UV Photoresponse of ZnO Nanowires. *Appl. Phys. Lett.* **2009**, *94* (2).

(34) Whittaker-Brooks, L.; McClain, W. E.; Schwartz, J.; Loo, Y. L. Donor-Acceptor Interfacial Interactions Dominate Device Performance in Hybrid P3HT-ZnO Nanowire-Array Solar Cells. *Adv. Energy Mater.* **2014**, *4* (16).

(35) Bao, J.; Shalish, I.; Su, Z.; Gurwitz, R.; Capasso, F.; Wang, X.; Ren, Z. Photoinduced Oxygen Release and Persistent Photoconductivity in ZnO Nanowires. *Nanoscale Res. Lett.* **2011**, *6*, 1–7.

(36) Cui, J. Zinc Oxide Nanowires. *Mater. Charact.* **2012**, *64* (0), 43–52.

(37) Lord, A. M.; Maffeis, T. G.; Allen, M. W.; Morgan, D.; Davies, P. R.; Jones, D. R.; Evans, J. E.; Smith, N. A.; Wilks, S. P. Surface State Modulation through Wet Chemical Treatment as a Route to Controlling the Electrical Properties of ZnO Nanowire Arrays Investigated with XPS. *Appl. Surf. Sci.* **2014**, *320*, 664–669.

(38) Zheng Wei Pan; Zu Rong Dai; Zhong Lin Wang. Nanobelts of Semiconducting Oxides. *Science* **2001**, *291* (5510), 1947–1949.

(39) Ruther, R. E.; Franking, R.; Huhn, A. M.; Gomez-Zayas, J.; Hamers, R. J. Formation of Smooth, Conformal Molecular Layers on ZnO Surfaces via Photochemical Grafting. *Langmuir* **2011**, *27* (17), 10604–10614.

(40) Smecca, E.; Motta, A.; Fragalaì, M. E.; Aleeva, Y.; Condorelli, G. G. Spectroscopic and Theoretical Study of the Grafting Modes of Phosphonic Acids on ZnO Nanorods. *J. Phys. Chem. C* **2013**, *117* (10), 5364–5372.

(41) Brahma, S.; Rao, K. J.; Shivashankar, S. Rapid Growth of Nanotubes and Nanorods of Würtzite ZnO through Microwave-Irradiation of a Metalorganic Complex of Zinc and a Surfactant in Solution. *Bull. Mater. Sci.* **2010**, *33* (2), 89–95.

(42) Tienes, B. M.; Perkins, R. J.; Shoemaker, R. K.; Dukovic, G. Layered Phosphonates in Colloidal Synthesis of Anisotropic ZnO Nanocrystals. *Chem. Mater.* **2013**, *25* (21), 4321–4329.

(43) Heo, Y. W.; Norton, D. P.; Tien, L. C.; Kwon, Y.; Kang, B. S.; Ren, F.; Pearton, S. J.; Laroche, J. R. ZnO Nanowire Growth and Devices. *Mater. Sci. Eng. R Reports* **2004**, *47* (1–2), 1–47.

(44) Singh, J.; Im, J.; Whitten, J. E.; Soares, J. W.; Meehan, a M.; Steeves, D. M. Adsorption of Mercaptosilanes on Nanocrystalline and Single Crystal Zinc Oxide Surfaces. *Nanophotonic Mater. V* **2008**, *7030*, 70300T.

(45) Baruah, S.; Dutta, J. Hydrothermal Growth of ZnO Nanostructures. *Sci. Technol. Adv. Mater.* **2009**, *10* (1), 013001.

(46) Nicholas, N. J.; Franks, G. V.; Ducker, W. A. Selective Adsorption to Particular Crystal Faces of ZnO. *Langmuir* **2012**, *28* (18), 7189–7196.

(47) Atkins, P.; De Paula, J. *Atkins' Physical Chemistry*, 10th ed.; Oxford University Press: Oxford; New York, 2006.

(48) Hewlett, R. M.; McLachlan, M. A. Surface Structure Modification of ZnO and the Impact on Electronic Properties. *Adv. Mater.* **2016**, *28* (20), 3893–3921.

(49) Van De Walle, C. G. Hydrogen as a Cause of Doping in Zinc Oxide. *Phys. Rev. Lett.* **2000**, *85* (5), 1012–1015.

(50) Koldemir, U.; Braid, J. L.; Morgenstern, A.; Eberhart, M.; Collins, R. T.; Olson, D. C.; Sellinger, A.

Molecular Design for Tuning Work Functions of Transparent Conducting Electrodes. *J. Phys. Chem. Lett.* **2015**, *6* (12), 2269–2276.

(51) Liang, J. K.; Su, H. L.; Chuang, P. Y.; Kuo, C. L.; Huang, S. Y.; Chan, T. S.; Wu, Y. C.; Huang, J. C. A. Origin of P-Type Conductivity of Sb-Doped ZnO Nanorods and the Local Structure around Sb Ions. *Appl. Phys. Lett.* **2015**, *106* (21).

(52) Sadananda Kumar, N.; Bangera, K. V.; Shivakumar, G. K. Properties of Antimony Doped ZnO Thin Films Deposited by Spray Pyrolysis Technique. *Semiconductors* **2015**, *49* (7), 899–904.

(53) Chouikh, F.; Beggah, Y.; Aida, M. S. Optical and Electrical Properties of Bi Doped ZnO Thin Films Deposited by Ultrasonic Spray Pyrolysis. *J. Mater. Sci. Mater. Electron.* **2011**, *22* (5), 499–505.

(54) Kumar, S. S.; Rubio, E. J.; Noor-A-Alam, M.; Martinez, G.; Manandhar, S.; Shutthanandan, V.; Thevuthasan, S.; Ramana, C. V. Structure, Morphology, and Optical Properties of Amorphous and Nanocrystalline Gallium Oxide Thin Films. *J. Phys. Chem. C* **2013**, *117* (8), 4194–4200.

(55) Kahn, A. Fermi Level, Work Function and Vacuum Level. *Mater. Horiz.* **2016**, *3* (1), 7–10.

(56) Schlesinger, R.; Xu, Y.; Hofmann, O. T.; Winkler, S.; Frisch, J.; Niederhausen, J.; Vollmer, A.; Blumstengel, S.; Henneberger, F.; Rinke, P.; Scheffler, M.; Koch, N. Controlling the Work Function of ZnO and the Energy-Level Alignment at the Interface to Organic Semiconductors with a Molecular Electron Acceptor. *Phys. Rev. B - Condens. Matter Mater. Phys.* **2013**, *87* (15), 1–5.

(57) Moormann, H.; Kohl, D.; Heiland, G. Work Function and Band Bending on Clean Cleaved Zinc Oxide Surfaces. *Surf. Sci.* **1979**, *80* (C), 261–264.

(58) Timpel, M.; Nardi, M. V.; Krause, S.; Ligorio, G.; Christodoulou, C.; Pasquali, L.; Giglia, A.; Frisch, J.; Wegner, B.; Moras, P.; Koch, N. Surface Modification of ZnO(0001)-Zn with Phosphonate-Based Self-Assembled Monolayers: Binding Modes, Orientation, and Work Function. *Chem. Mater.* **2014**, *26* (17), 5042–5050.

(59) Srikant, V.; Clarke, D. R. On the Optical Band Gap of Zinc Oxide. *J. Appl. Phys.* **1998**, *83* (10), 5447–5451.

(60) Keyes, B. M.; Gedvilas, L. M.; Li, X.; Coutts, T. J. Infrared Spectroscopy of Polycrystalline ZnO and ZnO:N Thin Films. *J. Cryst. Growth* **2005**, *281* (2–4), 297–302.

(61) Rhodes, C. L.; Lappi, S.; Fischer, D.; Sambasivan, S.; Genzer, J.; Franzen, S. Characterization of Monolayer Formation on Aluminum-Doped Zinc Oxide Thin Films. *Langmuir* **2008**, *24* (2), 433–440.

(62) Zhang, Z.; Yates, J. T. Band Bending in Semiconductors: Chemical and Physical Consequences at Surfaces and Interfaces. *Chem. Rev.* **2012**, *112* (10), 5520–5551.

(63) Sharma, A.; Kippelen, B.; Hotchkiss, P. J.; Marder, S. R. Stabilization of the Work Function of Indium Tin Oxide Using Organic Surface Modifiers in Organic Light-Emitting Diodes. *Appl. Phys. Lett.* **2008**, *93* (16).

(64) Zheng, H.; Zhang, F.; Zhou, N.; Sun, M.; Li, X.; Xiao, Y.; Wang, S. Self-Assembled Monolayer-Modified ITO for Efficient Organic Light-Emitting Diodes: The Impact of Different Self-Assemble Monolayers on Interfacial and Electroluminescent Properties. *Org. Electron.* **2018**.

(65) Bott, A. W. Electrochemistry of Semiconductors. *Curr. Sep.* **1998**, *17* (3), 87–91.

(66) King, P. D. C.; Veal, T. D.; Payne, D. J.; Bourlange, A.; Egdell, R. G.; McConville, C. F. Surface Electron Accumulation and the Charge Neutrality Level in In_2O_3. *Phys. Rev. Lett.* **2008**, *101* (11),

116808.

(67) Vasheghani Farahani, S. K.; Veal, T. D.; Mudd, J. J.; Scanlon, D. O.; Watson, G. W.; Bierwagen, O.; White, M. E.; Speck, J. S.; McConville, C. F. Valence-Band Density of States and Surface Electron Accumulation in Epitaxial SnO_2 Films. *Phys. Rev. B - Condens. Matter Mater. Phys.* **2014**, *90* (15), 1–9.

(68) Piper, L. F. J.; Colakerol, L.; King, P. D. C.; Schleife, A.; Zúñiga-Pérez, J.; Glans, P. A.; Learmonth, T.; Federov, A.; Veal, T. D.; Fuchs, F.; Muñoz-Sanjosé, V.; Bechstedt, F.; McConville, C. F.; Smith, K. E. Observation of Quantized Subband States and Evidence for Surface Electron Accumulation in CdO from Angle-Resolved Photoemission Spectroscopy. *Phys. Rev. B* **2008**, *78*, 165127.

(69) Colakerol, L.; Veal, T. D.; Jeong, H. K.; Plucinski, L.; Demasi, A.; Learmonth, T.; Glans, P. A.; Wang, S.; Zhang, Y.; Piper, L. F. J.; Jefferson, P. H.; Fedorov, A.; Chen, T. C.; Moustakas, T. D.; McConville, C. F.; Smith, K. E. Quantized Electron Accumulation States in Indium Nitride Studied by Angle-Resolved Photoemission Spectroscopy. *Phys. Rev. Lett.* **2006**, *97*, 237601.

(70) King, P. D. C.; Veal, T. D.; McConville, C. F. Nonparabolic Coupled Poisson-Schroedinger Solutions for Quantized Electron Accumulation Layers: Band Bending, Charge Profile, and Subbands at InN Surfaces. *Phys. Rev. B* **2008**, *77*, 125305.

(71) Veal, T. D.; King, P. D. C.; Hatfield, S. A.; Bailey, L. R.; McConville, C. F.; Martel, B.; Moreno, J. C.; Frayssinet, E.; Semond, F.; Zúñiga-Pérez, J. Valence Band Offset of the ZnO/AlN Heterojunction Determined by x-Ray Photoemission Spectroscopy. *Appl. Phys. Lett.* **2008**, *93* (20), 202108.

(72) Rombach, J.; Papadogianni, A.; Mischo, M.; Cimalla, V.; Kirste, L.; Ambacher, O.; Berthold, T.; Krischok, S.; Himmerlich, M.; Selve, S.; Bierwagen, O. The Role of Surface Electron Accumulation and Bulk Doping for Gas-Sensing Explored with Single-Crystalline In2O3 Thin Films. *Sensors Actuators, B Chem.* **2016**, *236*, 909–916.

(73) King, P. D. C.; Veal, T. D. Conductivity in Transparent Oxide Semiconductors. *J. Phys. Condens. Matter* **2011**, *23* (33).

(74) Petrovykh, D.; Yang, M.; Whitman, L. Chemical and Electronic Properties of Sulfur-Passivated InAs Surfaces. *Surf. Sci.* **2002**, *523*, 231–240.

(75) Batzill, M.; Diebold, U. The Surface and Materials Science of Tin Oxide. *Prog. Surf. Sci.* **2005**, *79*, 47–154.

(76) Wang, C.; Yin, L.; Zhang, L.; Xiang, D.; Gao, R. Metal Oxide Gas Sensors: Sensitivity and Influencing Factors. *Sensors* **2010**, *10*, 2088–2106.

(77) Wood, C.; Li, H.; Winget, P.; Brédas, J. L. Binding Modes of Fluorinated Benzylphosphonic Acids on the Polar ZnO Surface and Impact on Work Function. *J. Phys. Chem. C* **2012**, *116* (36), 19125–19133.

(78) Hunger, R.; Jaegermann, W.; Merson, A.; Shapira, Y.; Pettenkofer, C.; Rappich, J. Electronic Structure of Methoxy-, Bromo-, and Nitrobenzene Grafted onto Si(111). *J. Phys. Chem. B* **2006**, *110* (31), 15432–15441.

(79) Polydorou, E.; Zeniou, A.; Tsikritzis, D.; Soultati, A.; Sakellis, I.; Gardelis, S.; Papadopoulos, T. A.; Briscoe, J.; Palilis, L. C.; Kennou, S.; Gogolides, E.; Argitis, P.; Davazoglou, D.; Vasilopoulou, M. Surface Passivation Effect by Fluorine Plasma Treatment on ZnO for Efficiency and Lifetime Improvement of Inverted Polymer Solar Cells. *J. Mater. Chem. A* **2016**, *4* (30), 11844–11858.

(80) Bulusu, A.; Paniagua, S. A.; Macleod, B. A.; Sigdel, A. K.; Berry, J. J.; Olson, D. C.; Marder, S. R.; Graham, S. Efficient Modification of Metal Oxide Surfaces with Phosphonic Acids by Spray

Coating. *Langmuir* **2013**, *29* (12), 3935–3942.

(81) Li, H.; Paramonov, P.; Bredas, J.-L. Theoretical Study of the Surface Modification of Indium Tin Oxide with Trifluorophenyl Phosphonic Acid Molecules: Impact of Coverage Density and Binding Geometry. *J. Mater. Chem.* **2010**, *20* (13), 2630.

(82) Parthasarathy, M.; Ramgir, N. S.; Sathe, B. R.; Mulla, I. S.; Pillai, V. K. Surface-State-Mediated Electron Transfer at Nanostructured ZnO Multipod / Electrolyte Interfaces. *J. Phys. Chem. C* **2007**, *111*, 13092–13102.

(83) Chevtchenko, S.; Ni, X.; Fan, Q.; Baski, A. A.; Morkoç, H. Surface Band Bending of A-Plane GaN Studied by Scanning Kelvin Probe Microscopy. *Appl. Phys. Lett.* **2006**, *88* (12), 122104.

(84) Polak, L.; Wijngaarden, R. J. Two Competing Interpretations of Kelvin Probe Force Microscopy on Semiconductors Put to Test. *Phys. Rev. B* **2016**, *93* (19), 1–10.

(85) Melitz, W.; Shen, J.; Kummel, A. C.; Lee, S. Kelvin Probe Force Microscopy and Its Application. *Surf. Sci. Rep.* **2011**, *66* (1), 1–27.

(86) Moulder, J. F.; Chastain, J. *Handbook of X-Ray Photoelectron Spectroscopy: A Reference Book of Standard Spectra for Identification and Interpretation of XPS Data*; Chastain, J., Ed.; Physical Electronics Division, Perkin-Elmer Corporation, 1995.

(87) Mattox, D. M. *Substrate ("Real") Surfaces and Surface Modification*; 2010.

(88) McNeill, A. R.; Hyndman, A. R.; Reeves, R. J.; Downard, A. J.; Allen, M. W. Tuning the Band Bending and Controlling the Surface Reactivity at Polar and Nonpolar Surfaces of ZnO through Phosphonic Acid Binding. *ACS Appl. Mater. Interfaces* **2016**, *8* (45), 31392–31402.

(89) Ranke, W. Separation of the Partial S- and p-Densities of Valence States of ZnO from UPS-Measurements. *Solid State Commun.* **1976**, *19* (7), 685–688.

(90) Allen, C. G.; Baker, D. J.; Albin, J. M.; Oertli, H. E.; Gillaspie, D. T.; Olson, D. C.; Furtak, T. E.; Collins, R. T. Surface Modification of ZnO Using Triethoxysilane-Based Molecules. *Langmuir* **2008**, *24* (23), 13393–13398.

(91) Syuleiman, S. A.; Yakushova, N. D.; Pronin, I. A.; Kaneva, N. V.; Bojinova, A. S.; Papazova, K. I.; Gancheva, M. N.; Dimitrov, D. T.; Averin, I. A.; Terukov, E. I.; Moshnikov, V. A. Study of the Photodegradation of Brilliant Green on Mechanically Activated Powders of Zinc Oxide. *Tech. Phys.* **2017**, *62* (11), 1709–1713.

(92) Ozawa, K.; Suzuki, M.; Tochikubo, R.; Kato, H.; Sugizaki, Y.; Edamoto, K.; Mase, K. Electron-Donor Dye Molecule on ZnO$(10\bar{1}0)$, (0001), and $(000\bar{1})$ Studied by Photoelectron Spectroscopy and X-Ray Absorption Spectroscopy. *J. Phys. Chem. C* **2016**, *120* (16), 8653–8662.

(93) Gao, F.; Aminane, S.; Bai, S.; Teplyakov, A. V. Chemical Protection of Material Morphology: Robust and Gentle Gas-Phase Surface Functionalization of ZnO with Propiolic Acid. *Chem. Mater.* **2017**, *29* (9), 4063–4071.

(94) Pujari, S. P.; Scheres, L.; Marcelis, A. T. M.; Zuilhof, H. Covalent Surface Modification of Oxide Surfaces. *Angew. Chemie - Int. Ed.* **2014**, *53* (25), 6322–6356.

(95) Ulman, A. Formation and Structure of Self-Assembled Monolayers. *Chem. Rev.* **1996**, *96* (4), 1533–1554.

(96) Kedem, N.; Blumstengel, S.; Henneberger, F.; Cohen, H.; Hodes, G.; Cahen, D. Morphology-, Synthesis- and Doping-Independent Tuning of ZnO Work Function Using Phenylphosphonates. *Phys. Chem. Chem. Phys.* **2014**, *16* (18), 8310.

(97) Zhang, B.; Kong, T.; Xu, W.; Su, R.; Gao, Y.; Cheng, G. Surface Functionalization of Zinc Oxide by Carboxyalkylphosphonic Acid Self-Assembled Monolayers. *Langmuir* **2010**, *26* (6), 4514–4522.

(98) Lange, I.; Reiter, S.; Pätzel, M.; Zykov, A.; Nefedov, A.; Hildebrandt, J.; Hecht, S.; Kowarik, S.; Wöll, C.; Heimel, G.; Neher, D. Tuning the Work Function of Polar Zinc Oxide Surfaces Using Modified Phosphonic Acid Self-Assembled Monolayers. *Adv. Funct. Mater.* **2014**, *24* (44), 7014–7024.

(99) Perkins, C. L. Molecular Anchors for Self-Assembled Monolayers on ZnO: A Direct Comparison of the Thiol and Phosphonic Acid Moieties. *J. Phys. Chem. C* **2009**, *113* (42), 18276–18286.

(100) Ostapenko, A.; Klöffel, T.; Meyer, B.; Witte, G. Formation and Stability of Phenylphosphonic Acid Monolayers on ZnO: Comparison of in Situ and Ex Situ SAM Preparation. *Langmuir* **2016**, *32* (20), 5029–5037.

(101) Gao, W.; Dickinson, L.; Grozinger, C.; Morin, F. G.; Reven, L. Self-Assembled Monolayers of Alkylphosphonic Acids on Metal Oxides. *Langmuir* **1996**, *12* (26), 6429–6435.

(102) Ford, W. E.; Abraham, F.; Scholz, F.; Nelles, G.; Sandford, G.; Von Wrochem, F. Spectroscopic Characterization of Fluorinated Benzylphosphonic Acid Monolayers on AlO_x/Al Surfaces. *J. Phys. Chem. C* **2017**, *121* (3), 1690–1703.

(103) Paukku, Y.; Michalkova, A.; Leszczynski, J. Quantum-Chemical Comprehensive Study of the Organophosphorus Compounds Adsorption on Zinc Oxide Surfaces. *J. Phys. Chem. C* **2009**, *113* (4), 1474–1485.

(104) Wang, M.; Hill, I. G. Fluorinated Alkyl Phosphonic Acid SAMs Replace PEDOT:PSS in Polymer Semiconductor Devices. *Org. Electron. physics, Mater. Appl.* **2012**, *13* (3), 498–505.

(105) Paniagua, S. A.; Hotchkiss, P. J.; Jones, S. C.; Marder, S. R.; Mudalige, A.; Marrikar, F. S.; Pemberton, J. E.; Armstrong, N. R. Phosphonic Acid Modification of Indium-Tin Oxide Electrodes: Combined XPS/UPS/Contact Angle Studies. *J. Phys. Chem. C* **2008**, *112* (21), 7809–7817.

(106) Paniagua, S. A.; Li, E. L.; Marder, S. R. Adsorption Studies of a Phosphonic Acid on ITO: Film Coverage, Purity, and Induced Electronic Structure Changes. *Phys. Chem. Chem. Phys.* **2014**, *16* (7), 2874.

(107) Taylor, C. E.; Schwartz, D. K. Octadecanoic Acid Self-Assembled Monolayer Growth at Sapphire Surfaces. *Langmuir* **2003**, *19* (7), 2665–2672.

(108) Nuzzo, R. G.; Allara, D. L. Adsorption of Bifunctional Organic Disulphides on Gold Surfaces. *J.Am.Chem.Soc.* **1983**, *105* (13), 4481–4483.

(109) Castner, D. G.; Hinds, K.; Grainger, D. W. X-Ray Photoelectron Spectroscopy Sulfur 2p Study of Organic Thiol and Disulfide Binding Interactions with Gold Surfaces. *Langmuir* **1996**, *12* (21), 5083–5086.

(110) Garrell, R. L.; Chadwick, J. E.; Myles, D. C.; Severance, D. L.; McDonald, N. A. Adsorption of Sulfur Containing Molecules on Gold: The Effect of Oxidation on Monolayer Formation and Stability Characterized by Experiments and Theory. *J. Am. Chem. Soc.* **1995**, *117* (46), 11563–11571.

(111) Schoenfisch, M. H.; Pemberton, J. E. Air Stability of Alkanethiol Self-Assembled Monolayers on Silver and Gold Surfaces. *J. Am. Chem. Soc.* **1998**, *120* (18), 4502–5413.

(112) Dicke, C.; Morstein, M.; Hähner, G. Surface Inorganic Chemistry: The Reaction of Hydroxyl-Terminated Thiols on Gold with a Zirconium Coordination Compound. *Langmuir* **2002**, *18* (2),

336–344.

(113) Mani, G.; Johnson, D. M.; Marton, D.; Dougherty, V. L. Stability of Self-Assembled Monolayers on Titanium and Gold. *Langmuir* **2008**, *24* (c), 6774–6784.

(114) Vericat, C.; Vela, M. E.; Benitez, G.; Carro, P.; Salvarezza, R. C. Self-Assembled Monolayers of Thiols and Dithiols on Gold: New Challenges for a Well-Known System. *Chem. Soc. Rev.* **2010**, *39* (5), 1805.

(115) Smith, D. L.; Wysocki, V. H.; Colorado, R.; Shmakova, O. E.; Graupe, M.; Lee, T. R. Low-Energy Ion-Surface Collisions Characterize Alkyl- and Fluoroalkyl-Terminated Self-Assembled Monolayers on Gold. *Langmuir* **2002**, *18* (10), 3895–3902.

(116) Hoffman, R. V. *Organic Chemistry*; Saunders College Publishing: Orlando, Florida, 2004.

(117) Sadik, P. W.; Pearton, S. J.; Norton, D. P.; Lambers, E.; Ren, F. Functionalizing Zn- and O-Terminated ZnO with Thiols. *J. Appl. Phys.* **2007**, *101* (10), 1–6.

(118) Hanson, E. L.; Guo, J.; Koch, N.; Schwartz, J.; Bernasek, S. L. Advanced Surface Modification of Indium Tin Oxide for Improved Charge Injection in Organic Devices. *J. Am. Chem. Soc.* **2005**, *127* (28), 10058–10062.

(119) Li, M.; Zhai, J.; Liu, H.; Song, Y.; Jiang, L.; Zhu, D. Electrochemical Deposition of Conductive Superhydrophobic Zinc Oxide Thin Films. *J.Phys. Chem. B* **2003**, *107* (37), 9954–9957.

(120) Walba, D. M.; Liberko, C. A.; Korblova, E.; Farrow, M.; Furtak, T. E.; Chow, B. C.; Schwartz, D. K.; Freeman, A. S.; Douglas, K.; Williams, S. D.; Klittnick, A. F.; Clark, N. A. Self-Assembled Monolayers for Liquid Crystal Alignment: Simple Preparation on Glass Using Alkyltrialkoxysilanes. *Liq. Cryst.* **2004**, *31* (4), 481–489.

(121) Wei, J.; Ji, G.; Zhang, C.; Yan, L.; Luo, Q. Silane Capped ZnO Nanoparticles for Use as the Electron Transport Layer in Inverted Organic Solar Cells. **2018**.

(122) Verbakel, F.; Meskers, S. C. J.; Janssen, R. A. J. Surface Modification of Zinc Oxide Nanoparticles Influences the Electronic Memory Effects in ZnO-Polystyrene Diodes. *J. Phys. Chem. C* **2007**, *111* (28), 10150–10153.

(123) Chiang, C. T.; Roberts, J. T. Surface Functionalization of Zinc Oxide Nanoparticles: An Investigation in the Aerosol State. *Chem. Mater.* **2011**, *23* (23), 5237–5242.

(124) Liu, J. F.; Liu, E. Z.; Wang, H.; Su, N. H.; Qi, J.; Jiang, J. Z. Surface Magnetism in Amine-Capped ZnO Nanoparticles. *Nanotechnology* **2009**, *20* (16), 1–6.

(125) Coppel, Y.; Spataro, G.; Pagès, C.; Chaudret, B.; Maisonnat, A.; Kahn, M. L. Full Characterization of Colloidal Solutions of Long-Alkyl-Chain-Amine-Stabilized ZnO Nanoparticles by NMR Spectroscopy: Surface State, Equilibria, and Affinity. *Chem. - A Eur. J.* **2012**, *18* (17), 5384–5393.

(126) Li, Y.; Zuilhof, H. Photochemical Grafting and Patterning of Organic Monolayers on Indium Tin Oxide Substrates. *Langmuir* **2012**, *28* (12), 5350–5359.

(127) Franking, R. A.; Landis, E. C.; Hamers, R. J. Highly Stable Molecular Layers on Nanocrystalline Anatase TiO_2 through Photochemical Grafting. *Langmuir* **2009**, *25* (18), 10676–10684.

(128) Allongue, P.; Delamar, M.; Desbat, B.; Fagebaume, O.; Hitmi, R.; Pinson, J.; Savéant, J. M. Covalent Modification of Carbon Surfaces by Aryl Radicals Generated from the Electrochemical Reduction of Diazonium Salts. *J. Am. Chem. Soc.* **1997**, *114* (1), 201–207.

(129) Chehimi, M. M. *Aryl Diazonium Salts: New Coupling Agents and Surface Science*; Chehimi, M.

M., Ed.; Wiley-VCH: Weinheim, 2012.

(130) Mirkhalaf, F.; Mason, T. J.; Morgan, D. J.; Saez, V. Frequency Effects on the Surface Coverage of Nitrophenyl Films Ultrasonically Grafted onto Indium Tin Oxide. *Langmuir* **2011**, *27* (5), 1853–1858.

(131) Podvorica, F. I.; Combellas, C.; Delamar, M.; Kanoufi, F. A. A.; Pinson, J. Spontaneous Grafting of Iron Surfaces by Reduction of Aryldiazonium Salts in Acidic Water: Applications to the Inhibition of Iron Corrosion. *Passiv. Met. Semicond. Prop. Thin Oxide Layers* **2006**, No. 9, 697–702.

(132) Pinson, J.; Podvorica, F. Attachment of Organic Layers to Conductive or Semiconductive Surfaces by Reduction of Diazonium Salts. *Chem. Soc. Rev.* **2005**, *34* (5), 429.

(133) Adenier, A.; Barré, N.; Cabet-Deliry, E.; Chaussé, A.; Griveau, S.; Mercier, F.; Pinson, J.; Vautrin-Ul, C. Study of the Spontaneous Formation of Organic Layers on Carbon and Metal Surfaces from Diazonium Salts. *Surf. Sci.* **2006**, *600* (21), 4801–4812.

(134) Girard, A.; Geneste, F.; Coulon, N.; Cardinaud, C.; Mohammed-Brahim, T. SiGe Derivatization by Spontaneous Reduction of Aryl Diazonium Salts. *Appl. Surf. Sci.* **2013**, *282*, 146–155.

(135) Mesnage, A.; Lefèvre, X.; Jégou, P.; Deniau, G.; Palacin, S. Spontaneous Grafting of Diazonium Salts: Chemical Mechanism on Metallic Surfaces. *Langmuir* **2012**, *28* (32), 11767–11778.

(136) Mohamed, A. A.; Salmi, Z.; Dahoumane, S. A.; Mekki, A.; Carbonnier, B.; Chehimi, M. M. Functionalization of Nanomaterials with Aryldiazonium Salts. *Adv. Colloid Interface Sci.* **2015**, *225*, 16–36.

(137) Cao, C.; Zhang, Y.; Jiang, C.; Qi, M.; Liu, G. Advances on Aryldiazonium Salt Chemistry Based Interfacial Fabrication for Sensing Applications. *ACS Appl. Mater. Interfaces* **2017**, *9* (6), 5031–5049.

(138) Lee, L.; Brooksby, P. A.; Hapiot, P.; Downard, A. J. Electrografting of 4-Nitrobenzenediazonium Ion at Carbon Electrodes: Catalyzed and Uncatalyzed Reduction Processes. *Langmuir* **2016**, *32* (2), 468–476.

(139) Laforgue, A.; Addou, T.; Bélanger, D. Characterization of the Deposition of Organic Molecules at the Surface of Gold by the Electrochemical Reduction of Aryldiazonium Cations. *Langmuir* **2005**, *21* (15), 6855–6865.

(140) Bahr, J. L.; Yang, J.; Kosynkin, D. V.; Bronikowski, M. J.; Smalley, R. E.; Tour, J. M. Functionalization of Carbon Nanotubes by Electrochemical Reduction of Aryl Diazonium Salts: A Bucky Paper Electrode. *J. Am. Chem. Soc.* **2001**, *123* (27), 6536–6542.

(141) Menanteau, T.; Dias, M.; Levillain, E.; Downard, A. J.; Breton, T. Electrografting via Diazonium Chemistry: The Key Role of the Aryl Substituent in the Layer Growth Mechanism. *J. Phys. Chem. C* **2016**, *120* (8), 4423–4429.

(142) Doppelt, P.; Hallais, G.; Pinson, J.; Podvorica, F.; Verneyre, S. Surface Modification of Conducting Substrates. Existence of Azo Bonds in the Structure of Organic Layers Obtained from Diazonium Salts. *Chem. Mater.* **2007**, *19* (18), 4570–4575.

(143) Chen, X.; Chockalingam, M.; Liu, G.; Luais, E.; Gui, A. L.; Gooding, J. J. A Molecule with Dual Functionality 4-Aminophenylmethylphosphonic Acid: A Comparison between Layers Formed on Indium Tin Oxide by In Situ Generation of an Aryl Diazonium Salt or by Self-Assembly of the Phosphonic Acid. *Electroanalysis* **2011**, *23* (11), 2633–2642.

(144) English, C. R.; Hamers, R. J. Molecular Electronic Effects on the Thermal Grafting of Aryl Iodides

to TiO_2 Surfaces. *J. Phys. Chem. C* **2015**, *119* (50), 27972–27981.

(145) Koefoed, L.; Pedersen, S. U.; Daasbjerg, K. Covalent Modification of Glassy Carbon Surfaces by Electrochemical Grafting of Aryl Iodides. *Langmuir* **2017**, *33* (13), 3217–3222.

(146) Wang, C.; Huang, N.; Zhuang, H.; Jiang, X. Enhanced Performance of Nanocrystalline ZnO DNA Biosensor via Introducing Electrochemical Covalent Biolinkers. *ACS Appl. Mater. Interfaces* **2015**, *7* (14), 7605–7612.

(147) Bangle, R.; Sampaio, R. N.; Troian-Gautier, L.; Meyer, G. J. Surface Grafting of Ru(II) Diazonium-Based Sensitizers on Metal Oxides Enhances Alkaline Stability for Solar Energy Conversion. *ACS Appl. Mater. Interfaces* **2017**, *10*, 3121–3132.

(148) Chin, W. S.; Mok, C. Y.; Huang, H. H.; Masuda, S.; Kato, S.; Harada, Y. Penning Ionization Electron Spectra of Nitro Compounds. *J. Electron Spectros. Relat. Phenomena* **1992**, *60* (2), 101–116.

(149) Fujisawa, S.; Ohno, K.; Masuda, S.; Harada, Y. Penning Ionization Electron Spectroscopy of Monohalogenobenzenes: C6H5F, C6H5Cl, C6H5Br, and C6H5I. *J. Am. Chem. Soc.* **1986**, *108* (21), 6505–6511.

(150) Gao, F.; Teplyakov, A. V. Challenges and Opportunities in Chemical Functionalization of Semiconductor Surfaces. *Appl. Surf. Sci.* **2017**, *399*, 375–386.

(151) Ju, S.; Lee, K.; Janes, D. B.; Yoon, M. H.; Facchetti, A.; Marks, T. J. Low Operating Voltage Single ZnO Nanowire Field-Effect Transistors Enabled by Self-Assembled Organic Gate Nanodielectrics. *Nano Lett.* **2005**, *5* (11), 2281–2286.

(152) Kälblein, D.; Weitz, R. T.; Böttcher, H. J.; Ante, F.; Zschieschang, U.; Kern, K.; Klauk, H. Top-Gate ZnO Nanowire Transistors and Integrated Circuits with Ultrathin Self-Assembled Monolayer Gate Dielectric. *Nano Lett.* **2011**, *11* (12), 5309–5315.

(153) Qian, H.; Wang, Y.; Fang, Y.; Gu, L.; Lu, R.; Sha, J. High-Performance ZnO Nanowire Field-Effect Transistor with Forming Gas Treated SiO_2 Gate Dielectrics. *J. Appl. Phys.* **2015**, *117* (16), 164308.

(154) Zong, X.; Zhu, R. Zinc Oxide Nanorod Field Effect Transistor for Long-Time Cellular Force Measurement. *Sci. Rep.* **2017**, *7* (March), 1–8.

(155) Choo, T. F.; Saidin, N. U.; Kok, K. Y. Hydrogen Sensing Enhancement of Zinc Oxide Nanorods via Voltage Biasing. *R. Soc. Open Sci.* **2018**, *5*, 172372.

(156) Wang, H. T.; Kang, B. S.; Ren, F.; Tien, L. C.; Sadik, P. W.; Norton, D. P.; Pearton, S. J.; Lin, J. Hydrogen-Selective Sensing at Room Temperature with ZnO Nanorods. *Appl. Phys. Lett.* **2005**, *86* (24), 1–3.

(157) Wan, Q.; Li, Q. H.; Chen, Y. J.; Wang, T. H.; He, X. L.; Li, J. P.; Lin, C. L. Fabrication and Ethanol Sensing Characteristics of ZnO Nanowire Gas Sensors. *Appl. Phys. Lett.* **2004**, *84* (18), 3654–3656.

(158) Waclawik, E. R.; Chang, J.; Ponzoni, A.; Concina, I.; Zappa, D.; Comini, E.; Motta, N.; Faglia, G.; Sberveglieri, G. Functionalised Zinc Oxide Nanowire Gas Sensors: Enhanced NO 2 Gas Sensor Response by Chemical Modification of Nanowire Surfaces. *Beilstein J. Nanotechnol.* **2012**, *3* (1), 368–377.

(159) Wan, Q.; Li, Q. H.; Chen, Y. J.; Wang, T. H.; He, X. L.; Gao, X. G.; Li, J. P. Positive Temperature Coefficient Resistance and Humidity Sensing Properties of Cd-Doped ZnO Nanowires. *Appl. Phys. Lett.* **2004**, *84* (16), 3085–3087.

(160) Ahmad, R.; Ahn, M. S.; Hahn, Y. B. ZnO Nanorods Array Based Field-Effect Transistor Biosensor for Phosphate Detection. *J. Colloid Interface Sci.* **2017**, *498*, 292–297.

(161) Hagen, J. A.; Kim, S. N.; Bayraktaroglu, B.; Leedy, K.; Chávez, J. L.; Kelley-Loughnane, N.; Naik, R. R.; Stone, M. O. Biofunctionalized Zinc Oxide Field Effect Transistors for Selective Sensing of Riboflavin with Current Modulation. *Sensors* **2011**, *11* (7), 6645–6655.

(162) Hotchkiss, P. J.; Jones, S. C.; Paniagua, S. A.; Sharma, A.; Kippelen, B.; Armstrong, N. R.; Marder, S. R. The Modification of Indium Tin Oxide with Tuning of Surface Properties, and Potential for Use in Organic Electronic Applications. *Acc. Chem. Res.* **2011**, *45* (3), 337–346.

(163) Anta, J. A.; Guillén, E.; Tena-Zaera, R. ZnO-Based Dye-Sensitized Solar Cells. *J. Phys. Chem. C* **2012**, *116* (21), 11413–11425.

(164) Lund, T.; Nguyen, P. T.; Ruhland, T. Electrochemical Grafting of TiO_2-Based Photo-Anodes and Its Effect in Dye-Sensitized Solar Cells. *J. Electroanal. Chem.* **2015**, *758*, 85–92.

2 General Experimental and Analytical Methods

2.1 General Synthesis and Reagents

2.1.1 ZnO Substrates

Hydrothermally-grown 10 x 10 mm^2 single-crystal ZnO (Zn-polar, O-polar, and m-plane faces) were obtained from CrysTec GmbH, Germany and Tokyo Denpa, Japan. For all experiments, except those carried out in Chapter 5, samples were cut into smaller pieces using a diamond scribe. Directly before modification, each sample was sonicated in each of acetone, methanol, and isopropanol (IPA) for 4 min and dried with N_2. 'As-received samples' were cleaned by the same protocol and unless otherwise noted did not undergo any further treatment. For work performed in Chapter 5, as-received samples were cleaned with oxygen plasma prior to analysis to reduce carbon content.

Thin-film ZnO samples, grown by plasma-assisted molecular beam epitaxy (MBE) on sapphire substrates, were prepared by Adam Hyndman (non-doped) and Dr Rodrigo Martinez Gazoni (Sb-doped) (University of Canterbury), and characterised by Dr Gazoni. These samples grow in the O-polar orientation. Band gap and charge carrier concentrations are listed in Table 2.1; these were determined via UV-visible transmission spectroscopy and Hall Effect measurements with van der Pauw contacts, respectively. In this work, samples were diced using a wafer saw into 10 x 10 mm^2 or 5 x 10 mm^2 pieces where noted. For electrochemical work in Chapters 5 and 6, a ~1 mm Ti/Au contact strip was evaporated on the surface of the ZnO sample (MBE or single crystal) to provide good electrical contact. Dr Gazoni performed this step; contacts were shown previously to be ohmic on all three faces. Where noted (Chapter 6), as-received MBE-ZnO samples were further cleaned with oxygen plasma to reduce carbon content.

Table 2.1. Optical band gap and charge carrier concentrations for metal oxide substrates used in this work, experimentally-derived by Dr Rodrigo Martinez Gazoni (University of Canterbury).

Substrate	Band Gap (eV)	Carrier Concentration (cm^{-3})
CrysTec ZnO, single crystal		
Zn-polar	3.17	~1.4×10^{13}
O-polar	3.17	~5.0×10^{13}
m-plane	3.19	~4.1×10^{12}
Tokyo Denpa ZnO, single crystal		
Zn-polar	3.18	~1.5×10^{16}
O-polar	3.18	~3.0×10^{14}
m-plane	3.20	~4.0×10^{13}
MBE-grown Sb-doped ZnO, thin film		
O-polar	3.29	$9.1 \times 10^{18} \pm 0.5 \times 10^{18}$

2.1.2 Reagents and Solvents

Acetone (HPLC grade, VWR International), methanol (HPLC grade, Loba Chemie), isopropanol (IPA, HPLC grade, Sigma Aldrich), tetrahydrofuran (THF, HPLC grade, Sigma Aldrich), and acetonitrile (ACN, HPLC grade, Merck) were used as supplied. All water used in this work was either Nanopure water (Thermo Scientific Barnstead, Chapter 4) or Milli-Q water (Millipore, all other Chapters) with 18 MΩ resistivity.

2.1.3 Tetrabutylammonium Tetrafluoroborate

Tetrabutylammonium tetrafluoroborate ($[Bu_4N]BF_4$) was prepared according to literature:[1] 20 mL of 40% tetrabutylammonium hydroxide was diluted to 100 mL with water. 5 mL of fluoroboric acid (48%) was diluted to 25 mL with water and slowly added to the tetrabutylammonium hydroxide solution while stirring. A white precipitate formed, which was filtered and washed with water. It was dried in ambient conditions for 1 day, then stored in a ~60 °C oven.

2.1.4 Aryldiazonium Tetrafluoroborate Salts

NBD tetrafluoroborate and TFBD tetrafluoroborate were prepared according to literature:[2] 5 mmol of 4-nitro- or 4-trifluoromethyl-aniline was dissolved dropwise in dilute fluoroboric acid (2 mL water, 2 mL 48 % fluoroboric acid) and chilled in an ice bath. 5 mmol of sodium nitrite was dissolved in a small amount of water, cooled in an ice bath, and added dropwise to the aniline solution while stirring. A pale precipitate formed. The mixture was cooled in an ice bath for 20 minutes and the precipitate separated by filtration. To purify, the product was dissolved in a small amount of cold ACN, and cold diethyl ether was very slowly added. The product was filtered under vacuumed and allowed to dry for 30 minutes prior to use. Unused product was stored in the freezer.

2.2 Instrumental Methods

2.2.1 Atomic Force Microscopy

Topographical measurements of ZnO were performed using non-contact tapping mode AFM (Digital Instruments Dimensions 3100) with a silicon cantilever (Tap300Al-G) operating at a resonant frequency of ~280 kHz. Images were obtained at a scan rate of 0.5 or 0.3 Hz with 512 samples per line. Root mean square roughnesses were measured over a 2 × 2 μm^2 area. Where possible, the thickness of organic modification layers was measured using the procedure of Chen et al.,[3] whereby the surface film was physically removed using the cantilever tip in contact mode, with a set-point voltage of 0.6 V. A 1 × 1 μm^2 area of modifier was first removed, and then a 1 × 3 μm^2 area containing the scratched region was imaged in tapping mode. The depth of the scratch was calculated using the Step function in Nanoscope. This function finds the average sample height over a ~1 × 1 μm^2 area outside the scratched area, and the average sample height within the scratched area. The difference of these gave the scratch height. As it was not possible to fully remove the modifier layer without also scratching some of the underlying substrate, the calculated height was corrected for the scratch-depth on an identical bare ZnO substrate (cleaned using oxygen plasma), using the same instrument settings. This method was most successful for diazonium ion work (Chapters 5 and 6), where the thick multilayer

films allowed unambiguous determination of the thickness with a relatively small uncertainty (± 1 nm), which corresponded well with film thicknesses determined through XPS calculations. It was not successful for phosphonic acid or thiol work (Chapters 3 and 4) due the thinness of the modification monolayers (~ 1 nm) and adventitious carbon on the as-received samples.

2.2.2 Water Contact Angle Measurements

Static water contact angle (CA) measurements were performed with a homemade goniometer setup. Water droplets (1 µL) were placed on the surface with a micro syringe and photographed with an Edmund Scientific camera with macro lens. The images were the analysed using ImageJ v1.48 software (NIH, Bethesda, MD) with a drop analysis plug-in. At least 3 droplets were imaged per sample, with the mean value reported.

2.2.3 X-Ray and Ultraviolet Photoelectron Spectroscopy

Three X-ray photoelectron spectroscopy (XPS) instruments were used in this work: two with fixed photon energy and the second with a tuneable photon energy. Fixed-energy XPS spectra were plotted in Igor via an Excel macro,[4] and were typically normalised to give each sample of interest the same Zn $2p_{3/2}$ peak area. This normalisation was carried across the core level spectra for ease of reading. A UPS instrument was also used in this work.

2.2.3.1 XPS at the University of Wisconsin-Madison, USA

Fixed-energy XPS at the University of Wisconsin-Madison was used for experiments in Chapters 3 and 4. The custom-built XPS instrument (Physical Electronics Inc., Eden Prairie, MN) at the University of Wisconsin-Madison (UW), had a model 10-610 Al Kα source (1486.6 eV photon energy), a model 10-420 toroidal monochromator, and a model 10-360 hemispherical analyser (16-channel detector array). The electron take-off angle was 45°, giving a ZnO sampling depth of ~2.3 nm. The pass energy of the analyser was 29.35 eV, giving a resolution of 0.025 eV and an overall experimental error in peak area of ~10%. Atomic sensitivity factors (ASF) for this setup were obtained from the literature.[5] Spectra were calibrated such that the main C 1s peak (always present in adventitious carbon) was at 284.8 eV.

Peaks were fitted with Voigt functions (30% Gaussian, 70% Lorentzian unless otherwise stated), and Shirley or linear backgrounds where appropriate, using CasaXPS.

2.2.3.2 XPS at the University of Auckland, New Zealand

Fixed-energy XPS at the University of Auckland was used for experiments in Chapters 5 and 6. With help from Dr Colin Doyle, XPS was carried out with a Kratos Axis Ultra DLD spectrometer with a monochromatic Al Kα source. The electron take-off angle was 90° and ASF values were sourced from Kratos Analytical. Core-level spectra have an energy resolution of 0.4 eV and were calibrated to adventitious carbon at 284.8 eV, with peaks fitted with Voigt functions with either Shirley or linear backgrounds. The experimental error in measuring each element's peak intensity was 10%.

2.2.3.3 XPS at the Australian Synchrotron, Melbourne

The Australian Synchrotron (Melbourne) soft X-ray beamline was used for surface-sensitive measurements of the samples in Chapters 3 and 6. XPS was performed at room temperature at a base pressure of < 2 x 10^{-10} mbar. Spectra were collected by a Specs Phoibos 150 hemispherical analyser with the detector normal to the sample surface. The photon energies were selected such that the ejected photoelectrons all had kinetic energy of ~150 eV, corresponding to an escape depth of ~6.2 Å, estimated using the TPP-2M formula.[6] Unless otherwise noted, C 1s, N 1s, O 1s, F 1s, P 2p, Zn 2p core level and valence band (VB) spectra were collected using photon energies (*hv*) of 435, 548, 680, 835, 280, 1180, and 150 eV, respectively. Unlike fixed-energy XPS, the ASF values for these core levels measured at these energies are not known.

Samples were mounted on an electrically-grounded tantalum foil holder, negating the need for a flood gun so accurate relative shifts in binding energy (BE) could be measured via direct referencing of the zero BE to the Fermi level of each sample. The BE scale at each photon energy was calibrated to the Au 4f core level doublet and Fermi edge of an Au reference sample. Initial experiments used a photon slit size of 6 x 20 μm^2, but when it became apparent that sample damage was occurring during analysis, subsequent experiments were carried out using a photon slit of 6 x 9 μm^2. Preliminary tests showed

that this slit size reduced the flux of the incoming photons sufficiently to reduce the rate of decomposition of the modified sample to negligible levels. When deliberately examining the effects of X-ray irradiation, the slit was opened to 6 x 20 μm^2 and core levels (F 1s or N 1s) were repeatedly scanned for ~15 min to monitor changes. Spectra were typically fit using pseudo-Voigt (30:70 Gaussian:Lorentzian) functions, except where otherwise noted, with either linear or Shirley backgrounds in CasaXPS.

2.2.3.4 Ultraviolet Photoelectron Spectroscopy

Ultraviolet photoelectron spectroscopy (UPS) was carried out with the UW-Madison XPS/UPS system, using the He I α excitation line which gave an incoming photon energy of 21.2 eV. A negative bias of ~12 V was applied to all samples to ensure separation of secondary photoelectrons stemming from the analyser and sample. While this bias shifted the binding energy of the spectra, they were calibrated to E_F of Pt, freshly cleaned with piranha solution prior to each UPS procedure. (Caution: piranha solution is very corrosive and potentially explosive when introduced to organics) All spectra were collected at a pass energy of 2.95 eV, with the samples at a 45° angle between the incoming photons and the analyser.

2.2.3.5 Band Bending Calculations from XPS and UPS

Near-surface band bending was determined via linear extrapolation of the valence band (VB) edge of the VB spectrum to the XPS or UPS instrument background, as described by Chambers et al.[7,8] The intersect determines ζ, the energy difference between the VB maximum (E_v) and the Fermi level (E_F) in the near-surface (~6.2 Å) region. Band bending was then determined from $V_{bb} = E_g - \zeta - \xi$ (Figure 1.6) where E_g is the room-temperature bandgap of the ZnO substrate, determined from optical measurements, and $\xi = (kT/q) \ln(N_C/n)$ is the energetic separation between E_F and the conduction band minimum (E_C) in the bulk of the sample, where n is the bulk carrier concentration of the substrate, and N_C is the conduction band effective density of states for ZnO ($N_C = 2.94 \times 10^{18}$ cm^{-3}).[9] E_g and n for ZnO samples used here are listed in Table 2.1. Downwards band bending at the surface and

surface electron accumulation is indicated by negative values of V_{bb}, while positive values of V_{bb} indicates upwards band bending and near-surface electron depletion.[10,11] The error associated with V_{bb} was derived from the uncertainty of the linear extrapolations and was ± 5% for synchrotron XPS and fixed-energy UPS, and ~7% for fixed-energy XPS. For synchrotron XPS, VB spectra were calibrated to the Au 4f peaks of a clean gold sample, while for fixed-energy XPS, VB spectra were not calibrated.

2.2.4 Surface Coverage Calculations

The amounts of phosphonic acids and thiols on the surface was compared using the ratios of ASF-corrected peak areas of P 2p : Zn 2p or S 2p : Zn 2p, respectively. The inelastic mean free path (IMFP, the average distance a photoelectron will travel before losing kinetic energy) of P 2p and S 2p electrons through the modifying layer will vary slightly between modifiers and may influence quantification accuracy. However, Colorado and Lee found that the attenuation length of photoelectrons from fluorinated alkyl monolayers were indistinguishable from those from hydrocarbon monolayers.[12] Larger error is expected for Zn 2p electrons, which have short IMFP and are attenuated more for modifiers with long tails than shorter tails. This may artificially increase the P : Zn or S : Zn ratios. However, due to the deep sampling depths of fixed-energy XPS, in practice, the ratios did not appear to be significantly affected by modifier length and are a good indication of relative modifier concentrations on ZnO. For Synchrotron XPS, the P 2p : Zn 3s ratio is reported but was not ASF-corrected.

P:Zn ratios were also used to estimate, using a literature model, the molecular surface concentration for each modifier on each face. This approach is summarised by Timpel et al. and relates water CA to surface coverage of molecules.[13] Fractional surface coverage of a modification layer on ZnO is given by an equation based on Cassie's Law:[14]

$$\cos\theta = f\cos\theta_{ref} + (1-f)\cos\theta' \qquad (2.1)$$

where θ is the water CA of the modification layer, f is the fractional coverage of the layer on ZnO, θ_{ref} is the contact angle for an ideal, well-packed monolayer reference, and θ' is the water CA of the

unmodified substrate. In this case, a thiol analogue of F_{13}OPA on gold is considered as the ideal monolayer, with molecular coverage of 3.4 molecules nm^{-2} as determined by high-resolution AFM.[15] Using the measured water CA of a F_{13}OPA layer on ZnO, a fractional surface coverage can be calculated and thus, a molecular coverage determined based on the full-packed 3.4 molecules nm^{-2}. This method is only suitable for F_{13}OPA modification layers, because it is the only PA used here which has reliable estimates reported for its surface coverage. However, since XPS P:Zn and S:Zn ratios give relative surface concentrations between modifiers, the surface coverage of other PA modifiers can be calculated by comparing their P:Zn ratios with those of F_{13}OPA-modified ZnO samples with known surface coverage. Thus, estimated values of surface coverage can be determined for all PA modifiers, as was done by Timpel et al. for F_{13}OPA and trifluoromethylphenyl phosphonic acid.[13]

An alternative method for finding molecular surface concentrations was also investigated but found to be unsuitable. Franking et al.[16] outlined a method which compares the amount of carbon on an unmodified reference sample to the amount of carbon on a modified sample; it assumes attenuation of the Zn 2p signal when a modification layer is present. This proved to be untrue for some parts of this work, due to the varying amounts of adventitious carbon on the reference samples and the variability in the optimisation of the sample alignment with regards to the X-ray beam. During the majority of the phosphonic acid and thiol work, access to an oxygen plasma asher was not possible, and thus the amount of carbon on reference samples was significant.

2.2.5 Modification Layer Thickness Calculations

Grafting from aryldiazonium ion solution (Chapters 5 and 6) gives relatively thick organic layers (> 1 nm) with thicknesses that can be estimated directly from XPS data, provided it is analysed alongside a clean reference sample. For these calculations, as-received ZnO was cleaned with oxygen plasma prior to XPS analysis.

The thickness of the modification layer was calculated from:[17]

$$\frac{I}{I_0} = \exp(-\frac{d}{\lambda}\sin\theta) \qquad (2.2)$$

where I is the intensity of the Zn 2p signal on unmodified ZnO, I_0 is the Zn 2p intensity on modified ZnO, d is the thickness of overlayer, λ is IMFP of Zn 2p photoelectrons though a carbon modifier, and θ is the photoelectron take-off angle (90° for the University of Auckland XPS). The main source of error (estimated to be 20% for the present work) in this equation is the value of λ, which must be calculated from a model or found empirically. In the case of Laforgue et al., nitro- and carboxyphenyl films were attached to gold, and the value for λ they used was that of alkanethiols on gold (42 Å).[17] For the calculations in this work, the value of λ was 17.1 Å. This corresponds to the escape distance for Zn 2p photoelectrons through polystyrene and was calculated from the NIST IMFP Database.[18] This thickness calculation method was only applicable to the aryldiazonium ion work, where the use of an oxygen plasma asher allowed the reference samples to be almost completely clean from carbon contamination, allowing a significant difference in the Zn 2p signal stemming from the bare and modified samples.

2.2.6 Estimation of Modifier Lengths

Avogadro 1.1.1 freeware[19] was used to estimate the length of the modifiers used in this work. After the molecule was inputted and set to its lowest-energy configuration, the length was measured from the surface to the highest molecular atom and trigonometry was used to account for that atom's angle compared to the surface normal.

2.3 Modification Methods

Modification methods for phosphonic acids and thiols on ZnO are described in Chapters 3 and 4, respectively.

2.3.1 Aryldiazonium Grafting

2.3.1.1 O-Ring Method for Electrochemical Grafting

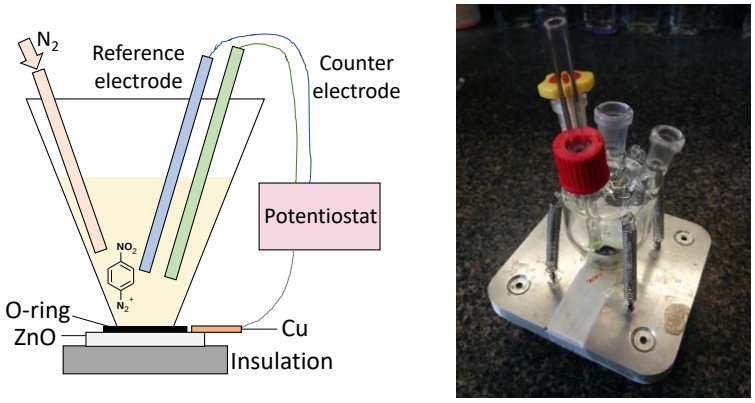

Figure 2.1. Electrochemical cell setup used for the O-ring method of electrochemically grafting from aryldiazonium salt solution.

The setup for typical electrochemical experiments on ZnO in this work (Chapters 5 and 6) is shown in Figure 2.1. This so-called 'O-ring method' was used for both electrochemical modification and reduction. Firstly, a long thin piece of copper foil was pressed onto the gold contact of a 10 x 10 mm^2 ZnO sample and secured with tape. The sample was sandwiched between an O-ring and an insulated base. A glass electrochemical cell with an aperture in the bottom was secured above, applying pressure to the O-ring to ensure that no electrolyte solution leakage. A freshly-sandpapered crocodile clip was attached to the dangling end of the copper foil, thus completing the working electrode circuit. A thin rubber tube for nitrogen purging was connected to the appropriate inlet. The counter electrode, a platinum mesh, was inserted into the cell, and 20 mL of the required solution carefully added. The open necks of the cell were stoppered, and nitrogen flowed through the solution for 15 minutes. Directly before grafting, the saturated calomel reference electrode was inserted, and the nitrogen flow halted. An alternative method ('dipping method') is outlined in Section 6.2.1.

Grafting was carried out using cyclic voltammetry with a scan rate of 200 mV s^{-1}, using various potential ranges. Unless otherwise specified, the aryldiazonium ion solutions used for electrochemical grafting were 2 mM aryldiazonium tetrafluoroborate salt and 100 mM $[Bu_4N]BF_4$ in ACN.

2.4 References

(1) Brooksby, P. A.; Downard, A. J. Electrochemical and Atomic Force Microscopy Study of Carbon Surface Modification via Diazonium Reduction in Aqueous and Acetonitrile Solutions. *Langmuir* **2004**, *20* (12), 5038–5045.

(2) Saunders, K. H.; Allen, R. L. M. *Aromatic Diazo Compounds*, 3rd ed.; Edward Arnold: London, 1985.

(3) Chen, J.; Ruther, R. E.; Tan, Y.; Bishop, L. M.; Hamers, R. J. Molecular Adsorption on ZnO($10\bar{1}0$) Single-Crystal Surfaces: Morphology and Charge Transfer. *Langmuir* **2012**, *28* (28), 10437–10445.

(4) Hurley, K. CasaXPS to Igor, Excel Macro. Christchurch 2017.

(5) Moulder, J. F.; Chastain, J. *Handbook of X-Ray Photoelectron Spectroscopy: A Reference Book of Standard Spectra for Identification and Interpretation of XPS Data*; Chastain, J., Ed.; Physical Electronics Division, Perkin-Elmer Corporation, 1995.

(6) Tanuma, S.; Powell, C. J. J.; Penn D. R.; Penn, D. R.; Penn D. R. Calculations of Electron Inelastic Mean Free Paths. III. Data for 15 Inorganic Compounds over the 50–2000 eV Range. *Surf. Interface Anal.* **1991**, *17* (13), 927–939.

(7) Chambers, S. A.; Droubay, T.; Kaspar, T. C.; Gutowski, M. Experimental Determination of Valence Band Maxima for $SrTiO_3$, TiO_2, and SrO and the Associated Valence Band Offsets with Si(001). *J. Vac. Sci. Technol. B* **2004**, *22* (4), 2205.

(8) King, P. D. C.; Veal, T. D.; Payne, D. J.; Bourlange, A.; Egdell, R. G.; McConville, C. F. Surface Electron Accumulation and the Charge Neutrality Level in In_2O_3. *Phys. Rev. Lett.* **2008**, *101* (11), 116808.

(9) Kassier, G. H.; Hayes, M.; Auret, F. D.; Mamor, M.; Bouziane, K. Electrical and Structural Characterization of As-Grown and Annealed Hydrothermal Bulk ZnO. *J. Appl. Phys.* **2007**, *102* (1).

(10) Heinhold, R.; Cooil, S. P.; Evans, D. A.; Allen, M. W. Stability of the Surface Electron Accumulation Layers on the Nonpolar ($10\bar{1}0$) and ($11\bar{2}0$) Faces of ZnO. *J. Phys. Chem. C* **2014**, *118* (42), 24575–24582.

(11) Heinhold, R.; Williams, G. T.; Cooil, S. P.; Evans, D. A.; Allen, M. W. Influence of Polarity and Hydroxyl Termination on the Band Bending at ZnO Surfaces. *Phys. Rev. B: Condens. Matter* **2013**, *88* (23), 235315.

(12) Colorado, R.; Lee, T. R. Physical Organic Probes of Interfacial Wettability Reveal the Importance of Surface Dipole Effects. *J. Phys. Org. Chem.* **2000**, *13* (12), 796–807.

(13) Timpel, M.; Nardi, M. V.; Krause, S.; Ligorio, G.; Christodoulou, C.; Pasquali, L.; Giglia, A.; Frisch, J.; Wegner, B.; Moras, P.; Koch, N. Surface Modification of ZnO(0001)-Zn with Phosphonate-Based Self-Assembled Monolayers: Binding Modes, Orientation, and Work Function. *Chem. Mater.* **2014**, *26* (17), 5042–5050.

(14) Cassie, A. B. D. Contact Angles. *Discuss. Faraday Soc.* **1948**, *3*, 11–16.

(15) Alves, C. A.; Porter, M. D. Atomic Force Microscopic Characterization of a Fluorinated Alkanethiolate Monolayer at Gold and Correlations to Electrochemical and Infrared Reflection Spectroscopic Structural Descriptions. *Langmuir* **1993**, *9* (12), 3507–3512.

(16) Franking, R. A.; Landis, E. C.; Hamers, R. J. Highly Stable Molecular Layers on Nanocrystalline Anatase TiO_2 through Photochemical Grafting. *Langmuir* **2009**, *25* (18), 10676–10684.

(17) Laforgue, A.; Addou, T.; Bélanger, D. Characterization of the Deposition of Organic Molecules at the Surface of Gold by the Electrochemical Reduction of Aryldiazonium Cations. *Langmuir* **2005**, *21* (15), 6855–6865.

(18) Powell, C. J.; Jablonski, A. *NIST Electron Inelastic-Mean-Free-Path Database*; National Institute of Standards and Technology: Gaithersburg, MD, 2010.

(19) Hanwell, M. D.; Curtis, D. E.; Lonie, D. C.; Vandermeersch, T.; Zurek, E.; Hutchison, G. R. Avogadro: An Advanced Semantic Chemical Editor, Visualisation, and Analysis Platform. *J. Chem. Informatics* **2012**, *4.17*, 1–17.

3 Phosphonic Acid Modification of Single-Crystal ZnO

3.1 Introduction

Phosphonic acids (PAs) and ZnO have an interesting relationship: PAs can be used to control the growth of ZnO nanocrystals,[1] while ZnO nanocrystals can be used as a catalyst to form PAs.[2] This is due to the strong affinity between PA head groups and metal oxides, making PAs a very promising starting point for ZnO surface modification. Covalent bonds form between PAs and a variety of metal oxides, including ZnO,[3–6] ITO,[7,8] and TiO_2,[9–12] via condensation reactions with the surface OH layer. Fluorinated,[6] aliphatic,[6,13] and aromatic PAs[13–15] have been successfully attached to ZnO nanorods,[16,17] nanowires,[18] single crystals,[6,18,19] and sputtered films.[3–5] This success has been attributed to the bi- and tridentate binding mode of PAs, which make attachment more stable than monodentate binding.

3.1.1 Preparation of Phosphonic Acid Modification Layers

The most common method for modifying ZnO with PAs involves soaking the sample in a solution of the acid. This appears to give weak binding between the acid and the surface,[5] as well as cluster or multilayer formation.[18] Covalent bonds between the modifier and the surface can be promoted by heating the ZnO after soaking. Though a study has been carried out on the effect of temperature on the binding of PAs to SiO_2,[20] no systematic study on optimal annealing temperature has been carried out for ZnO and a typical temperature of 140 °C is used.[6,21,22] The lowest annealing temperature recorded for PA on ZnO is 90 °C, used by Lange et al.,[19] while Perkins determined through temperature-dependent XPS that hexylphosphonic acid layers on O-polar ZnO are stable to 350 °C. Moreover, Perkins observed that for an unannealed sample, a basic potassium carbonate rinse removed hexylphosphonic acid layers from ZnO, while annealing at ~150 °C prevented this desorption.

A slight variation on the simple soaking technique is a method known as Tethering By Aggregation and Growth (T-BAG).[23] Here, the sample is held vertically in solution while the solvent evaporates until the sample is exposed to the air. The T-BAG method has been used to successfully modify both sputtered and single crystal ZnO with PAs, giving well-packed monolayers.[21,22] In experiments where the solvent

was not allowed to evaporate, Timpel et al. observed better homogeneity of the monolayer after repeating the immersion and annealing steps.[6]

A recent study on ITO, ZnO, and nickel oxide suggests an alternative method of modifying metal oxides with PAs: spray coating.[24] Aerosolised PAs are sprayed onto a heated surface and allowed to dry. For ZnO, the spray-coating method gave better surface concentration than dip-coating, but surprisingly, this did not significantly affect the work function. While spray-coating is a faster and perhaps more reliable method than those involving solvents, it requires specialist equipment.

3.1.2 Types of Phosphonic Acids

Many types of PAs, with varying properties, are available commercially. Three were selected for this work based on their similarities and differences (Table 3.1). ODPA was selected due to its popularity and long alkyl tail, which provides excellent van der Waals interaction stability.[25] Quiñones et al. showed that fluorinated PAs increased the stability and surface concentration of PA monolayers on ZnO nanoparticles compared to non-fluorinated analogues.[26] As well as this, fluorinated PAs generally have an opposing dipole moment to non-fluorinated derivatives[27] and this property is useful in terms of influencing electron density at the surface of ZnO.[28] For these reasons, a fluorinated analogue of ODPA (1*H*,1*H*,2*H*,2*H*-perfluorooctanephosphonic acid) was investigated in this work. F_{13}OPA is very similar to ODPA, though only has 8 carbons in its alkyl chain, of which 6 are perfluorinated. 2,3,4,5,6-pentafluorobenzyl phosphonic acid (PFBPA) has a fluorinated aromatic benzene ring, which can experience intermolecular π-π stacking interactions and stabilise the modification layer.[29] Timpel et al. saw that a trifluoromethyl-tagged phenyl PA resulted in higher surface concentration than F_{13}OPA and attributed this to the π–π interactions between the aromatic rings of the former when arranged on a surface.[6]

Table 3.1: PAs used to modify ZnO in the current work.

Name	**Octadecyl phosphonic acid**	**1*H*,1*H*,2*H*,2*H*-Perfluorooctane phosphonic acid**	**2,3,4,5,6-Pentafluorobenzyl phosphonic acid**
Abbreviation	ODPA	F_{13}OPA	PFBPA
Structure	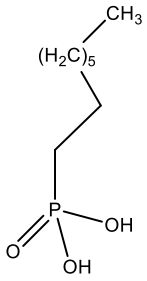	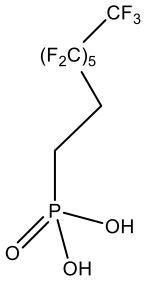	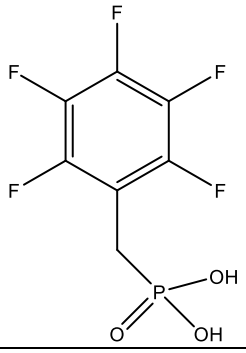

3.1.3 Aims

PAs form monolayers on ZnO and other metal oxide surfaces, and are a strong starting point for tuning the band bending of ZnO.[5,6,8,15,30,31] To date, there has not been a systematic study of the ability of PAs to attach to all three major faces of ZnO, nor a study of the band bending differences between the faces. Workfunction shift for several PAs has been experimentally measured on the polar faces,[6,19] while computational studies on the Zn- and O-polar faces have been carried out.[32] However, the experimental studies have mostly focussed on one particular type of PA, such as fluorinated. Shifts in work function are difficult to quantify as absolute values, as are changes in band bending, so a systematic comparison of a range of different PAs – and other modifiers – on the band bending of different ZnO faces is sought.

This chapter investigates a range of related PAs, as seen in Table 3.1, and their ability to bind to different faces of ZnO via an optimised modification method. Using synchrotron XPS, the binding mode and effect of modification on the surface band bending of ZnO was investigated. Finally, the stability of PA layers on ZnO over time and when exposed to UV light was studied by water contact angle (CA) and XPS measurements, as were their effects on the phenomenon of persistent photoconductivity (PPC).

3.2 Experimental Methods

3.2.1 Chemicals and Substrates

Octadecylphosphonic acid (ODPA), 1*H*,1*H*,2*H*,2*H*-perfluorooctanephosphonic acid (F_{13}OPA), and 2,3,4,5-pentafluorobenzylphosphonic acid (PFBPA) were used as received from Sigma Aldrich. ZnO single crystals from CrysTec and Tokyo Denpa, and MBE-grown thin film ZnO, were used after they were diced into 5 × 10 mm^2 samples. All samples were solvent-cleaned prior to modification, as outlined in Chapter 2, including reference samples which were not modified ('as-received').

3.2.2 Modification of ZnO with Phosphonic Acids

Unless stated otherwise, the procedure for modifying ZnO with PAs was based on that reported by Timpel et al., a diagram of which is shown in Figure 3.1.[6] After cleaning, ZnO samples were immersed vertically in vials containing 5 mL of 1 mM PA in THF. Vials were sealed to prevent evaporation and left in ambient conditions for 6 h. Following this, the samples were annealed on a hotplate at 140 °C for 2 h. They were then sonicated in THF for 4 min to remove physisorbed modifier molecules, before being dried in nitrogen. The soaking-annealing-sonication steps were carried out twice more, but with a 3 h soaking step and 30 min annealing.

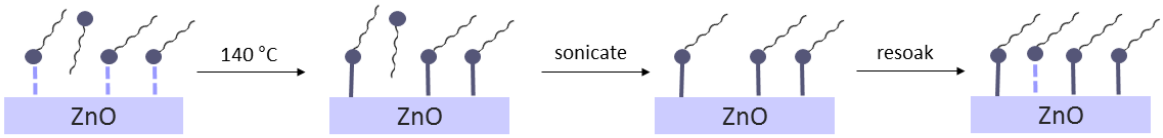

Figure 3.1. Diagram of the Timpel method for covalently bonding PAs to ZnO via repeated immersion, heating, and sonicating.

3.2.3 Thermogravimetric Analysis

Differential scanning calorimetry-thermogravimetric analysis was carried out using a Universal TA Instrument setup (v4.5A). 8.5 mg of sample was placed on a platinum pan and heated under nitrogen to 800 °C, with a step rate of 10 °C min^{-1}.

3.3 Results and Discussion

3.3.1 Method Optimisation for Phosphonic Acid Modification Layers on ZnO

The method for modifying ZnO with PAs was decided upon after trialling several different processes outlined in the literature.

3.3.1.1 Modification Solvent

Ethanol[3–5,19] and THF[6,17,22] have been used by other researchers as the solvent for PA modification of ZnO. The low dielectric constant of THF is claimed to aid the formation of dipole-oriented monolayers.[8] These two solvents were examined in this work for their ability to help form uniform molecular layers of PAs on ZnO.

MBE-grown ZnO (Adam Hyndman, University of Canterbury) was used for these preliminary studies; the modification method was similar to that described by Chockalingam et al.[31] After samples were cleaned in acetone, methanol, and IPA, they were immersed in separate 1 mM ODPA solutions for 18 h in either ethanol or THF. Samples were then rinsed briefly before annealing at 120 °C for 3 h. This was followed by sonication in the respective solvent. The effect of modification on surface wettability was monitored by measuring CA. CA were 68 ° ± 7 ° prior to modification and 107 ° ± 4° and 109 ° ± 2° after modification with ODPA in ethanol and THF, respectively (Figure 3.2). The increase in CA indicates the expected increase in hydrophobicity after modification, and the two solvents give modified surfaces with the same wettability.

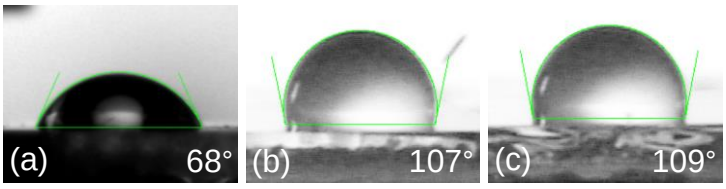

Figure 3.2: Water contact angles for MBE-grown ZnO (a) as-received, (b) modified with ODPA in ethanol, and (c) modified with ODPA in THF.

However, optical microscope images of the same samples revealed very different surfaces, as seen in Figure 3.3. The sample prepared in ethanol appeared to have residue on the surface, even after sonication, while the THF treatment yielded a very uniform surface. This may be due to the relative vapour pressures for THF and ethanol: THF has a higher vapour pressure and should be more readily removed from the sample after modification. Additionally, the viscosity of ethanol is higher than that of THF, so the ethanol may not be entirely removed during the nitrogen drying process. The apparent 'residue' may also be pitting: ZnO is highly susceptible to corrosion in acidic conditions, which the ethanolic solution may have provided. Indeed, modification of ZnO by Chen et al. using carboxylic acids in ethanol proved to etch the surface.[5] The polar non-protic THF was therefore selected as the solvent of choice for further PA modifications.

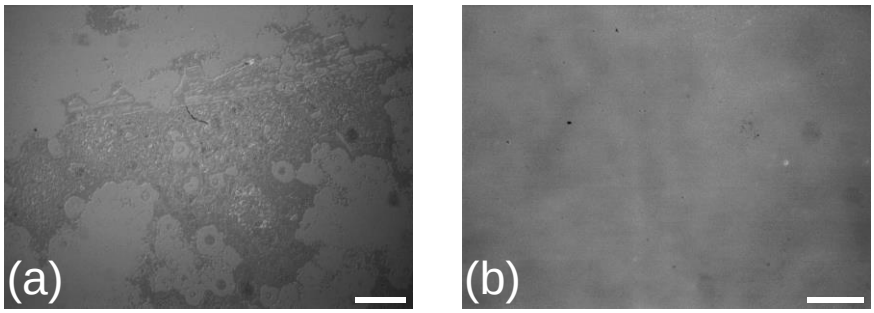

Figure 3.3: Microscope images of (A) ethanol- and (B) THF-treated MBE ZnO modified with ODPA. Scalebars are 125 µm.

3.3.1.2 Further Method Development

Three methods requiring shorter immersion times were investigated for PA modification: the 'Timpel method', which has repeated steps of soaking, annealing, and sonicating;[6] the 'T-BAG method', where the solvent is allowed to evaporate during the soaking step;[22] and the 'dip-coating method', where a very short immersion step is used.[33]

Table 3.2 shows the water CA results for these different modification methods tested on Zn-polar and m-plane ZnO. The CA for ODPA-treated titania was previously reported as 110°,[10] and on ITO, reported contact angles range from 103° to 117°.[8,21,34,35] A water contact angle of 103° was reported by Timpel

et al. for F_{13}OPA-modified Zn-polar ZnO,[6] which is similar to the results seen by Hotchkiss on ITO (101°)[36] but lower than that seen by Sharma (108°)[35] and Wang (108.67°) on ITO.[37] A higher contact angle for both ODPA- and F_{13}OPA-modified samples is assumed to be indicative of higher molecular density of the hydrophobic organic modifiers at the surface and a more successful modification method.[6] Additionally, the absolute error is an indication of how uniform the modification layer is across the sample, as it is the standard deviation of the angles of at least 3 water droplets for each sample.

*Table 3.2: Summary of PA modification methods trialled on single-crystal ZnO, and the corresponding water contact angle for each sample before and after modification. The concentration of PA was 1 mM in all solutions. *Solvent allowed to evaporate during modification. RT = room temperature.*

Method	Face	Modifying Solution	Time	Post-treatment	CA (°)
Unmod.	Zn-polar	-	-	-	64 ± 4
Unmod.	O-polar	-	-	-	56 ± 2
Unmod.	m-plane	-	-	-	48 ± 2
Timpel	Zn-polar	F_{13}OPA, THF, RT	6 h	Annealed at 140 °C in air; 2 h	108 ± 2
Timpel	Zn-polar	F_{13}OPA, THF, RT	6 h	As above; sonicated	95 ± 6
Timpel	Zn-polar	F_{13}OPA, THF, RT	3x 6 h	Annealed at 140 °C in air; 2 h; sonicated 3 min; repeated 2x	105 ± 2
Timpel	Zn-polar	F_{13}OPA, THF, RT	3x 6 h	As above; sonicated	109 ± 3
T-BAG	Zn-polar	F_{13}OPA, THF*, RT	3 h*	Rinsed and dried	92 ± 1
T-BAG	Zn-polar	F_{13}OPA, THF*, RT	3 h*	Sonicated	99 ± 2
Dip-coat	m-plane	ODPA, anisole, 60 °C	~3 s	Annealed at 150 °C in air; 30 min	105 ± 4
Dip-coat	m-plane	ODPA, anisole, 60 °C	~3 s	As above; rinsed in THF	98 ± 4
Dip-coat	m-plane	F_{13}OPA, anisole, 60 °C	~3 s	Annealed at 150 °C in air; 30 min	103 ± 2
Dip-coat	m-plane	F_{13}OPA, anisole, 60 °C	~3 s	As above; sonicated in THF (3 min)	102 ± 2

The highest CA (109°) was observed on the Zn-polar sample subjected to three iterations of the soaking, annealing, and sonicating Timpel process.[6] This angle was measured after the final sonication of the sample, indicating that the hydrophobic layer is stable and most likely chemisorbed to the ZnO surface. This contrasts with the sample which was treated only once with the soaking and annealing

process: before sonication, the water contact angle was 108°, but after sonication decreased to 95°. This result emphasises the necessity of sonication to remove any physisorbed PAs, followed by re-immersion to allow new PA molecules to move into the spaces previously blocked, and potentially form covalent bonds to ZnO upon annealing.

The dip-coating method by Chen et al. describes a rapid PA modification on mica and aluminium using anisole, a solvent with a very low dielectric constant of 4.3.[33] The sample was dipped briefly in a heated 1 mM solution of ODPA in anisole, and after annealing it was claimed that the result was a dense ODPA modification layer with a water contact angle of 110°. The process was followed in this work with ODPA and F_{13}OPA on ZnO. While the modified samples had acceptable water contact angles (105° and 103° respectively), in the case of ODPA, the contact angle decreased to 98° upon sonication of the sample. In contrast, the F_{13}OPA-modified sample retained its contact angle of ~103°. Its value was still lower than that found for the Timpel-modified Zn-polar face (109°).[6] This difference is not large and could be attributed to differences in the polarity of the two ZnO faces. However, the Timpel method, with 3 immersion and annealing steps, was chosen for all subsequent PA modifications.

3.3.2 AFM of Phosphonic Acid Modification Layers

The AFM images of as-received Zn-polar ZnO seen in Figure 3.4 shows step-like atomic features approximately 300 nm wide. Figure 3.4b shows the same sample directly after modification with PFBPA. After PFBPA modification, small circular features appear on the ZnO surface. The roughness increases from 0.1 nm to 0.2 nm but the characteristic terraces of the ZnO surface are still visible, suggesting the ZnO has been modified with a thin layer of PFBPA. The height of a PFBPA molecule upright on a flat surface is approximately 0.7 nm,[38] which is long enough to distort the details of the terraces, but not enough to completely obscure the terraces entirely. It is assumed that the circular features are clumps of PFBPA, and are comparable to those seen by Chen et al. of hexadecylPA on m-plane ZnO.[5]

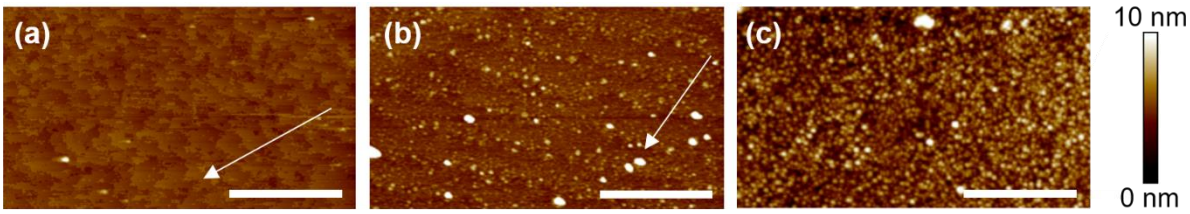

Figure 3.4. AFM images for high-quality Zn-polar ZnO: (a) as-received; (b) modified with PFBPA and imaged before synchrotron XPS analysis; (c) modified with PFBPA and imaged after synchrotron XPS analysis. Horizontal scale bars are 1 µm. Arrows have been added to show the approximate direction of terrace formation. Root mean square roughnesses are (a) 0.1 nm; (b) 0.2 nm; (c) 1.1 nm.

AFM was used to determine the topography changes for ZnO samples modified with ODPA, F_{13}OPA, and PFBPA, after synchrotron XPS analysis. This analysis order was chosen to minimise any contamination of the samples for the XPS analysis, but ultimately resulted in poor-quality surfaces for AFM, especially when compounded with external factors such as humidity.[39] To illustrate this point, Figure 3.4c shows an AFM image of PFBPA-modified sample after XPS analysis. The surface is clearly very different to that imaged before XPS analysis (Figure 3.4b), and the surface roughness is 1.1 nm compared to the freshly-modified surface roughness of 0.2 nm. This is most likely due to the repeated sample handling and transport required for synchrotron XPS analysis. Consequently, AFM imaging is not fully discussed here, although the images obtained of all samples after synchrotron XPS analysis can be found in Appendix 8.1.1.

3.3.3 Fixed-Energy XPS Analysis of Phosphonic Acid Modification of Single Crystal ZnO

Single-crystal Zn-polar, O-polar, and m-plane ZnO (CrysTec) were modified with ODPA, F_{13}OPA, and PFBPA (Table 3.1), and preliminary fixed-energy XPS analysis was performed to confirm that samples could be modified as expected. The atomic percentages of each modified sample and its as-received reference samples are shown in Table 3.3. Except for the as-received samples, evidence for PA modification layers was seen on all faces and with all PA derivatives. The results of core-level spectra

are presented and discussed in Appendix 8.1.2 and detailed analysis of samples by synchrotron XPS are discussed in Section 3.3.5.

Table 3.3. Fixed-energy XPS atomic percentages from survey spectra for OPDA-, F_{13}OPA-, and PFBPA-modified Zn-polar, O-polar, and m-plane ZnO faces.

Face	Modifier	Zn %	O %	C %	P %	F %
Zn-polar	As-received	23	45	32	0	0
	F_{13}OPA	17	37	17	2	26
	ODPA	8	30	59	3	0
	PFBPA	33	43	15	2	8
O-polar	As-received	21	43	36	0	0
	F_{13}OPA	17	36	18	2	27
	ODPA	14	35	49	2	0
	PFBPA	29	47	16	3	6
m-plane	As-received	27	41	33	0	0
	F_{13}OPA	16	29	20	2	33
	ODPA	9	28	60	3	0
	PFBPA	23	36	23	3	14

3.3.4 Water Contact Angles and Molecular Surface Concentration

Figure 3.5 shows the water CAs determined for each of the single-crystal PA-modified ZnO faces after analysis with synchrotron XPS (Appendix 8.1.3). The as-received samples have lower CA than the modified samples in all cases, confirming a change has occurred during modification to make the surfaces hydrophobic. However, all CA for modified samples are lower than expected due to sample handling and synchrotron XPS analysis prior to CA measurements. The values for ODPA-modified ZnO are 77°, 106°, and 97° for Zn-polar, O-polar, and m-plane ZnO, respectively. The O-polar value is closest to the literature values reported for ODPA monolayers: 108° on ZnO.[4] Barriet and Lee note that monolayers from fluorocarbon-based molecules typically have a lower packing density than their hydrocarbon analogues, attributed to the size increase from hydrogen to fluorine.[40] This is in contrast to the report by Quiñones et al., who saw denser packing of fluorinated PA on ZnO nanoparticles than

non-fluorinated PAs.[26] However, the present work uses planar surfaces, which are chemically and structurally different to nanoparticles. The values for F_{13}OPA-modified ZnO were ~89°, ~86° and ~93° for Zn-polar, O-polar, and m-plane samples, respectively. With the exception of the O-polar face, the error associated with these values places them within the region of 101°, as reported by Timpel et al. for Zn-polar ZnO.[6] This is lower than reported for the similar ODPA, a phenomenon attributed by Colorado and Lee to the interaction between water and the dipole of the fluorocarbons creating a more hydrophilic interface.[27] The CA for PFBPA monolayers has been reported as 87° on ITO.[41] Here, O-polar and m-plane samples matched this well, with values of ~83° and ~86° respectively. PFBPA-modified Zn-polar ZnO had a significantly lower value of ~76°, with a larger error associated with it. The high CA of F_{13}OPA-modified ZnO compared to those surfaces modified with PFBPA are due to the increased density of fluorine from the alkyl chains, resulting in a more hydrophobic surface.[42] Timpel et al. found a CA of 93° for p-(trifluoromethyl)phenylPA monolayers on ZnO and greater surface concentration of this molecule than F_{13}OPA.[6] This was attributed to the π-π interactions of the aromatic rings, and the binding modes.

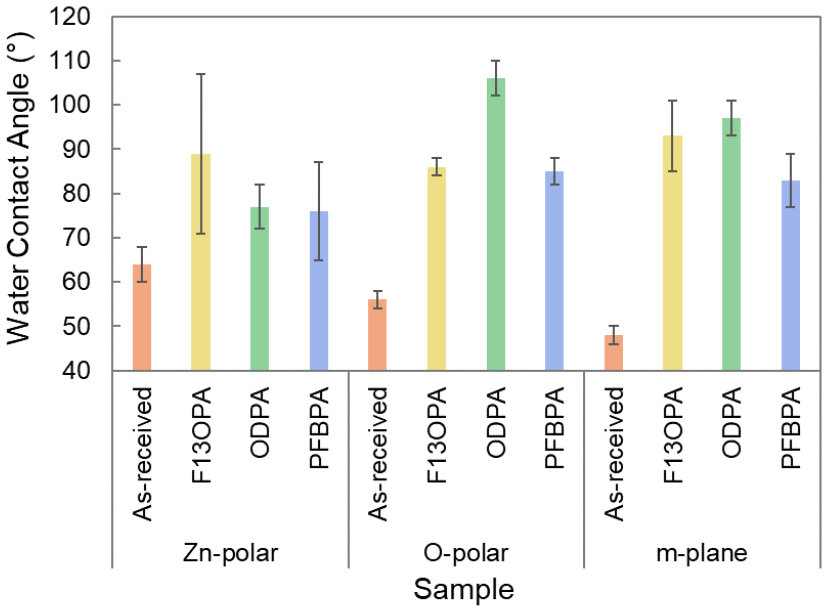

Figure 3.5. Water CAs for as-received and ODPA-, F_{13}OPA-, and PFBPA-modified Zn-polar, O-polar, and m-plane ZnO, measured after synchrotron XPS analysis.

Figure 3.6 displays CA for each of the as-received and modified faces against molecular surface concentrations, which were estimated by the F_{13}OPA CA and synchrotron XPS data as described in Chapter 2. Typical surface concentration calculations directly from XPS are limited by assumptions that are inappropriate for the carbon-heavy as-received ZnO samples used in this section. No trend across the faces is observed. Instead, it appears that modifiers have similar surface coverages on all three faces. These are distinct for all but ODPA-modified O-polar ZnO. Implications of these results for the binding mode are discussed in Section 3.3.6.

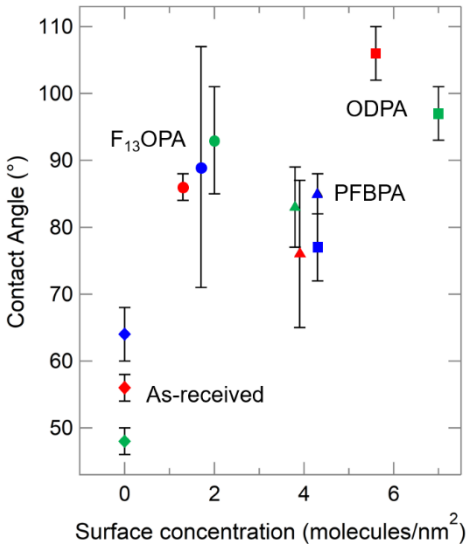

Figure 3.6. CA compared to molecular surface concentration of as-received (diamonds), ODPA-modified (circles), F_{13}OPA-modified (squares), and PFBPA-modified (triangles) Zn-polar (blue), O-polar (red), and m-plane (green) ZnO.

3.3.5 Synchrotron XPS Analysis of Phosphonic Acids on ZnO

Synchrotron XPS was used to obtain surface-sensitive chemical and electronic data for ODPA-, F_{13}OPA-, and PFBPA-modified Zn-polar, O-polar, and m-plane ZnO samples. Tokyo Denpa crystals were modified with the first two modifiers, while CrysTec samples were used for PFBPA modification.

3.3.5.1 ODPA- and F_{13}OPA-Modified ZnO

Figure 3.7 – Figure 3.9 show spectra obtained by synchrotron XPS for ODPA- and F_{13}OPA-modified Zn-polar, O-polar, and m-plane ZnO (Tokyo Denpa). Detailed data are shown in Appendix 8.1.4.

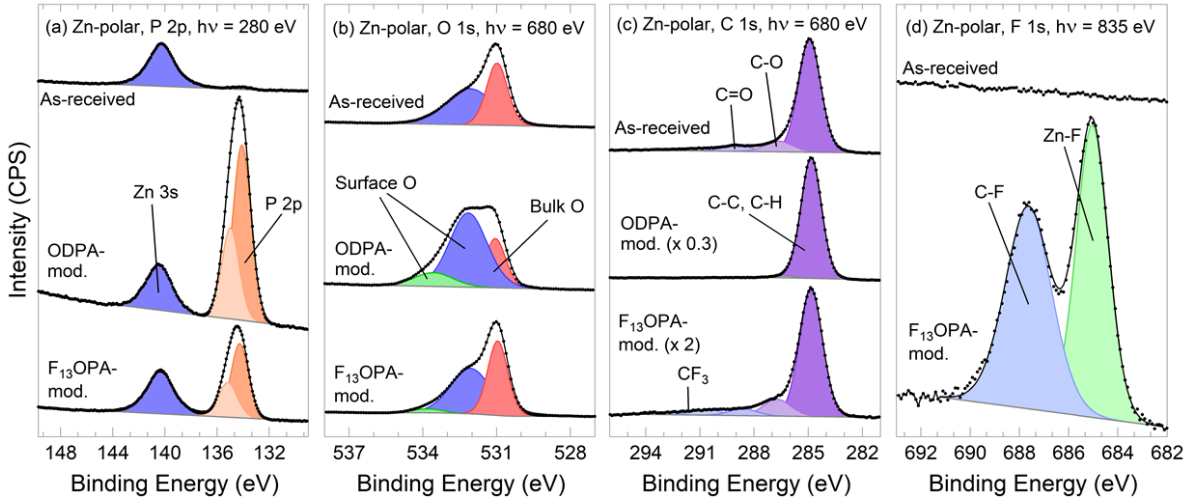

Figure 3.7: P 2p, C 1s, O 1s, and F 1s synchrotron XPS spectra for Zn-polar ZnO with and without modification with ODPA or F_{13}OPA. All spectra have been offset for clarity, with intensities normalised to the Zn 3s peak area of the as-received sample (BE = 140 eV).

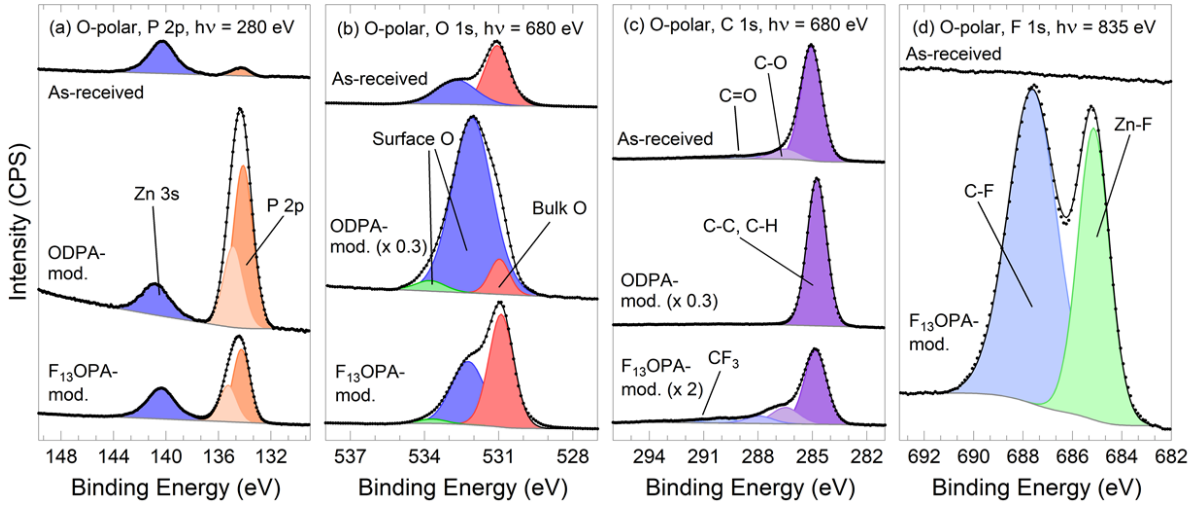

Figure 3.8: P 2p, C 1s, O 1s, and F 1s synchrotron XPS spectra for O-polar ZnO modified with and without modification with ODPA or F_{13}OPA. All spectra have been offset for clarity, with intensities normalised to the Zn 3s peak area of the as-received sample (BE = 140 eV).

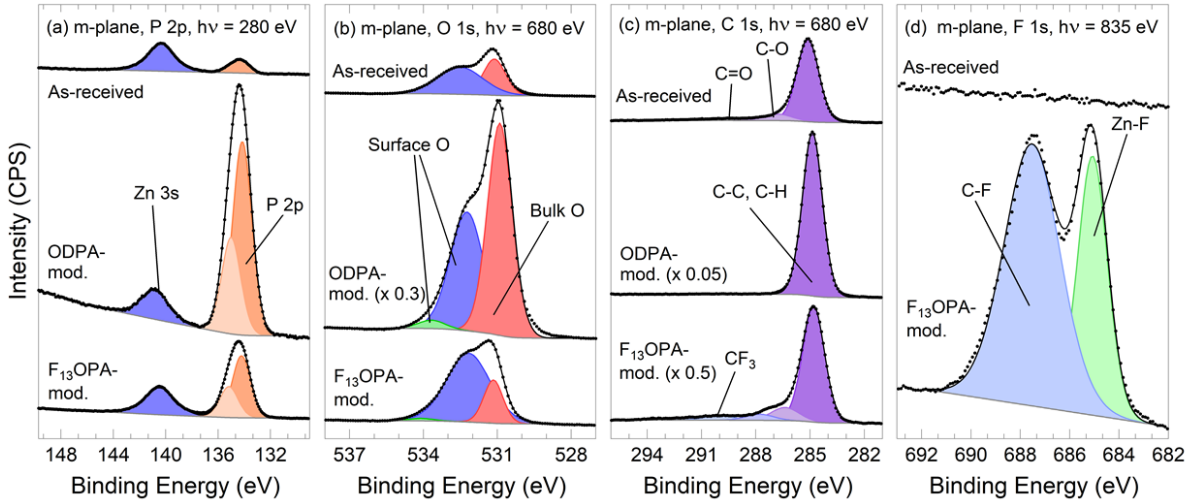

Figure 3.9: P 2p, C 1s, O 1s, and F 1s synchrotron XPS spectra for m-plane ZnO with and without modification with ODPA or F_{13}OPA. All spectra have been offset for clarity, with intensities normalised to the Zn 3s peak area of the as-received sample (BE = 140 eV).

P 2p

Figure 3.7a – Figure 3.9a show all modified samples have signal in the P 2p region (~134.5 eV),[5,6,43] which is possibly evidence of PA at the surface. The as-received samples have trace amounts of phosphorous present on the surface; this is attributed to cross-sample contamination from modified samples on the same analysis bar. Table 3.4 shows that ZnO faces modified with ODPA have a much larger P 2p signal than F_{13}OPA-modified samples, reflecting a larger surface concentration as seen by Hotchkiss et al.[36] and estimated in Figure 3.6. There is little difference in P 2p % between different ZnO faces modified with the same modifier: for ODPA, it ranges from 80 – 87%, while for F_{13}OPA it varies between 62 and 68%. While m-plane ZnO has more surface OH than the two polar faces (2.2×10^{-9} mol cm^{-2} compared to 1.8×10^{-9} mol cm^{-2}, respectively),[44,45] it appears that this does not increase the molecular surface concentration of PAs.

Table 3.4. Synchrotron XPS data from P 2p + Zn 3s and O 1s regions of as-received ('as-rec.'), ODPA- and F_{13}OPA-modified Zn-polar, O-polar, and m-plane ZnO. [a] Percentage of P 2p + Zn 3s region (hv = 280 eV). [b] Percentage of O 1s region (hv = 680 eV).

Sample		**Binding Energy (eV) and Assignment**				
		140.3 – 140.8 Zn 3s (%)[a]	134.3 – 134.8 P 2p (%)[a]	530.8 – 531.2 O $1s_{bulk}$ (%)[b]	531.8 – 532.3 O $1s_{surf.}$ (%)[b]	– Zn 3s : O $1s_{surf.}$
Zn-polar	As-rec.	95	5	43	57	1 : 3.3
	ODPA	20	80	18	82	1 : 7.6
	F_{13}OPA	38	62	36	64	1 : 3.7
O-polar	As-rec.	86	14	39	61	1 : 5.5
	ODPA	16	84	5	95	1 : 10. 5
	F_{13}OPA	32	68	29	71	1 : 5.9
m-plane	As-rec.	75	25	39	61	1 : 3.7
	ODPA	13	87	97	3	1 : 13.7
	F_{13}OPA	33	67	21	79	1: 4.7

O 1s

O 1s spectra are shown in Figure 3.7b – Figure 3.9b and quantified in Table 3.4. As-received ZnO faces show two distinct peaks related to bulk oxygen (531 eV) and surface oxygen (~532 eV) arising from OH groups, which are quantified in Table 3.4. These binding energies (BE) are similar to literature values.[46] Upon modification, a small peak at higher BE appears, and is attributed to different types of PA binding,[13] discussed later in Section 3.3.6. F_{13}OPA-modified ZnO samples show no significant difference from the as-received samples, while the ODPA-modified sample shows a significant increase in surface O, attributed to the large number of PA headgroups on the surface. Alongside the P 2p spectra, this is evidence for the ODPA-modified sample having more PA on the surface than the F_{13}OPA-modified sample. The addition of modification layers is expected to attenuate the bulk O signal relative to the surface O. However, the Zn 3s:O $1s_{surf}$ ratios indicate that ODPA has added a significant amount of O to the surface, while F_{13}OPA-modified samples have similar Zn 3s:O $1s_{surf}$ ratios to the as-

received samples. This suggests that ODPA and F_{13}OPA modifiers have different concentrations and binding modes on the surface, which will be discussed further in Section 3.3.6.

C1s

Adventitious carbon is always present in XPS analysis and limits the usefulness of C 1s spectra.[47] Figure 3.7c – Figure 3.9c and Table 3.5 show that ODPA-modified samples have a much larger C 1s signal than both the as-received samples and the F_{13}OPA-modified samples due to more carbon atoms present in the ODPA molecule (18). The F_{13}OPA modifier has only 8 carbons in its fluoroalkyl chain, which accounts for the sample having less carbon than the ODPA-modified sample. However, the F_{13}OPA C 1s signals on all ZnO faces are less intense than on the as-received samples. It may be that the fluorinated F_{13}OPA layer repels adventitious debris from the surface, resulting in a smaller amount of carbon on the surface.

Table 3.5. Synchrotron XPS data for the C 1s region of as-received and ODPA- and F_{13}OPA-modified Zn-polar, O-polar, and m-plane ZnO.

Sample		**Binding Energy (eV) and Assignment**				
		284.7 – 285.0 C-C, C-H	286.3 – 286.6 C-O	287.8 – 288.9 C=O	290.0 – 290.1 CF_2	292.2 – 292.3 CF_3
Zn-polar	As-received	84	10	6	-	-
	ODPA	98	2	-	-	-
	F_{13}OPA	78	12	5	4	2
O-polar	As-received	86	10	3	-	-
	ODPA	100	-	-	-	-
	F_{13}OPA	67	18	8	6	3
m-plane	As-received	87	9	4	-	-
	ODPA	100	-	-	-	-
	F_{13}OPA	79	11	5	4	2

Unlike fixed-energy XPS results (Appendix 8.1.2) and those reported by Timpel et al,[6] the synchrotron XPS C 1s spectrum for F_{13}OPA-modified ZnO did not show the intensity expected for the higher BE

peaks associated with CF_2 (290 eV) and CF_3 (292 eV) moieties (Table 3.5). This was determined from F 1s spectra to be due to degradation of fluorine bound to carbon.[40]

F 1s

Two peaks are observed in the F 1s spectra with approximately equal areas (Figure 3.7c – Figure 3.9c), quantified in Table 3.6. The peak at ~687 eV is assigned to C-bound F from the F_{13}OPA tail, while that at 685 eV is consistent with Zn-bound F. Evidently the synchrotron X-rays damaged the sample, liberating F from the modifier. It appears that this F interacts with the ZnO substrate.

Table 3.6. Synchrotron XPS data for the F 1s region of ODPA- and F_{13}OPA-modified Zn-polar, O-polar, and m-plane ZnO (hv = 835 eV).

Sample		**Binding Energy (eV)**	
		687.6 F-C (%)	685.0 – 685.1 F-Zn (%)
Zn-polar	As-received	-	-
	ODPA	-	-
	F_{13}OPA	50	50
O-polar	As-received	-	-
	ODPA	-	-
	F_{13}OPA	63	37
m-plane	As-received	-	-
	ODPA	-	-
	F_{13}OPA	60	40

Fluoropolymers are known to be unstable under XPS conditions,[40] but the possibility of thermal degradation of the modifiers during the annealing process was investigated by thermogravimetric analysis of F_{13}OPA (Figure 3.10). The molecule does not start to decompose until temperatures higher than ~170 °C. Samples were annealed at 140 °C during modification and therefore it is unlikely that the F-Zn interaction arose due to thermal degradation of the modification layer.

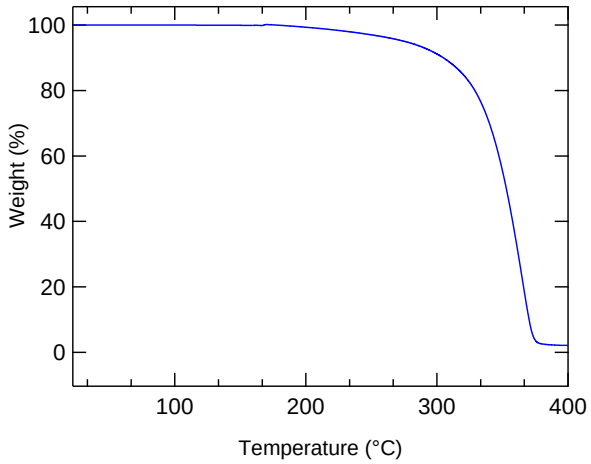

Figure 3.10: Thermogravimetric analysis of bulk F_{13}OPA, heated at a step rate of 10 °C min^{-1}.

For F_{13}OPA-modified ZnO, the total amount of CF_x degradation that occurred during XPS analysis could not be quantified, because the signal associated with F interacting with Zn does not include any liberated F that has been completely removed from the surface. While the Zn-polar face has a 1:1 ratio of organic:inorganic fluorine, and the O-polar and m-plane faces have ratios of ~3:2, these are not reliable due to differences in the number, type, and order of XPS scans on the three faces. It was concluded that photoelectrons from the X-ray source are the source of F_{13}OPA degradation[48] and following work sought to minimise the damage on PA-modified samples during XPS analysis.

3.3.5.2 PFBPA-Modified ZnO

PFBPA-modified ZnO was analysed with synchrotron XPS. The commercially-obtained crystals were from CrysTec, not Tokyo Denpa, and have lower charge carrier concentrations (Section 2.1.1). For these measurements, the photon flux for XPS measurements was decreased by reducing the slit size, which was successful in minimising the damage to the fluorinated modifier. Spectra are shown in Figure 3.11 – Figure 3.13.

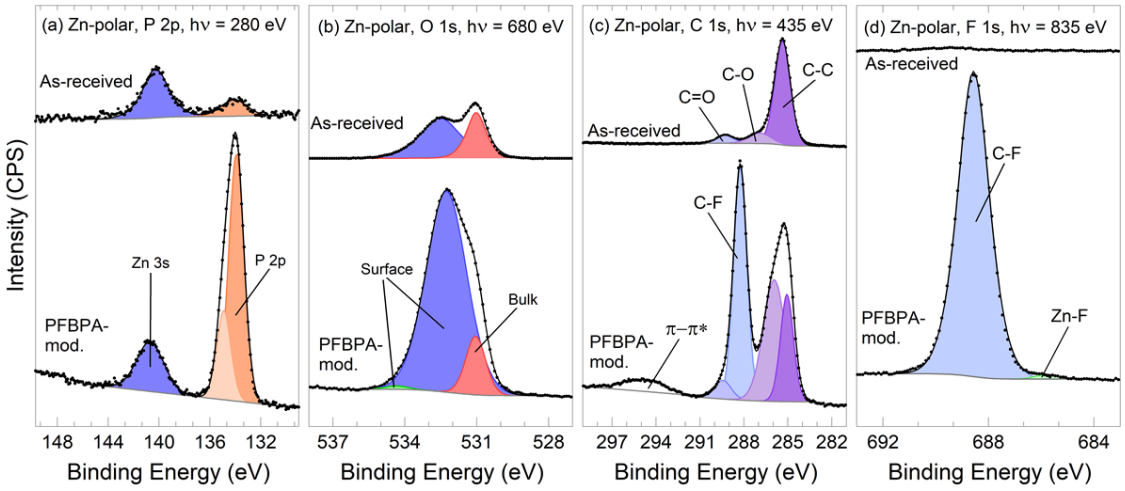

Figure 3.11. Synchrotron XPS spectra of (a) Zn 3s/P 2p, (b) O 1s, (c) C 1s, and (d) F 1s regions for PFBPA-modified Zn-polar ZnO. All spectra have been normalised to the same Zn 3s peak area.

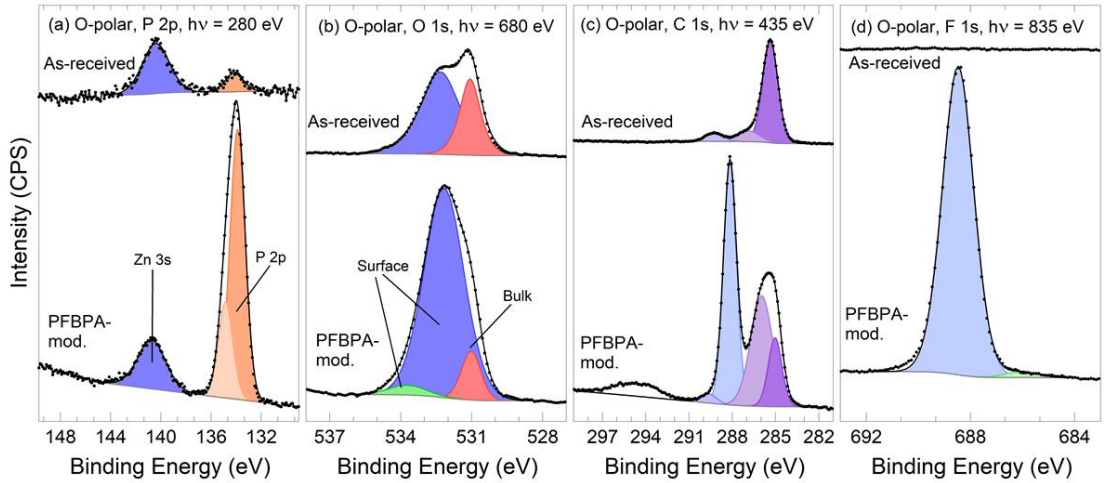

Figure 3.12. Synchrotron XPS spectra of (a) Zn 3s/P 2p, (b) O 1s, (c) C 1s, and (d) F 1s regions for PFBPA-modified O-polar ZnO. All spectra have been normalised to the same Zn 3s peak area.

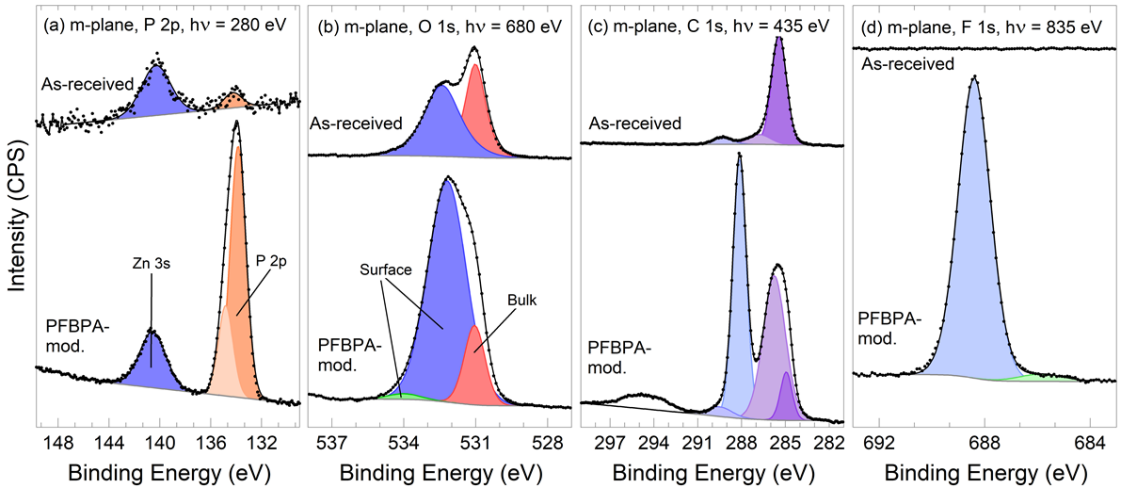

Figure 3.13. Synchrotron XPS spectra of (a) Zn 3s/P 2p, (b) O 1s, (c) C 1s, and (d) F 1s regions for PFBPA-modified m-plane ZnO. All spectra have been normalised to the same Zn 3s peak area.

All three ZnO faces showed clear XPS evidence of modification with PFBPA. As seen in Figure 3.11b – Figure 3.13b, a substantial pair of P 2p spin-orbit peaks is detected, while the as-received surface contains only a small amount of P contamination. The presence of the modifying layer attenuates the Zn 3s signal originating from the bulk ZnO and a similar effect is seen for bulk O 1s (Figure 3.11c – Figure 3.13c) where the increase in surface oxygen is likely due to attenuation of the signal arising from the bulk oxygen within the ZnO crystal. However, there is also a slight increase in surface O 1s:Zn 3s (Table 3.7) which is attributed to the PA headgroup of PFBPA not being fully coordinated to the surface.

Table 3.7 shows the percentages of P 2p signal in the P 2p + Zn 3s region. Like F_{13}OPA- and ODPA-modified samples, PFBPA-modified samples show little difference in P 2p surface concentration across the three faces, suggesting that coverage of PFBPA groups is governed by the bulk of the molecules themselves, not the chemical or physical properties of ZnO or how many OH groups are on the surface.

The presence of the modifying layer attenuates the Zn 3s signal originating from the bulk ZnO and a similar effect is seen for bulk O 1s (Figure 3.11c – Figure 3.13c) where the increase in surface oxygen is likely due to attenuation of the signal arising from the bulk oxygen within the ZnO crystal. However,

there is also a slight increase in surface O 1s:Zn 3s (Table 3.7) which is attributed to the PA headgroup of PFBPA not being fully coordinated to the surface.

Table 3.7. Synchrotron XPS data for O 1s, F 1s, and P 2p + Zn 3s regions of PFBPA-modified ZnO and as-received ZnO ('as-rec.'). [a] Percentage of O 1s region. [b] Percentage of F 1s region. [c] Percentage of Zn 3s + P 2p region.

Sample		**Binding Energy (eV) and Assignment**						
		531.0 – 531.2 O $1s_{bulk}$ (%)[a]	532.3 – 532.6 O $1s_{surf}$ (%)[2]	– Zn 3s : O $1s_{surf.}$	688.2 – 688.4 F-C (%)[b]	685.6 – 685.9 F-Zn (%)[b]	140.3 – 140.7 Zn 3s (%)[c]	134.1 – 134.4 P 2p (%)[c]
Zn-polar	As-rec.	36	64	1 : 6.5	-	-	76	24
	PFBPA	20	80	1: 10.6	99	1	21	79
O-polar	As-rec.	33	67	1 : 9.1	-	-	80	20
	PFBPA	17	83	1 : 11.1	98	2	20	80
m-plane	As-rec.	43	57	1 : 10.4	-	-	84	16
	PFBPA	22	78	1 : 7.9	99	1	22	78

Figure 3.11c – Figure 3.13c and Figure 3.11d – Figure 3.13d show clear evidence for the presence of fluorine on modified Zn-polar ZnO, with a C 1s peak arising at ~288 eV corresponding to the C bound to F, and a F 1s peak at ~689 eV corresponding to the fluorine interacting with C.[7,24] A very small amount of F interacting with Zn is seen at ~684 eV; unlike the measurements made on ODPA- and F_{13}OPA-modified surfaces, the XPS photon flux was carefully monitored and reduced to minimise damage. In the C 1s spectrum, the modified sample shows an increase in a peak centred at ~286 eV, a slightly lower BE than the C-O peak seen on the as-received sample (Table 3.8). This peak contains both adventitious C-O species as well as C-P bonds. The peak at 285 eV in the as-received spectrum arises from adventitious carbon. In PFBPA-modified samples there is a slightly smaller peak at a slightly lower BE than for as-received samples. The shift in BE is consistent with an assignment to C-C and C=C in PFBPA. The apparent decrease in adventitious carbon is attributed to the hydro- and oleo-phobic nature of PFBPA, which, like F_{13}OPA, has displaced a large amount of adventitious carbon upon modification and repelled any further contamination post-modification. The satellite peak at ~295 eV

also confirms the presence of aromatic rings on the surface: it is attributed to photoelectrons in the aromatic ring which underwent π-π* excitations before being ejected from the surface. m-Plane ZnO had the largest percentage of C-F bonds, followed by O-polar and Zn-polar. However, this difference is small and when compared with P 2p %, all faces have similar PFBPA surface concentrations.

Table 3.8. Synchrotron XPS data for the C 1s region of PFBPA-modified ZnO (hv = 435 eV).

Sample		**Binding Energy (eV)**					
		284.9 – 285.1 C=C (%)	285.4 C-C, C-H (%)	286.8 – 286.9 C-O (%)	289.3 C=O (%)	288.1 CF (%)	294.6 π-π* (%)
Zn-polar	As-received	-	82	12	7	-	-
	PFBPA	20	30	3	7	34	6
O-polar	As-received	-	80	12	8	-	-
	PFBPA	19	18	11	3	40	8
m-plane	As-received	-	82	11	7	-	-
	PFBPA	7	40	1	2	42	8

3.3.5.3 Band Bending of Phosphonic Acid-Modified ZnO

As outlined in Chapter 1 and detailed in Section 2.2.3, near-surface band bending (V_{bb}) can be derived from synchrotron XPS valence band (VB) spectra by extracting ζ ($E_F - E_V$). Although changes in V_{bb} can also be detected from BE shifts of bulk O 1s and Zn 3s core levels upon modification, the synchrotron soft X-ray beamline calibration is more stable and precise at 150 eV, so VB spectra are more accurate than core level measurements. V_{bb} is dependent on the X-ray energy and polarity of the crystal face, with values of –0.60 eV, –0.18 eV, and –0.23 eV for as-received Zn-polar, O-polar, and m-plane Tokyo Denpa ZnO (*hv* = 150 eV) respectively. CrysTec ZnO samples have much smaller V_{bb} differences across faces, with –0.59 eV, –0.52, and –0.61 eV for Zn-polar, O-polar, and m-plane ZnO (*hv* = 150 eV) respectively. This is attributed to lower-quality crystals having more strain in the ZnO lattice and thus reducing the electronic contrast between faces.

Figure 3.14a – c and Table 3.9 illustrate that ODPA and F_{13}OPA modification have shifted the VB edge to higher BE (larger ζ values) from that of as-received ZnO, meaning that downwards band bending

has increased. Thus, it appears that both modifiers have added electron density to the surface. ODPA has a dipole moment towards the surface (–2.3 D)[49] and is expected to donate electronic charge to the surface. ODPA-modified ZnO faces have the most negative band bending as well as the highest PA surface concentration (Figure 3.6) relative to F_{13}OPA-modified samples. However, it is unclear at this point whether the tail group or the PA headgroup itself has the major influence on band bending.

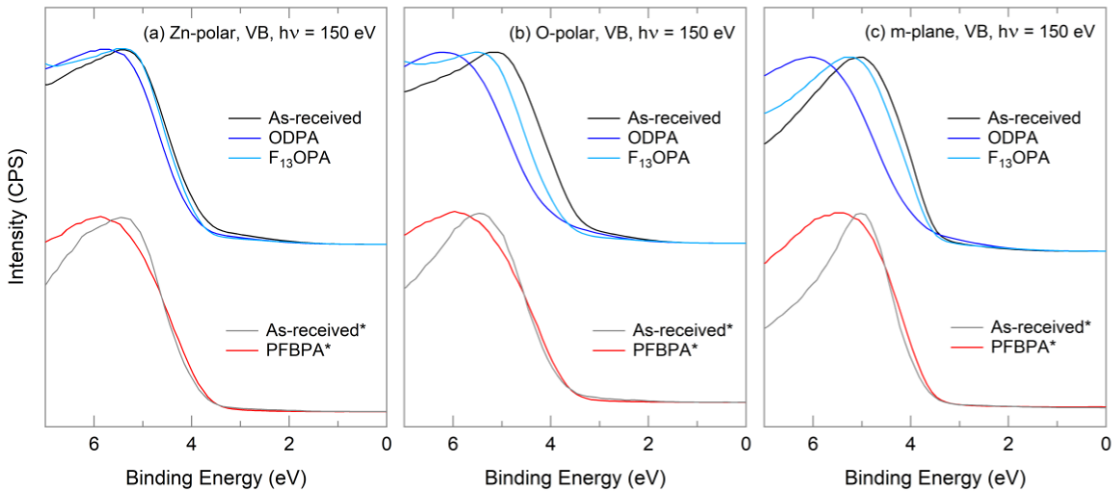

Figure 3.14. Valence band synchrotron XPS results for (a) Zn-polar, (b) O-polar, and (c) m-plane ZnO single crystals modified with ODPA, F_{13}OPA, and PFBPA. All samples Tokyo Denpa unless denoted by * (CrysTec).*

Two factors need to be considered for F_{13}OPA. It has a dipole in the opposite direction to the surface (+1.7 D)[49] arising from the strong electron withdrawing effect of F substituents. The $(CH_2)_2$ moiety between the PA headgroup and fluorinated tail will decrease this electron withdrawing effect, and it is likely that the aliphatic nature of F_{13}OPA prevents electron delocalisation which is required for efficient charge transfer away from the ZnO surface through the modifier.[19] Nevertheless, on all three ZnO faces the increase in downwards V_{bb} is smaller for F_{13}OPA than the ODPA modifier. The second factor to consider in relation to V_{bb} is that F 1s XPS spectra showed a large amount of Zn-F interactions on all three of the F_{13}OPA-modified samples (Figure 3.11d – Figure 3.13d). F is known to act as a shallow donor and will add electron density to its surroundings when part of the lattice, as opposed

to coordinated on the ZnO surface.[50,51] This was shown by Polydorou et al. who used SF_6 plasma to incorporate F into thin film ZnO and showed by UPS that it produced an increase in ζ and a downwards shift in surface bands. As evidenced by XPS measurements in this work, the Zn-polar face has the largest proportion of Zn-F to C-F yet has the smallest ζ change of the three faces. However, the small ζ changes observed on this face with each of the other two PA modifiers (Table 3.9) suggests that changing the band bending on the Zn-polar face is more difficult to achieve. Like ODPA, the effect of the F_{13}OPA headgroup on V_{bb} is unclear.

*Table 3.9. Band bending information for ODPA-, F_{13}OPA-, and PFBPA-modified Zn-polar, O-polar, and m-plane ZnO, from synchrotron XPS valence band regions (hv = 150 eV). Samples are Tokyo Denpa unless denoted by * (CrysTec). All V_{bb} values have an uncertainty of ± 5%.*

Sample	ζ (eV)	V_{bb} (eV)	ΔV_{bb} (eV)
Zn-polar			
As-received	3.74	-0.60	-
ODPA-modified	3.88	-0.74	-0.14
F_{13}OPA-modified	3.83	-0.69	-0.09
As-received*	3.88	-0.59	-
PFBPA-modified*	3.66	-0.37	+0.22
O-polar			
As-received	3.32	-0.18	-
ODPA-modified	3.94	-0.80	-0.62
F_{13}OPA-modified	3.74	-0.59	-0.42
As-received*	3.82	-0.52	-
PFBPA-modified*	3.53	-0.24	+0.28
m-plane			
As-received	3.37	-0.23	-
ODPA-modified	3.77	-0.63	-0.39
F_{13}OPA-modified	3.44	-0.30	-0.07
As-received*	3.90	-0.61	-
PFBPA-modified*	3.53	-0.24	+0.37

Figure 3.14a – c and Table 3.9 show that PFBPA modification decreases downwards band bending by several hundred meV on all ZnO faces. The direction of the ζ shift corresponds to that reported by Timpel et al. for fluorinated PA modifiers on ZnO, which strongly suggests that the opposite ζ shift seen on the F_{13}OPA-modified ZnO in this work was governed by F-Zn interactions.[6] This highlights the need for maintaining the stability of the PA modifier and preventing the formation of donor-like F species. The magnitude of the band bending decrease is smaller than expected and highlights the influence of the phosphonate-ZnO interface dipole on the charge transfer process.

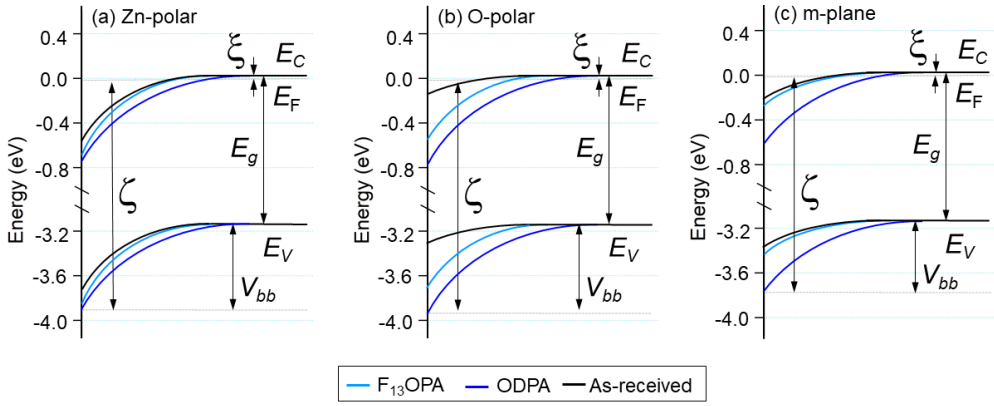

Figure 3.15. Energy-level diagrams showing surface band bending on as-received (black), F_{13}OPA-modified (light blue) and ODPA-modified (blue) faces of (a) Zn-polar, (b) O-polar, and (c) m-plane ZnO.

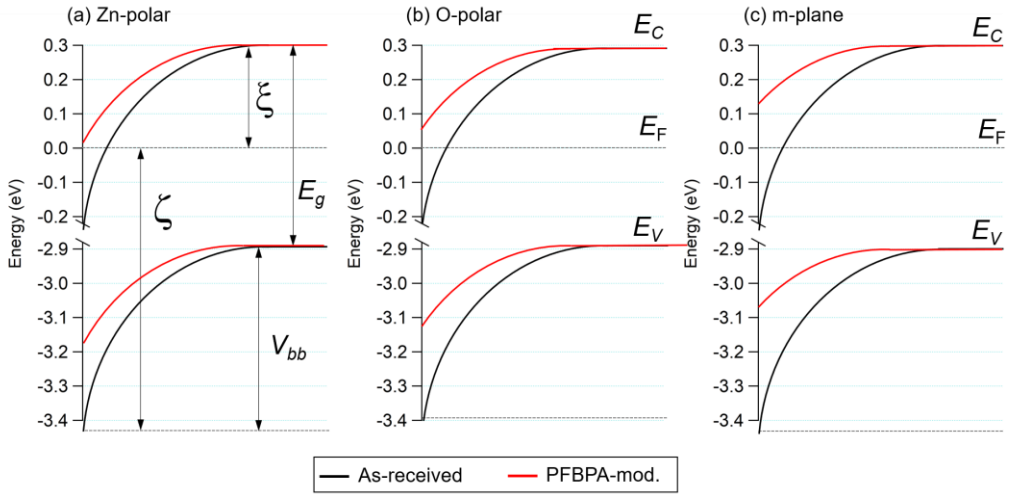

Figure 3.16. Energy-level diagrams showing surface band bending on as-received (black) and PFBPA-modified (red) faces of (a) Zn-polar, (b) O-polar, and (c) m-plane CrysTec ZnO.

Figure 3.15 and Figure 3.16 are energy-level diagrams showing the effects of each modifier (Figure 3.15, ODPA and F_{13}OPA; Figure 3.16, PFBPA). It is assumed that the valence and conduction band bending is the same, though literature suggests this might not be the case. King et al.[52] used angle-resolved photoemission spectroscopy to show that electron accumulation layers on semiconductor surfaces can reduce the band gap by way of increased interactions between the electrons. Consequently, the conduction band would have more downward band bending than the valence band. This effect means that the downwards band bending in the above Tables and Figures may be overestimated, but the relative changes of V_{bb} upon surface modification are still valid. The value of ξ (= kT/q ln(N_c/n), defined in Chapters 1 and 2) is different for each set of crystals: for Tokyo Denpa, it is 0.04 eV, which places the conduction band slightly above the Fermi level, and for CrysTec, it is 0.3 eV, meaning the conduction band is well above the Fermi level. CrysTec samples have lower carrier concentrations that the higher-quality Tokyo Denpa crystals, so the band bending is affected more easily as fewer electrons are present.[53]

Work done in this section showed that ODPA and F_{13}OPA modifiers increased downwards V_{bb} on ZnO, while PFBPA decreased downwards V_{bb}. This indicates that PA tail groups can influence the electron density at ZnO surfaces. Chen et al. reported that hexadecylPA decreased V_{bb} on m-plane ZnO, as measured by Mott-Schottky analysis.[5] However, they noted that the surface attachment was very weak and suggested that the PA was likely bound only by hydrogen bonds. No sonication or annealing was used to remove physisorbed species or form covalent bonds, respectively, so the results are not comparable with this work.

Timpel et al. used synchrotron XPS/UPS to show that F_{13}OPA on Zn-polar ZnO decreased V_{bb}.[6] Importantly, they included supplementary information to show that the F_{13}OPA modifier had not been significantly damaged by XPS. This strongly suggests that the increased downward V_{bb} seen in this work for F_{13}OPA-modified ZnO was significantly influenced by the XPS-induced degradation of F_{13}OPA and subsequent interactions of F with Zn. The expected decrease in V_{bb} was seen on PFBPA-modified

ZnO, which corresponded with the results of Timpel et al. for F_{13}OPA and similar fluorinated PA:[6] A separate XPS and UPS study by Timpel et al. showed p-(trifluoromethyl)phenylPA and phenylPA decreased V_{bb} by 0.1 eV.[30] These PA have no methyl group between the PA and tail group, as for PFBPA and F_{13}OPA, and PFBPA has a weaker dipole than p-(trifluoromethyl)phenylPA (–1.75 D compared to –2.24 D).[54] However, differences in carrier concentrations of the ZnO samples may explain why PFBPA in this work had a larger effect on V_{bb} than stronger electron-withdrawing PA used by Timpel et al. Timpel et al. annealed the ZnO samples to 1000 °C, which is known to increase the carrier concentration at the surface due the migration of shallow donors such as Li and Na into the bulk.[55]

3.3.6 Binding Modes of Phosphonic Acids on ZnO

Several theoretical and experimental studies have investigated binding modes for PAs on ZnO.[6,13,19,30] Consideration of molecular surface concentrations, the relative intensities and BE separation between bulk and surface O (Δ_{surf}) in XPS, and the band bending direction as determined by XPS measurements may all give insight into the PA binding mode.

3.3.6.1 XPS O 1s Spectra and Molecular Surface Concentration

From theoretical studies, an XPS BE shift of surface O 1s relative to bulk O 1s (Δ_{surf}) value of +1.1 eV is associated with tridentate coordination of PA to ZnO, while a value of +2.1 eV corresponds to bidentate binding.[6,13,30] Unbound PA were calculated to have Δ_{surf} of +3.75 eV.[13] These changes occur due to increased electron density near surface O upon PA modification. For as-received ZnO, Δ_{surf} depends on the ZnO face. Table 3.10 shows Δ_{surf} values for as-received ZnO; these were +1.2 eV, +1.7 eV, and +1.4 eV for Zn-polar, O-polar, and m-plane Tokyo Denpa ZnO, respectively, and +1.5 eV, +1.3 eV, and +1.5 eV for Zn-polar, O-polar, and m-plane CrysTec ZnO, respectively. These are similar to that reported for fully-hydroxylated ZnO (1.4 eV).[44] The differences in Δ_{surf} are attributed to the different type of OH termination for each face: such polarity-related differences have been previously observed on polar and non-polar faces of ZnO.[44,46] The differences between the two types of crystals are attributed to the subtleties involved with peak-fitting the XPS spectra.

*Table 3.10. Molecular surface concentrations, Δ_{surf} values, and Zn 3s : O 1s ratios for ODPA-, F_{13}OPA-, and PFBPA-modified Zn-polar, O-polar, and m-plane ZnO. The fractional surface coverage of * was found by comparison of water contact angle with literature values. Synchrotron XPS Zn 3s : P 2p ratios were then used to estimate surface concentrations for other faces and modifiers. ‡ is the as-received sample for PFBPA-modified ZnO (CrysTec).*

Face	Modifier	Molecules nm^{-2}	O 1s Δ_{surf} (eV)	Zn 3s : O 1s
Zn-polar	As-received	-	+1.2	1 : 3.3
	F_{13}OPA*	2	+1.1, +2.5	1 : 3.7
	ODPA	4	+1.1, +2.8	1 : 7.6
	As-received‡	-	+1.5	1 : 6.5
	PFBPA	4	+1.2, +3.3	1 : 10.6
O-polar	As-received	-	+1.7	1 : 5.5
	F_{13}OPA	1	+1.2, +2.3	1 : 5.9
	ODPA	6	+1.1, +2.8	1 : 10.5
	As-received‡	-	+1.3	1 : 9.1
	PFBPA	4	+1.2, +2.7	1 : 11.1
m-plane	As-received	-	+1.4	1 : 3.7
	F_{13}OPA	2	+1.0, +1.9	1 : 4.7
	ODPA	7	+1.2, +2.9	1 : 13.7
	As-received‡	-	+1.5	1 : 10.4
	PFBPA	4	+1.1, +3.0	1 : 7.9

In this work, Δ_{surf} values around ~+1.1 eV are seen on all PA-modified ZnO faces, which suggest the main binding mode is tridentate. However, there are also less-intense O 1s peaks at higher BE. For F_{13}OPA-modified ZnO, the Δ_{surf} values for these are around ~+2.2 eV, consistent with a bidentate binding mode.[6,13] On ODPA- and PFBPA-modified faces, small peaks at ~2.9 eV greater BE than bulk O 1s are present, halfway between literature Δ_{surf} values for bidentate binding (+2.1 eV) and unbound PA (+3.75 eV).[13] This may relate to the surfaces having a combination of these modes. However, relative to the dominant peak, which is indicative of tridentate binding, none of the peaks

corresponding to bidentate or unbound PA are significantly intense, suggesting that tridentate binding is the major binding mode.

From experimental XPS data, Timpel et al. found that F_{13}OPA prefers tridentate binding on ZnO but also had a small amount of bidentate coordination. However, Wood et al. did not experimentally observe bidentate binding for a range of benzylPAs and concluded that bidentate binding is not probable. XPS O 1s studies of hexylPA on O-polar ZnO performed by Perkins revealed only one surface O 1s peak, which was assigned to tridentate binding.[3] These results are consistent with XPS results shown here and suggest that ODPA, F_{13}OPA, and PFBPA are mainly tridentate on all ZnO faces, although ODPA and PFBPA may have some multilayer formation.

In contrast to these results, calculated molecular surface concentrations are shown in Table 3.10. Surface concentration of F_{13}OPA was estimated by comparison of F_{13}OPA-modified ZnO water CA with a literature value. The relationship between XPS P 2p: Zn 3s ratios and molecular surface concentration was used to extrapolate concentrations to other modifiers and faces. A dense PA surface concentration is assumed to indicate bidentate modes; a sparse coverage indicates tridentate binding.[6] Table 3.10 shows that F_{13}OPA modification layers have molecular surface concentrations in agreement with the theoretical maximum surface concentration (2.73 molecules nm^{-2}) for tridentate binding (2, 1, and 2 molecules nm^{-2} for Zn-polar, O-polar, and m-plane faces, respectively). This corresponds to a surface coverage of ~3×10^{-10} mol cm^{-2}, accounting for ~50% of the surface OH groups on Zn-polar and O-polar ZnO, and ~40% of surface OH groups on m-plane ZnO, participating in tridentate PA binding. Coverage of ODPA (4 – 7 molecules nm^{-2}) is much higher than the theoretical maximum surface concentration predicted for tridentate-bound PAs on ZnO and are instead closer to the surface concentration predicted for bidentate binding (5.47 molecules nm^{-2}).[6] This corresponds to ~90% (~75%) of the surface OH groups on the polar (m-plane) ZnO faces participating in bidentate PA binding. However, the presence of multilayers would also cause a higher PA surface concentration, so cannot be ruled out. Timpel et al. were able to observe and attribute peaks to both tri- and bi-dentate

modes for PA-modified ZnO through computationally-aided XPS, but the XPS fitting required for this could not be satisfactorily reproduced for the O 1s spectra obtained in this work. This suggests that the higher molecular surface concentrations observed here for ODPA might be due to physisorbed multilayers on top of a tridentate-bound layer. This would explain the water CA being slightly lower than literature values, as hydrophilic PA groups might be at the air-surface interface. The large surface O 1s signal for ODPA- and PFBPA-modified samples relative to those for as-received ZnO (Table 3.10) can also be explained by such a layer structure. AFM images (Figure 3.4) showed evidence of small clumps of PFBPA on ZnO, similar to other PA modifiers. Multilayer 'islands' have previously been reported on PA-modified ZnO,[5] but have been assumed to be removed via sonication.[22,56]

3.3.6.2 Band Bending Direction

In a computational study, Wood et al. calculated that bidentate binding of PA on ZnO gives a ζ value dictated by O 2p orbitals of the ZnO surface and PA head group.[13] In contrast, tridentate binding allows for the effect of the attached PA tail group to influence ζ. In this work, ODPA-modified ZnO samples have more positive ζ values than as-received samples. This could be due to the electron-donating alkyl chain, or bidentate binding of the PA contributing to increased downwards V_{bb}; this binding mode is thus unclear. For PFBPA-modified ZnO, the value of ζ shifted to more negative values, reflecting the electron-withdrawing properties of the fluorinated aromatic ring. This suggests tridentate binding for PFBPA. F_{13}OPA cannot be reliably considered this way, because of the presence of Zn-F interactions whose effect on V_{bb} is likely significant.

3.3.6.3 Summary

Table 3.11 summarises the binding mode results based on molecular surface concentrations derived from F_{13}OPA water contact angles and synchrotron XPS (Figure 3.6), O 1s intensities and BE shifts (Table 3.4), and the direction of band bending derived from synchrotron XPS (Table 3.9). For each modifier, there was no significant difference between ZnO faces. Evidence presented in Table 3.11 determines conclusively that F_{13}OPA is bound in a tridentate arrangement on Zn-polar, O-polar, and

m-plane ZnO. This is in accord with literature reports.[6] For PFBPA and ODPA, the evidence is less clear and it is most likely that they bind with a mixture of bi- and tri-dentate coordination on all faces, with PFBPA likely having significant tridentate coordination. Infrared spectroscopy by Hotchkiss et al. suggested that ODPA is bound tridentate on ZnO, though lesser amounts of bidentate binding modes could not be ruled out. Ostapenko et al. carried out a thorough study on the binding mode of phenylPA on Zn-polar, O-polar, and m-plane ZnO using XPS, near-edge X-ray adsorption fine structure spectroscopy, thermal desorption spectroscopy, and computational work.[57] They observed that for unhydroxylated ZnO, tridentate binding was only possible on Zn-polar ZnO due to steric constraints. However, OH-terminated ZnO was able to promote deprotonation of phenylPA to give tridentate binding as well as bidentate binding on all faces. This is consistent with the work presented here. Finally, the high surface concentrations of ODPA and PFBPA on ZnO suggest that there is some multilayer formation on these modified surfaces.

Table 3.11. Summary of experimental evidence for bi- or tri-dentate binding modes of F_{13}OPA, ODPA, and PFBPA on ZnO. Findings apply to all ZnO faces.

Modifier	Molecular surface concentration	XPS O 1s spectrum (Δ_{surf})	Amount of surface O 1s	Band bending direction
F_{13}OPA	Tri	Tri	Tri	(Uncertain)
ODPA	Bi or multilayer	Tri	Bi or multilayer	Tri/bi
PFBPA	Bi or multilayer	Tri	Bi or multilayer	Tri

3.3.7 Stability of Phosphonic Acid-Modified ZnO in Air and Darkness

Freshly-prepared ODPA- and PFBPA-modified O-polar ZnO samples were analysed with fixed-energy XPS before and after storage in air at 22 ± 2 °C in the dark for 60 d. Results are summarised in Table 3.12. The P 2p + Zn 3s regions, shown in Figure 3.17a and b, were accidentally truncated but a comparison between freshly-prepared and 60-day-old samples was still possible by taking a linear background for all P 2p regions and comparing the peak area to the corresponding Zn 2p peak area

(BE = 1022 eV). This fitting understates the true intensity of the P 2p peak, as it does not account for the overlap with the neighbouring Zn 3s peak, but for the purposes of comparison, it is valid.

Table 3.12. Atomic percentages from fixed-energy XPS survey spectra on ODPA- and PFBPA-modified O-polar ZnO before (fresh) and after storage for 60 d (after) in ambient dark conditions.

Atomic %	C 1s %	O 1s %	P 2p %	F 1s %	Zn 2p %
ODPA, fresh	34	49	0.3	-	17
ODPA, after	40	37	0.3	-	23
PFBPA, fresh	51	25	0.4	0.7	23
PFBPA, after	46	28	0.4	0.7	25

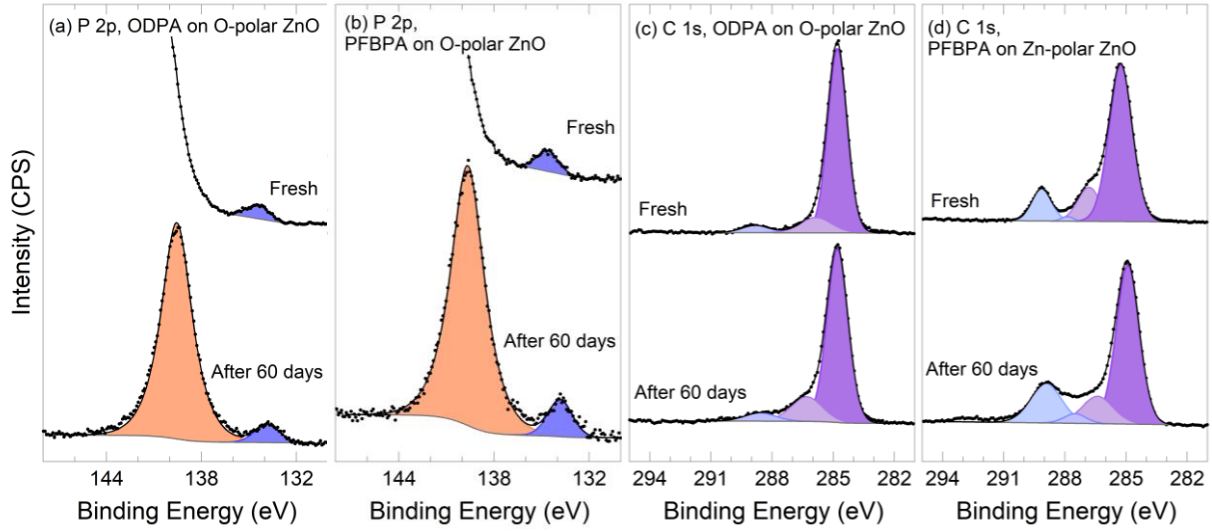

Figure 3.17. (a, b) XPS P 2p spectra and (c, d) XPS C 1s spectra for (a, c) ODPA-modified O-polar and (b, d) PFBPA-modified Zn-polar ZnO 1 d after modification and 60 d after analysis and storage in ambient lab conditions. Spectra are normalised to the same Zn 2p peak area. The Zn 3s peaks are fitted with GL(70). Due to poor communication with XPS technician, the fresh P 2p spectra lack the Zn 3s peak.

Figure 3.17a and b show that no significant change in the P 2p intensities occurs on either sample after storage. The C 1s spectra (Figure 3.17c and d) are as expected for ODPA and PFBPA modification layers. Of interest are the C-C region for ODPA-modified ZnO (BE = 284.8 eV), and the C-F region for PFBPA (BE = 289 eV). Minor changes in the amount of adventitious C-O and C=O present on the PFBPA surface are seen over time.

ODPA- and PFBPA-modified ZnO were both stable when stored for 60 d at room temperature in the dark, with no significant loss of PA head group or tail group. This is a promising start for use of PA-modified ZnO in device applications.

3.3.8 Persistent Photoconductivity on ODPA-Modified ZnO

As outlined in Section 1.1.3, ZnO possesses persistent photoconductivity (PPC) properties which are not ideal for UV-related device applications. ODPA-modified ZnO was tested to determine if the modification layer led to a change in the PPC behaviour. As resistivity measurements are not surface-sensitive, MBE-grown thin-film O-polar ZnO (210 nm) was used to minimise the effects of bulk ZnO. Figure 3.18 shows there is a decrease in resistivity upon UV illumination at 365 nm of bare ZnO which returns to its original value after 2 d in air, though storage in vacuum or nitrogen prolongs the PPC effect (inset, Figure 3.18). The results for the ODPA-modified sample show that the initial resistivity was larger than for the as-received sample, showing that the attachment of PA molecules increased the overall resistivity. Similarly, the minimum resistivity reached upon UV illumination was achieved after 30 s for the bare sample, and 10 min for the ODPA-modified sample. After UV illumination was removed, the ODPA-modified sample (Figure 3.18) took a much longer time to recover to its initial resistivity, with a total recovery time of ~2 weeks (not shown). This is ~8 times longer than taken for as-received ZnO to return to its initial resistivity. As discussed in Section 1.1.3, the proposed mechanism for PPC is dependent on desorption and physisorption of atmospheric species on the surface of ZnO,[58] and these data show that PPC decreases faster when oxygen and air species are present. The ODPA modification, which gave the densest modification of all the trialled PAs, is expected to block the transfer of species from the air to the ZnO surface, and vice versa, and enhance the PPC effect. The difference between the illumination time required to reach a minimum resistivity value on the bare and modified samples (20 times longer for the modified sample) suggests that the ODPA molecules hindered the desorption of physisorbed O_2 and H_2O from the ZnO surface as well as re-adsorption.

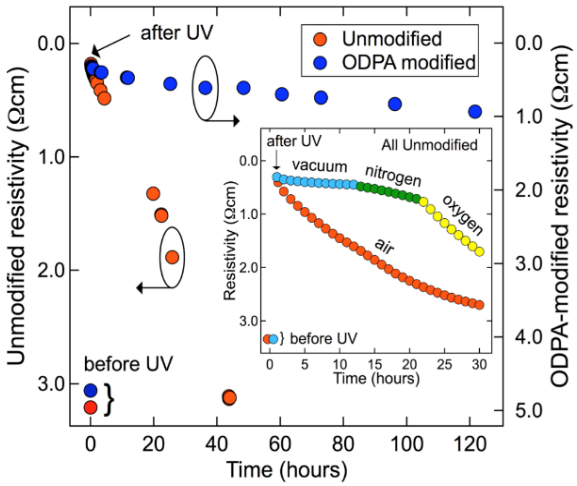

Figure 3.18. Resistivity changes of as-received and ODPA-modified MBE-grown O-polar ZnO upon and after UV illumination in air (hv = 365 nm). Inset: Effect of atmosphere (vacuum, 1 atm nitrogen, 1 atm oxygen, air) on the recovery time of as-received ZnO. Collected by Adam Hyndman.

The increased lifetime of PPC on ODPA-modified ZnO points to surface modification as a possible method for stabilising device performance. These applications would require the PA films be stable long-term to UV light, so this factor was investigated in further experiments.

3.3.9 Effect of Light on Phosphonic Acid-Modified ZnO

3.3.9.1 Water Contact Angle Analysis of the Effect of UV Light on Phosphonic Acid-Modified ZnO

The UV stability of ODPA and F_{13}OPA films on each of the ZnO faces was probed via water CA measurements. It is known that as-received ZnO surfaces become hydrophilic when exposed to UV light;[59] this is thought to be due to the desorption of hydrophobic molecular O_2 from the surface.[60] Figure 3.19 shows this effect on each of the unmodified Zn-polar, O-polar, and m-plane faces of single-crystal ZnO after 1 h of irradiation with 0.2 mW, 300 nm UV light. CA measured after the UV irradiation show that the surfaces become much less hydrophobic but return to their original levels of hydrophobicity within several days of storage in the dark.

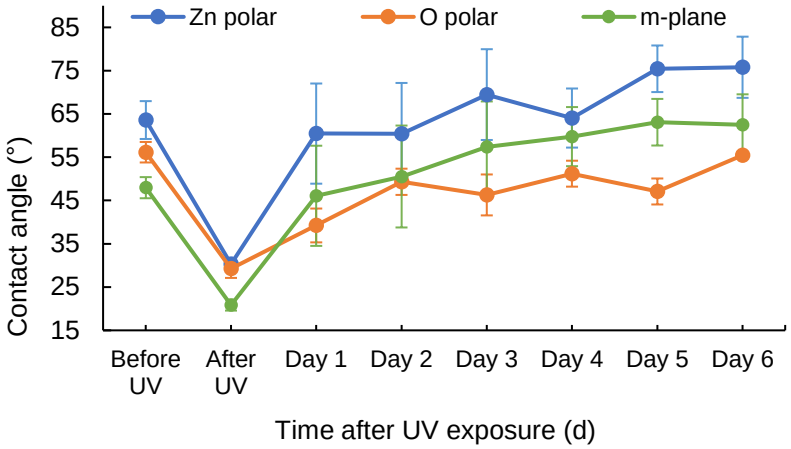

Figure 3.19: Water contact angles on bare Zn-polar, O-polar, and m-plane ZnO before and after irradiation with 1 h of 0.2 mW, 300 nm UV light.

The large decrease in hydrophobicity was not seen when the same treatment was given to samples which had been modified with PA layers (Figure 3.20). The surfaces proved to be mostly unchanged by UV light, with only a small decrease in CA upon irradiation, and CAs remained consistent in the days following, during which the samples were stored in the dark. Water CA is determined by the wettability of the PA modification layer, not the underlying ZnO substrate. As such, UV-induced changes on the PA-modified ZnO surface should not affect the CA. However, a week later the samples were re-irradiated with UV light, and a significant increase in hydrophilicity was seen. Section 3.3.7 showed that minimal decomposition of PA layers occurs in storage in the dark, so this is attributed to the deterioration of the PA films under UV light that allowed for the water droplet to penetrate the organic layer and in turn be affected by the UV-affected ZnO surface itself. This was observed on all faces except for the ODPA-modified O-polar and m-plane faces, suggesting that these two modified faces are more stable to UV light than their as-received counterparts. From XPS, the ODPA-modified O-polar and m-plane faces were shown to have much higher calculated surface concentrations than the ODPA-modified Zn-polar face and all F_{13}OPA-modified faces, and the increased molecular density and van der Waals attractions of the ODPA layers on O-polar and m-plane ZnO may account for the increased stability of the monolayers on these two faces. Additionally, the increased catalytic nature

of Zn-polar ZnO compared to O-polar ZnO may contribute to faster degradation of ODPA on Zn-polar ZnO (Section 1.1.1.1).

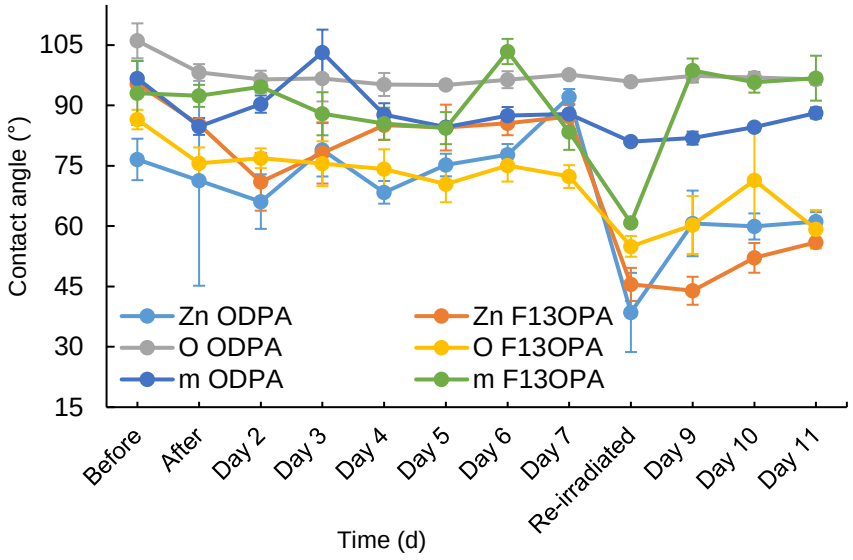

Figure 3.20: Water contact angles over time after UV irradiation (1 h, 300 nm, 0.2 mW) for ODPA- and F_{13}OPA-modified Zn-polar, O-polar, and m-plane ZnO.

3.3.9.2 Fixed-Energy XPS Analysis of Effect of UV Light on PFBPA-Modified ZnO

XPS measurements were carried out to further investigate the effect of UV light on PA layer stability. PFBPA was used for these measurements because F is a useful marker and the modification layers underwent minimal degradation during XPS analysis (Section 3.3.5.2). Here, fixed-energy XPS was used to probe the stability of PFBPA layers under UV irradiation, using F and P as a measure of molecular degradation. Atomic percentages and core level XPS spectra, before and after UV irradiation, can be seen in Table 3.13 and Figure 3.21, respectively.

Table 3.13. Atomic percentages from fixed-energy XPS survey spectra for PFBPA-modified ZnO, before (fresh) and after hv = 300 nm UV irradiation (after UV).

Atomic %	C 1s %	O 1s %	P 2p %	F 1s %	Zn 2p %
PFBPA, fresh	31	38	3	8	19
PFBPA, after UV	20	49	3	2	26

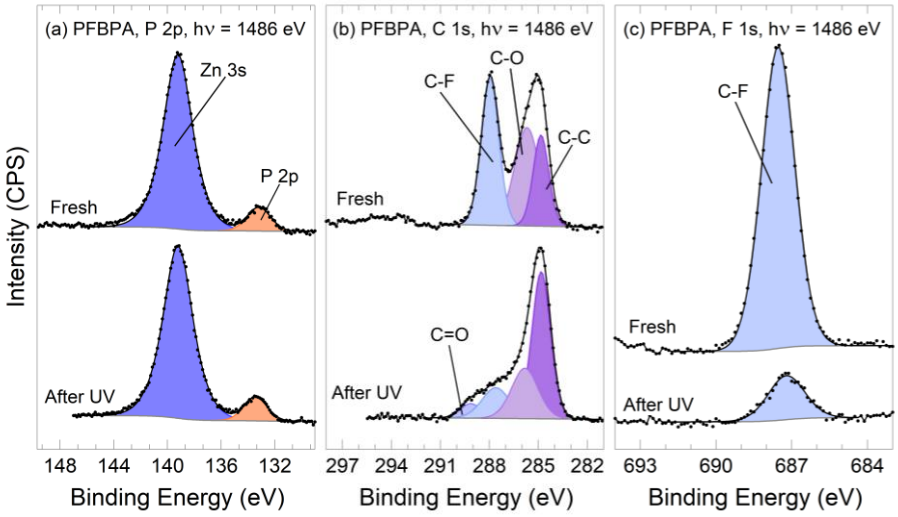

Figure 3.21. Fixed-energy XPSP 2p, C 1s, and F 1s spectra for PFBPA-modified m-plane ZnO before and after UV irradiation (hν = 254 nm). Spectra have been normalised to the same Zn 2p peak area and offset for clarity.

Figure 3.21a shows that the amount of phosphorous on the PFBPA-modified sample was very similar before and after UV exposure. However, the C 1s and F 1s spectra (Figure 3.21b and c) show a decrease in the amount of F on the surface after UV treatment. In the case of C 1s, the C-F signal at ~288 eV is significantly reduced by 67% while the F 1s peak is attenuated also, by 84%. Interestingly, there is no evidence of Zn-F interactions, as seen under X-ray damage conditions with synchrotron XPS (Section 3.3.9.3). This indicates that either the cleavage mechanism is different when induced by UV or by photoelectrons produced during fixed-energy XPS analysis, and/or that the PFBPA molecules on this sample are better-packed and as such do not allow liberated F to interact with the ZnO surface. However, even with surface-sensitive synchrotron XPS, only a small signal originating from F-Zn interactions was seen on PFBPA-modified ZnO, suggesting that PFBPA films are generally less porous to liberated F than F_{13}OPA layers.

The C 1s satellite peak at around 295 eV, attributed to π-π*, disappears when the sample is irradiated. This suggests that not only is the modification layer losing F, but its aromatic rings are also degrading. A 11% decrease in C 1s signal is also seen. While a peak at 289 eV appears on the irradiated sample,

this corresponds to C=O bonds in adventitious carbon, and it is likely that it is also present in the fresh sample but masked by the large C-F signal.

Evidently the effect of UV irradiation on PFBPA-modified ZnO is similar for ODPA on titania: Kanta et al. reported no change in XPS P 2p signal after UV exposure on ODPA-modified titania surfaces, but saw degradation of the alkyl chain and attributed it to the catalytic properties of titania.[10] It is concluded that UV light degrades the tail end of PA layers but does not cleave the phosphonate linkage.

3.3.9.3 Effect of Light-Induced Damage on Band Bending of PFBPA-Modified ZnO

To investigate the effect of PFBPA degradation on the band bending of ZnO, in situ degradation of PFBPA modification layers was undertaken using synchrotron XPS. This modifier was of interest as it was the only PA to give a reduction in downward band bending on ZnO and exhibited only small amounts of Zn-F interactions. By examining the effect of deliberately decomposing the tail group and liberated F on the band bending, it was expected to give insight into the factors affecting band bending of F_{13}OPA. PFBPA layers on Zn-polar and m-plane faces were repeatedly scanned in the F 1s region (hv = 835 eV) for approximately 15 min, at a higher photon flux than usually employed. In the F 1s spectrum (Figure 3.22b and Figure 3.23a), liberation of F from the organic film can be seen, as can a small increase in the Zn-F signal. The total amount of F on each surface remained constant. Figure 3.22b and Figure 3.23b show negligible change in P 2p signal after X-ray irradiation.

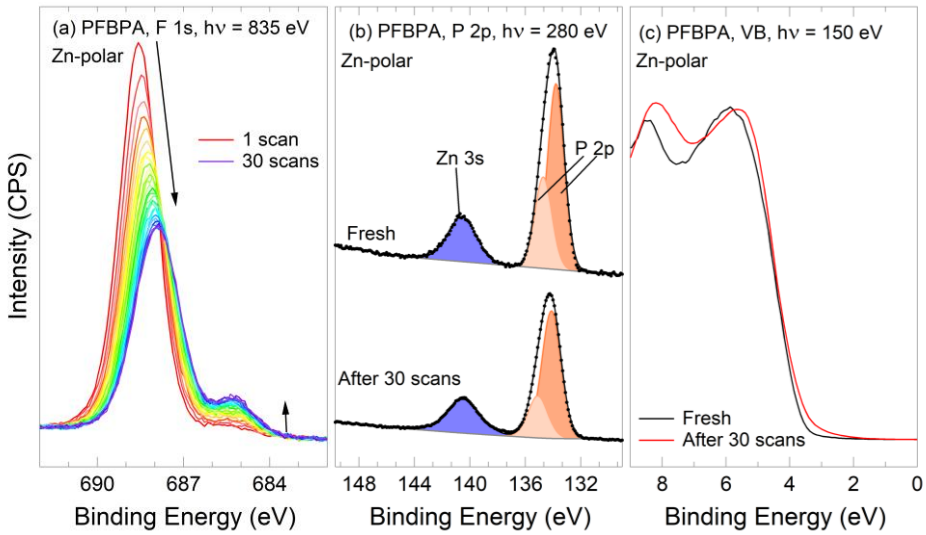

Figure 3.22. Synchrotron XPS spectra for PFBPA-modified Zn-polar ZnO. (a) F 1s region upon continuous single scans for 15 min, (b) P 2p + Zn 3s region before and after the continuous scans on the F 1s region, and (c) valence band region for the same.

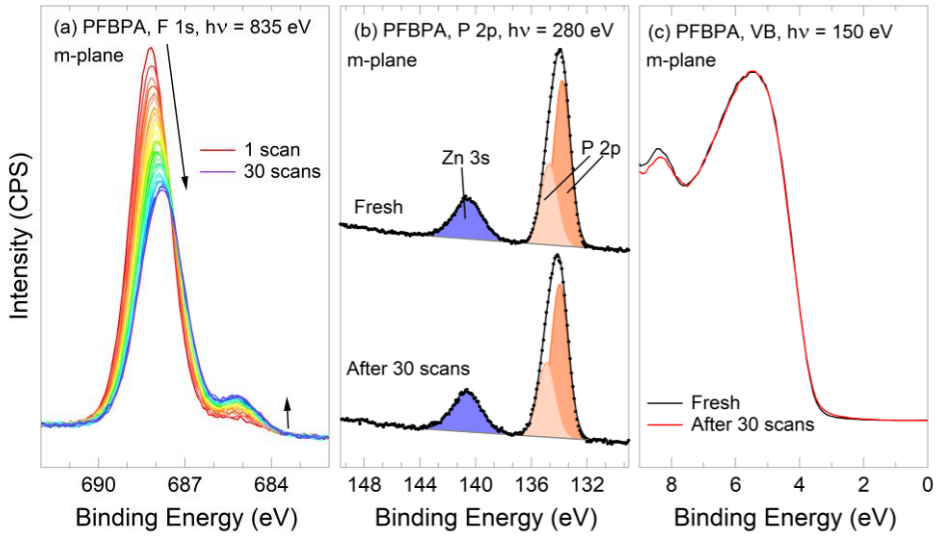

Figure 3.23. Synchrotron XPS spectra for PFBPA-modified m-plane ZnO. (a) F 1s region upon continuous single scans for 15 min, (b) P 2p + Zn 3s region before and after the continuous scans on the F 1s region, and (c) valence band region for the same.

There is very little change in the band bending on either face after degradation of PFBPA. This suggests that band bending is mainly influenced on the PA headgroup, as expected for a bidentate-bound PA.[13] However, there is still significant signal arising from C-F bonds after the repeated scans were stopped,

suggesting that not all the PFBPA was decomposed, which may explain why no change in band bending was seen (Figure 3.22c and Figure 3.23c). Compared to the damage noted on F_{13}OPA-modified ZnO (Section 3.3.5.1), the ratio of Zn-F:C-F for PFBPA-modified samples is very small and the corresponding effect on band banding is assumed to be negligible. The shape of the Zn-polar VB changes with PFBPA degradation. Given that both Zn-polar and m-plane PFBPA had similar levels of PFBPA decomposition, but Zn-polar ZnO had a larger amount of Zn-F form, this change in valence band is attributed to the Zn-F interactions. If these are minimised, as for m-plane ZnO, the change in the valence band region is apparently also minimised.

Table 3.14 quantifies the changes that occurred upon continued XPS scanning. Initially, Zn-polar and m-plane faces have similar ratios of C-F and Zn-F in the F 1s region, although the m-plane face has a slightly higher P 2p %, indicating that it has more PAs on the surface. During the F 1s scans, the C-F peaks on both faces decrease by ~65%. However, the Zn-F peak on the Zn-polar face increases 3 times in size, compared to the m-plane which increases by less than a factor of 2. This shows that a fraction of the liberated F interacts with the Zn-polar face more than the m-plane face, probably due to a combination of different facial geometry and terminating atoms, and a more complete PA surface concentration on the m-plane face.

Table 3.14. Synchrotron XPS data for PFBPA-modified Zn-polar and m-plane ZnO before and after continuous scans at the F 1s region for 15 min. [a] *Percentage of F 1s spectrum.* [b] *Percentage of Zn 3s + P 2p spectrum.*

Samples	**Percentages**					
	C-F %[a]	Zn-F %[a]	$C\text{-}F_{fin}/C\text{-}F_{ini}$	$Zn\text{-}F_{fin}/Zn\text{-}F_{ini}$	Zn 3s %[b]	P 2p %[b]
Zn-polar						
Fresh	96	4	-	-	26	74
After 30 scans	85	15	0.6	3.1	25	75
m-plane						
Fresh	93	7	-	-	21	79
After 30 scans	88	12	0.7	1.4	22	78

3.4 Conclusions

A variety of PAs has been attached to Zn-polar, O-polar, and m-plane ZnO surfaces using an optimised method, with the highest surface concentration typically calculated for the O-polar and m-plane faces. F_{13}OPA is shown to bind to ZnO in a highly-dominant tridentate mode, while ODPA and PFBPA bind in a mixture of bi- and tri-dentate modes, with the formation of multilayers likely.

Synchrotron XPS revealed that downward surface band bending on ZnO became more negative upon attachment of ODPA and F_{13}OPA, while PFBPA reduced the downward band bending by ~0.2 eV, assumed to be due to the aromatic, electron-withdrawing effects of the PFBPA tail group. This suggests that PFBPA has significant tridentate coordination, which allows for the tail group to influence the band bending. While tridentate-bound F_{13}OPA was expected to have a similar effect as PFBPA, decomposition of the PA during XPS analysis resulted in F interactions with Zn, which are thought to have an electron donating effect.

While the modifiers showed excellent stability when stored in dark conditions for 2 months, the stability was poor under UV light and synchrotron XPS irradiation. Degradation of PFBPA under XPS X-rays did not show a significant change in band bending, emphasising that the phosphonate head group plays a large role in determining the surface charge transfer and therefore band bending, and that PFBPA modification layers do not have to be fully intact to retain their effect on the band bending. This behaviour is consistent with bidentate coordination, although the PFBPA modifiers were not completely decomposed. Although PFBPA layers on both Zn-polar and m-plane ZnO underwent the same quantitative loss of organic F, the Zn-polar face saw double the amount of Zn-bound F than the m-plane. This suggested that the layers were denser on the m-plane and showed that the amount of Zn-F interactions does change the VB spectra.

PPC effects on ZnO were prolonged by the addition of ODPA, showing that the modification layer slows down the transfer of atmospheric species from air to the ZnO surface, and vice versa. While the organic film is not impermeable to atmospheric species, it increases the time taken to return to

original resistivity from 2 d to 2 weeks. This is a promising start to making photostable devices with ZnO, though it should be noted that ODPA modification also doubled the resistivity of the as-received sample, which may introduce other practical problems.

In summary, several PA modification layers were successfully attached to Zn-polar, O-polar, and m-plane ZnO via immersion and annealing. They provide an excellent route for increasing the negative band bending of ZnO, provided they are not exposed to UV light. Although PFBPA was able to decrease the band bending, it could not remove it entirely. The following chapters describe investigations of other modifiers and their effects on band bending.

3.5 References

(1) Guerrero, G.; Alauzun, J. G.; Granier, M.; Laurencin, D.; Mutin, P. H. Phosphonate Coupling Molecules for the Control of Surface/Interface Properties and the Synthesis of Nanomaterials. *Dalt. Trans.* **2013**, *42* (35), 12569.

(2) Kassaee, M. Z.; Movahedi, F.; Masrouri, H. ZnO Nanoparticles as an Efficient Catalyst for the One-Pot Synthesis of α-Amino Phosphonates. *Synlett* **2009**, No. 8, 1326–1330.

(3) Perkins, C. L. Molecular Anchors for Self-Assembled Monolayers on ZnO: A Direct Comparison of the Thiol and Phosphonic Acid Moieties. *J. Phys. Chem. C* **2009**, *113* (42), 18276–18286.

(4) Hotchkiss, P. J.; Malicki, M.; Giordano, A. J.; Armstrong, N. R.; Marder, S. R. Characterization of Phosphonic Acid Binding to Zinc Oxide. *J. Mater. Chem.* **2011**, *21* (9), 3107–3112.

(5) Chen, J.; Ruther, R. E.; Tan, Y.; Bishop, L. M.; Hamers, R. J. Molecular Adsorption on ZnO($10\bar{1}0$) Single-Crystal Surfaces: Morphology and Charge Transfer. *Langmuir* **2012**, *28* (28), 10437–10445.

(6) Timpel, M.; Nardi, M. V.; Krause, S.; Ligorio, G.; Christodoulou, C.; Pasquali, L.; Giglia, A.; Frisch, J.; Wegner, B.; Moras, P.; Koch, N. Surface Modification of ZnO(0001)-Zn with Phosphonate-Based Self-Assembled Monolayers: Binding Modes, Orientation, and Work Function. *Chem. Mater.* **2014**, *26* (17), 5042–5050.

(7) Paniagua, S. A.; Hotchkiss, P. J.; Jones, S. C.; Marder, S. R.; Mudalige, A.; Marrikar, F. S.; Pemberton, J. E.; Armstrong, N. R. Phosphonic Acid Modification of Indium-Tin Oxide Electrodes: Combined XPS/UPS/Contact Angle Studies. *J. Phys. Chem. C* **2008**, *112* (21), 7809–7817.

(8) Chen, X.; Luais, E.; Darwish, N.; Ciampi, S.; Thordarson, P.; Gooding, J. J. Studies on the Effect of Solvents on Self-Assembled Monolayers Formed from Organophosphonic Acids on Indium Tin Oxide. *Langmuir* **2012**, *28* (25), 9487–9495.

(9) Gao, W.; Dickinson, L.; Grozinger, C.; Morin, F. G.; Reven, L. Self-Assembled Monolayers of Alkylphosphonic Acids on Metal Oxides. *Langmuir* **1996**, *12* (26), 6429–6435.

(10) Kanta, A.; Sedev, R.; Ralston, J. The Formation and Stability of Self-Assembled Monolayers of Octadecylphosphonic Acid on Titania. *Colloids Surfaces A* **2006**, *291* (1–3), 51–58.

(11) Rivest, J. B.; Li, G.; Sharp, I. D.; Neaton, J. B.; Milliron, D. J. Phosphonic Acid Adsorbates Tune the Surface Potential of TiO_2 in Gas and Liquid Environments. *J. Phys. Chem. Lett.* **2014**, *5* (14), 2450–2454.

(12) Geldof, D.; Tassi, M.; Carleer, R.; Adriaensens, P.; Roevens, A.; Meynen, V.; Blockhuys, F. Binding Modes of Phosphonic Acid Derivatives Adsorbed on TiO_2 Surfaces: Assignments of Experimental IR and NMR Spectra Based on DFT/PBC Calculations. *Surf. Sci.* **2017**, *655* (July 2016), 31–38.

(13) Wood, C.; Li, H.; Winget, P.; Brédas, J. L. Binding Modes of Fluorinated Benzylphosphonic Acids on the Polar ZnO Surface and Impact on Work Function. *J. Phys. Chem. C* **2012**, *116* (36), 19125–19133.

(14) Braid, J. L.; Koldemir, U.; Sellinger, A.; Collins, R. T.; Furtak, T. E.; Olson, D. C. Conjugated Phosphonic Acid Modified Zinc Oxide Electron Transport Layers for Improved Performance in Organic Solar Cells. *ACS Appl. Mater. Interfaces* **2014**, *6* (21), 19229–19234.

(15) Lange, I.; Reiter, S.; Kniepert, J.; Piersimoni, F.; Pätzel, M.; Hildebrandt, J.; Brenner, T.; Hecht, S.; Neher, D. Zinc Oxide Modified with Benzylphosphonic Acids as Transparent Electrodes in Regular and Inverted Organic Solar Cell Structures. *Appl. Phys. Lett.* **2015**, *106* (11), 113302.

(16) Smecca, E.; Motta, A.; Fragalaì, M. E.; Aleeva, Y.; Condorelli, G. G. Spectroscopic and Theoretical Study of the Grafting Modes of Phosphonic Acids on ZnO Nanorods. *J. Phys. Chem. C* **2013**, *117* (10), 5364–5372.

(17) Kedem, N.; Blumstengel, S.; Henneberger, F.; Cohen, H.; Hodes, G.; Cahen, D. Morphology-, Synthesis- and Doping-Independent Tuning of ZnO Work Function Using Phenylphosphonates. *Phys. Chem. Chem. Phys.* **2014**, *16* (18), 8310.

(18) Zhang, B.; Kong, T.; Xu, W.; Su, R.; Gao, Y.; Cheng, G. Surface Functionalization of Zinc Oxide by Carboxyalkylphosphonic Acid Self-Assembled Monolayers. *Langmuir* **2010**, *26* (6), 4514–4522.

(19) Lange, I.; Reiter, S.; Pätzel, M.; Zykov, A.; Nefedov, A.; Hildebrandt, J.; Hecht, S.; Kowarik, S.; Wöll, C.; Heimel, G.; Neher, D. Tuning the Work Function of Polar Zinc Oxide Surfaces Using Modified Phosphonic Acid Self-Assembled Monolayers. *Adv. Funct. Mater.* **2014**, *24* (44), 7014–7024.

(20) Vega, A.; Thissen, P.; Chabal, Y. J. Environment-Controlled Tethering by Aggregation and Growth of Phosphonic Acid Monolayers on Silicon Oxide. *Langmuir* **2012**, *28* (21), 8046–8051.

(21) Hotchkiss, P. J. *Design, Synthesis, and Use of Phosponic Acids for the Surface Modification of Metal Oxides*; 2008.

(22) Gouzman, I.; Dubey, M.; Carolus, M. D.; Schwartz, J.; Bernasek, S. L. Monolayer vs. Multilayer Self-Assembled Alkylphosphonate Films: X-Ray Photoelectron Spectroscopy Studies. *Surf. Sci.* **2006**, *600* (4), 773–781.

(23) Hanson, E. L.; Schwartz, J.; Nickel, B.; Koch, N.; Danisman, M. F. Bonding Self-Assembled, Compact Organophosphonate Monolayers to the Native Oxide Surface of Silicon. *J. Am. Chem. Soc.* **2003**, *125* (51), 16074–16080.

(24) Bulusu, A.; Paniagua, S. A.; Macleod, B. A.; Sigdel, A. K.; Berry, J. J.; Olson, D. C.; Marder, S. R.; Graham, S. Efficient Modification of Metal Oxide Surfaces with Phosphonic Acids by Spray Coating. *Langmuir* **2013**, *29* (12), 3935–3942.

(25) Gawalt, E.; Avaltroni, M.; Koch, N.; Schwartz, J. Self-Assembly and Bonding of Alkane Phosphonic Acids on the Native Oxide Surface of Titanium. *Langmuir* **2001**, No. 17, 5736–5738.

(26) Quiñones, R.; Shoup, D.; Behnke, G.; Peck, C.; Agarwal, S.; Gupta, R.; Fagan, J.; Mueller, K.; Iuliucci, R.; Wang, Q. Study of Perfluorophosphonic Acid Surface Modifications on Zinc Oxide Nanoparticles. *Materials* **2017**, *10* (12), 1363.

(27) Colorado, R.; Lee, T. R. Physical Organic Probes of Interfacial Wettability Reveal the Importance of Surface Dipole Effects. *J. Phys. Org. Chem.* **2000**, *13* (12), 796–807.

(28) Ford, W. E.; Abraham, F.; Scholz, F.; Nelles, G.; Sandford, G.; Von Wrochem, F. Spectroscopic Characterization of Fluorinated Benzylphosphonic Acid Monolayers on AlO_x/Al Surfaces. *J. Phys. Chem. C* **2017**, *121* (3), 1690–1703.

(29) Dou, R. F.; Ma, X. C.; Xi, L.; Yip, H. L.; Wong, K. Y.; Lau, W. M.; Jia, J. F.; Xue, Q. K.; Yang, W. S.; Ma, H.; Jen, A. K. Y. Self-Assembled Monolayers of Aromatic Thiols Stabilized by Parallel-Displaced π-π Stacking Interactions. *Langmuir* **2006**, *22* (7), 3049–3056.

(30) Timpel, M.; Nardi, M. V.; Ligorio, G.; Wegner, B.; Pätzel, M.; Kobin, B.; Hecht, S.; Koch, N. Energy-Level Engineering at ZnO/Oligophenylene Interfaces with Phosphonate-Based Self-Assembled Monolayers. *ACS Appl. Mater. Interfaces* **2015**, *7* (22), 11900–11907.

(31) Chockalingam, M.; Darwish, N.; Le Saux, G.; Gooding, J. J. Importance of the Indium Tin Oxide Substrate on the Quality of Self-Assembled Monolayers Formed from Organophosphonic Acids. *Langmuir* **2011**, *27* (6), 2545–2552.

(32) Paukku, Y.; Michalkova, A.; Leszczynski, J. Quantum-Chemical Comprehensive Study of the Organophosphorus Compounds Adsorption on Zinc Oxide Surfaces. *J. Phys. Chem. C* **2009**, *113* (4), 1474–1485.

(33) Chen, D.; Yin Wu, H. K.; Naderi-Gohar, S.; Wu, Y.; Huang, Y.; Nie, H.-Y. An Extremely Rapid Dip-Coating Method for Self-Assembly of Octadecylphosphonic Acid and Its Thermal Stability on an Aluminum Film. *J. Mater. Chem. C* **2014**, *2* (46), 9941–9948.

(34) Koh, S. E.; McDonald, K. D.; Holt, D. H.; Dulcey, C. S.; Chaney, J. A.; Pehrsson, P. E. Phenylphosphonic Acid Functionalization of Indium Tin Oxide: Surface Chemistry and Work Functions. *Langmuir* **2006**, *22* (14), 6249–6255.

(35) Sharma, A.; Kippelen, B.; Hotchkiss, P. J.; Marder, S. R. Stabilization of the Work Function of Indium Tin Oxide Using Organic Surface Modifiers in Organic Light-Emitting Diodes. *Appl. Phys. Lett.* **2008**, *93* (16).

(36) Hotchkiss, P. J.; Jones, S. C.; Paniagua, S. A.; Sharma, A.; Kippelen, B.; Armstrong, N. R.; Marder, S. R. The Modification of Indium Tin Oxide with Tuning of Surface Properties, and Potential for Use in Organic Electronic Applications. *Acc. Chem. Res.* **2011**, *45* (3), 337–346.

(37) Wang, M.; Hill, I. G. Fluorinated Alkyl Phosphonic Acid SAMs Replace PEDOT:PSS in Polymer Semiconductor Devices. *Org. Electron.* **2012**, *13* (3), 498–505.

(38) Hanwell, M. D.; Curtis, D. E.; Lonie, D. C.; Vandermeersch, T.; Zurek, E.; Hutchison, G. R. Avogadro: An Advanced Semantic Chemical Editor, Visualisation, and Analysis Platform. *J. Chem. Informatics* **2012**, *4.17*, 1–17.

(39) Chang, H.-P.; Chu, E.-D.; Yeh, Y.-T.; Wu, Y.-C.; Lo, F.-Y.; Wang, W.-H.; Chern, M.-Y.; Chiu, H.-C. Influence of Oxygen Vacancies on the Frictional Properties of Nanocrystalline Zinc Oxide Thin Films in Ambient Conditions. *Langmuir* **2017**, 8362–8371.

(40) Barriet, D.; Lee, T. R. Fluorinated Self-Assembled Monolayers: Composition, Structure and Interfacial Properties. *Curr. Opin. Colloid Interface Sci.* **2003**, *8* (3), 236–242.

(41) Zheng, H.; Zhang, F.; Zhou, N.; Sun, M.; Li, X.; Xiao, Y.; Wang, S. Self-Assembled Monolayer-

Modified ITO for Efficient Organic Light-Emitting Diodes: The Impact of Different Self-Assemble Monolayers on Interfacial and Electroluminescent Properties. *Org. Electron.* **2018**, 89–95.

(42) Lee, S.; Puck, A.; Graupe, M.; Colorado, R.; Shon, Y. S.; Lee, T. R.; Perry, S. S. Structure, Wettability, and Frictional Properties of Phenyl-Terminated Self-Assembled Monolayers on Gold. *Langmuir* **2001**, *17* (23), 7364–7370.

(43) Paniagua, S. A.; Li, E. L.; Marder, S. R. Adsorption Studies of a Phosphonic Acid on ITO: Film Coverage, Purity, and Induced Electronic Structure Changes. *Phys. Chem. Chem. Phys.* **2014**, *16* (7), 2874.

(44) Heinhold, R.; Williams, G. T.; Cooil, S. P.; Evans, D. A.; Allen, M. W. Influence of Polarity and Hydroxyl Termination on the Band Bending at ZnO Surfaces. *Phys. Rev. B: Condens. Matter* **2013**, *88* (23), 235315.

(45) Morkoç, H.; Özgür, Ü. *Zinc Oxide: Fundamentals, Materials and Device Technology*; Wiley-VCH: Weinheim, 2009.

(46) Heinhold, R.; Cooil, S. P.; Evans, D. A.; Allen, M. W. Stability of the Surface Electron Accumulation Layers on the Nonpolar $(10\bar{1}0)$ and $(11\bar{2}0)$ Faces of ZnO. *J. Phys. Chem. C* **2014**, *118* (42), 24575–24582.

(47) Tosatti, S.; Michel, R.; Textor, M.; Spencer, N. D. Self-Assembled Monolayers of Dodecyl and Hydroxy-Dodecyl Phosphates on Both Smooth and Rough Titanium and Titanium Oxide Surfaces. *Langmuir* **2002**, *18* (9), 3537–3548.

(48) Laibinis, P. E.; Graham, R. L.; Biebuyck, H. A.; Whitesides, G. M. X-Ray Damage to CF_3CO_2-Terminated Organic Monolayers on Silicon/Gold Supports Is Due Primarily to X-Ray Induced Electrons. *Science* **1991**, *254* (5034), 981–983.

(49) Schulmeyer, T.; Paniagua, S. A.; Veneman, P. A.; Jones, S. C.; Hotchkiss, P. J.; Mudalige, A.; Pemberton, J. E.; Marder, S. R.; Armstrong, N. R. Modification of $BaTiO_3$ Thin Films: Adjustment of the Effective Surface Work Function. *J. Mater. Chem.* **2007**, *17* (43), 4563.

(50) Zhang, S. B.; Wei, S. H.; Zunger, A. Intrinsic n-Type versus p-Type Doping Asymmetry and the Defect Physics of ZnO. *Phys. Rev. B: Condens. Matter* **2001**, *63* (7), 1–7.

(51) Van De Walle, C. G. Defect Analysis and Engineering in ZnO. *Phys. B* **2001**, *308*, 899–903.

(52) King, P. D. C.; Veal, T. D.; McConville, C. F.; Zúñiga-Pérez, J.; Muñoz-Sanjosé, V.; Hopkinson, M.; Rienks, E. D. L.; Jensen, M. F.; Hofmann, P. Surface Band-Gap Narrowing in Quantized Electron Accumulation Layers. *Phys. Rev. Lett.* **2010**, *104* (25), 1–4.

(53) Vasheghani Farahani, S. K.; Veal, T. D.; Mudd, J. J.; Scanlon, D. O.; Watson, G. W.; Bierwagen, O.; White, M. E.; Speck, J. S.; McConville, C. F. Valence-Band Density of States and Surface Electron Accumulation in Epitaxial SnO_2 Films. *Phys. Rev. B: Condens. Matter* **2014**, *90* (15), 1–9.

(54) Hotchkiss, P. J.; Li, H.; Paramonov, P. B.; Paniagua, S. A.; Jones, S. C.; Armstrong, N. R.; Brédas, J. L.; Marder, S. R. Modification of the Surface Properties of Indium Tin Oxide with Benzylphosphonic Acids: A Joint Experimental and Theoretical Study. *Adv. Mater.* **2009**, *21* (44), 4496–4501.

(55) Kassier, G. H.; Hayes, M.; Auret, F. D.; Mamor, M.; Bouziane, K. Electrical and Structural Characterization of As-Grown and Annealed Hydrothermal Bulk ZnO. *J. Appl. Phys.* **2007**, *102* (1).

(56) Nie, H. Y.; Walzak, M. J.; McIntyre, N. S. Bilayer and Odd-Numbered Multilayers of

Octadecylphosphonic Acid Formed on a Si Substrate Studied by Atomic Force Microscopy. *Langmuir* **2002**, *18* (7), 2955–2958.

(57) Ostapenko, A.; Klöffel, T.; Meyer, B.; Witte, G. Formation and Stability of Phenylphosphonic Acid Monolayers on ZnO: Comparison of In Situ and Ex Situ SAM Preparation. *Langmuir* **2016**, *32* (20), 5029–5037.

(58) Bao, J.; Shalish, I.; Su, Z.; Gurwitz, R.; Capasso, F.; Wang, X.; Ren, Z. Photoinduced Oxygen Release and Persistent Photoconductivity in ZnO Nanowires. *Nanoscale Res. Lett.* **2011**, *6*, 1–7.

(59) Sun, R.-D.; Nakajima, A.; Fujishima, A.; Watanabe, T.; Hashimoto, K. Photoinduced Surface Wettability Conversion of ZnO and TiO_2 Thin Films. *J. Phys. Chem. B* **2001**, *105* (10), 1984–1990.

(60) Li, Y.; Della Valle, F.; Simonnet, M.; Yamada, I.; Delaunay, J.-J. Competitive Surface Effects of Oxygen and Water on UV Photoresponse of ZnO Nanowires. *Appl. Phys. Lett.* **2009**, *94* (2).

4 Alkanethiol Modification of Single Crystal ZnO

4.1 Introduction

4.1.1 Alkanethiols on ZnO

As detailed in Chapter 1, some researchers have reported that alkanethiol monolayers are physically stable on metal oxides such as ZnO,[1,2] while other reports suggest that forming a well-organised thiol monolayer is difficult and requires very specific preparation parameters.[3,4] These differences may be due to the variety of modifiers used, but may also be due to the different reactivities of ZnO faces: Chen et al.[1] observed that on m-plane ZnO, octadecanethiol (ODT) forms better-organised SAMs than hexadecylphosphonic acids, while Perkins observed that hexylphosphonic acid SAMs on O-polar ZnO have superior stability to hexanethiol monolayers.[5] Other factors that differ between studies include modifier concentration, reaction time, modification solvent, and post-modification treatment (rinsing and heating). A summary of the experimental conditions used in the preparation of alkanethiol monolayers on ZnO is seen in Table 4.1.

The binding mode of thiols on ZnO is reported as being either thiolate (Zn-S) or sulfonate (Zn-O-S), as determined by XPS.[6] A S 2p BE of ~169 eV is indicative of Zn-O-S bonds and a BE of ~163 eV arises from Zn-S bonds. The exact nature of 'sulfonate' species at ZnO is unclear, but this work will be consistent with previous reports by referring to S 2p BE peaks at ~169 eV as 'sulfonate' peaks, or oxidised S. Similarly, S 2p peaks at ~163 eV will be referred to as 'thiolate' peaks or 'non-oxidised' S. Alkanethiolate SAMs are well-studied on Au surfaces, but the mechanism for thiol adsorption and oxidation at ZnO is much less clear. Literature reports give inconsistent data as to the binding modes involved in alkanethiol SAMs on ZnO (Table 4.1), and their stability.[1,2,5–7] For example, Pesika et al. report that the major S 2p peak on octanethiol-modified Zn-polar ZnO arises from sulfonate bonds,[6] whereas Sadik et al. observed thiolate bonds on dodecanethiol-modified Zn-polar ZnO.[2] Sadik et al.,[2] Pesika et al.,[6] and Perkins[5] all report thiolate as the main S 2p environment for alkanethiol-modified O-polar ZnO, while Ogata et al.[4] observed that sulfonate was the major S 2p peak at O-polar ZnO. In

terms of stability, Sadik et al.[2] reported that dodecanethiol-modified Zn-polar and O-polar ZnO were stable to 400 °C and 350 °C, respectively. On the other hand, Perkins observed that the S 2p peak intensity remained unchanged for hexanethiol-modified O-polar ZnO to 400 °C but that C-S scission started to occur at temperatures > 100 °C.[5] The authors listed in Table 4.1 have used a wide range of preparation methods and further investigation of the parameters for sulfonate and thiolate bond formation is warranted.

Table 4.1: Summary of conditions used to prepare SAMs of alkanethiols on ZnO and the binding modes as determined from XPS S 2p BE. 'S' indicates an XPS S 2p peak at ~ 169 eV (sulfonate), while 'T' refers to a S 2p peak at ~163 eV (thiolate).

Ref.	Modifier	Conc. (mM)	Solvent	Time	Face	Post Treatment	Major S 2p Peak	Minor S 2p Peak
Pesika[6]	Octanethiol	3	IPA	24 h	Zn	None	S	T
	Octanethiol	3	IPA	24 h	Zn	IPA rinse	S	-
	Octanethiol	3	IPA	24 h	Zn	IPA + H_2O rinse	S	-
	Octanethiol	3	IPA	24 h	O	None	T	S
	Octanethiol	3	IPA	24 h	O	IPA rinse	T	-
	Octanethiol	3	IPA	24 h	O	IPA + H_2O rinse	T	-
Sadik[2]	Dodecanethiol	10	IPA	7 d	Zn	IPA rinse; 50 °C	T	-
	Dodecanethiol	10	IPA	7 d	Zn	IPA rinse; 200 °C	T	-
	Dodecanethiol	10	IPA	7 d	Zn	IPA rinse; 400 °C	T	-
	Dodecanethiol	10	IPA	7 d	Zn	IPA rinse; 500 °C	-	-
	Dodecanethiol	10	IPA	7 d	O	IPA rinse; 50 °C	T	S
	Dodecanethiol	10	IPA	7 d	O	IPA rinse; 150 °C	T	S
	Dodecanethiol	10	IPA	7 d	O	IPA rinse; 400 °C	T	-
	Dodecanethiol	10	IPA	7 d	O	IPA rinse; 500 °C	-	-
Perkins[5]	Hexanethiol	2	EtOH	16 h	O	EtOH rinse	T	S
	Hexanethiol	2	EtOH	16 h	O	EtOH; 300 °C	T	S
	Hexanethiol	2	EtOH	16 h	O	EtOH; 350 °C	T	-
	Hexanethiol	2	EtOH	16 h	O	EtOH; 500 °C	T	-
Ogata[4]	Propanethiol	100	IPA	Overnight	O	IPA rinse	S	T
	Propanethiol	100	IPA	Overnight	O	IPA rinse; 100 °C	S	-
	Propanethiol	100	IPA	Overnight	O	IPA rinse; 400 °C	S	-
Chen[1]	ODT	1	EtOH	Overnight	m	None	T	-

Another type of S-containing molecule is isothiocyanate (R-N=C=S, ITC). Work by Hamers et al. showed that both phenyl- and methyl-ITC give well-defined attachment to Si(001) surfaces, binding through

the N=C moiety as determined by XPS.[8] In work by Loscutoff et al., germanium was modified with phenyl ITC in UHV in efforts to elucidate its binding structure from XPS, FTIR, and DFT calculations.[9] The authors determined that the major product was that of a [2 + 2] cycloaddition across the C=S moiety where the ITC was bound through both C and S, each on a different Ge atom (Figure 4.1, Structure a). The minor product was the [2 + 2] cycloaddition across the C=N bond (Figure 4.1, Structure b).

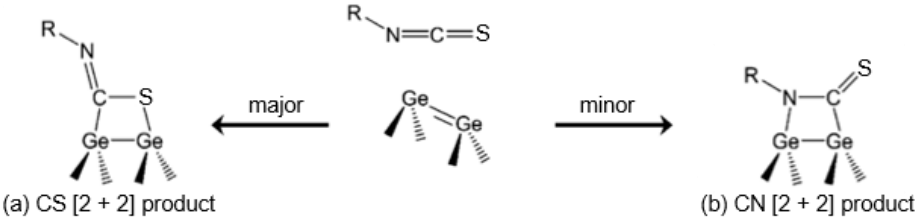

Figure 4.1: Proposed products formed upon the reaction of isothiocyanate (R-N=C=S) with Ge(100)-2 × 1 surface dimer. Adapted from Loscutoff et al.[9]

To date, no work on the attachment of ITC to metal oxides has been carried out. ZnO lacks the proximity of the metal atoms seen in Ge, yet dative bonds may be able to form between Zn and either the N or S in the ITC molecule.

4.1.2 Aims

Due to contradictions and some incompleteness of previous studies of thiol-modified ZnO (Table 4.1), the work in this Chapter systematically investigates the stability and binding mode of alkanethiols on Zn-polar, O-polar, and m-plane ZnO. No other studies of alkanethiol modification of Zn-polar, O-polar, and m-plane ZnO under the same conditions have been reported. Several alkane- and arylthiol modifiers (Table 4.2) are compared for their surface coverage on ZnO and their effect on band bending. Octadecanethiol (ODT) and 1*H*,1*H*,2*H*,2*H*-perfluorooctanethiol (F_{13}OT) were selected for their similarities to ODPA and F_{13}OPA used in Chapter 3. 4-trifluoromethylbenzyl mercaptan (4TFMBM) was selected as it has similar properties to PFBPA. Although 3,5-bis(trifluoromethyl)phenyl

isothiocyanate (ITC) is not a thiol, it is also trialled alongside the thiol modifiers due to reports of successful isothiocyanate binding on Si and GaAs.[8,9]

Table 4.2: Structures and abbreviations of thiol and isothiocyanate derivatives used to modify ZnO in this work.

Name	**1-Octadecane thiol**	**1*H*,1*H*,2*H*,2*H*-perfluoro octanethiol**	**4-trifluoromethyl benzyl mercaptan**	**3,5-bis(trifluoromethyl) phenyl isothiocyanate**
Abbreviation	ODT	$F_{13}OT$	4TFMBM	ITC
Structure	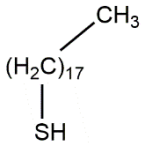	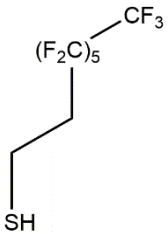	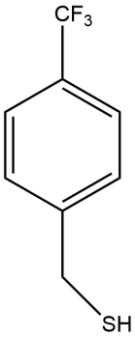	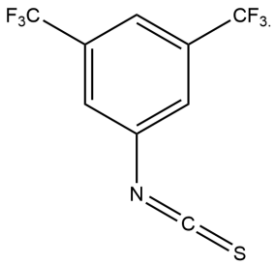

4.2 Experimental Methods

All modifications and analyses in this Chapter were performed at the University of Wisconsin-Madison, USA. 3 × 5 mm^2 single-crystal CrysTec ZnO samples (Zn-polar, O-polar, and m-plane faces) were solvent-cleaned prior to modification as outlined in Chapter 2. The modification method reported by Chen et al.[1] was followed, but with a change in reaction solvent. Unless stated otherwise, thiol derivatives were reacted with cleaned single-crystal ZnO samples by soaking in 5 mL of 1 mM thiol solution in THF for 16 h in ambient laboratory atmosphere. Samples were then rinsed in THF, dried with nitrogen, and stored in air and darkness prior to XPS analysis. The ZnO samples were too small to be clipped into the standard XPS sample holder. They were instead attached using conductive colloidal silver paste, directly after modification. In early experiments, as in Section 4.3.1.1, the sample holder was immediately inserted into the load lock of the XPS instrument before the silver paste had cured. This method was detrimental to the UHV system and was modified so that the silver paste and samples were cured in a 50 °C oven for 30 min prior to loading the sample. This procedure was followed for

ZnO samples described in Section 4.3.1.3, but still did not solve the problems associated with maintaining the efficiency of the UHV system. For all other experiments, the silver paste was cured in ambient conditions for 22 h before the sample holder was loaded into the XPS instrument.

The concentrations of modifiers on the surface were estimated from XPS measurements as described in Chapter 2.2.4. For many samples examined in this Chapter, the S signal was small (low signal:noise) and so there is a large uncertainty in both the amount of S on the surface and the molecular surface concentration. For some sets of samples, the % Zn and % S do not show a consistent relationship, indicating that the Zn signal has been affected by non-S-containing adventitious contamination. This adds to the uncertainty in surface concentration estimations, which should be assumed to be at least 20%.

4.3 Results and Discussion

4.3.1 Method Optimisation for Thiol Modification of ZnO

4.3.1.1 Role of Modifier Concentration in Octadecanethiol Modification of ZnO

Prior studies on thiol attachment to ZnO used a range of modifier concentrations for the immersion step (1 to 10 mM).[1,2,5,6] Given the different results of these earlier works, a study was undertaken to determine the effect of changing the thiol concentration on the resulting surface coverage on O-polar ZnO. ODT was used because it is commonly used to form SAMs and was readily available.[1] After immersion of ZnO samples in THF solutions of ODT, samples were rinsed with water and immediately analysed by XPS.

Figure 4.2 shows the XPS survey and core level S 2p spectra for ODT-modified ZnO, and Table 4.3 lists XPS data. Full survey spectrum peak assignments for as-received ZnO are discussed in Appendix 8.1.2. Peaks in the ODT-modified survey spectra (Figure 4.2a) are attributed to the presence of Zn, O, S, and C; the Zn 2p peak intensity decreases as the ODT concentration increases and as the C 1s and S 2p signals increase, indicating an increased alkanethiol coverage that attenuates the bulk ZnO signal. The S 2p signal is very small and is best examined through the core level scan (Figure 4.2b), where the

signal at 163 eV can be fitted by two peaks arising from S $2p_{1/2}$ and S $2p_{3/2}$ spin-orbit splitting.[1] As mentioned in Section 4.1, previous reports indicate that the S 2p peak at ~168 eV can be attributed to sulfonate species, where S is attached to O.[2,6] However, the exact structure of oxidised S is unclear. Due to the weakness of the sulfonate signal, the peak at ~168 eV was not deconvoluted into spin-orbit doublets.

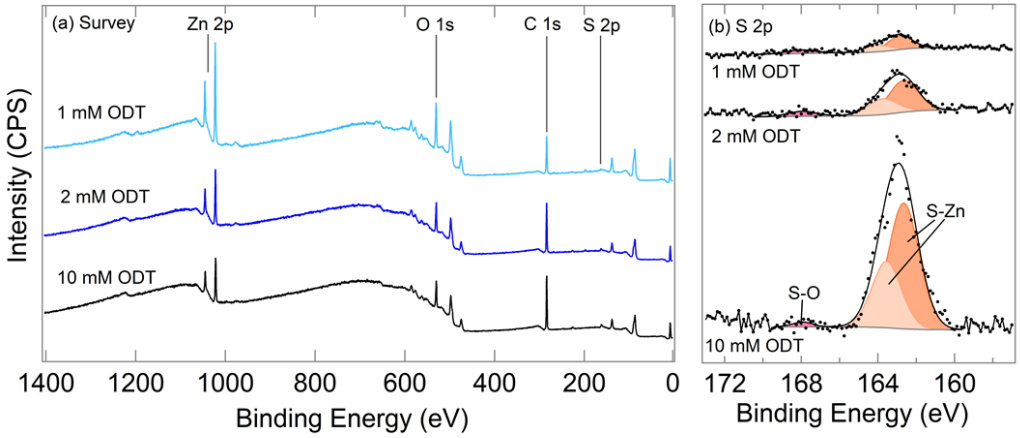

Figure 4.2: Fixed-energy XPS (a) survey spectra and (b) S 2p core level spectra for O-polar ZnO, modified in 1 mM, 2 mM, and 10 mM ODT in THF (ambient conditions). After modification, samples were rinsed with water and analysed immediately, without heating. Spectra have been offset for clarity. Spectra in (b) have been normalised to the same Zn 2p peak area.

Using the methods described in Chapter 2, the ASF-corrected Zn:S ratios were calculated and water-CA-derived molecular surface concentrations were estimated (Table 4.3).[10–13] Increasing the ODT concentration from 1 to 10 mM increased the percentage of S on O-polar ZnO from 1 – 3%, and the calculated modifier surface concentration from 15 to 50 molecules nm^{-2}. Chen et al. calculated from XPS data a surface concentration of ~4.2 ODT molecules nm^{-2} on m-plane ZnO and described this as near-monolayer coverage because the same molecules on gold formed highly-ordered, close-packed SAMs with a surface concentration of ~3.9 molecules nm^{-2} (~6.5×10^{-10} mol cm^{-2}). In this work, SAM preparation using 1 mM ODT appears to give a surface concentration greater than a monolayer. However, the sulfonate species on O-polar ZnO modified with 1 mM ODT have a surface concentration of ~3 molecules nm^{-2}, which is close to a monolayer. This might suggest that a chemisorbed sulfonate

monolayer is present at ZnO, and that non-oxidised ODT are physisorbed on top of this layer and not removed during the brief post-modification water rinsing.[1] However, it is also possible that a mixed thiolate-sulfonate monolayer is chemisorbed to ZnO, with a mixed thiol and sulfonate ODT multilayer on top.

Table 4.3: Atomic percentages from fixed-energy XPS survey spectra, sulfur oxidation state ratios from S 2p core level XPS spectra, and estimated molecular surface concentrations for ODT-modified O-polar ZnO modified in 1 mM, 2 mM, and 10 mM ODT in THF (ambient conditions). After modification, samples were rinsed with water and analysed immediately, without heating.

[ODT] (mM)	Zn %	C %	O %	S %	Thiolate : Sulfonate	Molecule/nm^2
1	20	37	41	1	4 : 1	15
2	9	67	20	3	7 : 1	80
10	8	70	19	3	21 : 1	100

ODT concentrations greater than 1 mM resulted in even larger surface concentration values and presumably thicker multilayers. Modification of O-polar ZnO in 10 mM ODT gave a sulfonate surface concentration of ~4 molecules nm^{-2}, which adds weight to the explanation of a sulfonate monolayer with a non-oxidised ODT multilayer. However, it is not strong evidence as the 2 mM ODT modification gave a sulfonate surface density of ~10 sulfonate molecules nm^{-2}, which is greater than a monolayer and therefore suggests that at least some physisorbed ODT are oxidised. As explained above, the nature of 'sulfonate' ODT is unclear: it may indicate a S-O-Zn bond or a physisorbed oxidised thiol (R-SO_4^- or R-SO_3^-).[6] Similarly, the nature of 'thiolate' ODT is unclear: it appears likely that a significant number of these ODT molecules are unreacted thiols (BE = 163.6 eV)[14] which form multilayers, but they cannot be distinguished from the thiolate (Zn-S) signal (~163 eV). For convenience, the non-oxidised form of the modifier which may be present as the thiol or thiolate will be referred to as 'thiolate' except when it is necessary to discuss the two forms separately. Disulfides, a product of thiol oxidation, also have a binding energy of ~163 eV, so cannot be discounted as being present on the

surface.[14] To minimise formation of multilayers, a modifier concentration of 1 mM was chosen for the remainder of the alkanethiol work.

4.3.1.2 Preparation of Octadecanethiol-Modified ZnO in Inert Atmosphere

The presence of an oxidised S signal on ODT-modified ZnO as discussed above was investigated further by carrying out the ODT modification on Zn-polar and O-polar ZnO in an Ar-filled glovebox. Samples were rinsed with water after modification, and XPS analysis was performed after 22 h storage in air. Figure 4.3 shows the resulting fixed-energy XPS S 2p spectra, and Table 4.4 gives XPS data. Both samples show evidence of oxidised (168 eV) and non-oxidised S (~163 eV) on the surface. The large modifier surface concentrations (~20 and ~30 molecules nm^{-2} for Zn-polar and O-polar ZnO, respectively) are attributed to multilayers of ODT which were not rinsed away by water and did not desorb from the surface during exposure to air. This is not unexpected due to the long alkyl chain of ODT, which is not soluble in water nor highly volatile.

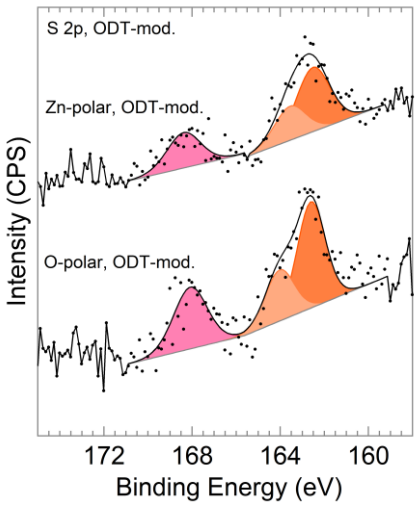

Figure 4.3. Fixed-energy XPS S 2p core level spectra for Zn-polar and O-polar ZnO, modified in 1 mM ODT in THF in an Ar-filled glovebox. After modification, samples were rinsed with water, stored for 22 h in air, and analysed. Spectra have been normalised to the same Zn 2p peak area and offset for clarity.

Both Zn-polar and O-polar ZnO have similar thiolate:sulfonate ratios, and sulfonates account for ~6 – ~9 molecules nm^{-2}. Since these values are greater than a monolayer, some physisorbed ODT molecules

must be sulfonate-like. However, it is unclear whether sulfonates are directly coordinated to the ZnO surface.

Table 4.4. Atomic percentages and sulfonate:thiolate ratios from fixed-energy XPS survey and S 2p spectra for ODT-modified Zn-polar and O-polar ZnO. Modification was carried out in an Ar-filled glovebox with 1 mM ODT in THF; samples were rinsed with water after modification and analysed after 22 h storage in air.

Sample	Zn %	C %	O %	S %	Thiolate:Sulfonate	Molecules/nm^2
Zn-polar	14	50	35	1	2 : 1	20
O-polar	11	55	33	1	2: 1	30

Comparing Figure 4.2b and Figure 4.3 and their corresponding Tables, it appears that modification of O-polar ZnO in 1 mM ODT (THF) carried out in ambient conditions and analysed immediately after water rinsing gives multilayer ODT coverage with ~20% of the modifiers as sulfonate. When the same experiment is carried out in inert conditions but with 22 h storage in air, sulfonates account for ~33% of the ODT present. This suggests that ODT oxidises during modification regardless of the presence of O_2, as seen by Perkins,[5] but that a more significant degree of oxidation occurs when the modified sample is exposed to air during storage. Thus, it appears that the post-modification treatment of samples is more important than the modification conditions and hence, the remaining thiol modifications in this work were carried out in ambient laboratory conditions.

4.3.1.3 Effect of Rinsing Solvent on Octadecanethiol Layers on ZnO

Castner et al. highlighted the importance of correct solvent choice for rinsing alkanethiol-based SAMs on Au because of the strong tendency for unbound thiol or disulfide groups to remain on the surface.[15] Likewise, Pesika et al. highlighted the importance of rinsing ZnO samples after thiol modification. They found that for the Zn-polar face, a 'thiolate' S 2p XPS signal disappeared after rinsing with IPA and water, leaving only a sulfonate peak (Table 4.1). The reverse was true for the O-polar face: prior to

rinsing, the main S 2p peak was in the thiolate region, and a small sulfonate peak was also visible. After rinsing with both IPA and water, only a thiolate signal was detected.[6]

The post-modification treatment used in Sections 4.3.1.1 and 4.3.1.2 involved rinsing the samples with water before drying with nitrogen gas. However, the observed multilayer coverage suggested that this process did not remove physisorbed modifiers. To determine the best rinsing procedure, 4 ODT-modified Zn-polar ZnO samples were subjected to different post-modification treatments and the S coverage was analysed via XPS. The rinsing steps were: no rinse, rinsed with water, rinsed with THF, and sonicated in THF (4 min). After rinsing, all samples were dried with nitrogen and immediately inserted into the XPS instrument.

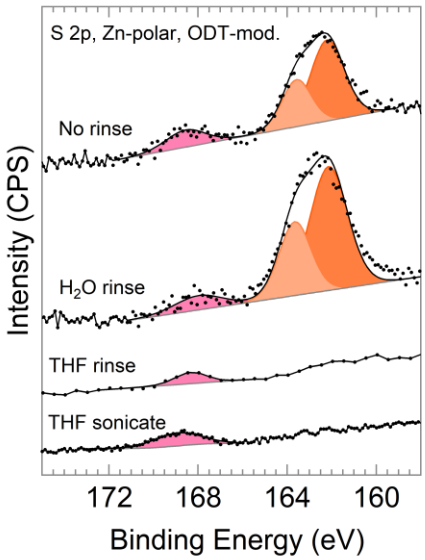

Figure 4.4: Fixed-energy XPS S 2p core level spectra for 4 different Zn-polar ZnO samples modified in 1 mM ODT in THF (ambient conditions). Post modification treatments were: not rinsed, rinsed with water, rinsed with THF, or sonicated in THF for 4 min. All samples were dried with nitrogen and immediately analysed by XPS. The spectrum of the THF-rinsed sample was taken with a larger BE step size. Spectra have been normalised to the same Zn 2p peak area and offset for clarity.

Figure 4.4 shows that unrinsed ODT-modified Zn-polar ZnO has a large S 2p signal in the thiolate region, and a small sulfonate peak at higher BE. A sample which had been rinsed with water after ODT

modification has a S 2p spectrum with very similar features, consistent with spectra seen in Figure 4.2b and Figure 4.3. However, when ODT-modified Zn-polar ZnO was rinsed or sonicated in THF, the 'thiolate' peak decreased significantly to leave only trace amounts, which suggests that non-oxidised thiols were physisorbed as multilayers. In contrast, there was only a small decrease in the sulfonate signal after THF rinsing or sonication. The calculated molecular surface concentrations shown in Table 4.5 for the unrinsed sample and the THF-rinsed and THF-sonicated samples (~4 molecules nm^{-2}, ~7 × 10^{-10} mol cm^{-2}) are consistent with an approximate monolayer of modifiers remaining after rinsing, bound to the surface as the sulfonate. This surface coverage is less than half that of the reported Zn-polar ZnO OH surface concentration (~1.8 × 10^{-9} mol cm^{-2}). This suggests that either the modifiers are monodentate and there is still a significant amount of unreacted OH groups on the surface, or that the modifiers have bonded to ZnO in a bi- or tridentate fashion.

The effect of solvent rinsing seen here is consistent with that reported by Pesika et al, who rinsed Zn-polar samples with IPA (the same solvent as their modifying solution) and saw the sulfonate signal decrease slightly while the thiolate signal disappeared (Table 4.1).[6] Surface concentrations of modifiers were not reported, however Pesika et al. concluded that the sulfonate was more stable than the thiolate on the Zn-polar face. Ogata et al reported sub-monolayer coverage of sulfonate-type propanethiol on O-polar ZnO after being rinsed well with IPA.[6] The present work indicates that under the conditions used, the sulfonate is more stable than non-oxidised thiols on Zn-polar ZnO. Given that any application of surface-modified ZnO is expected to require stable layers, the THF rinsing step was retained in further investigations to ensure that only strongly-bound modifiers remained on the surface. Sonicating the sample in THF did not significantly change the ODT coverage from that obtained with a simple rinsing step, and so was omitted in future work.

Table 4.5: Fixed-energy XPS survey and S 2p spectra data gathered on 4 different ODT-modified Zn-polar samples which were subjected to several post-modification cleaning methods: no rinsing, rinsing with water, rinsing with THF, and sonication with THF.

Post-modification treatment	Zn %	C %	O %	S %	Thiolate : Sulfonate	Molecules/nm^2
No rinse	12	58	27	3	3.0 : 1	58
Water rinse	9	66	23	3	6.3 : 1	78
THF rinse	31	21	48	0.5	0 : 1	4
THF sonication	26	21	52	0.4	0 : 1	4

4.3.1.4 Role of Solvent in Octadecanethiol-Modification of ZnO

Ethanol and IPA have been commonly used in the preparation of alkanethiol-based SAMs on ZnO (Table 4.1).[1,2,5,6] However, THF was used for the preparation of PA SAMs on ZnO (Chapter 3) because Chen et al. reported that using a low dielectric solvent was important in forming ordered PA SAMs on ITO.[16] Hence, the preparation of SAMs of ODT on ZnO was compared using ethanol and THF as the modification solvents. After immersion in the thiol solution, the samples were rinsed with their respective modification solvent and heated at 50 °C for 30 min. A heating step was included because the use of heat is proposed to promote covalent bonding of PA modifiers to ZnO. Samples were then immediately analysed by XPS.

Figure 4.5 shows fixed-energy XPS S 2p spectra for Zn-polar, O-polar, and m-plane ZnO after modification with ODT in THF, and Zn-polar and O-polar ZnO after modification with ODT in ethanol. All three THF-treated faces show a signal in the ~169 eV binding energy range, indicating oxidised S is present. Only the O-polar face shows evidence of non-oxidised alkanethiols on its surface. Similar results to Figure 4.5a were observed for ZnO modified in ethanol solution (Figure 4.5b), where Zn-polar ZnO has no thiolate peak and O-polar ZnO has both thiolate and sulfonate signals.

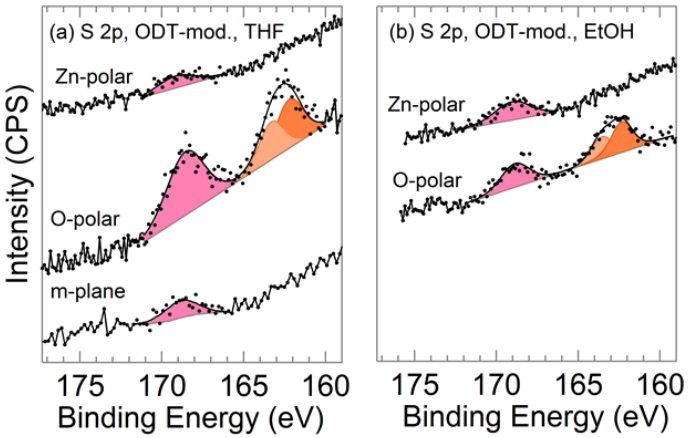

Figure 4.5: Fixed-energy XPS S 2p core level spectra for (a) Zn-polar, O-polar, and m-plane ZnO modified in 1 mM ODT in THF (ambient conditions), and (b) Zn-polar and O-polar ZnO modified in 1 mM ODT in ethanol (ambient conditions). After modification, samples were rinsed with the modification solvent, heated (50 °C, 30 min), and immediately analysed. Spectra have been normalised to the same Zn 2p peak area and offset for clarity.

Figure 4.5 and Table 4.6 show that Zn-polar ZnO had more S on the surface when modified with ODT in ethanol than when modified in THF, while O-polar ZnO had more S when modified with ODT in THF than when modified in ethanol. O-polar ZnO had significantly more S on the surface than the other two faces, regardless of the solvent used. The thiolate:sulfonate ratio was higher for O-polar ZnO modified in ethanol than in THF. The surface concentration of ODT on both O-polar samples was greater than that expected for a monolayer, indicating that multilayers were present. Overall, the data in Table 4.6 suggest that the surface thiol concentration depends more on the ZnO face than the modification solvent. This is discussed later.

Table 4.6: Fixed-energy XPS survey and S 2p spectra data for Zn-polar, O-polar, and m-plane ZnO modified with 1 mM ODT in THF or ethanol (in ambient conditions). After modification, samples were rinsed with the modification solvent, heated (50 °C, 30 min), and immediately analysed. m-Plane ZnO was not reacted with ODT in ethanol.

Face	Solvent	Zn %	C %	O %	S %	Thiolate : Sulfonate	Molecules/nm^2
Zn-polar	THF	29	27	43	0.2	0 : 1	2
	Ethanol	20	33	46	0.3	0 : 1	4
O-polar	THF	18	45	36	1.2	1.0 : 1	16
	Ethanol	20	37	42	0.8	1.7 : 1	9
m-plane	THF	15	36	48	0.1	0 : 1	2

A contrast can be drawn between O-polar ZnO, and Zn-polar and m-plane ZnO: Figure 4.5 shows that non-oxidised, unreacted ODT molecules desorb completely from Zn-polar and m-plane surfaces during either or both of THF rinsing and mild heating (Figure 4.4 also shows this behaviour for the Zn-polar face), while on O-polar ZnO, a significant peak at BE ~163 eV is still present after both treatments. Evidently thiolates are more stable on O-polar ZnO than on Zn-polar or m-plane ZnO. Using UHV conditions, Perkins observed that the sulfonate signal from hexanethiol on O-polar ZnO was stable until 350 °C under UHV, while the thiolate-type signal remained on the surface to 500 °C.[5] This demonstrates that thiolate bonding is more stable than sulfonate binding on O-polar ZnO. Assuming that this is also the case at Zn-polar and m-plane ZnO, the lack of thiolates at these surfaces can be attributed to the higher catalytic activity of the Zn-polar and m-plane faces, as suggested by Pesika et al.[6] Under the conditions used here, thiolates at these faces are oxidised to sulfonates, whereas oxidation does not occur to the same degree at O-polar ZnO.

4.3.1.5 Summary of Octadecanethiol Oxidation at ZnO

Several previous studies have investigated the formation of alkanethiol SAMs on ZnO via S 2p XPS, yet the resulting modification layers differ greatly in terms of extent of thiol oxidation, as seen in Table 4.1. As shown in Table 4.7, results in this work showed that reaction of alkanethiols with Zn-polar, O-

polar, and m-plane ZnO gave modification layers with which also incorporated sulfonates, irrespective of modification solvent (Figure 4.5). The possibility that the stock ODT used in this work was oxidised prior to preparation of SAMs was considered. However, the NMR spectrum for the ODT sample showed no evidence of oxidised species (Appendix 8.2.1) and the results of various modification experiments were not consistent with progressive oxidation of the stock ODT. It is therefore more likely that oxidation of ODT occurs during and/or after modification of ZnO.

*Table 4.7. Summary of XPS S 2p data for ODT-modified ZnO from the current work. 'S' indicates an XPS S 2p peak at ~169 eV (sulfonate) and 'T' refers to an S 2p peak at ~163 eV (thiolate). 'S and T' indicates that the sulfonate and thiolate peaks were of the same intensity. *Denotes samples which were not analysed within 3 h of modification.*

Face	Conc. (mM)	Solvent	Atmosphere	Post Treatment	Major S 2p Peak	Minor S 2p Peak
Zn-polar	1	THF	Air	THF rinse, 50 °C	S	-
Zn-polar	1	THF	Argon	H_2O rinse*	T	S
Zn-polar	1	THF	Air	No rinse	T	S
Zn-polar	1	THF	Air	THF rinse	S	-
Zn-polar	1	Ethanol	Air	Ethanol rinse, 50 °C	S	-
Zn-polar	1	THF	Air	THF sonicate	S	-
O-polar	1	THF	Argon	H_2O rinse*	T	S
O-polar	1	THF	Air	THF rinse, 50 °C	S and T	-
O-polar	1	Ethanol	Air	Ethanol rinse, 50 °C	T	S
O-polar	1	THF	Air	H_2O rinse	T	S
O-polar	2	THF	Air	H_2O rinse	T	S
O-polar	10	THF	Air	H_2O rinse	T	S
m-plane	1	THF	Air	THF rinse, 50 °C	S	-

Thiols can be oxidised by atmospheric species[17] as well as by ZnO itself.[5] Even when freshly-modified O-polar ZnO samples were directly loaded into the XPS instrument, a small sulfonate signal was observed (Figure 4.2). Likewise, Perkins observed a small amount of oxidised thiols on hexanethiol-modified polycrystalline ZnO, despite the modification and analysis being carried out in oxygen-free

conditions. The author proposed that thiols were reacting with O in the ZnO sublattice, aided by lattice steps and other surface defects. It is likely that a similar mechanism occurred in this work. From Figure 4.6, it is seen that oxidation of ODT layers occurs after modification, and from the results in Figure 4.2 and Figure 4.3, it appears that a more significant fraction of ZnO-bound ODT is oxidised upon exposure to air after modification than during modification. However, it is still unclear whether preformed sulfonates bond to ZnO, or alternatively, whether thiolates bind to the surface and are subsequently oxidised to sulfonates. Both processes may occur concurrently.

On metal substrates, long-chain alkanethiols (> 10 CH_x) generally have high packing density and uniform thiolate structures due to the high number of van der Waals attractions between the alkyl chains.[18] Once self-assembled, these alkanethiols are more stable to oxidation than their shorter counterparts, as they form more effective barriers to oxidants.[19] This is consistent with work carried out by Sadik et al. using dodecanethiol on ZnO:[2] the authors observed that a densely-packed layer on Zn-polar ZnO was in the thiolate form, while a less-dense layer on O-polar ZnO was bound by sulfonates despite being more uniform.[2] The modification layers were prepared by immersion in the alkanethiol solution for 7 d (by far the longest time reported for preparation of alkanethiol layers on ZnO), and hence it is possible that the long preparation time gives more densely-packed layers on Zn-polar ZnO which are more difficult for oxidising species to penetrate. Sadik et al.'s results suggest that that the modification layer on the O-polar face, despite the uniformity of the layer, was not dense enough to prevent oxidising species from migrating to the surface. Although Chen et al. modified m-plane ZnO with ODT using a much shorter reaction time (overnight), and reported only thiolate signal,[1] the authors did not mention a rinsing step; therefore the XPS S 2p signal could be largely due to physisorbed molecules.

Schoenfisch et al.[17] and Love et al.[20] observed that alkanethiol SAMs on different metal substrates oxidise at different rates, suggesting that the substrate plays a role in oxidation. Similarly, in this work it was observed that long-chain ODT layers on Zn-polar and O-polar ZnO, modified in the same

conditions (Figure 4.5), had different amounts of oxidation. Thus, it appears that oxidation of ODT on ZnO depends on the substrate. This is consistent with work carried out by Pesika et al.,[6] who also observed differences between Zn-polar and O-polar ZnO: octanethiol modification of Zn-polar ZnO resulted in sulfonate bonds after solvent rinsing, while the same procedure on O-polar ZnO resulted in thiolate bonds. This suggested that on the Zn-polar face, sulfonate formation is favoured compared to the O-polar face. The authors attributed this to the more catalytic nature of the Zn-polar face compared to O-polar ZnO. Thus, it seems likely that in this work, the higher catalytic reactivity of Zn-polar and m-plane faces increase the oxidation rate on these faces relative to O-polar ZnO. Sulfonate-type ODT molecules are expected to be more soluble and less prone to physisorption than their non-oxidised counterparts, and it may be that the multilayers on Zn-polar and m-plane ZnO are catalytically oxidised to sulfonates prior to THF rinsing, making them easily removed by THF. On the O-polar face, the same extent of catalytic oxidation does not occur, and the multilayer still has significant non-oxidised ODT which is more strongly adsorbing and not as easily removed by ethanol or THF. Photooxidation of thiols to sulfonates has also been reported in literature;[21] samples in this work were largely kept in the dark, but the effect of brief exposure to ambient light on the oxidation process cannot be ruled out.

4.3.2 Long-Term Stability of ODT Modifiers in Air

The long-term stability of the ODT modification layers remaining on ZnO after heating to 50 °C for 30 min was investigated. The ODT-modified, THF-rinsed, and heat-treated Zn-polar, O-polar, and m-plane ZnO samples shown in Figure 4.5 were analysed with XPS on the day of modification and were analysed again after 40 d storage in air and darkness. Figure 4.6 compares the Day 1 and Day 40 XPS spectra, and XPS data are given in Figure 4.7.

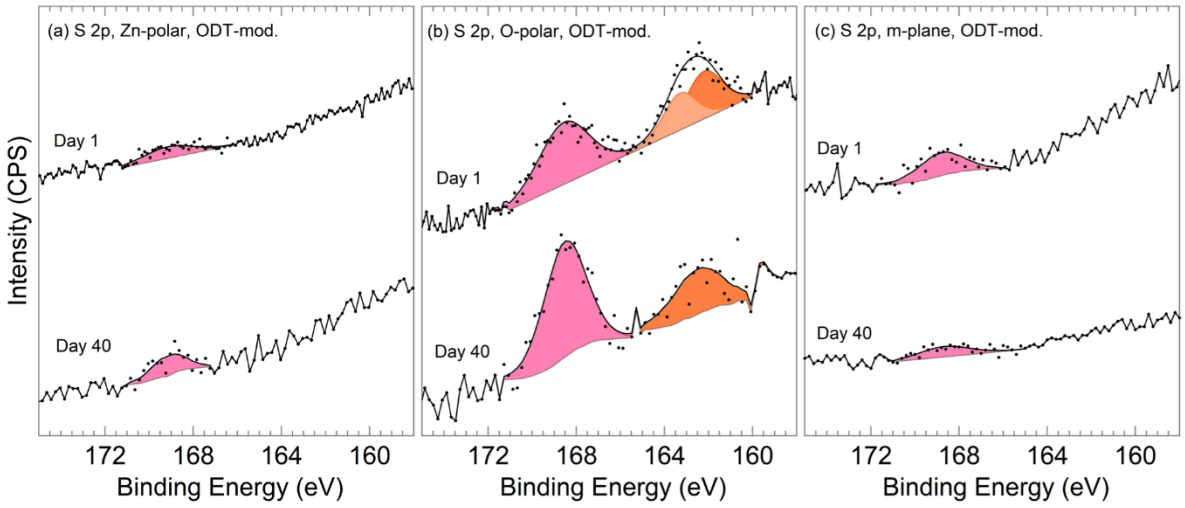

Figure 4.6. Fixed-energy S 2p XPS for (a) Zn-polar, (b) O-polar, and (c) m-plane ZnO faces modified with 1 mM ODT in THF (ambient conditions), rinsed with THF, and heated (50 °C, 30 min). Spectra were obtained immediately after heating (Day 1) and after 40 d storage in air and darkness (Day 40). Spectra have been normalised to the same Zn 2p peak area and offset for clarity. The Day 1 spectra are also shown in Figure 4.5.

Zn-polar and m-plane ZnO showed a loss of S from the surface after 40 d, as evidenced by a decrease in the S:Zn ratio in Table 4.8. On the O-polar face, the S:Zn ratio and consequently the calculated surface concentration of modifiers indicative of a multilayer coverage, remained the same over 40 d. However, the thiolate:sulfonate ratio on the O-polar face decreased from 1:1 to 1:3, indicating that some thiolate modifiers were oxidised to sulfonate moieties during the 40 d of storage, with minimal loss of total S. This is consistent with previous work on substrates other than Au, such as that done by Love et al., who observed that alkanethiol layers on Pd exposed to air over 5 d were oxidised to sulfonate or sulfate anion species.[20]

Table 4.8: Fixed-energy S 2p XPS data for Zn-polar, O-polar, and m-plane ZnO faces modified with 1 mM ODT in THF (ambient conditions), rinsed with THF, and heated (50 °C, 30 min). Spectra were obtained immediately after heating (Day 1) and 40 d later (Day 40). Day 1 data are also listed in Table 4.6.

	Day 1			Day 40		
Face	Thiolate : Sulfonate	S : Zn	Molecule/nm^2	Thiolate : Sulfonate	S : Zn	Molecule/nm^2
Zn-polar	0 : 1	0.007 : 1	2	0 : 1	0.005 : 1	1
O-polar	1 : 1	0.07 : 1	16	1 : 3	0.06 : 1	16
m-plane	0 : 1	0.008 : 1	2	0 : 1	0.004 : 1	1

To test the generality of the results, a similar experiment was carried out on the fluorinated analogue of ODT (F_{13}OT), but without the heating step. XPS analysis of freshly-prepared F_{13}OT-modified, THF-rinsed ZnO was carried out 22 h after preparation. In contrast to ODT, the O-polar face did not have a thiolate S signal: all three faces showed evidence of sulfonate bonding only, with the m-plane face having the highest surface coverage. After 3 d of storage in the air and darkness, the samples were re-analysed. The XPS results from the S 2p, C 1s, and F 1s scans can be seen in Figure 4.7.

In the Day 2 spectra, the presence of sulfonate and F peaks in the S 2p and F 1s regions, respectively, indicate that the three faces were successfully modified with F_{13}OT. CF_2 and CF_3 signals are present at ~292 and ~294 eV, as expected (Figure 4.7c).[22] The m-plane face had the largest signal for both elements, indicating the largest F_{13}OT surface concentration (Table 4.9). However, all three faces had two signals in the F 1s region. The larger of these, at 689 eV, is attributed to fluorocarbon bonds, as expected from a fluorinated alkanethiol. The lower-energy shoulder has a BE indicative of Zn-F interactions[23] and suggests that either the F_{13}OT is orientated such that the intact fluorinated backbone is capable of interacting with the ZnO surface, or that the molecule has decomposed, releasing F-containing fragments that interact with the surface.[14] The decomposition of fluorinated

molecules under X-ray irradiation is well-established (discussed in Chapter 3),[22,24–27] thus the latter explanation is most likely. Examination of the F:S ratios (Table 4.9), derived from F 1s and S 2p spectra, shows that the total amount of F on the surface for m-plane ZnO is consistent with $F_{13}OT$ (~12 F : 1 S) while for the polar ZnO faces, the ratios are slightly smaller (~9 F : 1 S). This suggests that for all faces, most F is still present on the surface and has not desorbed following C-F bond cleavage.

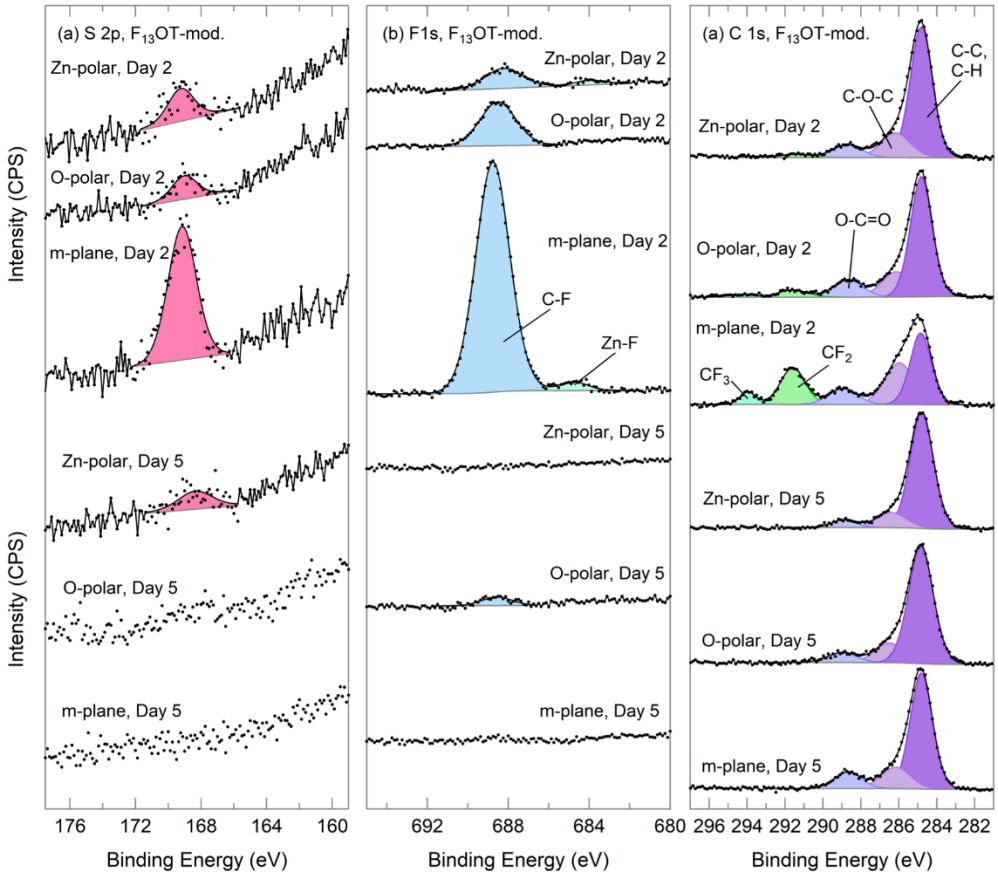

Figure 4.7: Fixed-energy XPS (a) S 2p, (b) F 1s, and (c) C 1s spectra for $F_{13}OT$-modified Zn-polar, O-polar, and m-plane ZnO modified with 1 mM $F_{13}OT$ in THF (ambient conditions) and rinsed with THF (no heating step). Spectra were obtained 22 h after preparation (Day 2) and 3 d later (Day 5). Spectra have been normalised to the same Zn 2p peak area and offset for clarity.

Calculated molecular surface concentrations, listed in Table 4.9, show that when examined 22 h after preparation (Day 2), Zn-polar and O-polar ZnO had sub-monolayer coverage of $F_{13}OT$ (2 molecules nm^{-2}), while m-plane ZnO appeared to have multilayer coverage (12 molecules nm^{-2}). The difference

between faces and to the surface coverage of ODT on m-plane ZnO (3 molecules nm^{-2}) is attributed to physisorbed, oxidised $F_{13}OT$ not being fully rinsed from m-plane ZnO due to its fluorinated alkyl chain. Unlike results seen with ODT, $F_{13}OT$-modified O-polar ZnO does not show any thiolate signal, which suggests that surprisingly, $F_{13}OT$ appears to oxidise more readily than ODT on ZnO.

Table 4.9: Fixed-energy S 2p and F 1s XPS data for $F_{13}OT$-modified Zn-polar, O-polar, and m-plane ZnO modified with 1 mM $F_{13}OT$ in THF (ambient conditions) and rinsed with THF (no heating). Data was obtained 22 h after preparation (Day 2) and 3 d later (Day 5).

Face	S 2p type	S : Zn	F : Zn	F : S	Molecules nm^{-2}
$F_{13}OT$-modified ZnO, Day 2					
Zn-polar	Sulfonate	0.01 : 1	0.1 : 1	8 : 1	2
O-polar	Sulfonate	0.01 : 1	0.1 : 1	9 : 1	2
m-plane	Sulfonate	0.05 : 1	0.6 : 1	12 : 1	12
$F_{13}OT$-modified ZnO, Day 5					
Zn-polar	Sulfonate	0.005 : 1	0 : 1	0 : 1	1
O-polar	None	0 : 1	0.02 : 1	0 : 1	0
m-plane	None	0 : 1	0 : 1		0

After 3 d storage in air and darkness, no S 2p signal was observed on O-polar or m-plane ZnO. This does not follow the results seen with ODT, where a S signal – especially that in the sulfonate region – was still observed for all three faces after 40 d. The lower stability for $F_{13}OT$ than ODT is attributed to fewer stabilising van der Waals interactions and the increased steric bulk of fluorinated modifiers. It is also possible that the heating step used for the ODT modification increased the amount of covalent bonding to the surface, but this was not further investigated. Although a small S signal is obtained for Zn-polar ZnO after 3 d storage in air and darkness, no F 1s signal is evident, indicating decomposition of the fluorinated tail. The nature of S-containing species remaining on the surface is unclear.

In summary, F_{13}OT-modified ZnO was not stable when stored in air and darkness for several days. ODT-modified ZnO was more stable, with loss of thiols from Zn-polar and m-plane ZnO. No S was lost from ODT-modified O-polar ZnO, but thiolates were oxidised to sulfonates.

4.3.3 Comparison of Thiol Modifiers and ZnO Faces

4.3.3.1 Molecular Surface Concentration

Having explored some of the variables involved in preparation of SAMs from thiols, two additional modifiers were examined: the aromatic thiol 4TFMBM and the isothiocyanate, ITC (Table 4.2). Samples were modified in 1 mM of modifier in THF (ambient conditions), rinsed with THF, and kept in the dark for 22 h prior to XPS measurement. Figure 4.8 shows the results of XPS analysis of these samples and, for convenience, data for F_{13}OT-modified ZnO, modified and analysed under the same conditions, are also shown in Figure 4.8. (These results are those shown in Figure 4.7). Similarly, XPS spectra of ODT-modified samples which were rinsed in THF and heated for 30 min (50 °C) immediately prior to analysis are also included in Figure 4.8. (These spectra are also shown in Figure 4.5). Atomic percentages are listed in Appendix 8.2.2.

Figure 4.8 (a, e, i) shows that except for ODT-modified O-polar ZnO, all S 2p signal arises from sulfonate species. The very small, broad peak seen at lower binding energy (~159 eV) arises from a plasmon loss from the Zn 3s transition and is not related to S.[5] The F 1s and C 1s spectra show that organic F species are present where expected, alongside some minor Zn-F interactions, except for 4TFMBM-modified Zn-polar and m-plane ZnO which have no F 1s signal. The O 1s spectra (Figure 4.8d, h, l) are largely unchanged for modified ZnO, but attenuation of the bulk O 1s peak can be seen in the spectra for ODT- and ITC-modified ZnO. For ODT-modified ZnO, this is attributed to the attenuating effect of the long alkyl chain of ODT, and for the O-polar sample, to the substantial amount of sulfonate on the surface which may increase the amount of surface O. However, for ITC-modified ZnO, both bulk and surface O signals are significantly attenuated while the S:Zn ratio indicates only a monolayer is present. The nature of the modifying layer formed by ITC is thus not clear.

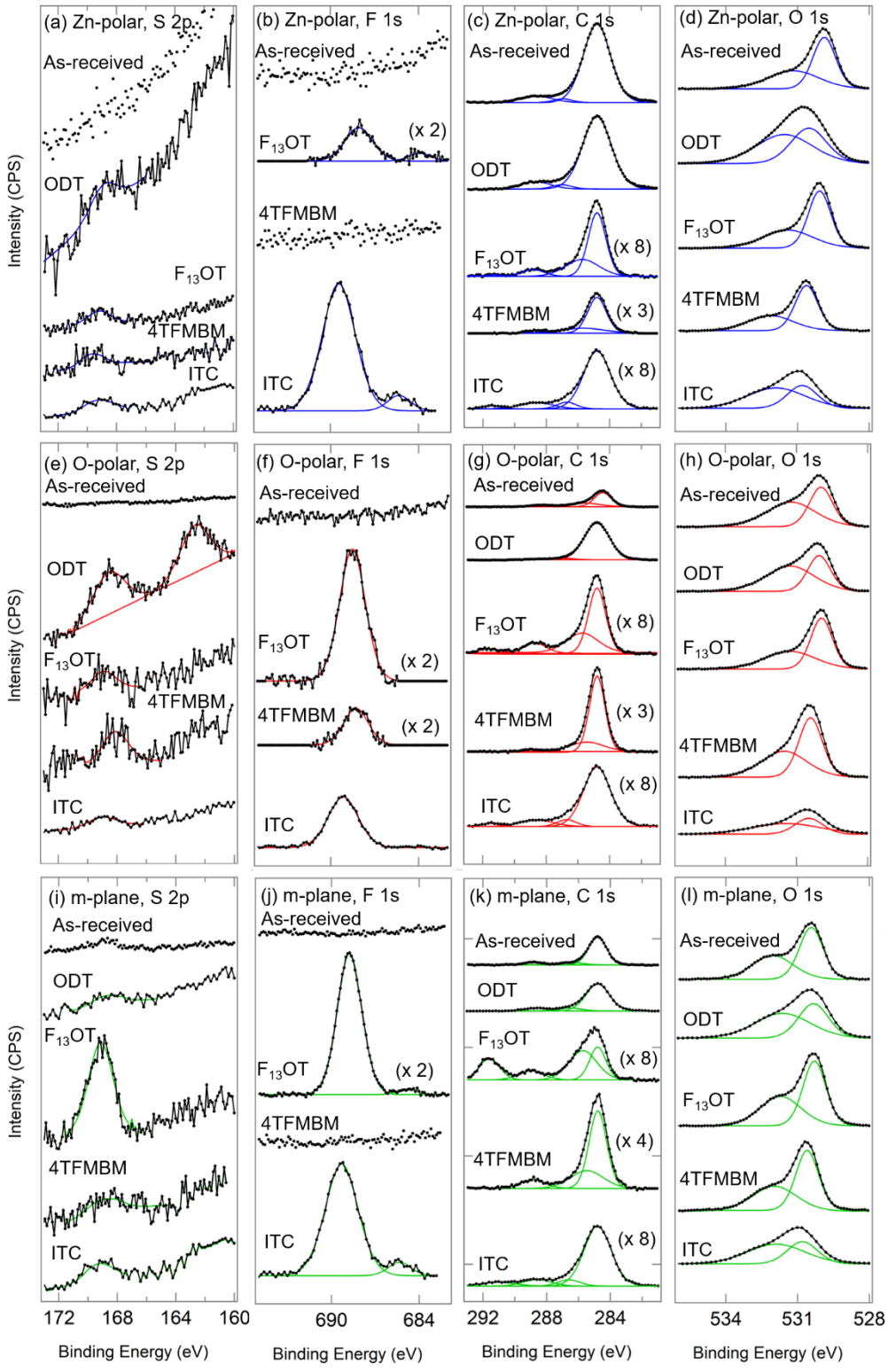

Figure 4.8: Fixed-energy XPS S 2p, F 1s, C 1s, O 1s, and Zn 2p spectra collected on (a – d) Zn-polar, (e – h) O-polar, and (i – l) m-plane ZnO, as-received and modified with 1 mM ODT, F_{13}OT, 4TFMBM, and ITC (ambient conditions). All samples were rinsed with THF after modification. Except for ODT-modified

ZnO, all samples were kept in the dark for 22 h prior to XPS analysis. ODT-modified samples were heated after modification (30 min, 50 °C) and immediately analysed with XPS. Spectra are offset for clarity and normalised to the Zn 2p peak area, scaled where noted. The spectra for ODT- and F_{13}OT-modified samples are also shown in Figures 4.5 and 4.7, respectively.

Table 4.10 gives a summary of fixed-energy XPS results, water CA, and estimated modifier surface concentrations (derived from S:Zn ratios and water CA as described in Section 2.2.4) on the modified surfaces. Only ODT-modified O-polar ZnO and F_{13}OT-modified m-plane ZnO had molecular surface concentrations greater than a monolayer, and only the former sample had evidence of non-oxidised modifiers. This suggests that sulfonate bonds are more likely than direct Zn-S bonds regardless of the modifier type. Garrell et al. observed through surface-enhanced Raman spectroscopy that aromatic thiolate monolayers on Au are less prone to oxidation than alkanethiolate monolayers, but this difference is not seen in the present work:[28] 4TFMBM and ITC modifiers both have a sulfonate signal. Their calculated molecular coverages are approximately a monolayer. However, these were calculated using S:Zn ratios, which do not account for decomposition of the modifiers as seen below. It is thus unclear how many molecules are on the surface, and the species on the surface after reaction with ITC could not be determined from XPS.

All ZnO surfaces showed an increase in water CA and therefore hydrophobicity after reaction with the modifiers. Due to the relatively large margin of error for contact angle measurements, only angle differences > 10° were considered significant. The CAs for the modified ZnO samples are not always consistent with the calculated Zn:S ratios (Table 4.10); this is assumed to be related to the uniformity of the modifiers at the surface. Further, the CA are smaller than those observed on PA-modified ZnO (Chapter 3). This is consistent with work by Perkins, who observed that hexanethiol-modified ZnO had significantly smaller water CA than did analogous hexylPA-modified surfaces, due to differences in uniformity.[5]

*Table 4.10: Fixed-energy XPS data for thiol surface coverage on Zn-polar, O-polar, and m-plane ZnO modified with 1 mM ODT, F_{13}OT, 4TFMBM, and ITC in THF (ambient conditions). All samples were rinsed with THF after modification. Except for ODT-modified ZnO, all samples were kept in the dark for 22 h prior to XPS analysis. *ODT-modified samples were heated (30 min, 50 °C) and immediately analysed with XPS. All water contact angles have an uncertainty of ± 10°.*

Sample	S 2p type	S : Zn	S : F	S : N	Water CA (°)	Molecule nm^{-2}
Zn-polar						
As-received	-	-	-	-	64	-
*ODT	Sulfonate	0.007 : 1	-	-	88	2
F_{13}OT	Sulfonate	0.012 : 1	1 : 6	-	104	3
4TFMBM	Sulfonate	0.012 : 1	1 : 0	-	73	3
ITC	Sulfonate	0.009 : 1	1 : 21	1 : 1	84	2
O-polar						
As-received	-	-	-	-	56	-
*ODT	Sulfonate & thiolate	0.07 : 1	-	-	101	16
F_{13}OT	Sulfonate	0.013 : 1	1 : 10	-	78	3
4TFMBM	Sulfonate	0.018 : 1	1 : 2	-	83	4
ITC	Sulfonate	0.015 : 1	1 : 9	1 : 1	80	4
m-plane						
As-received	-	-	-	-	48	-
*ODT	Sulfonate	0.007 : 1	-	-	-	2
F_{13}OT	Sulfonate	0.048 : 1	1 : 12	-	99	11
4TFMBM	Sulfonate	0.015 : 1	1 : 0	-	68	4
ITC	Sulfonate	0.013 : 1	1 : 16	1 : 1	80	3

The S:F ratios for 4TFMBM-modified ZnO are much smaller than expected, which is attributed to C-F cleavage during XPS and loss of F from the surface. For ITC-modified ZnO, the S:F ratios are much larger than expected, while the S:N ratios for ITC are ~1:1. This suggests that ITC has decomposed, liberating S and N in equal amounts from the surface, and leaving organic F on the surface. As the C % is similar to other modifiers (Appendix 8.2.2), it is tentatively proposed that the phenyl ring remains intact. This was not further investigated. Generally, O-polar ZnO has less evidence of modifier disintegration,

which is consistent with the O-polar face being the least reactive face of the three faces,[29] but this evidence is not statistically significant. It is unknown why 4TFMBM appears more susceptible to decomposition than ITC or F_{13}OT.

4.3.3.2 Band Bending at Thiol-Modified ZnO

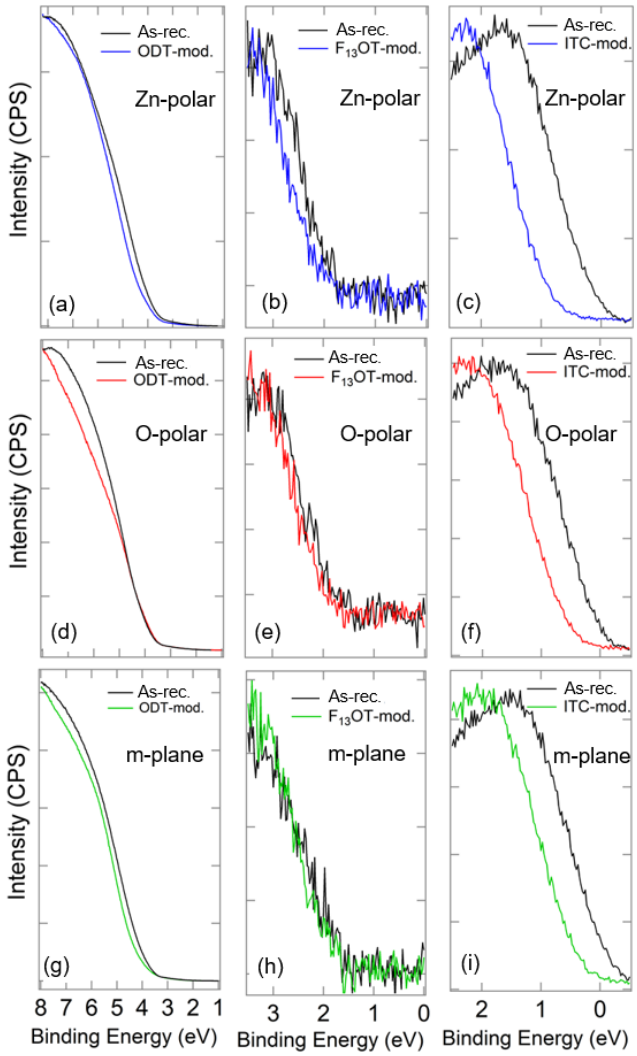

Figure 4.9: UPS (a, d, g) and XPS (all others) VB spectra for and ODT-, F_{13}OT-, and ITC-modified Zn-polar (a – c), O-polar (d – f), and m-plane (g – i) ZnO. On all spectra, the black trace indicates the spectrum of the corresponding as-received ('as rec.') ZnO sample. The spectra have been normalised in the y-direction for visual clarity, but no calibration has been applied to the binding energy scale. As such, all values are relative to the respective as-received ZnO sample.

The effects of ODT, F_{13}OT, and ITC on the VB spectrum of ZnO were studied using fixed-energy XPS (*hv* = 1486.6 eV) and UPS (*hv* = 21.2 eV). 4TFMBM was not investigated as core level XPS spectra (Figure 4.8) showed that it had significantly decomposed on the surface. The results, seen in Figure 4.9, indicated that all modifiers had only a small effect on band bending, except for ITC. This is most likely due to a significant amount of OH remaining on the surface after modification, and perhaps the high level of thiol oxidation gives a surface interaction similar to that for PAs.

The spectra in Figure 4.9 obtained using XPS show large BE differences between the as-received ZnO samples used in different experiments. The values of ζ derived from XPS spectra for as-received ZnO varied hugely, from 1.5 eV to -0.5 eV. Such values are inconsistent with previous work on ZnO, which showed that ZnO has a typical ζ value > 3.2 eV, giving downwards band bending. This difference is most likely due the XPS instrument used, which had not been calibrated for many years, and the lack of external reference sample.[30] UPS spectra were calibrated to freshly-cleaned Pt and thus gave the expected ζ values and absolute band bending values for the surface region probed at *hv* = 21.2 eV. However, for all samples, the calculated $\Delta\zeta$ values are reliable (Table 4.11), showing the change in band bending for a modified sample relative to an as-received sample measured in the same experiment with a particular photon energy.

The use of UPS to study the ODT-modified samples means that the band bending closer to the surface is being probed than when using fixed-energy XPS. The low photon energy (*hv* = 21.2 eV) can be problematic as contributions from the molecular orbitals of the modifiers can convolute the VB spectra. This may be seen in Figure 4.9d on O-polar ZnO; it is more difficult to know where the VB edge is compared to XPS VB spectra. However, it appears that the downwards band bending on ODT-modified Zn-polar and m-plane ZnO has increased by ~0.3 eV, while for ODT-modified O-polar ZnO, downwards band bending has decreased by ~0.1 eV. This difference is most likely due to the different oxidation states and surface coverage of ODT on the surface: Zn-polar and m-plane ZnO had a sub-monolayer of sulfonate modifiers whereas O-polar ZnO had a thick multilayer with 50% of the S 2p

signal attributed to thiolates. Chen et al. performed Mott-Schottky analysis on thiolate-bound ODT on m-plane ZnO and observed that the ODT modifier decreased the negative band bending.[1] This evidence, coupled with the decreased negative band bending on ODT-modified O-polar ZnO seen in this work, suggests that thiolate-bound ODT may decrease negative surface band bending at ZnO surfaces, while ODT bound as Zn-O-S increases the negative band bending. Ozawa et al. also observed a decrease in downwards band bending on Zn-polar ZnO when tetrathiafulvalene was non-dissociatively bound to ZnO via S-Zn bonds, which adds weight to this explanation.[31]

*Table 4.11: Surface band bending for ZnO samples modified with ODT, F_{13}OT, and ITC, from valence band XPS data. * Samples were analysed using UPS and calibrated to the Fermi level of a Pt reference sample.*

Sample	Δζ (eV)	Abs. BB
Zn-polar ZnO		
ODT	-0.34 ± 0.05*	-0.80 ± 0.05*
F_{13}OT	-0.3 ± 0.2	-
ITC	-0.8 ± 0.1	-
O-polar ZnO		
ODT	+0.13 ± 0.05*	-0.39 ± 0.05*
F_{13}OT	-0.2 ± 0.2	-
ITC	-0.6 ± 0.1	-
m-plane ZnO		
ODT	-0.26 ± 0.05*	-0.90 ± 0.05*
F_{13}OT	-0.0 ± 0.2	-
ITC	-0.5 ± 0.1	-

Due to the poor resolution of the VB spectra for F_{13}OT-modified ZnO, the uncertainty of Δζ is high. However, a clear shift to higher BE can be seen for the VB edge of F_{13}OT-modified Zn-polar ZnO, consistent with an increase in downwards band bending of ~−0.3 eV (Table 4.11). The F_{13}OT surface coverage for this sample was significantly less than seen for m-plane ZnO, which showed no change in ζ. It is thus unlikely that the sulfonate modification produced this band bending change. Instead it is

proposed that F interacting directly with Zn, as was observed in the F 1s core level spectrum (Figure 4.8a), acts as a donor on the Zn-polar surface.[23] This was also observed for decomposed F_{13}OPA on ZnO in Chapter 3.

The most significant and reliable $\Delta\zeta$ was seen for ITC-modified ZnO; all faces showed an increase in downwards band bending of > 0.5 eV (Table 4.11). This is a significant change, but its origins are not clear. While elemental S acts as a donor in ZnO,[31] S was present as sulfonate (or similar) on ITC-modified ZnO, and so it seems unlikely to be able to act as a donor. Further, the smallest band bending change is seen on m-plane ZnO, which had a similar S:Zn ratio to the O-polar face, whereas the largest $\Delta\zeta$ was observed for ITC-modified Zn-polar ZnO (−0.8 eV), which had the smallest S:Zn ratio of the three ZnO faces (Table 4.10). In terms of F, significant F-Zn interactions were observed on the F 1s spectrum for Zn-polar and m-plane ZnO. In contrast to other F-containing modifiers (F_{13}OT and 4TFMBM), the S:F ratio was considerably lower than expected, suggesting that the bistrifluoromethylphenyl moiety is interacting with the surface after loss of S. However, the trend in $\Delta\zeta$ does not match the amount of Zn-F on the surface. Another factor to consider is the S:N ratio; this is approximately 1:1 for all three ZnO faces but the degree to which decomposition has occurred is not known. While elemental N acts as an acceptor in ZnO and would shift ζ to lower BE,[32] it is possible that the N=C moiety acts as a donor. An alternative mechanism is nucleophilic attack on the carbon in N=C=S by the ZnO hydroxyl groups, giving a thiourea Zn-O-C linkage (Figure 4.10). The sulfur would have to undergo subsequent oxidation in order to give the XPS S 2p signal at ~169 eV.

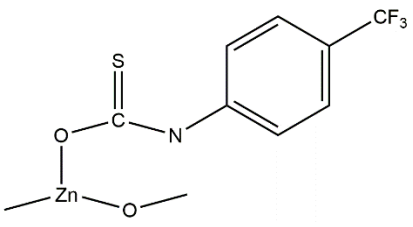

Figure 4.10. Possible binding mode for ITC on ZnO.

Although the shift in ζ on ITC-modified ZnO is significant and interesting, when the samples were re-analysed 5 days after modification (Appendix 8.2.3), XPS spectra showed that the significant amounts of S and F had been lost from the surface and that band bending had returned to the same values as as-received ZnO samples. This indicates that the increase in downwards band bending observed on ITC-modified ZnO is short-lived and that ITC modification therefore appears not be a practical modification method.

4.4 Conclusion

A method was developed for ODT modification of ZnO; during this process, a number of observations about the nature of ODT on ZnO were made. Firstly, multilayers of non-oxidised thiols readily form on the surface. These undergo oxidation to a small degree during modification, but more significantly when exposed to air for even a short time (< 1 d). Thiolate multilayers can be removed from Zn-polar and m-plane ZnO by rinsing in a solvent which dissolves thiols to give approximately monolayer surface coverage on ZnO. On O-polar ZnO, a single THF rinse was not successful in removing these multilayers. It is suggested that thiols are more easily oxidised on, and removed from, Zn-polar and m-plane ZnO due to the increased catalytic nature of these faces compared to O-polar ZnO, and a lower tendency of sulfonates to physisorb compared to thiolates. Other workers reported both thiolate and sulfonate bonds on ZnO faces, but it is difficult to detect any trend because of variations in modification procedures in those experiments. From this work, it appears that ODT modification of all three ZnO faces results in approximately a monolayer of sulfonate-type ODT, but it is not clear whether modifiers bind to the surface as sulfonates or bind as thiolates and oxidise to sulfonates post-modification.

The difficulty of obtaining close-packed, well-characterised thiol-derived monolayers on ZnO means that surface modification layers are somewhat irreproducible, and it was therefore difficult to observe a trend in the reactivities of Zn-polar, O-polar, and m-plane ZnO towards modification with different thiol derivatives and ITC. It was seen that O-polar ZnO had the highest surface concentration of ODT, and m-plane ZnO had the highest surface coverage of F_{13}OT, but these large multilayer surface

coverages did not lead to large changes in the surface band bending of ZnO. This is evidence that significant amounts of ODT and F_{13}OT were not directly bound to ZnO and had no effect on its electron density. ITC-modification of ZnO had the largest effect on band bending, increasing the downwards band bending by ~0.7 eV on all ZnO faces. However, the modifier layer was not stable, desorbing from the surface within several days.

While some authors have reported that alkanethiols are useful for assembling SAMs on ZnO, the present work shows that reproducible alkanethiol modification of ZnO is difficult and that the resulting layers are not stable. Overall, thiols gave lower surface concentrations and had poorer stability than PAs on ZnO. Sulfonate-type ODT monolayers remain on the surface of O-polar ZnO after 40 d storage in air and darkness, while significant desorption was observed on ODT-modified Zn-polar and m-plane ZnO in the same conditions.

This work aimed to systematically study the formation of thiol SAMs on ZnO and untangle several contradictory reports from previous studies. It did not establish conditions where reproducible thiolate SAMs were formed on the surface, but results suggest that the large variability in previous reports are due to the catalytic nature of ZnO, which is expected to vary with crystal quality as well as face. Differences in the modification and post-modification treatments also play an important role. This work highlighted the importance of rinsing modified ZnO with a solvent that can dissolve thiols. It was conclusively demonstrated that preparing SAMs from alkanethiols is not an attractive route to modified ZnO substrates for practical applications.

4.5 References

(1) Chen, J.; Ruther, R. E.; Tan, Y.; Bishop, L. M.; Hamers, R. J. Molecular Adsorption on ZnO($10\bar{1}0$) Single-Crystal Surfaces: Morphology and Charge Transfer. *Langmuir* **2012**, *28* (28), 10437–10445.

(2) Sadik, P. W.; Pearton, S. J.; Norton, D. P.; Lambers, E.; Ren, F. Functionalizing Zn- and O-Terminated ZnO with Thiols. *J. Appl. Phys.* **2007**, *101* (10), 1–6.

(3) Taratula, O.; Galoppini, E.; Wang, D.; Chu, D.; Zhang, Z.; Chen, H.; Saraf, G.; Lu, Y. Binding Studies of Molecular Linkers to ZnO and MgZnO Nanotip Films. *J. Phys. Chem. B* **2006**, *110* (13), 6506–6515.

(4) Ogata, K.; Hama, T.; Hama, K.; Koike, K.; Sasa, S.; Inoue, M.; Yano, M. Characterization of Alkanethiol/ZnO Structures by X-Ray Photoelectron Spectroscopy. *Appl. Surf. Sci.* **2005**, *241* (1–2), 146–149.

(5) Perkins, C. L. Molecular Anchors for Self-Assembled Monolayers on ZnO: A Direct Comparison of the Thiol and Phosphonic Acid Moieties. *J. Phys. Chem. C* **2009**, *113* (42), 18276–18286.

(6) Pesika, N. S.; Hu, Z.; Stebe, K. J.; Searson, P. C. Quenching of Growth of ZnO Nanoparticles by Adsorption of Octanethiol. *J. Phys. Chem. B* **2002**, *106* (28), 6985–6990.

(7) Rhodes, C. L.; Lappi, S.; Fischer, D.; Sambasivan, S.; Genzer, J.; Franzen, S. Characterization of Monolayer Formation on Aluminum-Doped Zinc Oxide Thin Films. *Langmuir* **2008**, *24* (2), 433–440.

(8) Hamers, R. J.; Coulter, S. K.; Ellison, M. D.; Hovis, J. S.; Padowitz, D. F.; Schwartz, M. P.; Greenlief, C. M.; Russell, J. N. Cycloaddition Chemistry of Organic Molecules with Semiconductor Surfaces. *Acc. Chem. Res.* **2000**, *33* (9), 617–624.

(9) Loscutoff, P. W.; Wong, K. T.; Bent, S. F. Reaction of Phenyl Isocyanate and Phenyl Isothiocyanate with the Ge(100)-2 × 1 Surface. *J. Phys. Chem. C* **2010**, *114* (33), 14193–14201.

(10) Laforgue, A.; Addou, T.; Bélanger, D. Characterization of the Deposition of Organic Molecules at the Surface of Gold by the Electrochemical Reduction of Aryldiazonium Cations. *Langmuir* **2005**, *21* (15), 6855–6865.

(11) Timpel, M.; Nardi, M. V.; Krause, S.; Ligorio, G.; Christodoulou, C.; Pasquali, L.; Giglia, A.; Frisch, J.; Wegner, B.; Moras, P.; Koch, N. Surface Modification of ZnO(0001)-Zn with Phosphonate-Based Self-Assembled Monolayers: Binding Modes, Orientation, and Work Function. *Chem. Mater.* **2014**, *26* (17), 5042–5050.

(12) Cassie, A. B. D. Contact Angles. *Discuss. Faraday Soc.* **1948**, *3*, 11–16.

(13) Alves, C. A.; Porter, M. D. Atomic Force Microscopic Characterization of a Fluorinated Alkanethiolate Monolayer at Gold and Correlations to Electrochemical and Infrared Reflection Spectroscopic Structural Descriptions. *Langmuir* **1993**, *9* (12), 3507–3512.

(14) NIST X-Ray Photoelectron Spectroscopy Database, Version 4.1, 2012. National Institute of Standards and Technology, Gaithersburg. http://srdata.nist.gov/xps/ (accessed Oct 18, 2015).

(15) Castner, D. G.; Hinds, K.; Grainger, D. W. X-Ray Photoelectron Spectroscopy Sulfur 2p Study of Organic Thiol and Disulfide Binding Interactions with Gold Surfaces. *Langmuir* **1996**, *12* (21), 5083–5086.

(16) Chen, X.; Luais, E.; Darwish, N.; Ciampi, S.; Thordarson, P.; Gooding, J. J. Studies on the Effect of Solvents on Self-Assembled Monolayers Formed from Organophosphonic Acids on Indium Tin Oxide. *Langmuir* **2012**, *28* (25), 9487–9495.

(17) Schoenfisch, M. H.; Pemberton, J. E. Air Stability of Alkanethiol Self-Assembled Monolayers on Silver and Gold Surfaces. *J. Am. Chem. Soc.* **1998**, *120* (18), 4502–5413.

(18) Jang, L. S.; Keng, H. K. Modified Fabrication Process of Protein Chips Using a Short-Chain Self-Assembled Monolayer. *Biomed. Microdevices* **2008**, *10* (2), 203–211.

(19) Laibinis, P. E.; Whitesides, G. M. Self-Assembled Monolayers of *n*-Alkanethiolates on Copper Are Barrier Films That Protect the Metal against Oxidation by Air. *J. Am. Chem. Soc.* **1992**, *114* (23), 9022–9028.

(20) Love, J. C.; Wolfe, D. B.; Haasch, R.; L, M.; Paul, K. E.; Whitesides, G. M.; Nuzzo, R. G.; Chabinyc,

M. L. Formation and Structure of Self-Assembled Monolayers of Alkanethiolates on Palladium. **2003**, 2597–2609.

(21) Huang, J.; Hemminger, J. C. Photooxidation of Thiols in Self-Assembled Monolayers on Gold. *J. Am. Chem. Soc.* **1993**, *115* (8), 3342–3343.

(22) Ferraria, A. M.; Lopes da Silva, J. D.; Botelho do Rego, A. M. XPS Studies of Directly Fluorinated HDPE: Problems and Solutions. *Polymer* **2003**, *44* (23), 7241–7249.

(23) Polydorou, E.; Zeniou, A.; Tsikritzis, D.; Soultati, A.; Sakellis, I.; Gardelis, S.; Papadopoulos, T. A.; Briscoe, J.; Palilis, L. C.; Kennou, S.; Gogolides, E.; Argitis, P.; Davazoglou, D.; Vasilopoulou, M. Surface Passivation Effect by Fluorine Plasma Treatment on ZnO for Efficiency and Lifetime Improvement of Inverted Polymer Solar Cells. *J. Mater. Chem. A* **2016**, *4* (30), 11844–11858.

(24) Kissa, E. Analysis of Fluorinated Surfactants. In *Fluorinated Surfactants and Repellents*; Marcel Dekker, Inc.: New York, 2001; pp 390–450.

(25) Thermo Scientific: XPS Simplified. Fluorine, 2013. http://xpssimplified.com/elements/fluorine.php (accessed Dec 2, 2016).

(26) Ravichandran, L.; Selvam, K.; Swaminathan, M. Photoassisted Catalytic Cleavage of the C-F Bond in Pentafluorophenol with ZnO and the Effect of Operational Parameters. *Aust. J. Chem.* **2007**, *60* (12), 951–956.

(27) Barriet, D.; Lee, T. R. Fluorinated Self-Assembled Monolayers: Composition, Structure and Interfacial Properties. *Curr. Opin. Colloid Interface Sci.* **2003**, *8* (3), 236–242.

(28) Garrell, R. L.; Chadwick, J. E.; Myles, D. C.; Severance, D. L.; McDonald, N. A. Adsorption of Sulfur Containing Molecules on Gold: The Effect of Oxidation on Monolayer Formation and Stability Characterized by Experiments and Theory. *J. Am. Chem. Soc.* **1995**, *117* (46), 11563–11571.

(29) Akhter, S.; Lui, K.; Kung, H. H. Comparison of the Chemical Properties of the Zinc-Polar, the Oxygen-Polar, and the Nonpolar Surfaces of Zinc Oxide. *J. Phys. Chem.* **1985**, *89* (10), 1958–1964.

(30) Scheithauer, U. Long Time Stability of the Energy Scale Calibration of a Quantum 2000. *J. Electron Spectros. Relat. Phenomena* **2012**, *184* (11–12), 542–546.

(31) Ozawa, K.; Munakata, S.; Edamoto, K.; Mase, K. Electron Donor Molecule on the Oxide Surface: Influence of Surface Termination of ZnO on Adsorption of Tetrathiafulvalene. *J. Phys. Chem. C* **2011**, *115* (44), 21843–21851.

(32) Morkoç, H.; Özgür, Ü. *Zinc Oxide: Fundamentals, Materials and Device Technology*; Wiley-VCH: Weinheim, 2009.

5 Aryldiazonium Ion Chemistry at Single Crystal ZnO Surfaces

5.1 Introduction

As detailed in Chapter 1, aryldiazonium ions are a common precursor for covalently-bound organic layers on carbon,[1–4] metals,[5,6] and semiconductors such as silicon,[7,8] ITO,[9–11] TiO_2,[11,12] MnO_2,[13] iron oxide,[14] SnO_2,[11,12] and ZnO.[11,15] The diazonium ion can either be formed in situ or prepared as a salt beforehand through straightforward one-step reactions.[16] Tetrafluoroborate salts are commonly used because of their stability and lack of explosion risk: due to the bulky anion, the diazonium ion will decompose via the Balz-Schiemann reaction to form fluoroaryl groups.[17] However, they are still sensitive to heat and light and must be stored in appropriate conditions.[18]

Electrochemistry was the first reported method of forming aryl layers from aryldiazonium salt solutions.[19] It is a relatively simple way of supplying electrons for the reduction of aryldiazonium ions, although some substrates are capable of spontaneously reducing aryldiazonium ions without applied potential.[20–22] Typically, cyclic voltammetry (CV) is carried out with a three-electrode cell, where the substrate to be modified acts as the working electrode. The solution consists of the aryldiazonium salt in its tetrafluoroborate form and a supporting electrolyte such as H_2SO_4 or tetrabutylammonium tetrafluoroborate ($[Bu_4N]BF_4$) in aqueous or non-aqueous conditions, respectively.[11,23] Once grafted to a substrate, further chemistry can be carried out on the layer to achieve specific functionalisation for applications such as sensors.[6]

5.1.1 Electrochemical Grafting from Aryldiazonium Ions at Gold and Carbon

CVs give information on the electrochemical reduction of aryldiazonium ions occurring at the substrate during grafting. A typical CV for NBD reduction at a gold electrode is shown in Figure 5.1. Here, three scans were performed between +0.65 V and −0.1 V. On the first cycle, a large current density peak is seen around +0.58 V, corresponding to the reduction of NBD to NP radicals. Correspondingly, the mass of the grafted film increases, as seen on the mass-potential curve. On the second and third CV scans, very little current is seen, indicating that NP grafting has occurred and is

blocking the electrode from further electron transfer and thus reduction processes. However, grafting still occurs according to the mass-potential curves. A complicating factor in CV interpretation is that the current output relates to how many aryldiazonium ions have been reduced, not how many radicals have then grafted to the substrate, and the grafting efficiency is not 100%.

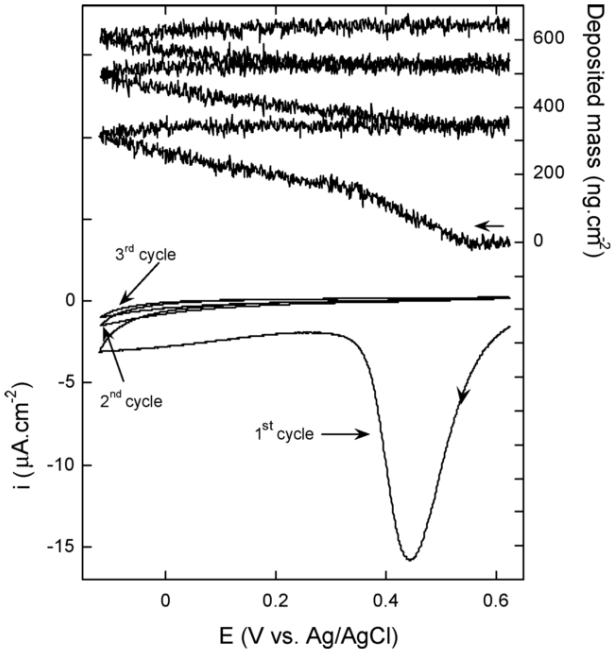

Figure 5.1. Repeat CVs and mass-potential curves of an Au electrode in 5 mM NBD, 0.1 M $[Bu_4N]BF_4$-ACN. Scan rate = 5 mV s^{-1}. Adapted from Laforgue et al.[24]

Although the reduction of a diazonium ion is a one-electron process, the mechanisms that occur are complicated. This is reflected in the variety of CVs observed for different substrates, modifiers,[25,26] modifier concentrations,[27] scan rates,[3] and potential ranges.[3,15] Importantly, there have been reports of different CVs obtained at similar substrates in identical conditions.[3,28] This highlights the subtleties of aryldiazonium ion reduction, which are not fully understood. For example, Benedetto et al. studied the CVs obtained during reduction of a highly-passivating, fluorinated aryldiazonium salt at three different types of Au surfaces, shown in Figure 5.2.[28] These surfaces were:

A-Au: polycrystalline Au on glass

B-Au: Au(111) on mica

C-Au: Au deposited on bronze by galvanoplasty.

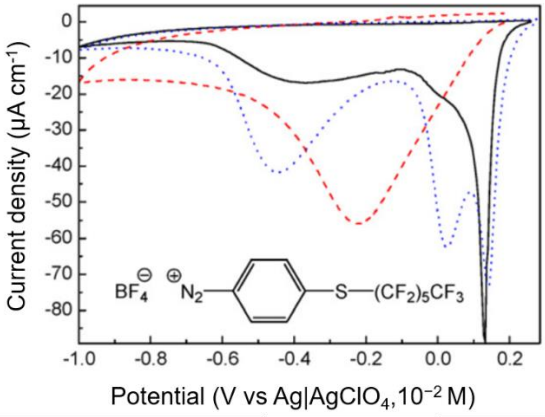

Figure 5.2. Single CVs acquired during grafting at 3 different Au surfaces from a fluorinated aryldiazonium salt (inset) in ACN-[Et_3N]PO_4H_3. Blue = Au-A (polycrystalline Au on glass); Black = B-Au (Au(111) on mica); Red = Au-C (Au on bronze). Adapted from Benedetto et al.[28]

Experiments were carried out in inert atmosphere to observe differences in the grafting CVs for each of these three substrates. For A-Au, the authors observed three separate peaks in the CV (Figure 5.2, blue), while for C-Au, a single broad peak was seen (red). B-Au showed one high-current peak with two broader, less-distinct peaks at more negative potential (black). The authors first noted that the cleanness of the Au substrates was important: for freshly-cleaned A-Au surfaces, the three CV peaks were present as in Figure 5.2, while substrates that had been exposed to air for a longer time produced a CV with only one broad peak. The authors point to this as an explanation for why most CVs reported elsewhere lack multiple reduction peaks.

The second main conclusion Benedetto et al. drew was that the crystal orientation of the Au substrate was important. This was not a new observation, but they were able to attribute the peak at positive potential to the reduction of the aryldiazonium ion at Au(111), the more negative peak to reduction at Au(100), and the most negative peak to reduction at the remaining crystal facets present, including those with lattice defects. These were assigned by comparing the work functions and corresponding points of zero charge of each crystallographic orientation of Au in solution.

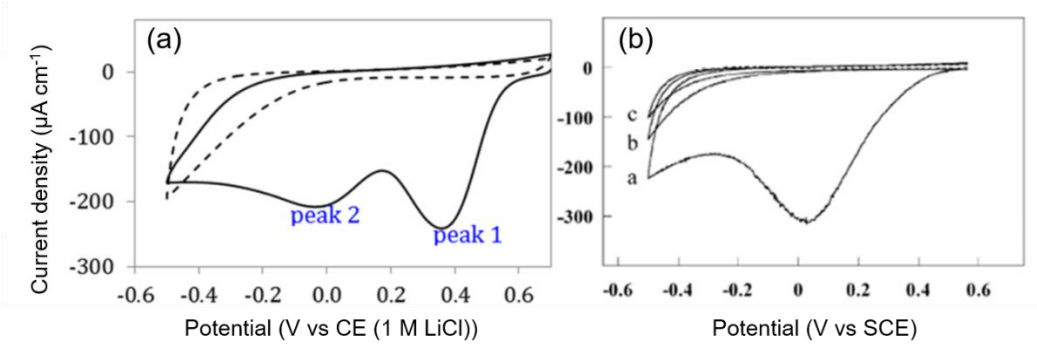

Figure 5.3. Repeat CVs (scan rate = 200 mV s^{-1}) on glassy carbon surfaces, obtained in 0.1 M $[Bu_4N]BF_4$–ACN of (a) 1 mM NBD (solid line = first scan; dashed line = second scan) [3] *and (b) 2 mM NBD (a, c, d = first, second, third scans). (a) Obtained by Lee et al.*[3] *(b) Obtained by Adenier et al.*[22]

CVs for aryldiazonium ion reduction at carbon are also complicated. Lee et al.[3] compared a CV of nitrobenzene diazonium (NBD) reduction obtained at glassy carbon (GC) to that observed by Adenier et al. (Figure 5.3).[22] While Adenier et al. observed only one broad reduction peak in the first scan (Figure 5.3b), the CV collected by Lee et al. showed two peaks (Figure 5.3a). For second and subsequent scans, the CVs are similar: the current attenuates due to the presence of a blocking nitrophenyl (NP) film on the carbon electrode. Cline et al. had proposed that, like that observed on Au surfaces, the presence of 2 peaks vs only one peak was due to the cleanness of the carbon substrate.[29] Lee explored this further and examined NBD grafting at three types of carbon surfaces: glassy carbon (GC), highly-ordered pyrolytic graphite (HOPG), and pyrolyzed photoresist films (PPF).[3] The results can be seen in Figure 5.4.

Similar to the work of Benedetto et al. on Au, Lee et al. observed that NBD reduction at two carbon surfaces (GC and PPF) produced two distinct reduction peaks, while NBD reduction at HOPG resulted in one dominant peak and a low-current, broad peak at more negative potential.[3] The authors confirmed through film thickness measurements that both peaks result in NP grafting. They tentatively proposed that a catalytic reduction of NBD can occur at a clean carbon surface, giving a sparse multilayer which grows until the NBD can no longer interact with the surface. This manifests in a reduction peak at a relatively positive potential. Then, when a more negative potential is applied, it

drives non-catalytic reduction to result in NP radicals 'filling in the gaps' of the sparse film already present on the surface. However, the catalysed reduction peak was observed for all carbon surfaces (GC, HOPG, PPF) despite HOPG consisting mainly of basal planes and GC and PPF consisting mainly of edge planes. This meant that Lee et al. were unable to assign the catalytic reaction to a particular carbon site.

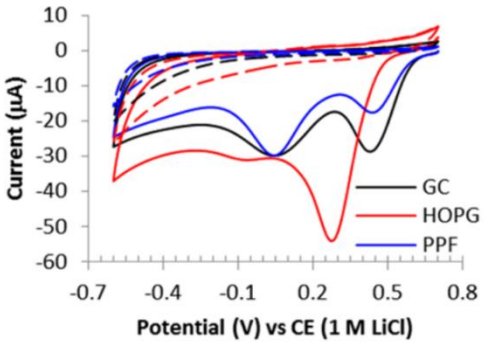

Figure 5.4. Repeat CVs obtained in 1 mM NBD in 0.1 M $[Bu_4N]BF_4$-ACN (scan rate = 50 mV s^{-1}) at GC (black), HOPG (red), and PPF (blue). Solid line = first scan; dashed line = second scan. Adapted from Lee et al.[3]

Another complicating factor with CV interpretation is 'spontaneous' reduction – where the aryldiazonium ion is reduced without an applied potential – which can occur on substrates such as carbon.[20,25,30] If an electrode is kept in the grafting solution prior to application of potential, spontaneous reduction and grafting can occur, affecting the appearance of the subsequent CVs.[3]

5.1.2 Electrochemical Grafting from Aryldiazonium Ions at ZnO

As mentioned in Chapter 1, Wang et al. used electrochemistry to graft NP layers to Al-doped nanocrystalline ZnO films in $[Bu_4N]BF_4$-ACN (anhydrous).[15] Figure 5.5 shows the CVs for this process over short and long potential ranges. In Figure 5.5a, one broad peak can be seen at −0.3 V vs Ag/Ag^+, which is attenuated on the second scan. On subsequent scans, the peak is not significantly attenuated further. Figure 5.5b shows the same system over a wider potential range, and 3 peaks at more negative potentials, in addition to the peak seen in Figure 5.5a. Of these, the one at −1.12 V vs Ag/Ag^+ was

attributed to a 'small amount of unattached' NBD, while the peaks at −1.32 and −1.50 V vs Ag/Ag^+ were attributed to the reduction of grafted NP groups (see Section 5.1.3). This reduction is chemically reversible in anhydrous ACN.

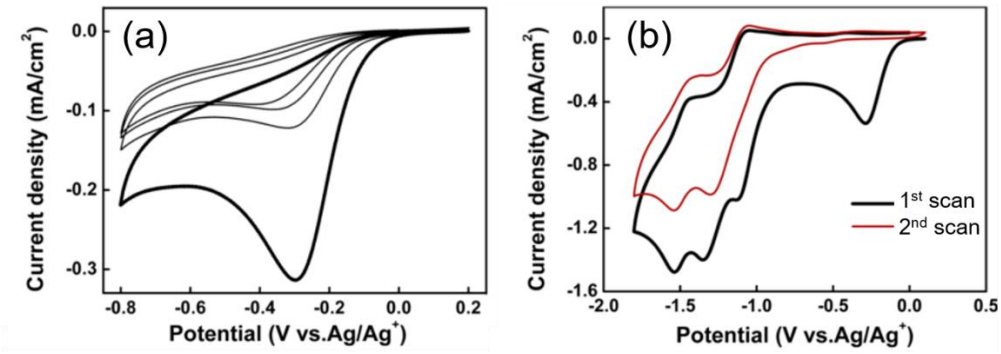

Figure 5.5: Repeat CVs at nanocrystalline ZnO films in 1 mM NBD in anhydrous $[Bu_4N]BF_4$-ACN at 200 mV s^{-1}. (a) Scanning range +0.2 to −0.8 V vs Ag/Ag^+; (b) Scanning range 0 to −1.8 V vs Ag/Ag^+. (Highest current is Scan 1) Adapted from Wang et al.[15]

Bangle et al. modified a ZnO nanoparticle film on FTO with diazonium ion-based ruthenium complexes formed in situ and grafted by applying a fixed potential for 30 min. They noted that the optimal potential for grafting to ZnO ranged from +0.14 V vs NHE (−0.1 V vs SCE) to −0.2 V vs NHE (−0.44 V vs SCE).[11] This range varied across other metal oxides such as SnO_2, ZrO_2, and TiO_2 and was convoluted by the non-planar nanoparticles. No further explanation for the different CVs was given.

Electrochemical grafting from aryldiazonium ions at carbon, Au, and ZnO surfaces involves complicated processes. CVs can offer a limited insight into these processes, but they are not fully understood.

5.1.3 Reduction of Nitrophenyl Films

NBD has been used for electrochemically grafting multi-layered NP films on a range of substrates.[2,4,31] The grafted NP groups have a distinctive N 1s XPS binding energy (BE) which offers a useful tag for analysis. Furthermore, nitro groups can be reduced to amino groups, which are versatile functional groups commonly used in linking reactions such as with carboxylic acids to form amides.[32] The nature

of aryldiazonium salt synthesis from anilines precludes straightforward preparation of isolated arylamine diazonium salts, so the amine functionality is often produced post-grafting.

Grafted NP groups can be fully reduced to form aminophenyl groups via a 6 electron process (Equations 5.1 and 5.2), or partially reduced to NHOH groups via a 4 electron pathway (Equation 5.1 only):[4]

$$C_6H_4(NO_2) \xrightarrow{+\,4H^+ + 4e^-} C_6H_4(NHOH) + H_2O \qquad (5.1)$$

$$C_6H_4(NHOH) \xrightarrow{+\,2H^+ + 2e^-} C_6H_4(NH_2) + H_2O \qquad (5.2)$$

Yu et al. trialled a range of techniques for reducing NP films on carbon substrates.[4] These were electrochemical reduction methods in various media (0.25 M H_2SO_4; 0.1 M KCl in 1:9 ethanol:H_2O, and 20 mM benzoic acid in 0.1 M $[Bu_4N]BF_4$-ACN) and a chemical reduction process using ethanolic Na_2S. It was found that the latter method gave the cleanest and most complete conversion from nitro to amine groups, while the ACN-based electrochemical method was the least effective. $NaBH_4$ has also been used as a chemical reducing agent for NP groups.[33]

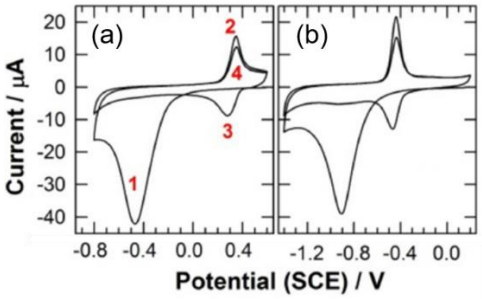

Figure 5.6. CV scans at 200 mV s^{-1} of thin NP films on glassy carbon in (a) 0.5 H_2SO_4 and (b) 0.2 M $KOH_{(aq)}$. Adapted from Brooksby et al.[23]

Electrochemical reduction can be used to characterise the surface concentration of grafted NP groups by relating the charge to the number of electrons participating in the reduction (Equations 5.1 and 5.2). Brooksby et al. carried out a series of experiments to investigate the reduction process in acidic

and basic conditions on carbon.[23] The CVs obtained in these conditions are shown in Figure 5.6. The peaks are numbered in order of appearance: Peak 1 is due to NP reduction, while Peaks 2/4 and 3 represent the reversible redox reaction in Equation 5.3, where NHOH groups (produced by Equation 5.1) are oxidised to NO (Peaks 2/4) and NO groups are reduced to NHOH (Peak 3).

$$C_6H_4(NHOH) \rightleftharpoons C_6H_4(NO) + 2H^+ + 2e^- \qquad (5.3)$$

Acidic conditions were recommended over basic media for reducing NP films as the reduction process is better understood in acid, resulting in more reliable surface concentration calculations.[23] Regardless of pH, NP groups located far from the electrode in the multi-layered film can be electrochemically inactive, leading to underestimations of surface concentration.[2]

There are numerous reports of NP films undergoing reduction during analysis with XPS,[7,34–36] or by deliberately exposing NP-modified surfaces to electrons to achieve localised reduction via electron beam lithography.[37–39] These will be discussed in Chapter 6.

5.1.4 Aims

Aryldiazonium ion chemistry gives robust multilayer films on a wide range of substrates. As described in Chapter 1, although various metal oxides have been modified in this way, very little work has been done on ZnO.[11,15] Furthermore, no work to date has characterised the nature of films and bonding on ZnO. There have been no reports of the effect of aryl layers on the surface band bending of ZnO, although the aromaticity of such multilayers has been proposed as a potential path for charge transfer.[7]

In this Chapter, electrografting from NBD to well-defined Zn-polar, O-polar, and m-plane ZnO faces at ZnO surfaces was explored. The results were characterised with AFM and XPS, including the effects on surface band bending. Secondly, grafted NP films were subjected to electrochemical and chemical reduction conditions and analysed using XPS. Finally, the ability of nitrobenzene diazonium ions (NBD) to undergo 'spontaneous' reduction at single crystal ZnO was investigated.

5.2 Methods

5.2.1 Chemicals and Materials

Unless otherwise stated, 10 × 10 mm^2 single-crystal Zn-polar, O-polar, and m-plane ZnO from CrysTec, Germany, were used. To ensure good electrical contact to samples, thin Ti/Au contacts were thermally evaporated onto a small section of the ZnO prior to modification as described in Chapter 2. NBD and $[Bu_4N]BF_4$ were synthesised as detailed in Chapter 2. Samples that were not modified and used as comparisons to modified samples ('as-received' samples) were cleaned with O_2 plasma to enable accurate modification layer thicknesses to be derived from XPS data.

5.2.2 Modification Methods

5.2.2.1 Electrochemical Grafting of Nitrophenyl Films

Single-crystal ZnO samples were modified using cyclic voltammetry in 2 mM NBD in $[Bu_4N]BF_4$-ACN using the O-ring set-up, as detailed in Chapter 2. The scan rate was 200 mV s^{-1} in all cases. All ZnO samples were solvent-cleaned prior to CV measurements, and not cleaned with O_2 plasma unless stated otherwise.

5.2.2.2 Reduction of Nitrophenyl Films

Electrochemical reduction was undertaken via cyclic voltammetry (O-ring set-up) in 0.2 M $KOH_{(aq)}$, with a scan rate of 200 mV s^{-1}. The potential was scanned from 0.6 V to −1.1 V vs SCE for 10 cycles. Prior to reduction, the electrochemical cell was purged with nitrogen for 15 min. After modification, samples were sonicated in ACN for 3 min, and rinsed with acetone, MeOH, and IPA prior to N_2 drying.

For chemical reduction, NP-modified samples were immersed for 2 h in stirred 0.8 M Na_2S in 1:1 ethanol:H_2O at ~50 °C. Afterwards, samples were sonicated in ethanol for 3 min, then rinsed in each of acetone, MeOH, and IPA and blown dry with N_2.

5.2.2.3 'Spontaneous' Grafting of Nitrophenyl Films

Single crystal m-plane ZnO samples were soaked for 4 h in the dark in one of:

1. ACN

2. ACN and NBD

3. Water and NBD.

In each case, the concentration of NBD was 25 mM. Two different pre-treatments were also investigated to enhance the electron accumulation layer at the m-plane surface:[40,41]

1. *UVA treatment*: 30 min under a 365 nm mercury lamp, then immersed in ACN and NBD

2. *Base treatment*: 30 min in pH 12 $NaOH_{(aq)}$, then immersed in ACN and NBD.

5.3 Results and Discussion

5.3.1 Electrochemical Grafting of Nitrophenyl Films on ZnO

Electrochemical grafting from NBD solution in ACN was performed on single-crystal ZnO samples using the O-ring format outlined in Section 2.3.1.1. Similar conditions and parameters to those previously reported on carbon surfaces were used, though the potential range and pre-modification treatment of ZnO were varied.

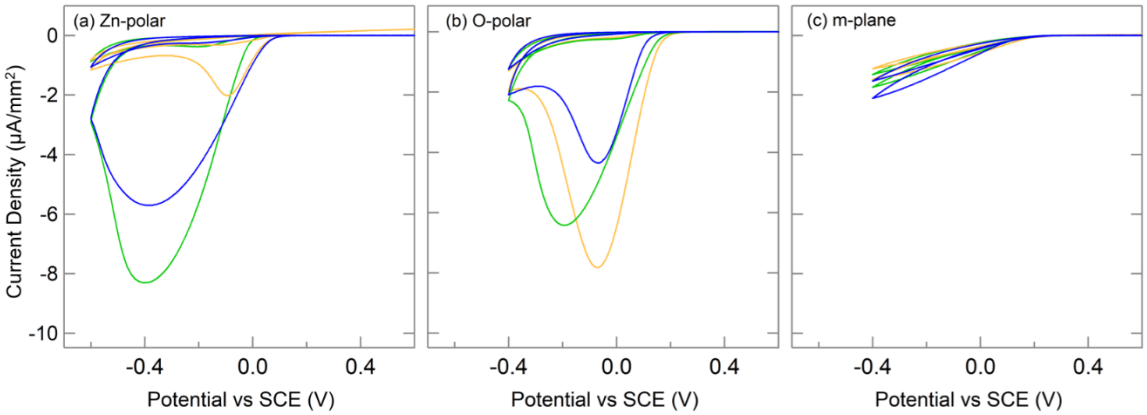

Figure 5.7. Repeat CVs (scan rate = 200 mV s^{-1}) for electrochemical grafting of NBD in $[Bu_4N]BF_4$-ACN at three different samples of each of (a) Zn-polar, (b) O-polar and (c) m-plane ZnO over a short potential range. In each panel, the 2 CVs of the same colour represent repeat scans (largest peak current density is Scan 1).

Figure 5.7 shows CVs collected during the reduction of 2 mM NBD in $[Bu_4N]BF_4$-ACN at separate samples of single-crystal ZnO over a relatively narrow potential range (0.6 to −0.4 V for O-polar and m-plane ZnO, and 0.6 to −0.6 V for Zn-polar ZnO). On the two polar faces, the first scan elicits a large reduction current peak. As discussed in Section 5.1.1 and 5.1.2, this is attributed to the reduction of the NBD ion to an NP radical that can then graft to ZnO and to each other as shown in Figures 1.17 and 1.18. On the second CV scan, the reduction current is significantly attenuated, indicating that the grafted NP film has blocked further electron transfer from ZnO and thus NBD reduction can no longer proceed to the same extent as before.[23] All three short-potential-range CVs on m-plane ZnO lack an obvious reduction peak, and very little current is seen relative to polar ZnO faces.

The reduction peak potential on Zn-polar ZnO (Figure 5.7a) varies for each sample over a range of 0.3 V. The reduction peaks in the O-polar modification process are slightly less variable, with peak potentials ranging from −0.05 to −0.20 V.

Figure 5.8 shows NP grafting CVs for Zn-polar, O-polar, and m-plane ZnO over a wider potential range than used in Figure 5.7. Like Figure 5.7a and b, the CVs for Zn-polar and O-polar ZnO show a large reduction peak which is greatly attenuated on the second scan (Figure 5.8a and b). An additional reduction process occurs at ~−0.8 V. Assuming similar electron behaviour as discussed on carbon electrodes (Section 5.1.1), both processes may be assigned to reduction of NBD at sites of different reactivities. The onset of reduction current on O-polar ZnO occurs at a more positive potential than the other faces, indicating that electron transfer from O-polar ZnO is more facile than from the other faces.

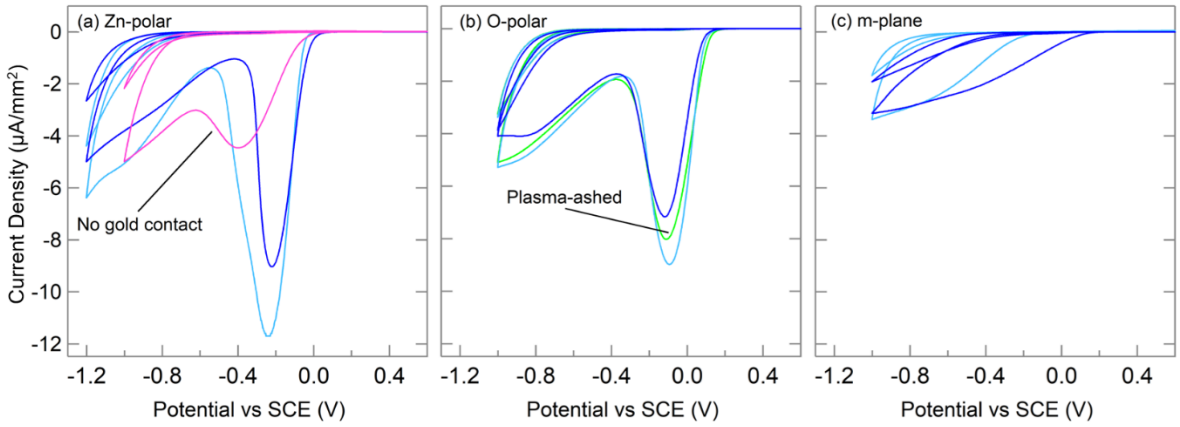

Figure 5.8. Two repeat CVs of 2 mM NBD in 0.1 M $[Bu_4N]BF_4$-ACN for electrochemical grafting of NBD (scan rate = 200 mV s^{-1}) at (a) 3 samples of Zn-polar, (b) 3 samples of O-polar and (c) two samples of m-plane ZnO over a wide potential range. Unless otherwise noted, all samples had gold contacts and were solvent-cleaned with no plasma ashing. In each panel, the 2 CVs of the same colour represent repeat scans (largest peak current density is Scan 1).

A very broad low-current reduction process is observed on m-plane ZnO (Figure 5.8c), in contrast with polar ZnO faces. This is consistent with the relatively low carrier concentration for this material. As listed in Table 2.1, m-plane CrysTec ZnO has the lowest charge carrier concentration of the three faces, with $\mu = 4.1 \times 10^{12}$ cm^{-3} compared to $\mu = 1.4 \times 10^{13}$ cm^{-3} for Zn-polar ZnO and $\mu = 5.0 \times 10^{13}$ cm^{-3} for O-polar ZnO. Table 5.1 lists the potentials of their reduction peaks. With the exception of the m-plane, these values fall within the range observed by Bangle et al. (Section 5.1.2),[11] and the Zn-polar ZnO has a more negative reduction potential than O-polar ZnO, as expected from the relative charge carrier concentrations. Alternatively, or concurrently, the more negative reduction potential for NBD at Zn-polar ZnO could be due to the significant chemical differences of the crystal terminations and the differences in work function (Table 1.1), which affect the potential of zero charge and thus the reduction potential, as outlined in Section 5.1.1.

Table 5.1. Reduction peak potentials for CVs (scan rate = 200 mV s^{-1}) in 2 mM NBD in $[Bu_4N]BF_4$-ACN on Zn-polar, O-polar, and m-plane face (Figure 5.7 and Figure 5.8). Data from the sample without a Ti/Au contact is not included.

Face	Reduction peak potential range (V vs SCE)	Reduction peak potential mean (V vs SCE)
Zn-polar	−0.40 – −0.10	−0.27
O-polar	−0.20 – −0.05	−0.18
m-plane	< −0.50	< −0.50

Several modification parameters were varied to determine the optimal grafting conditions at ZnO. Firstly, the importance of the Ti/Au strip on the crystal surface was investigated. The CV for NBD reduction at a Zn-polar sample without a gold contact, shown in Figure 5.8a, has significantly smaller maximum current and more negative reduction current onset and peak potential than seen on other Zn-polar samples. This confirms that the Ti/Au contact is advantageous, and it was therefore used for all subsequent experiments. The effect of sample cleaning by O_2 plasma prior to electrochemistry was also examined. Figure 5.8b shows that this step made no significant difference to the grafting CV at Zn-polar ZnO so was not pursued.

To probe the effect of charge carrier concentration on reduction peak position further, Tokyo Denpa single crystals which are of higher quality (fewer defects) than the CrysTec crystals, were used in the same NP grafting process as above; the CV results can be seen in Figure 5.9.

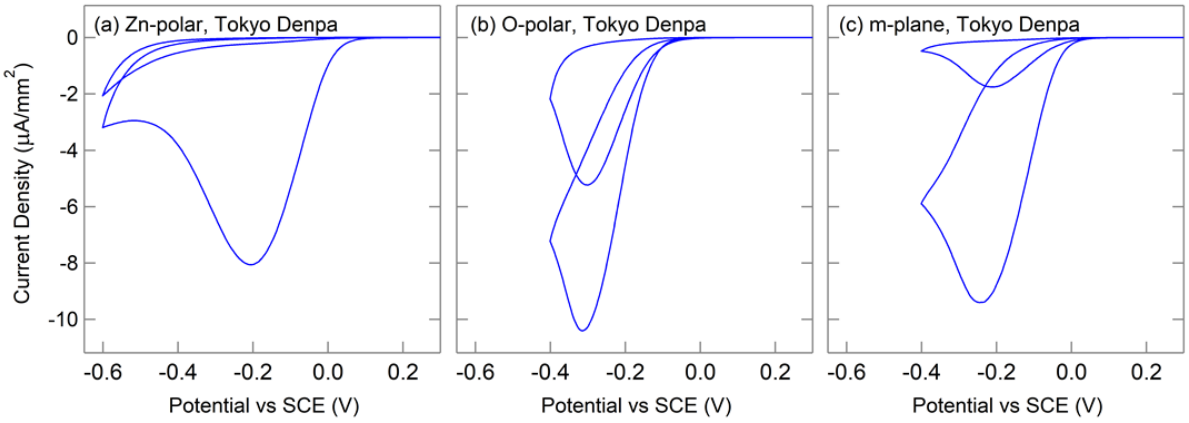

Figure 5.9. Two repeat CVs of NP grafting on Tokyo Denpa (a) Zn-polar, (b) O-polar, and (c) m-plane ZnO in 2 mM NBD in $[Bu_4N]BF_4$-ACN. Scan rate = 200 mV s^{-1}. In each panel, the scan with the largest peak current density is the first scan.

For each ZnO face, Tokyo Denpa crystals have a higher charge carrier concentration than CrysTec samples: for Zn-polar, O-polar, and m-plane single crystals, μ = 1.5 × 10^{16} cm^{-3}, 3.0 × 10^{14} cm^{-3}, and 4.0 × 10^{13} cm^{-3}, respectively. Figure 5.9c shows that a well-defined, relatively high-current reduction peak at −0.25 V is now visible on the m-plane CV, where none was visible on CrysTec m-plane ZnO. The Zn-polar face has a very broad reduction peak centred around −0.20 V, while the O-polar face has a narrow but high current peak at −0.30 V. It is interesting that the NBD reduction peak potential is 0.1 V more negative at Tokyo Denpa O-polar ZnO than at the CrysTec O-polar face, and that Tokyo Denpa Zn-polar and m-plane ZnO have similar NBD reduction potentials to each other, despite having ~3 orders of magnitude difference in charge carrier concentration. Across the two sets of samples, there is no clear trend between the NBD reduction peak potential and charge carrier concentration of the sample, nor between the peak potential and the crystal face. This is maybe not surprising due to the range of reduction peak potentials observed at different crystallographic faces of Au and carbon, as discussed in Section 5.1.1.[3,28] It shows that the reduction potential of each face is likely dependent on a combination of charge carrier concentration, chemical termination, and work function (and thus the potential of zero charge).

Notably, on both O-polar and m-plane ZnO, the second CV scan also shows a significant reduction peak, indicating that the surface was not completely blocked to further electron transfer as seen on the Zn-polar face. The more negative potential limit used for the CVs at the Zn-polar face, resulting in a thicker grafted film, is the most likely explanation for this observation.

Overall, it appears that O-polar ZnO gives the most reproducible CVs, with a peak potential ranging from −0.05 V to −0.2 V for the CrysTec samples that were used for further investigations. The CrysTec m-plane face is too resistive to have the typical features of an NBD grafting CV. Electrochemical behaviour of NBD at the different crystal faces of the 2 brands of crystals is of fundamental interest in the context of aryldiazonium ion reduction. Unfortunately, practical factors prevented further investigations at these interesting systems: each crystal could only be used once, and the cost made more detailed electrochemistry investigations unfeasible.

5.3.1.1 Nitrophenyl Film Thicknesses at CrysTec ZnO from AFM

AFM depth profiling, outlined in Section 2.2.1, was carried out to determine the thickness of NP films grafted over a short potential range (Figure 5.7, green trace) or a long potential range (Figure 5.8, light blue trace). The AFM images and line profiles can be seen in Figure 5.10. It is immediately clear that the films produced under a wide potential range are thicker than those produced using a shorter range (6 – 8 nm compared 1 – 5 nm). The results are consistent with thicknesses reported on carbon surfaces.[17] The total charge passed for reduction of NBD is greater during the wide potential range scans than the shorter range scans, leading to a greater number of aryl radicals and hence a thicker film. All films, except for that grafted over the short potential range on m-plane ZnO (Figure 5.10c), are clearly multilayers given that the height of an individual NP moiety, vertically aligned on a flat surface, is 0.6 nm (calculated using Avogadro).[42] The thinness of that NP film on m-plane ZnO is consistent with the small reduction current seen in the grafting CV (Figure 5.7c). Given the clear differences in thickness between films grafted over ‘short’ and ‘wide’ potentials, the samples will be referred to as ‘thin’ and ‘thick’ films from now on.

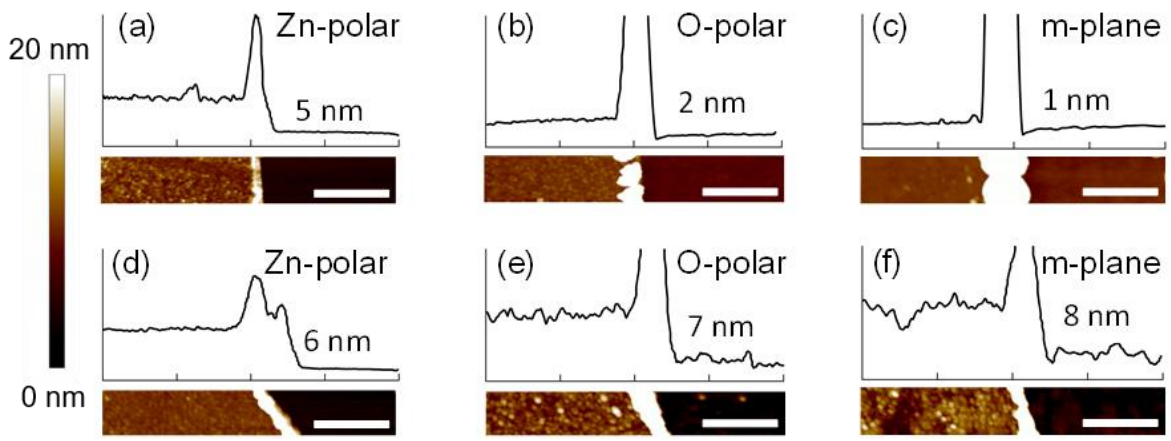

Figure 5.10. Tapping-mode AFM images, corresponding line profiles, and blank-corrected film thickness of (a – c) Zn-polar, O-polar, and m-plane ZnO modified with NP groups over a short potential range, and (d – f) the same crystal faces modified with NP groups over a wide potential range. The height scale is 20 nm, and horizontal scale bars are 500 nm.

5.3.1.2 Fixed-Energy XPS Analysis of Nitrophenyl Films on Single-Crystal ZnO

XPS survey spectra were collected on thin and thick NP-modified Zn-polar, O-polar, and m-plane ZnO samples (CrysTec) to obtain elemental percentages of NP films. The films are those generated in the grafting CVs shown in Figure 5.7 (green) and Figure 5.8 (light blue). An example of the XPS survey spectra obtained from the samples is shown in Figure 5.11 for Zn-polar ZnO; other faces are not shown due to the similar spectra, however all results are tabulated in Table 5.2.

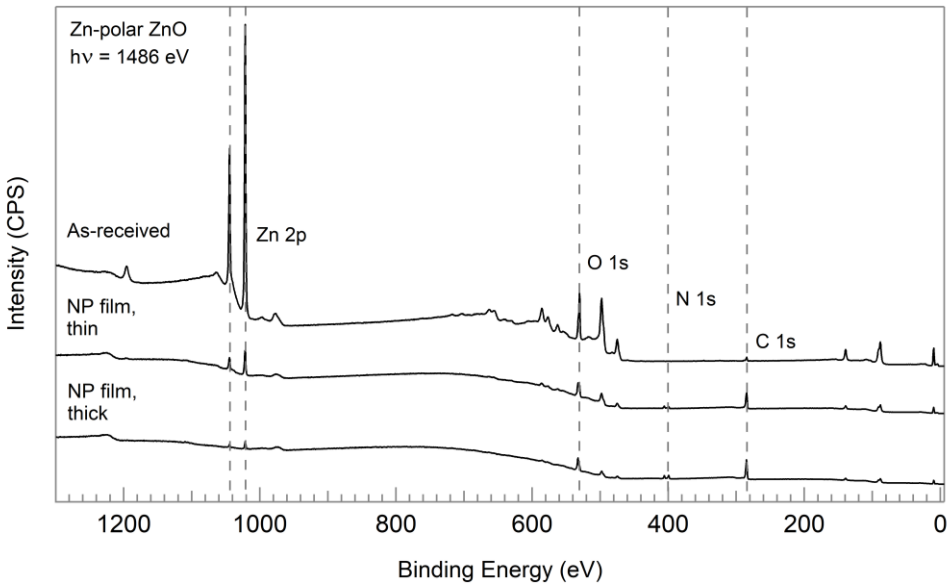

Figure 5.11. Fixed-energy XPS survey spectra for Zn-polar ZnO, as-received and modified with thin and thick NP films on Zn-polar ZnO. Elements of interest are noted. Spectra are not scaled but are offset for clarity.

As-received Zn-polar ZnO has an XPS survey spectrum typical for single crystal ZnO, with two large Zn 2p signals at ~1020 eV, an O 1s signal at ~530 eV, and a small C 1s signal at ~285 eV. No evidence for N on the surface was seen. The appearance of a signal near 400 eV (N 1s) and the significant increase in the C 1s signal on both NP-modified samples suggests that electrochemical NP grafting has been successful. The thin NP film on m-plane shows a smaller amount of N on the surface than the other two faces (Table 5.2), consistent with low thickness. The Zn 2p signal has been greatly attenuated by the grafted layers, as has the total O 1s signal. The C 1s carbon signal is greater on thick samples than it is on thin samples, as expected for an increase in the number of aryl layers on the surface. No sample shows the presence of F, which suggests that BF_4, used as both an electrolyte and the NBD counter ion, is not present on the surface.

Table 5.2. Elemental percentages and XPS- and AFM-derived thicknesses of Zn-polar, O-polar, and m-plane ZnO modified with thin and thick NP films.

	C %	N %	O %	Zn %	F %	Thickness (nm) from XPS	Thickness (nm) from AFM
Zn-polar							
As-received	18	0	46	36	0	-	-
Thin	63	9	25	4	0	4.2 ± 0.8	5 ± 1
Thick	69	12	18	1	0	6 ± 1	6 ± 1
O-polar							
As-received	25	0	49	26	0	-	-
Thin	51	8	31	10	0	2.3 ± 0.5	2 ± 1
Thick	70	12	18	1	0	7 ± 1	7 ± 1
m-plane							
As-received	26	0	45	28	0	-	-
Thin	40	2	39	19	0	1.1 ± 0.2	1 ± 1
Thick	68	10	21	1	0	6 ± 1	8 ± 1

The Zn 2p signal ratios of as-received and modified samples were used to calculate the thicknesses of the NP film. A comparison of the values obtained from XPS and AFM measurements is seen in Table 5.2. There is excellent agreement between the two methods which gives confidence in both methods for determining film thickness.

N 1s

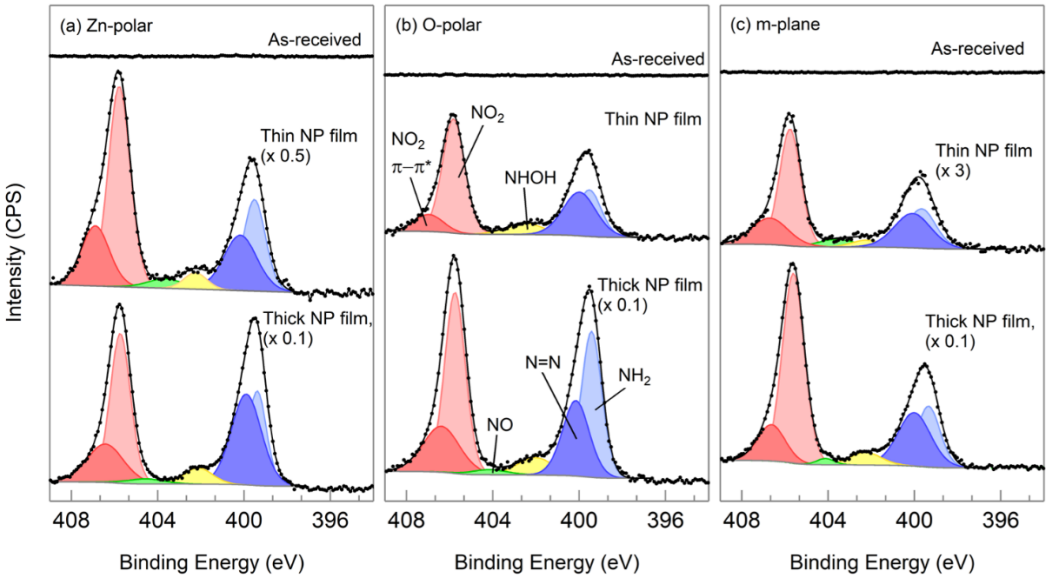

Figure 5.12. Fixed-energy XPS N 1s spectra for (a) Zn-polar, (b) O-polar, and (c) m-plane ZnO, as-received and modified with thin and thick NP films. Spectra are normalised to the same Zn 2p peak area, scaled where noted and vertically offset for clarity.

Figure 5.12 shows the N 1s core level XPS spectra for Zn-polar, O-polar, and m-plane ZnO, as-received and modified with thin and thick NP films on. Thin NP films on each of the three main ZnO faces have very similar features in the N 1s spectrum, which are consistent with those reported for NP films on other substrates.[7,13] A peak arising from $\underline{N}O_2$ groups is present at ~406 eV, as expected for NP films.[8] This peak has a shoulder at slightly higher BE (407 eV), which is a satellite peak that arises from photoelectrons which have undergone $\pi - \pi^*$ transitions in NO_2 prior to being ejected from the surface.[7] Together, these peaks are evidence for the presence of NP films on the ZnO surface. There is a broad signal at lower BE, which can be deconvoluted into two peaks: azo ($\underline{N}$=N) linkages around 400 eV,[31] and amino groups ($\underline{N}H_2$, ~399.7 eV).[7] An azo signal is commonly seen in XPS spectra for films grafted from aryldiazonium ions, formed from unreduced aryldiazonium ions which graft either to the substrate or to already-grafted organic groups (Figures 1.18 and 1.19).[7,8,10] Chen et al. formed diazonium ions in situ from 4-aminophenylmethylphosphonate, which were electrochemically

reduced at ITO.[10] They suggested that 7.99% of the resulting film was grafted to ITO with azo bonds as opposed to ITO-C or phosphonate bonds.

Typically, amino groups are assumed to arise from NO_2 functionalities that have been reduced during the electrochemical grafting process in aqueous solutions and/or during XPS measurements, as noted on other surfaces.[2,7,31,33] Mirkhalaf et al. used ultrasonication to induce NP grafting on ITO and observed that at high frequencies (≥ 582 kHz), grafted NP groups were reduced to aminophenyl groups.[33] The possibility that NP films in this work were reduced during the sonication step of the post-modification cleaning process was considered. However, Mirkhalaf et al. observed that minimal NP reduction occurred at 20 kHz, which is very similar to the frequency of the sonicator used in this work (37 kHz, Elmasonic). It is therefore unlikely that NP groups were reduced by sonication, and as grafting was carried out in non-aqueous ACN solution, reduction of NP groups during XPS measurements is the most likely explanation.

The remaining peaks, centred around 404 eV and 402 eV, are attributed to partially-reduced NP groups: NO and NHOH, respectively.[7]

Table 5.3. Fixed-energy XPS N 1s peak assignments, percentages, and azo ratios for Zn-polar, O-polar, and m-plane ZnO modified with thin and thick NP films on.

Binding Energy	Assignment	Zn-polar (%)		O-polar (%)		m-plane (%)	
		Thin	Thick	Thin	Thick	Thin	Thick
407.2 – 406.7	π-π* (NO_2)	16	15	8	15	15	11
405.9 – 405.7	NO_2	41	32	43	33	39	47
404.2 – 403.6	NO	3	2	0	2	4	1
402.4 – 402.1	NHOH	4	5	7	6	3	4
400.3 – 399.8	N=N	17	29	24	18	20	20
399.6 – 399.1	NH_2	19	18	18	27	18	16
-	Azo : NP	1 : 5	1 : 10	1 : 6	1 : 9	1 : 8	1 : 8

As seen in Table 5.3, the percentage of NO_2 of the N $1s_{total}$ is similar across the faces and for different thicknesses. The ratios of N=N signal to (NO_2 + reduced NO_2 signal) for thin and thick NP films on Zn-polar face are 1:5 and 1:2.5. These correspond to one azo linkage for every 10 grafted NP groups and one azo linkage for every 5 grafted NP groups, respectively (Table 5.3). On the thin NP film on O-polar ZnO, it appears that azo linkages form once every 6 NP groups, while the thick film has 9 NP groups per azo linkage. Although it is difficult to be confident of the fitting of the N 1s signal near 400 eV, the data suggests that azo linkages are more prone to form near the ZnO surface than further away, as the azo:NP ratios are greater for the thin NP films on Zn-polar and O-polar ZnO than the thick films. This is unexpected, as reduction of NBD groups are more likely to occur closer to the ZnO surface where electron transfer occurs, while non-reduced species are likely to be further from the surface. On the m-plane, azo linkages occur every 8 NP groups in both thin and thick films. While this was not explored further, an explanation is that the polar faces are capable of stabilising positive aryldiazonium cations at the surface due to electrostatic interactions with Zn-OH termination (Zn-polar face) or O-H termination (O-polar face). This could increase the number of unreduced NBD that form azo linkages near the ZnO/organic interface. As the film grows, the ZnO surface would no longer be able to interact with NBD species, and thus the preferred grafting mode would switch to grafting via phenyl radicals. While there is no evidence for direct azo linkages with the ZnO surface, this possibility cannot be ruled out.

O 1s

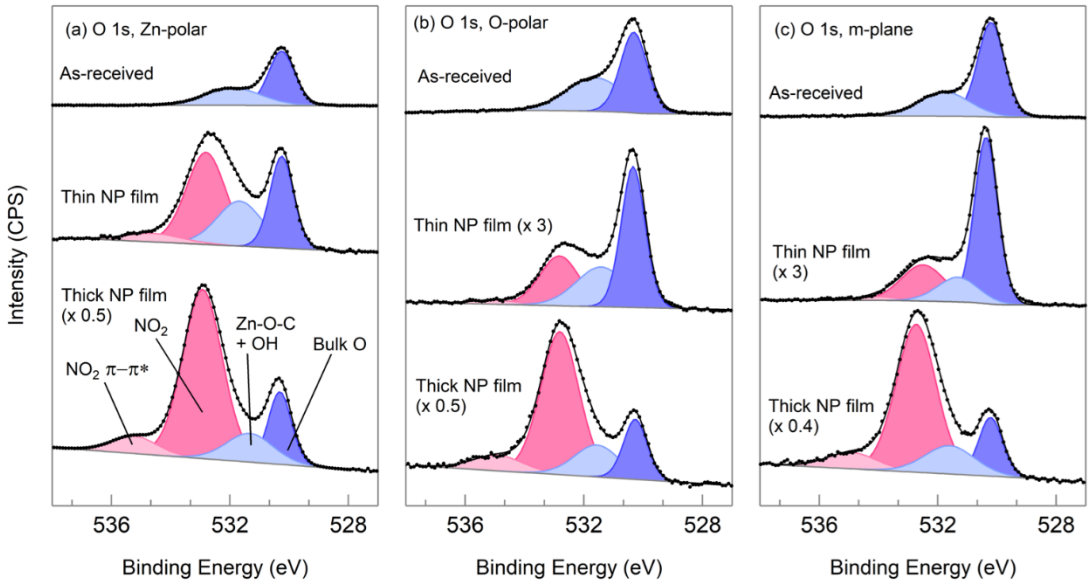

Figure 5.13. Fixed-energy XPS O 1s spectra for (a) Zn-polar, (b) O-polar, and (c) m-plane ZnO, as-received and modified with thin and thick NP films. Spectra have been normalised to the same Zn 2p peak area, scaled where noted and offset for clarity.

The O 1s results for NP-modified ZnO are shown in Figure 5.13. The two peaks seen in the as-received Zn-polar, O-polar, and m-plane ZnO spectra arise from bulk and surface O,[43] as seen in previous thesis Chapters. Upon NP modification, another peak appears in the spectra at ~533 eV, shown in pink. The intensity of this peak is greatest for thick NP films and the 'thin' NP film on Zn-polar sample, which is thick relative to the other thin films (Table 5.2). This observation is consistent with assigning the peak to $N\underline{O}_2$, as reported by others.[7,8] To further confirm this, the ASF-corrected O 1s $N\underline{O}_2$ peak area of thick NP film on Zn-polar ZnO was compared to the corresponding ASF-corrected N 1s $\underline{N}O_2$ peak. As expected, the peak area ratio of N:O was 1:2. Accurate fitting of the O 1s NO_2 peak on the thin film samples was subsequently aided by loosely constraining the $N\underline{O}_2$ peak area to double that of the $\underline{N}O_2$ peak (considering ASFs and satellite peaks). A small satellite peak next to the $N\underline{O}_2$ peak is also visible

on NP-modified samples at 535 eV. It is attributed to the π-π* shake-up peak for N<u>O</u>$_2$, and its intensity is small relative to that of the main N<u>O</u>$_2$ peak.[8]

There are no other expected sources of O in NP-modified samples, so the remainder of the O 1s signal is assigned to the presence of surface OH groups that have not reacted during the modification process, and from Zn-O-C bonds between the aryl groups and the ZnO substrate, should these be present. Assuming an OH coverage of ~1 monolayer,[43] the density of OH groups on Zn-polar and O-polar ZnO is ~1.8 × 10^{-9} mol cm^{-2} and ~2.2 × 10^{-9} mol cm^{-2} on m-plane ZnO,[44] but the computed ideal packed monolayer of phenyl rings on flat surface is ~1.3 × 10^{-9} mol cm^{-2}.[45] These means that ~30% of the surface OH groups on polar ZnO, and ~40% of OH on m-plane ZnO, cannot react with NP radicals due to steric effects. Furthermore, previous reports on gold and carbon substrates suggested that the density of NP groups bound directly to the substrate was ~2.5 – 4.0 × 10^{-10} mol cm^{-2}; this corresponds to ~20 – 33% of a close-packed NP monolayer and suggests the multilayer here is also loosely-packed.[2,45]

Because there is a wide range of reported XPS BEs for metal-O-C moieties on metal oxides, and none reported for Zn-O-C,[13,46,47,48] deconvoluting Zn-O-C signals from OH signals with confidence proved difficult. As such, they were grouped together in a peak centred around 532 eV but are discussed further in Chapter 6.

The N<u>O</u>$_2$ peak is significantly larger for thick NP films when compared to thin films (Table 5.4). This is the result of more NP groups on the surface, which contribute to a larger N<u>O</u>$_2$ peak but also attenuate the signal from bulk O. This is most noticeable on the Zn-polar face, further strengthening the results of XPS and AFM thickness calculations which showed that the Zn-polar face had the thickest 'thin' aryl modification layer. This can be compared to the CVs in Figure 5.7a, which showed that the largest NBD reduction peak current density of the three ZnO faces was observed on the Zn-polar face, while the m-plane face showed the smallest current density (Figure 5.7c) and the thinnest 'thin' NP film.

Table 5.4. Binding energies and percentage peak areas from O 1s XPS spectra for Zn-polar, O-polar, and m-plane ZnO modified with thin and thick NP films.

	Bulk O (%)	**Zn-O-C / OH (%)**	**NO_2 (%)**	**π–π* (NO_2) (%)**
Binding Energy (eV)	530.2 – 529.8	531.6 – 531.2	533.2 – 532.8	535.6 – 534.8
Zn-polar				
As-received	45	55	0	0
Thin	26	24	44	6
Thick	16	13	64	8
O-polar				
As-received	52	47	0	0
Thin	44	27	26	3
Thick	15	16	60	9
m-plane				
As-received	67	34	0	0
Thin	59	15	24	2
Thick	15	15	62	9

C 1s

Figure 5.14 shows the C 1s spectra for as-received and NP-modified ZnO. As-received ZnO samples were cleaned with O_2 plasma prior to XPS analysis to achieve a low-carbon surface: consequently, the amount of adventitious carbon on the as-received samples is very small. Upon NP modification, the C 1s signal increases significantly. On both thin and thick NP films, the largest peak at 284.8 eV is assigned to C-C, C-H, and the aromatic carbon rings. The large intensity of the peak at ~286 eV suggests that C-N bonds are present,[49] but the C-O signal from adventitious carbon has the same BE, so the amount of C-N bonds cannot be quantified. O-C=O signal at ~288.5 eV is also typical of adventitious carbon. However, a satellite peak around 291 eV is visible on the NP-modified samples but not the as-received samples and is associated with the π-π* excitations which occurred within the aryl rings on the surface. It is the strongest C 1s evidence of successful NP grafting. This peak is most intense on the thicker films, as expected due to the increased number of aryl groups present.

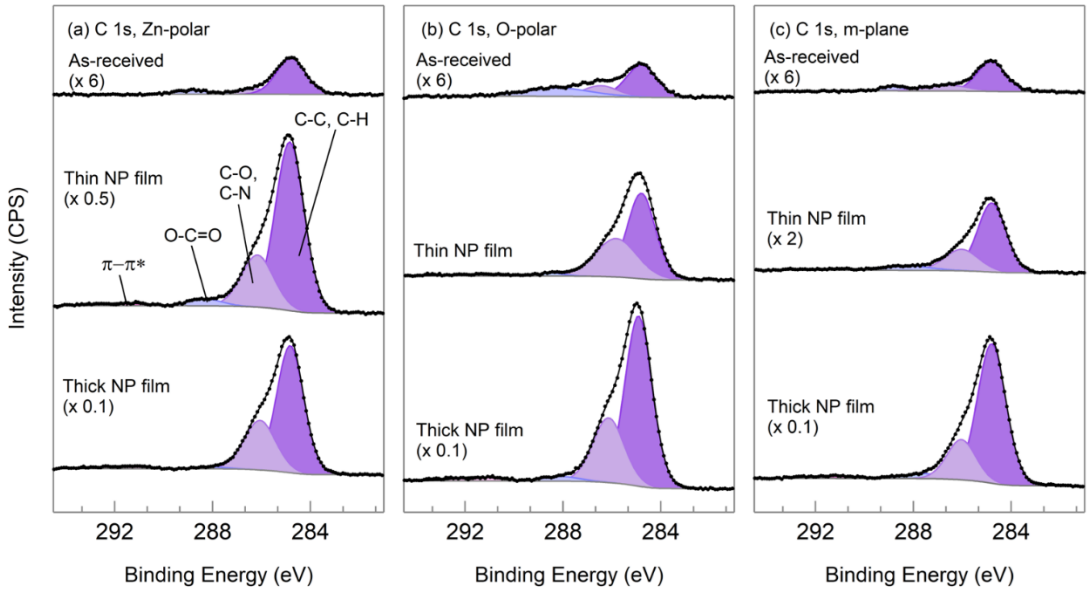

Figure 5.14. Fixed-energy XPS C 1s spectra for (a) Zn-polar, (b) O-polar, and (c) m-plane ZnO, as-received and modified with thin and thick NP films. Spectra have been normalised to the same Zn 2p peak area, scaled where noted and offset for clarity.

Importantly, the absence of a C 1s peak at low BE (~281 eV) suggests that Zn-C bonds are not present.[11] The films are resistant to sonicating, suggesting that they are covalently bound to the substrate, and thus it seems likely that the NP groups are bound through Zn-O-C bonds as noted in the O 1s section and observed on other metal oxides.[12–14,50] The mechanism for surface grafting is expected to be similar to those proposed in the literature for hydrogenated silicon, where electrons provided by the negatively-biased substrate generate aryl radicals (Figure 5.15). Abstraction of surface H by one aryl radical forms a surface radical which can combine with another aryl radical to give Zn-O-C covalent bonds.[51,52] Heinhold et al. reported that H was less easily removed from Zn-polar ZnO than O-polar ZnO via heating in UHV,[43] so it might be expected that H-abstraction occurs more easily on O-polar and m-plane ZnO to give more Zn-O-C bonds than on the Zn-polar face; however, due to the different grafting potentials used and the ambiguity of the O 1s Zn-O-C peak area, this hypothesis cannot be tested using the present data.

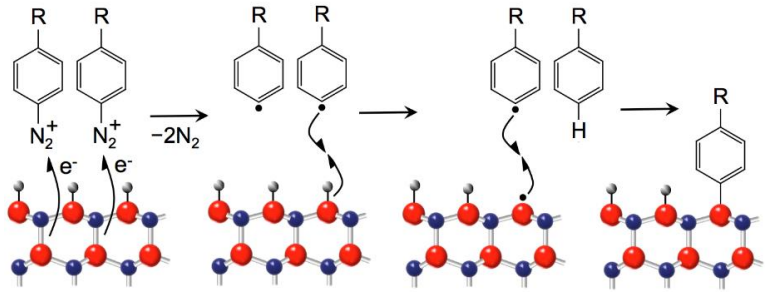

Figure 5.15. Proposed mechanism for the electrografting of aryl groups to the O-polar ZnO surface by reduction of aryldiazonium ions.

5.3.1.3 Band Bending of Nitrophenyl-Modified Single Crystal ZnO

Figure 5.16 shows the valence band spectra (*hv* = 1486 eV) for NP-modified Zn-polar, O-polar, and m-plane ZnO.

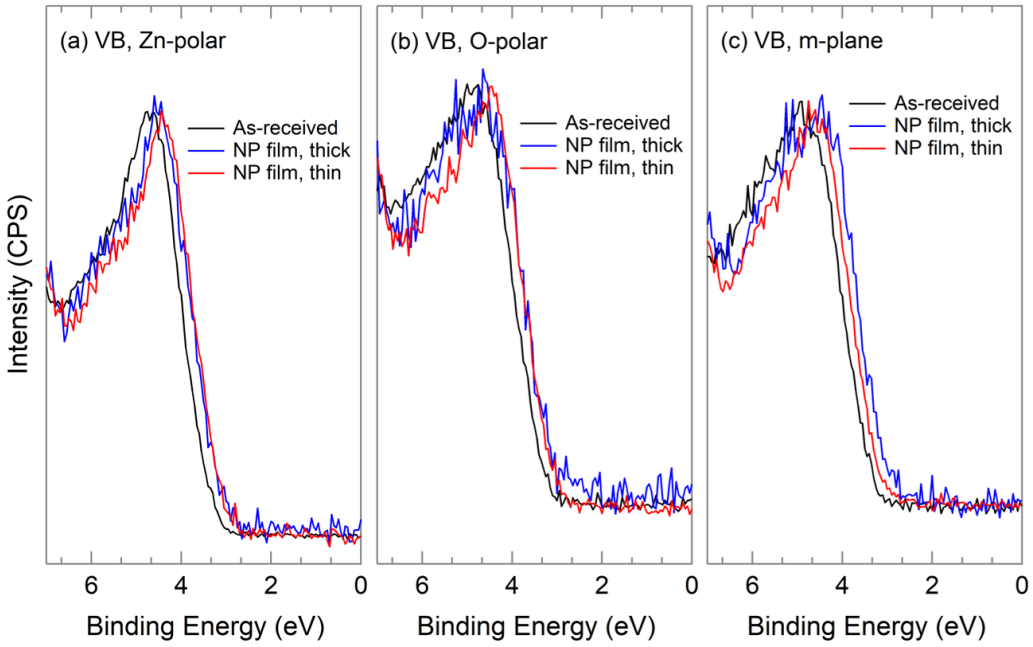

Figure 5.16. Fixed-energy XPS valence band spectra for (a) Zn-polar, (b) O-polar, and (c) m-plane ZnO, as-received and modified with thin and thick NP films.

The VB XPS spectra are noisy due to the small number of scans collected. However, it is still evident that the addition of a NP film decreases the value of ζ on all ZnO faces compared to as-received samples, which corresponds to a decrease in downwards band bending. Data are listed in Table 5.5;

these were not calibrated to either an external reference or adventitious carbon (284.8 eV), as were the core-level XPS spectra, but are relative values.

Table 5.5. ζ and band bending (V_{bb}) values from fixed-energy XPS valence band spectra of Zn-polar, O-polar, and m-plane ZnO, as-received and modified with thin and thick NP films. Uncertainty ± 7%.

	Zn-polar			O-polar			m-plane		
NP-modification	ζ (eV)	V_{bb} (eV)	ΔV_{bb} (eV)	ζ (eV)	V_{bb} (eV)	ΔV_{bb} (eV)	ζ (eV)	V_{bb} (eV)	ΔV_{bb} (eV)
As-received	3.34	-0.47	-	3.30	-0.40	-	3.34	-0.49	-
Thin	3.08	-0.21	+0.26	3.09	-0.19	+0.21	3.17	-0.32	+0.17
Thick	3.11	-0.24	+0.23	3.07	-0.17	+0.23	3.09	-0.24	+0.25

On the Zn-polar face, essentially the same ζ shift is seen for the thin and thick NP films (~+0.24 eV). The same trend is seen on the O-polar face, where ζ shifts by ~+0.22 eV for both thicknesses of film. This suggests that V_{bb} is affected the same regardless of whether the NP film is 4 – 5 nm or 6 nm (Zn-polar face), or 2 – 2.5 nm or 7 nm (O-polar face). In contrast, the thin NP film on the m-plane face (~1 nm) induces a ζ shift of only +0.17 eV compared to +0.25 eV seen on the thick NP film (~7 nm). It thus appears that to achieve the maximum effect on ζ, the thickness of the NP film should be greater than 1 nm. Furthermore, while NP-modified O-polar ZnO has the least negative surface band bending, the largest band bending change upon modification was seen on the Zn-polar face. This could be due to the as-received Zn-polar face having a lower charge carrier concentration and more downwards band bending than O-polar ZnO, meaning that the bands are more easily influenced by electron-withdrawing substituents.[53] However, the difference in this case is probably negligible. Regardless of the crystal face or thickness, NP films are successful in decreasing the downwards band bending on ZnO.

5.3.2 Electrochemical Reduction of Nitrophenyl Films on ZnO

5.3.2.1 Electrochemical Reduction of Nitrophenyl Films on ZnO in Basic Conditions

A second set of thin and thick NP films on Zn-polar, O-polar, and m-plane ZnO were used to investigate the electrochemical reduction of NP films (the corresponding grafting CVs are the dark blue lines in Figure 5.7 and Figure 5.8). Although acidic conditions are most commonly used in electrochemical reduction of NP films to generate aminophenyl groups, basic solution was chosen so as to not dissolve the ZnO. Reduction of NP films in basic conditions is also reported to yield aminophenyl groups although the details of the reaction are not clear.[23] The reduction is reported to occur at ~−0.9 V vs SCE at 200 mV s^{-1} on glassy carbon.[23] Figure 5.17 shows control CVs obtained while cycling as-received Zn-polar ZnO in basic conditions after variable periods of N_2 purging. Even after 30 min of purging with N_2, a well-defined reduction process is observed. This occurs at the same potential as the air-saturated solution, suggesting that either residual O_2 or ZnO itself is participating in some reduction process.

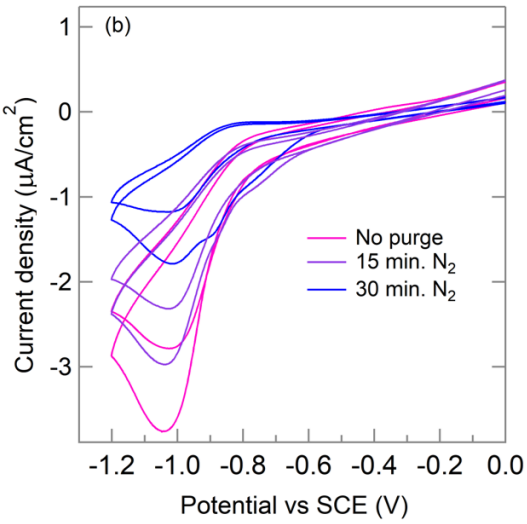

Figure 5.17. As-received Zn-polar ZnO in 0.2 M $KOH_{(aq)}$ at 200 mV s^{-1}, cycled after increasing degassing times. Scans of the same colour correspond to 2 repeat CVs obtained after a period of N_2 purging. The peak with the larger current density was the first scan of each pair.

Figure 5.18 shows the CVs for the reduction of NP-modified ZnO in 0.2 M KOH. The thin NP film on Zn-polar ZnO has a similar CV to the response on as-received ZnO, suggesting that the reduction process

is unrelated to the NP film. Reduction of an NP film is expected to be irreversible and close to complete on the first scan. Hence the persistence of the reduction also indicates it is not due to reduction of NP groups. The CV for reduction of the thick NP film on Zn-polar ZnO has a somewhat different shape, with the initial appearance of a reduction peak that decreases on each scan but does not disappear even after 10 scans.

Both thin and thick NP films on O-polar ZnO had similar CV responses, with the first scan showing a relatively large reduction current that decreases rapidly on repeat scans. The CVs show a small redox couple at ~−0.4 V that only appears after the first scan. This response matches those reported for NP films on carbon, where the first scan reduces NO_2 groups to NHOH and NH_2 at ~−0.4 V in 0.2 M KOH (Equation 5.1 and 5.2); on the return scan, NHOH are then oxidised to NO (Equation 5.3). The reduction peak at −0.5 V on the second sweep is due to NO groups which are reduced back to NHOH.

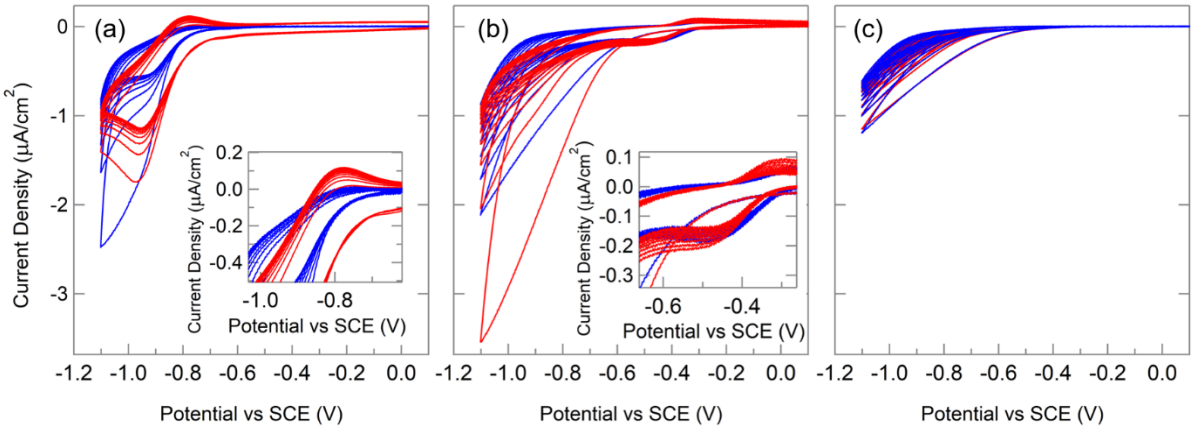

Figure 5.18. Repeat CVs in 0.2 M $KOH_{(aq)}$ at 200 mV s^{-1}after 15 min N_2 purging for thick (blue) and thin (red) NP films on (a) Zn-polar, (b) O-polar, (c) m-plane ZnO. 10 scans were run per sample: largest current density = first scan. Inset: Closer view of areas of interest.

Both thin and thick films on m-plane ZnO had the same electrochemical response with relatively low current and no reduction peak. This response indicates that this substrate is more resistive than polar ZnO, as observed for NP grafting CVs on m-plane ZnO (Figure 5.7).

In summary, the CVs in Figure 5.18 show little evidence for reduction of NP films. Only for O-polar ZnO, where a couple assigned to NHOH/NO redox reaction is observed, is NP reduction definitely indicated.

5.3.2.2 XPS Characterisation of Electrochemically Reduced Nitrophenyl Films on ZnO

Electrochemically-reduced thick and thin NP films on Zn-polar, O-polar, and m-plane ZnO were characterised by fixed-energy XPS. All these were reduced by 10 scans under the conditions stated in the Figure 5.18 caption. Note that these are separate samples from those shown in Figure 12 – Figure 14; the grafting CVs can be seen in Figure 5.7 and Figure 5.8 (dark blue traces).

Table 5.6 shows the atomic percentages and film thicknesses derived from XPS survey spectra. As-received ZnO samples have no evidence of nitrogen on the surface, while all modified samples have a significant N 1s signal. Within the margin of error, the film thicknesses and N % of the reduced samples do not differ from the freshly-modified samples in Section 5.3.1.2 (Table 5.2), except for the thin O-polar modification layer which is only half the thickness and N % seen previously, consistent with a relatively small peak current seen in the grafting CV (Figure 5.7b). This demonstrates that, with the one exception, the electrochemical modification has good reproducibility and that the reduction process did not remove significant amounts of modifier or NO_2 groups from the films.

Table 5.6. Atomic percentages and film thicknesses from fixed-energy XPS of Zn-polar, O-polar, and m-plane ZnO, modified with thin and thick NP films and electrochemically reduced.

	C %	N %	O %	Zn %	Thickness (nm) from XPS
Zn-polar					
As-received	18	0	46	36	-
Thin reduced	62	6	26	5	2.8 ± 0.6
Thick reduced	75	9	16	0	7 ± 1
O-polar					
As-received	25	0	49	26	-
Thin reduced	53	5	30	12	1.0 ± 0.2
Thick reduced	73	10	16	1	5 ± 1
m-plane					
As-received	26	0	45	28	-
Thin reduced	59	3	27	11	1.3 ± 0.3
Thick reduced	72	7	19	2	4.1 ± 0.8

N 1s

Figure 5.19 shows the N 1s spectra obtained for each sample, the peaks of which are quantified in Table 5.7. Figure 5.19a shows the XPS N 1s spectra of NP-modified Zn-polar ZnO after electrochemical reduction. No obvious difference in the $\underline{N}O_2$:$\underline{N}H_2$ ratio is seen relative to that shown in Figure 5.12 and Table 5.3 (non-reduced); again, the $\underline{N}O_2$ signal is more intense than the lower BE $\underline{N}H_2$ signal for both the thin and thick NP films. These XPS data provide no evidence for reduction of NP groups which supports the conclusion from CV experiments that the response seen in Figure 5.18 is due to reduction of O_2 or ZnO itself, not the NP films. The reason why NP films cannot be reduced on Zn-polar ZnO is not clear but may be related to its relatively low carrier concentration and thick NP films; Richard et al. observed that the reaction rate for NP reduction in acidic conditions is limited by electron transfer from the carbon substrate rather than proton migration from the electrolyte through the modification layer.[1]

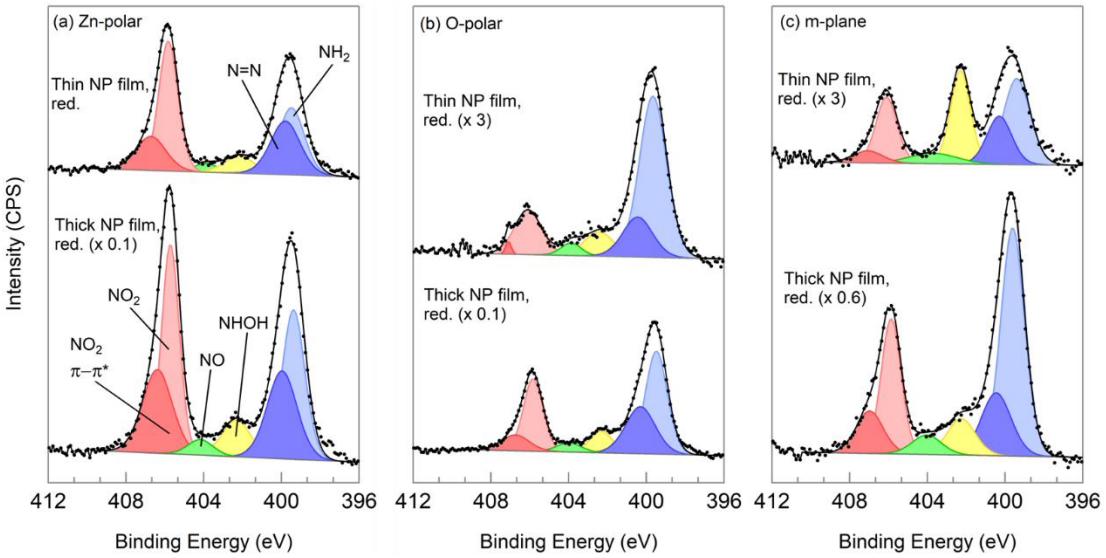

Figure 5.19. Fixed-energy XPS N 1s spectra for electrochemically-reduced thin and thick NP films on (a) Zn-polar, (b) O-polar, and (c) m-plane ZnO. Spectra were normalised to the same Zn 2p peak area, scaled and offset for clarity.

On the O-polar face (Figure 5.19b), a large difference is seen between the freshly-prepared NP films (Figure 5.12b) and those that have undergone electrochemical reduction. On the reduced thin NP film, there is very little $\underline{N}O_2$ signal and the $\underline{N}H_2$ peak is dominant. The thick NP film also shows greater $\underline{N}H_2$ signal than $\underline{N}O_2$, suggesting that reduction of NO_2 groups occurred. The remaining NO_2 groups may be electrochemically inactive due to their position in the film, as mentioned in Section 5.1.3. This is consistent with the reduced thick NP film (5 nm thick) having relatively more NO_2 than the reduced thin film (1 nm thick), because electron transfer rate decreases with distance and so NO_2 groups in the outer regions of the film may not be reduced.[54] It is also possible that a thicker film restricts access of electrolyte solution to the inner regions of the film, thereby preventing reduction.

From the N 1s spectra of NP-modified m-plane samples, both samples appear to have been reduced. The thick NP film now has 30% of its N 1s signal attributed to $\underline{N}H_2$ groups (Table 5.7) compared to 16% for a non-reduced sample (Table 5.30). The thin NP film appears to also be reduced, as the $\underline{N}O_2$ peak intensity of the reduced thin NP film now only accounts for 23% of the N 1s signal (including π-π*), instead of 54% as on the non-reduced sample. Interestingly, the $\underline{N}$HOH peak at 402 eV is very intense

on the thin NP film on m-plane ZnO and is the dominant peak with 30% of the N 1s signal. From Equation 5.1, this suggests that only partial reduction involving 4 electrons has occurred. This may be due to the higher resistivity of the m-plane sample making electron transfer less facile than on the other two ZnO faces.

Table 5.7. Fixed-energy XPS N 1s peak assignments and percentages for thin and thick NP films on Zn-polar, O-polar, and m-plane ZnO after electrochemical reduction treatment.

Binding Energy	**Assignment**	**Zn-polar (%)**		**O-polar (%)**		**m-plane (%)**	
(eV)		**Thin**	**Thick**	**Thin**	**Thick**	**Thin**	**Thick**
407.2 – 406.7	π-π* (NO_2)	13	18	1	7	5	9
405.9 – 405.7	NO_2	33	25	16	23	18	21
404.2 – 403.6	NO	3	3	3	4	7	5
402.4 – 402.1	NHOH	7	8	9	8	24	8
400.3 – 399.8	N=N	21	19	15	23	16	15
399.6 – 399.1	NH_2	23	25	56	36	30	42

O 1s

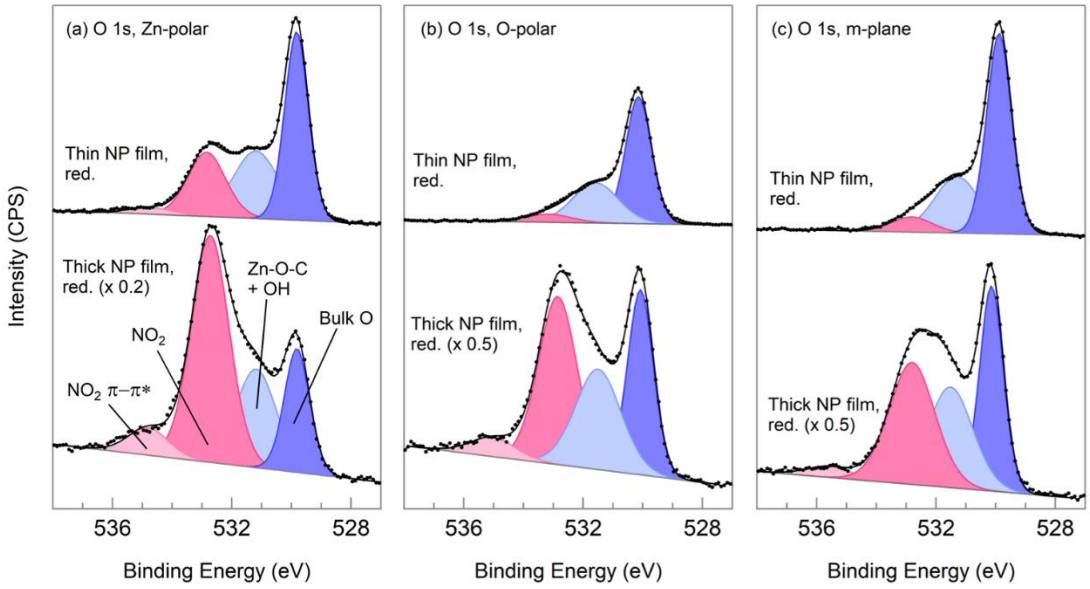

Figure 5.20. Fixed-energy XPS O 1s spectra for electrochemically-reduced thin and thick NP films on (a) Zn-polar, (b) O-polar, and (c) m-plane ZnO. Spectra were normalised to the same Zn 2p peak area, scaled and offset for clarity.

Figure 5.20 shows the O 1s spectra for electrochemically 'reduced' thin and thick NP films on Zn-polar, O-polar, and m-plane ZnO. The data are qualified in Table 5.8. On the Zn-polar face, the thinness of the 'reduced' thin NP film (2.8 nm) compared to the freshly-prepared thin NP film (5 nm) results in a smaller NO_2 peak than for the non-reduced thin NP film (Figure 5.13 and Table 5.4). The 'reduced' thick NP film, however, bears resemblance to the freshly-modified thick NP film, which is consistent with the evidence from the N 1s spectrum suggesting that the film was not reduced.

From N 1s spectra, it was clear that successful reduction processes occurred only on NP films on O-polar and m-plane ZnO. Similarly, the O 1s spectra for thin NP films on O-polar and m-plane ZnO show significantly less NO_2 signal than either the freshly-modified samples, or the thin NP film on Zn-polar ZnO. Furthermore, the π-π* shake-up peak for NO_2 is negligible in these films.[7] The O 1s spectrum of thick NP film on O-polar ZnO still has significant NO_2 signal, which contrasts with its N 1s spectrum where NO_2 signal accounted for only 23% of the total N 1 signal. However, the ASF-corrected peak

area ratio for $\underline{N}O_2$:$N\underline{O}_2$ is 1:2, as expected. The thicker NP film has unreacted NO_2 groups, and it is likely the thickness of the film attenuates the bulk O signal and thus exaggerates the $N\underline{O}_2$ peak on the O 1s spectrum. The thick NP film on m-plane ZnO has 39% of its O 1s signal attributed to $N\underline{O}_2$, compared to 71% on non-reduced thick NP film (Table 5.4).

Table 5.8. Binding energies and percentage peak areas from O 1s XPS spectra for Zn-polar, O-polar, and m-plane ZnO modified with electrochemically-reduced thin and thick NP films.

	% Bulk O	**% Zn-O-C / OH**	**% NO_2**	**% π–π* (NO_2)**
Binding Energy (eV)	530.2 – 529.8	531.6 – 531.2	533.2 – 532.8	535.6 – 534.8
Zn-polar				
Thin, reduced	43	30	24	3
Thick, reduced	19	24	51	7
O-polar				
Thin, reduced	60	34	7	0
Thick, reduced	28	27	39	5
m-plane				
Thin, reduced	60	31	7	1
Thick, reduced	31	29	36	3

5.3.2.3 Band Bending of Electrochemically-Reduced Nitrophenyl Films on Single Crystal ZnO

The fixed-energy XPS VB spectra for NP-modified Zn-polar, O-polar, and m-plane ZnO electrochemically treated in basic conditions are shown in Figure 5.21, and values of interest are listed in Table 5.9. Because non-reduced and reduced NP-modified samples were prepared and analysed at different times without external calibration, there is difference in the absolute ζ values between Table 5.5 and Table 5.9. However, as explained earlier, the changes in band bending relative to the as-received reference sample (ΔV_{bb}) can be directly compared.

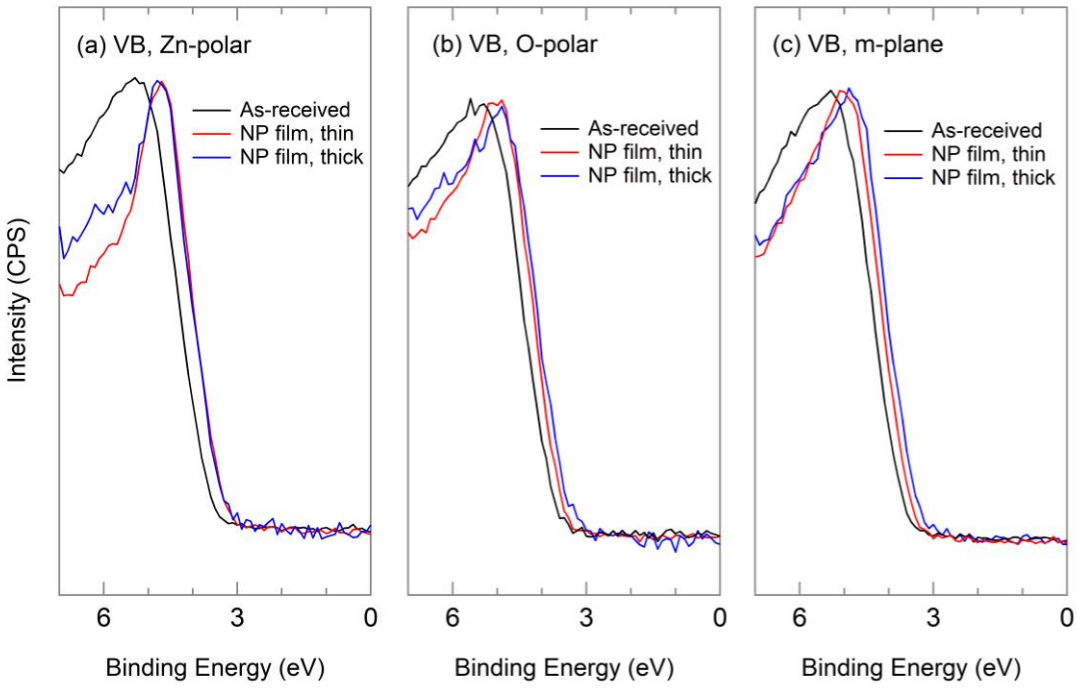

Figure 5.21. Fixed-energy XPS valence band spectra for as-received and NP-modified (a) Zn-polar, (b) O-polar, and (c) m-plane ZnO, after electrochemical reduction in $KOH_{(aq)}$. As-received ZnO samples are shown in black.

On the Zn-polar face, where N 1s and CV data suggested that the reduction had not been successful, both thin and thick NP films have similar values of ζ (3.35 eV), and their ΔV_{bb} closely match those of the non-reduced analogues (~+0.25 eV for 'reduced', ~+0.24 eV for non-reduced).

The reduced thin NP film on O-polar ZnO, which showed evidence of reduction occurring in the N 1s spectrum, had ΔV_{bb} of +0.17 eV relative to the as-received sample, which is 0.04 eV smaller than the band bending change seen on the freshly-prepared NP film (Table 5.5). This suggests that the reduction and the resulting amino groups have slightly affected V_{bb} and have resulted in a small shift towards the original band banding of the as-received sample, as expected for electron-donating aryl substituents. However, the reduction has not completely removed the decrease in downwards band bending, despite the significant decrease in the number of electron-withdrawing NP groups. It is possible that there is a competing effect between the amino groups and the non-reduced nitro groups: the N 1s spectrum suggests that 17% of the N 1s signal still originates from nitro groups, compared to

54% on the unreduced sample. The relative locations of the groups may also influence the effect on surface band bending.

Table 5.9. ζ and band bending (V_{bb}) values from fixed-energy XPS valence band spectra of Zn-polar, O-polar, and m-plane ZnO modified with thin and thick NP films and electrochemically reduced. Values have not been calibrated. Uncertainty ± 6%.

	Zn-polar			**O-polar**			**m-plane**		
NP-modification	ζ (eV)	V_{bb} (eV)	ΔV_{bb} (eV)	ζ (eV)	V_{bb} (eV)	ΔV_{bb} (eV)	ζ (eV)	V_{bb} (eV)	ΔV_{bb} (eV)
As-received	3.60	-0.73	-	3.74	-0.84	-	3.66	-0.81	-
Thin, 'reduced'	3.35	-0.48	+0.25	3.57	-0.67	+0.17	3.51	-0.66	+0.15
Thick, 'reduced'	3.36	-0.49	+0.24	3.53	-0.63	+0.21	3.44	-0.58	+0.23

The reduced thick NP film on O-polar ZnO, which was not as well-reduced as the thin layer, had slightly smaller V_{bb} than the unreduced sample by 0.02 eV. This is not a significant difference, which suggests that the electron-withdrawing ability of the partially-reduced NP film was not changed.

The thin NP films on m-plane ZnO, which was reduced to give 3 different N 1s signals (Figure 5.19), also had an insignificant (−0.02 eV) change in V_{bb} compared to the non-reduced sample. The prominent NHOH reduction product is expected to have electron-withdrawing characteristics similar to NO_2. XPS results (Table 5.7) indicated that a greater fraction of NP groups was reduced in the thin film than the thick film. The reduced thick NP film also had a −0.02 eV change in band bending relative to its non-reduced sample; this is attributed to a significant amount of NO_2 groups remaining on the surface which may be competing with the NH_2 groups (Figure 5.19).

Overall, the band bending did not significantly change for any NP-modified sample after electrochemical reduction. This suggests that the NP groups closest to the ZnO have the most influence on the band bending: if these are not reduced during electrochemical reduction, then any successfully-reduced electron-donating amino groups further up in the film can have little effect on band bending. This could be investigated using chemical reduction methods.

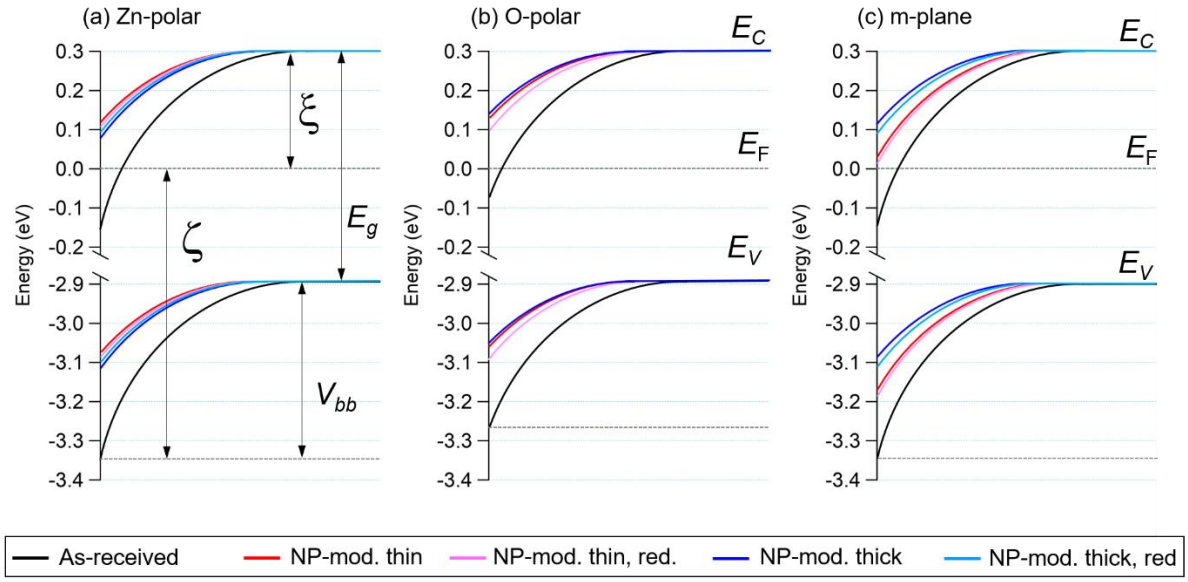

Figure 5.22. Schematic energy level diagrams of as-received, NP-modified, and reduced NP-modified (a) Zn-polar, (b) O-polar, and (c) m-plane ZnO surfaces, using the ζ and V_{bb} values extracted from the fixed-energy XPS VB spectra in Figure 5.16 and Figure 5.21 with the zero of the energy scale equal to E_F, which is assumed to not change after NP modification as it is a bulk property. For ease of reading, the energy scale has been shifted to give the as-received samples the same ζ.

Figure 5.22 compares band bending on non-reduced and reduced NP films. As-received samples have been calibrated to the same energy for visual clarity: the ζ value for the as-received sample of each face for spectra collected during analysis of non-reduced (Table 5.5) and reduced (Table 5.9) samples were set to the values in Table 5.5.

In summary, the addition of thin and thick NP films decreased the downwards band bending on all ZnO faces. On Zn-polar ZnO, there is little difference between thin and thick, 'reduced' and unreduced films, which is attributed to the thickness of the thin films, and the unsuccessful reduction of NP groups. On the O-polar face, the band bending effects of both thin and thick films are similar, and successful partial reduction of both NP films slightly increased the downwards band bending compared to a freshly-prepared sample. The direction of this shift is expected, due to the amine-type products having electron donating character, but the small magnitude of the shift suggests that there

are competing influences. On m-plane ZnO, it was seen that a very thin NP film changed the band bending less than did a thicker film. After reduction of NO_2 groups to electron-withdrawing NHOH, the downwards band bending on thin NP films shifted by a small amount towards the original band bending of as-received m-plane ZnO. The thick NP film on m-plane, when reduced, showed a smaller decrease in downwards band bending relative to the freshly-modified sample, consistent with the main product of the reduction being amino groups.

On as-received Zn-polar, O-polar, and m-plane ZnO, downwards band bending of ~−0.40 eV positions the Fermi level within the conduction band near the surface. Upon NP modification, the band bending decreases, which separates the Fermi level from the conduction band on all faces. This means that fewer electrons populate the conduction band than on as-received ZnO; this could be a reason for subsequent poor electrochemical behaviour of the modified materials. On the other hand, the lack of external calibration of ζ values means that Figure 5.22 is illustrative and does not contain absolute values.

Figure 5.23a summarises the changes in band bending associated with each film thickness, including the samples which had undergone electrochemical reduction. Several observations can be made. Firstly, the thin reduced films (1 – 1.3 nm) had, as expected, the smallest change in V_{bb} as nearly all of the NO_2 groups were reduced, while the thicker analogues (4 – 5 nm) on the O-polar and m-plane faces still had significant NO_2 signals and thus had V_{bb} values which reflected that. In general, it appears that NP films < 2.5 nm thick have relatively little effect on V_{bb} (< 0.2 eV) while thicker films of 3 – 7 nm may have larger band bending changes. It also appears that films in the range of 6 – 7 nm have smaller ΔV_{bb} than those of 4 – 5 nm, however, the uncertainty for film thickness shown here (± 20%) and the small number of samples do not allow for a firm conclusion to be made. The largest ΔV_{bb} is seen on Zn-polar ZnO, suggesting that the bands are more easily changed compared to O-polar and m-plane faces.

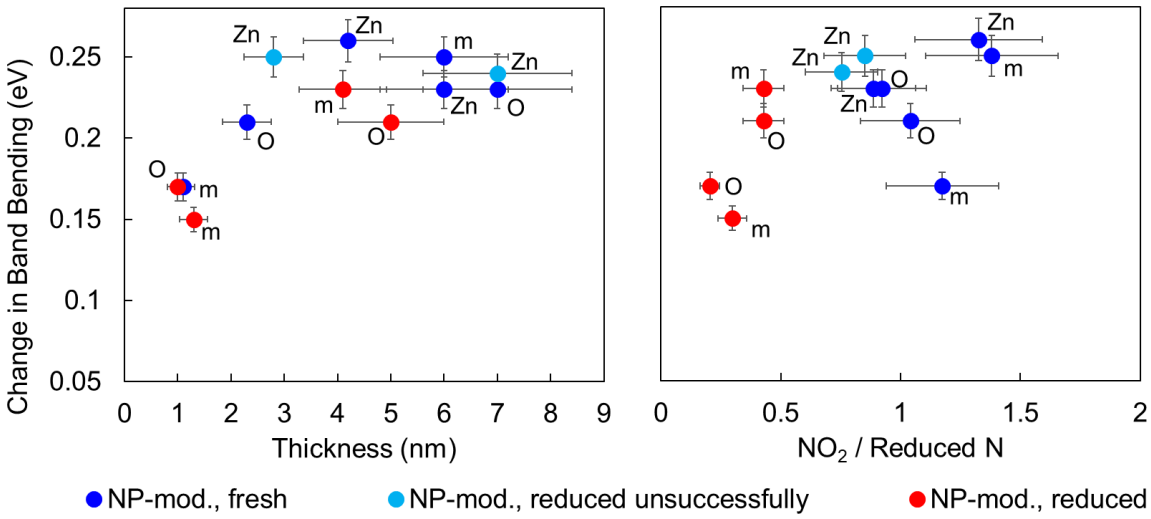

Figure 5.23. Band bending changes relative to the as-received samples for NP-modified and NP-modified, then reduced, Zn-polar, O-polar, and m-plane ZnO, as compared to (a) NP-layer thickness and (b) the NO_2/reduced N XPS fraction.

Figure 5.23b shows how V_{bb} changes with respect to the amount of NO_2 relative to reduced N species on the surface. It appears that the change in V_{bb} increases with the amount of NO_2 (if the film is thick enough), but there is no clear trend and the role of NO_2 in band bending relative to reduced N groups is uncertain. The range of ΔV_{bb} values for the successfully reduced NP films on O-polar and m-plane ZnO, where the amount of NO_2 is less than the amount of reduced N, is very similar to the range of values seen on non-reduced NP films, which have larger amounts of NO_2 than reduced N species. The possibility of aryl rings acting to withdraw electrons from ZnO, regardless of the aryl substituents, therefore cannot be ruled out. Study of a known electron-donating substituent on the aryl group would be useful to explore this further.

5.3.3 Chemical Reduction of Nitrophenyl Films on ZnO

As electrochemical reduction of NP films was incomplete, a direct chemical reduction method was investigated. O-polar ZnO was first modified with a thin film on NP before immersion in an ethanolic Na_2S solution and heated to ~40 °C.[4] It was analysed with AFM and fixed-energy XPS.[4]

5.3.3.1 Surface Morphology of Chemically-Reduced Nitrophenyl Films on ZnO

Figure 5.24 shows AFM images of Na_2S-treated, NP-modified O-polar ZnO and as-received O-polar ZnO. While the as-received sample has a small amount of debris and polishing scratches on the surface, the modified sample has undergone large changes in topography and roughness. Notably, there are large raised islands several hundred nm in diameter and 20 – 60 nm in height, as well as smaller features. These appeared unlikely to be due to the NP film as these were not seen previously.

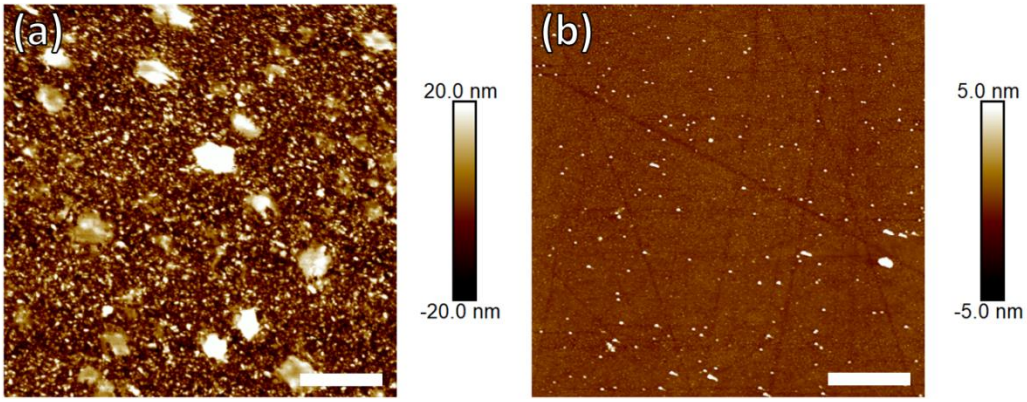

Figure 5.24. AFM images of (a) Na_2S-treated NP-modified O-polar ZnO and (b) as-received O-polar ZnO. Scale bar is 1 µm.

5.3.3.2 XPS Characterisation of Chemically Reduced Nitrophenyl-Modified O-polar ZnO

Na_2S-treated NP-modified O-polar ZnO was analysed with fixed-energy XPS. As-received O-polar ZnO with a Ti/Au contact strip was also subjected to the same Na_2S treatment as a control. Figure 5.25 shows the survey XPS spectra for these samples and for an as-received sample; Table 5.10 shows the atomic percentages.

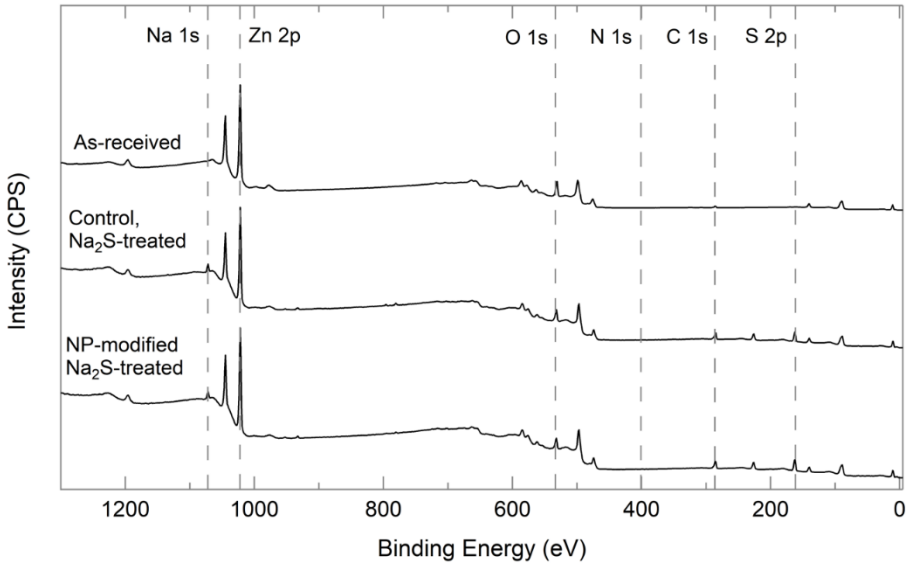

Figure 5.25. Fixed-energy XPS survey spectra for as-received O-polar ZnO, O-polar ZnO with a Ti/Au contact strip treated with Na_2S ('control'), and NP-modified O-polar ZnO modified treated with Na_2S. Spectra offset and resized for clarity. Core levels of interest are noted.

Table 5.10. ASF-corrected atomic percentages and overlayer thicknesses from fixed-energy XPS survey spectra for as-received O-polar ZnO, O-polar ZnO with a Ti/Au contact strip treated with Na_2S ('control'), and NP-modified O-polar ZnO treated with Na_2S.

	% Zn 2p	% C 1s	% O 1s	% N 1s	% S 2p	% Na 1s	Overlayer Thickness (nm)
As-received	41	15	40	-	4	-	-
Control	22	35	18	-	20	5	1.8 ± 0.4
NP and Na_2S	23	36	16	-	21	5	1.7 ± 0.3

In Figure 5.25, there is no detectable N 1s signal from any sample, including NP-modified O-polar ZnO. This indicates that N was lost from NP-modified ZnO during Na_2S treatment, via either NO_2 cleavage from the phenyl rings, or desorption of entire NP groups. The second scenario is more likely, as the NP-modified sample has the same C:Zn ratio as the control sample (1.6:1). The percentage of Zn in the survey spectrum decreases from 41% to 22% upon Na_2S treatment of both O-polar ZnO samples; this gives a similar calculated overlayer thickness on both samples of ~1.8 ± 0.5 nm, which is similar to that

reported by Love et al. for Na_2S-treated Pd.[55] The overlayers on the treated surfaces likely consist of C, S, and Na, as the percentage of these elements increases on these samples. The percentages of each of these elements is consistent across the control and NP-modified surfaces. The Na:S ratio is ~1:4, suggesting that S is more likely to adsorb strongly to the surface than Na.

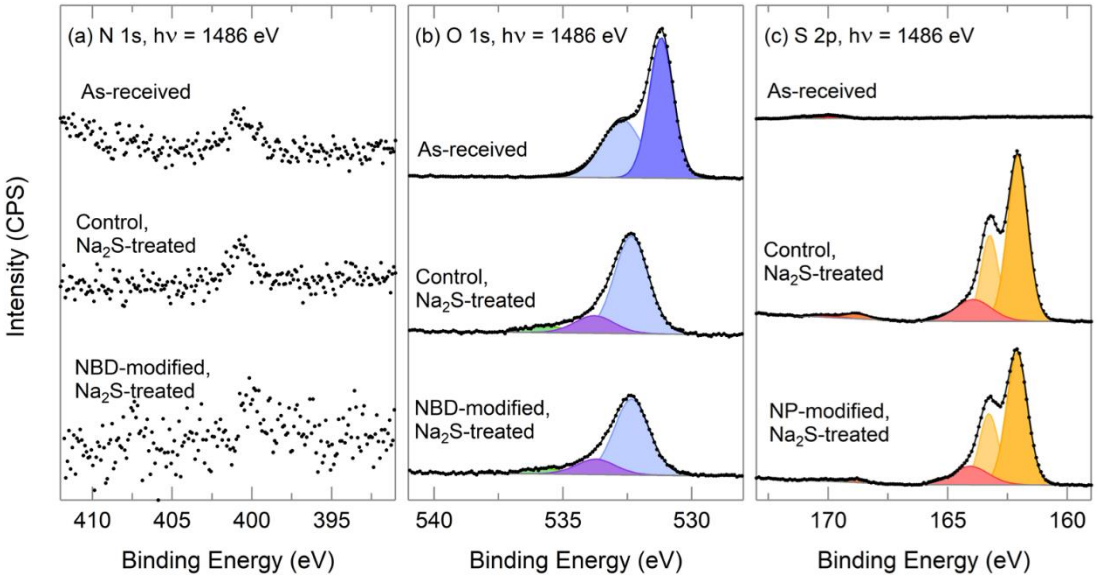

Figure 5.26. Fixed-energy XPS (a) N1s, (b) O 1s, and (c) S 2p spectra for as-received O-polar ZnO, 'control' O-polar ZnO treated with Na_2S, and NP-modified O-polar ZnO treated with Na_2S. Spectra are normalised to the same Zn 2p peak area and vertically offset for clarity.

Figure 5.26 shows the N 1s, O 1s, and S 2p core level spectra. Figure 5.26a further shows that only trace N is present on the samples. This confirms loss of NO_2 and azo groups from the NP-modified sample; combined with the modified samples having similar amounts of C on the surface (Table 5.10), this suggests that the entire NP film was removed during the Na_2S treatment.

Figure 5.26b shows unusual O 1s spectra for both Na_2S-treated samples compared to the as-received sample, which has the typical two peaks indicative of bulk and surface oxygen as discussed previously. On the Na_2S-modified samples it appears that the bulk O peak at ~531 eV has disappeared. Either an overlayer containing C, S, Na, and O is present, masking the bulk O signal, or a large shift in the core levels has shifted the bulk O signal to higher BE (~533 eV) and there is a very small amount of surface

O at ~534 eV. The bulk O BE shift of +1.35 eV required for the latter explanation is not consistent with BE shifts in other spectra. For example, the BE difference between the S 2p peak at ~170 eV for as-received O-polar ZnO and Na_2S-treated ZnO is 0.39 eV; for Zn 2p, it is 0.34 eV. These are significantly smaller shifts than 1.35 eV, as proposed for the O 1s spectra. On the other hand, the high percentages of C, S, and Na on control and NP-modified Na_2S-treated samples, alongside the attenuation of the Zn 2p signal, suggest that loss of the bulk O 1s signal due to attenuation by an overlayer is more likely. However, it is unusual that the Zn 2p signal has not been attenuated by a similar amount; this cannot be attributed to a difference in BE of Zn 2p and O 1s as the O 1s signal should be attenuated less than Zn 2p due to O 1s having a lower BE and therefore a longer IMFP. This is currently unexplained, but an unusually limited penetration depth of Na_2S-treated Pd was also observed by Love et al,[55] who observed a PdS metal sulfide layer had formed after 24 h in 10 mM $Na_2S_{(aq)}$ (RT).

A significant amount of S is seen in the S 2p region of both Na_2S-treated samples (Figure 5.26c). A trace amount of oxidised S contamination is present on the as-received sample (~168 eV), while the strongest signal for the Na_2S-treated samples is at BE ~162 eV, consistent with S bound to Zn.[56] This shows that S was strongly adsorbed to the modified surface and able to withstand sonication. Spin-orbit splitting of the S 2p peak is evident in both the ~170 eV and ~161.5 eV regions, while small peaks at 167 eV and 163 eV are currently unassigned but likely arise from different oxidation states of S. All Na_2S-treated samples have a similar amount of S on the surface.

The results described above demonstrate that Na_2S treatment was not successful in reducing NP groups on NP modification films, and instead removed NP groups and contaminated the ZnO surfaces. However, the highly unusual O 1s spectra are intriguing and hence the effect of Na_2S treatment on surface band bending was investigated.

5.3.3.3 Band Bending of O-polar ZnO After Treatment with Na_2S

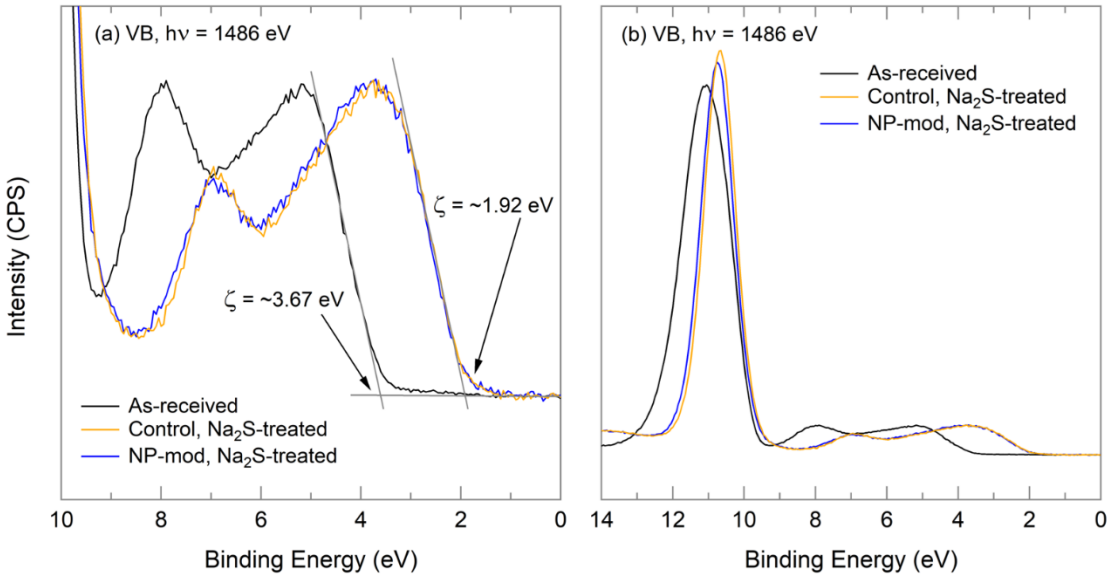

Figure 5.27. Fixed-energy VB spectra for as-received O-polar ZnO (black), O-polar ZnO contacted with a Ti/Au strip prior to treatment with Na_2S ('control', orange), and NP-modified O-polar ZnO treated with Na_2S (blue). (a) BE scale 10 to 0 eV; (b) BE scale 14 to 0 eV. Spectra are normalised to the same intensity of the lowest BE peak.

Figure 5.27 shows VB spectra measured for NP-modified O-polar ZnO subjected to Na_2S treatment. For comparison, an as-received O-polar ZnO sample is plotted, as are spectra for as-received O-polar ZnO, with a Ti/Au contact, treated with Na_2S ('control'). It is immediately clear that both Na_2S-treated samples have undergone a large change in surface properties, with a decrease in ζ of ~1.75 eV (Figure 5.27a). Table 5.11 tabulates ζ and the corresponding band bending values for each sample. While not shown, an identical treatment of NP-modified MBE-grown ZnO gave similar results with average $\Delta\zeta = -1.75$ eV, confirming reproducibility. The ζ change on the Na_2S-treated samples is highly significant, as it indicates that the surface now has upwards band bending of +0.95 – 0.96 eV. This is an extremely large change, especially as it was measured using high-energy photons of $h\nu = 1486.6$ eV, which means that the surface now has an insulating nature that extends well into the bulk of ZnO.

The shapes of the VB spectra for the modified samples are qualitatively similar to that of the as-received O-polar ZnO, indicating that the material is still ZnO. However, there is a small decrease in intensity for the peak located at higher BE (8 eV for as-received ZnO; 7 eV for Na_2S-treated ZnO). This peak is assigned to hybridised O 2p and Zn 4s states,[57] and its attenuation upon modification may reflect the attenuation of the bulk O signal as seen in core level spectra. Again, little evidence of Zn attenuation is seen: the Zn 3d peaks situated at ~11 eV have similar intensities for all three samples. On the Na_2S-treated samples, the Zn 3d peak is shifted by ~−0.4 eV relative to as-received O-polar ZnO, while the hybridised O 2p and Zn 4s peak is shifted by ~−1 eV. This suggests that a large change has occurred in the VB of ZnO upon Na_2S treatment.

Table 5.11. ζ and band bending data for as-received O-polar ZnO, O-polar ZnO contacted with Ti/Au prior to treatment with Na_2S ('control'), and NP-modified O-polar ZnO treated with Na_2S, determined from fixed-energy XPS valence band spectra.

Sample	**ζ (eV)**	**Δζ (eV)**	**V_{bb} (eV)**
As-received	3.67	-	−0.80
Control, Na_2S-treated	1.92	−1.75	0.95
NP-modified, Na_2S treated	1.91	−1.76	0.96

The amount of S on the two Na_2S-treated samples is similar (Table 5.10), so it is proposed that S may play a role in their similar band bending changes. However, the direction of the band bending shift is unexpected if this is the case. Ozawa et al. observed that S atoms bound on ZnO faces via dissociative adsorption of tetrathiafulvalene act as dopants, not acceptors, and would be expected to shift the VB to more positive BE.[58] Several studies report that spin-coated thin films of Na_2S change the band bending at semiconductor surfaces: Petrovykh et al. observed increased downwards on band bending n-type InAs when treated this way, but that the effects only lasted for several days.[59] Besser and Helms used Na_2S on n-type GaAs and also observed that downwards band bending increased.[60] In another study, the same authors trialled both sodium and ammonium sulfides on n-type GaAs; while Na_2S

treatment resulted in an oxygenated surface, $(NH_4)_2S$ left very little surface O.[61] However, both treatments increased downwards band bending. In contrast, Chen et al. observed a decrease in downwards band bending on *p*-type GaAs after soaking the substrate in dilute $(NH_4)_2S$ at 50 °C for 10 – 25 min.[62] The different doping type of the two *n*- and *p*-type materials explains the difference in ΔV_{bb} direction.

The possibility of ZnS formation on top of the ZnO surface in the present work was considered, since O signal has been attenuated while Zn signal was not, suggesting that Zn species are still present at the surface.[55] However, if the VB spectrum was dominated by ZnS, the value of ζ would be expected to shift to a higher BE, not a lower BE, because hexagonal ZnS has a bandgap of 3.91 eV, which is ~0.6 eV greater than that of ZnO.[63] Furthermore, the shape of the VB spectra are consistent with that of ZnO, not ZnS.[64] This could be due to the low surface sensitivity of the fixed-energy XPS and would be worth investigating with a tuneable X-ray source or angle-resolved XPS.

The amounts of Na on each Na_2S-treated sample are also similar (Table 5.10). Na is known to be a shallow acceptor in ZnO,[44,65] and may be responsible for the large shift of ζ towards lower BE. The nature of Na adsorption on ZnO is not known, however. At this time, no explanation for this large and reproducible band bending shift is given and further investigation into this interesting phenomenon is required.

5.3.4 Characterisation of 'Spontaneous' NBD-Treated m-Plane ZnO

5.3.4.1 Surface Morphology of 'Spontaneous' NBD-Treated m-Plane ZnO

Having determined that ZnO can be grafted with NP layers using electrochemical reduction of NBD, the ability of the same reaction to occur 'spontaneously' – that is, without applied potential – was investigated. This is a desirable modification method due to its simplicity.

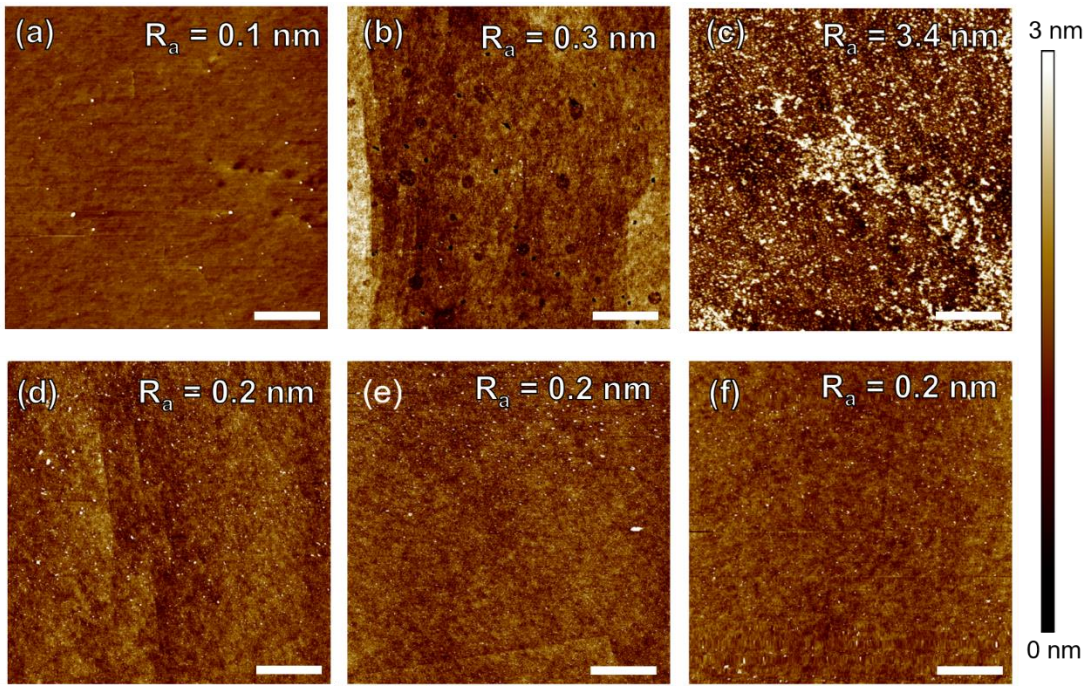

Figure 5.28: AFM images for (a) as-received m-plane ZnO, and m-plane ZnO after immersion in (b) ACN, (c) water and NBD, and (d), (e), (f) ACN and NBD. Sample (e) was treated with UV prior to immersion, and sample (f) was treated with NaOH before immersion. Scale bars are 1 µm.

Figure 5.28 shows AFM images obtained for m-plane ZnO samples subjected to the 'spontaneous' grafting procedures outlined in 5.2.2.3, and their corresponding surface roughness values.

As-received m-plane ZnO (Figure 5.28a) is very smooth, with small specks of dust present on the surface as well as several small pits < 1 nm deep due to sonication. When analysed after immersion in ACN (Figure 5.28b), m-plane ZnO shows clear evidence of increased pitting, with pits ranging from 50 – 350 nm wide. The larger pits are less than 2 nm deep, while the narrow pits are up to 30 nm deep. No significant changes in surface topography or roughness are seen for any of the samples treated with ACN and NBD (Figure 5.28d, e and f) regardless of UV or base pre-treatment, which suggests that none of these samples were successfully modified with NP groups. On the other hand, the lack of pitting compared to the ACN control sample may indicate that the samples have been modified with NP groups, which have either 'filled-in' the pits caused by ACN or prevented the pits from forming.

The m-plane sample which was immersed in water and NBD (Figure 5.28c) shows a significant increase in surface roughness from 0.1 nm (as-received) to 3.4 nm, with very rough surface features clearly visible. This is thought to be due to etching by the slightly acidic Milli-Q water used for the diazonium salt solution (pH ~6.4). (Carbon dioxide is known to dissolve into deionised water from the atmosphere, lowering the pH.) Acidic conditions are known to lead to etching of ZnO, especially on the m-plane, and are most likely the cause of the roughened surface.[66] However, the roughness could also possibly be due to disordered layers of precipitated NBD or covalently-bound NP groups on the surface.

However, fixed-energy XPS spectra of NBD-treated m-plane samples, and synchrotron XPS spectra of NBD-treated Zn-polar, O-polar, and m-plane ZnO, did not show any evidence of successful NP grafting (Appendix 8.3) or changes in band bending. This is consistent with the above AFM images. Evidently, the 2DEG at ZnO surfaces is unable to spontaneously participate in the NBD reduction process. Further investigation was not deemed necessary considering that the use of electrochemistry is a well-known technique for acquiring aryl layers from aryldiazonium salt solutions.

5.4 Conclusions

Grafting of NP groups on ZnO does not occur spontaneously during immersion in either aqueous or non-aqueous NBD salt solution, indicating that the 2DEG is not readily available for the reduction reaction. However, ZnO can be modified via electrochemical means to give NP film thicknesses ranging from 1 – 7 nm depending on the potential range used and the ZnO crystal face. The thicker films were grafted by extending the potential limit to a more negative value. In general, using the same modification conditions, thinner films are grafted to m-plane ZnO, with Zn-polar ZnO gaining the thickest NP layers. These differences are attributed to the surfaces' resistivities, where m-plane ZnO has the highest resistivity of the three faces. Despite the different compositions of the Zn-polar, O-polar, and m-plane ZnO crystal faces, no clear dependence of the electrochemical behaviour of NBD at the different faces could be identified. As shown in this Chapter, the shape of the grafting CV is not

a reliable indicator of the success of a grafting process: for example, the grafting CV for a thin NP film on m-plane ZnO had very little current density relative to the polar faces, yet XPS and AFM measurements revealed that the surface was modified with 2 or 3 layers of NP groups. This cannot be attributed to a contribution from spontaneous grafting occurring during the degassing process (15 min) as spontaneous grafting was shown not to occur at ZnO. Chapter 6 investigates electrografting from aryldiazonium salt solutions on Sb-doped ZnO, which has a higher charge carrier concentration than bulk crystals.

While attempts to determine the exact binding mode of the aryl groups on ZnO were made through detailed examination of XPS data, an emission uniquely attributable to Zn-O-C bonds could not be identified. However, due to the lack of evidence for Zn-C bonds, and the fact that the films can withstand sonication, it is proposed that the films attach to all three ZnO faces via Zn-O-C bonds. The mechanism previously proposed for grafting from aryldiazonium ion solutions at Si may account for formation of Zn-O-C bonds. This is consistent with previous reports of metal-O-C bonds for other metal oxides modified by aryldiazonium ion chemistry. In Chapter 6, surface-sensitive synchrotron XPS is used to further characterise the binding mode.

NP films were found to decrease downwards band bending from ZnO surfaces by ~+0.2 eV ($h\nu$ = 1486.6 eV), with thicker NP films (> 2.5 nm) having the greatest effect. Beyond this thickness, no further decrease in band bending is seen. Upon electrochemical reduction of some nitro groups to amino groups, the downwards band bending increases but remains smaller than that of as-received ZnO. Chapter 6 investigates XPS-induced reduction of NP groups.

Finally, a large upwards shift in band bending was seen on O-polar ZnO when treated with Na_2S. Although XPS showed that all NP modifiers were removed by this treatment, S and Na remained on the surface. As S is expected to increase downwards band bending, Na is tentatively proposed to act as an acceptor on ZnO. However, the exact mechanism behind this band bending shift is unclear and the nature of the modified surface deserves further investigation.

5.5 References

(1) Richard, W.; Evrard, D.; Gros, P. New Insight into 4-Nitrobenzene Diazonium Reduction Process: Evidence for a Grafting Step Distinct from NO_2 Electrochemical Reactivity. *J. Electroanal. Chem.* **2012**, *685*, 109–115.

(2) Brooksby, P. A.; Downard, A. J. Electrochemical and Atomic Force Microscopy Study of Carbon Surface Modification via Diazonium Reduction in Aqueous and Acetonitrile Solutions. *Langmuir* **2004**, *20* (12), 5038–5045.

(3) Lee, L.; Brooksby, P. A.; Hapiot, P.; Downard, A. J. Electrografting of 4-Nitrobenzenediazonium Ion at Carbon Electrodes: Catalyzed and Uncatalyzed Reduction Processes. *Langmuir* **2016**, *32* (2), 468–476.

(4) Yu, S. S. C.; Tan, E. S. Q.; Jane, R. T.; Downard, A. J. An Electrochemical and XPS Study of Reduction of Nitrophenyl Films Covalently Grafted to Planar Carbon Surfaces. *Langmuir* **2007**, *23* (22), 11074–11082.

(5) Kullapere, M.; Marandi, M.; Matisen, L.; Mirkhalaf, F.; Carvalho, A. E.; Maia, G.; Sammelselg, V.; Tammeveski, K. Blocking Properties of Gold Electrodes Modified with 4-Nitrophenyl and 4-Decylphenyl Groups. *J. Solid State Electrochem.* **2012**, *16* (2), 569–578.

(6) Liu, G.; Böcking, T.; Gooding, J. J. Diazonium Salts: Stable Monolayers on Gold Electrodes for Sensing Applications. *J. Electroanal. Chem.* **2007**, *600* (2), 335–344.

(7) Roodenko, K.; Gensch, M.; Rappich, J.; Hinrichs, K.; Esser, N.; Hunger, R. Time-Resolved Synchrotron XPS Monitoring of Irradiation-Induced Nitrobenzene Reduction for Chemical Lithography. *J. Phys. Chem. B* **2007**, *111* (26), 7541–7549.

(8) Hunger, R.; Jaegermann, W.; Merson, A.; Shapira, Y.; Pettenkofer, C.; Rappich, J. Electronic Structure of Methoxy-, Bromo-, and Nitrobenzene Grafted onto Si(111). *J. Phys. Chem. B* **2006**, *110* (31), 15432–15441.

(9) Tajik, N.; Peng, Z.; Kuyanov, P.; LaPierre, R. R. Sulfur Passivation and Contact Methods for GaAs Nanowire Solar Cells. *Nanotechnology* **2011**, *22* (22), 225402.

(10) Chen, X.; Chockalingam, M.; Liu, G.; Luais, E.; Gui, A. L.; Gooding, J. J. A Molecule with Dual Functionality 4-Aminophenylmethylphosphonic Acid: A Comparison Between Layers Formed on Indium Tin Oxide by In Situ Generation of an Aryl Diazonium Salt or by Self-Assembly of the Phosphonic Acid. *Electroanalysis* **2011**, *23* (11), 2633–2642.

(11) Bangle, R.; Sampaio, R. N.; Troian-Gautier, L.; Meyer, G. J. Surface Grafting of Ru(II) Diazonium-Based Sensitizers on Metal Oxides Enhances Alkaline Stability for Solar Energy Conversion. *ACS Appl. Mater. Interfaces* **2017**, *10*, 3121–3132.

(12) Lund, T.; Nguyen, P. T.; Ruhland, T. Electrochemical Grafting of TiO_2-Based Photo-Anodes and Its Effect in Dye-Sensitized Solar Cells. *J. Electroanal. Chem.* **2015**, *758*, 85–92.

(13) Bell, K. J.; Brooksby, P. A.; Polson, M. I. J.; Downard, A. J. Evidence for Covalent Bonding of Aryl Groups to MnO_2 Nanorods from Diazonium-Based Grafting. *Chem. Commun.* **2014**, *50* (89), 13687–13690.

(14) Brymora, K.; Fouineau, J.; Eddarir, A.; Chau, F.; Yaacoub, N.; Grenèche, J. M.; Pinson, J.; Ammar, S.; Calvayrac, F. Grafting of Diazonium Salts on Oxides Surface: Formation of Aryl-O Bonds on Iron Oxide Nanoparticles. *J. Nanoparticle Res.* **2015**, *17* (11), 1–9.

(15) Wang, C.; Huang, N.; Zhuang, H.; Jiang, X. Enhanced Performance of Nanocrystalline ZnO DNA

Biosensor via Introducing Electrochemical Covalent Biolinkers. *ACS Appl. Mater. Interfaces* **2015**, *7* (14), 7605–7612.

(16) Mohamed, A. A.; Salmi, Z.; Dahoumane, S. A.; Mekki, A.; Carbonnier, B.; Chehimi, M. M. Functionalization of Nanomaterials with Aryldiazonium Salts. *Adv. Colloid Interface Sci.* **2015**, *225*, 16–36.

(17) Pinson, J.; Podvorica, F. Attachment of Organic Layers to Conductive or Semiconductive Surfaces by Reduction of Diazonium Salts. *Chem. Soc. Rev.* **2005**, *34* (5), 429.

(18) Milanesi, S.; Fagnoni, M.; Albini, A. (Sensitized) Photolysis of Diazonium Salts as a Mild General Method for the Generation of Aryl Cations. Chemoselectivity of the Singlet and Triplet 4-Substituted Phenyl Cations. *J. Org. Chem.* **2005**, *70* (2), 603–610.

(19) Allongue, P.; Delamar, M.; Desbat, B.; Fagebaume, O.; Hitmi, R.; Pinson, J.; Savéant, J. M. Covalent Modification of Carbon Surfaces by Aryl Radicals Generated from the Electrochemical Reduction of Diazonium Salts. *J. Am. Chem. Soc.* **1997**, *114* (1), 201–207.

(20) Mesnage, A.; Lefèvre, X.; Jégou, P.; Deniau, G.; Palacin, S. Spontaneous Grafting of Diazonium Salts: Chemical Mechanism on Metallic Surfaces. *Langmuir* **2012**, *28* (32), 11767–11778.

(21) Podvorica, F. I.; Combellas, C.; Delamar, M.; Kanoufi, F. A. A.; Pinson, J. Spontaneous Grafting of Iron Surfaces by Reduction of Aryldiazonium Salts in Acidic Water: Applications to the Inhibition of Iron Corrosion. *Passiv. Met. Semicond. Prop. Thin Oxide Layers* **2006**, No. 9, 697–702.

(22) Adenier, A.; Cabet-Deliry, E.; Chaussé, A.; Griveau, S.; Mercier, F.; Pinson, J.; Vautrin-Ul, C. Grafting of Nitrophenyl Groups on Carbon and Metallic Surfaces without Electrochemical Induction. *Chem. Mater.* **2005**, *17* (3), 491–501.

(23) Brooksby, P. A.; Shields, J. D.; Farquhar, A. K.; Downard, A. J. Reduction of Nitrophenyl Films in Aqueous Solutions: How Many Electrons? *ChemElectroChem* **2016**, *3* (12), 2021–2026.

(24) Laforgue, A.; Addou, T.; Bélanger, D. Characterization of the Deposition of Organic Molecules at the Surface of Gold by the Electrochemical Reduction of Aryldiazonium Cations. *Langmuir* **2005**, *21* (15), 6855–6865.

(25) Chaussé, A.; Chehimi, M. M.; Karsi, N.; Pinson, J.; Podvorica, F.; Vautrin-Ul, C. The Electrochemical Reduction of Diazonium Salts on Iron Electrodes. The Formation of Covalently Bonded Organic Layers and Their Effect on Corrosion. *Chem. Mater.* **2002**, *14* (1), 392–400.

(26) Combellas, C.; Jiang, D.; Kanouf, F.; Pinson, J.; Podvorica, F. I. Steric Effects in the Reaction of Aryl Radicals on Surfaces. *Langmuir* **2009**, No. 25, 286–293.

(27) Chevalier, C. L.; Landis, E. C. Electrochemical Attachment of Diazonium-Generated Films on Nanoporous Gold. *Langmuir* **2015**, *31* (31), 8633–8641.

(28) Benedetto, A.; Balog, M.; Viel, P.; Le Derf, F.; Sallé, M.; Palacin, S. Electro-Reduction of Diazonium Salts on Gold: Why Do We Observe Multi-Peaks? *Electrochim. Acta* **2008**, *53* (24), 7117–7122.

(29) Cline, K. K.; Baxter, L.; Lockwood, D.; Saylor, R.; Stalzer, A. Nonaqueous Synthesis and Reduction of Diazonium Ions (without Isolation) to Modify Glassy Carbon Electrodes Using Mild Electrografting Conditions. *J. Electroanal. Chem.* **2009**, *633* (2), 283–290.

(30) Farquhar, A. K.; Dykstra, H. M.; Waterland, M. R.; Downard, A. J.; Brooksby, P. A. Spontaneous Modification of Free-Floating Few-Layer Graphene by Aryldiazonium Ions: Electrochemistry, Atomic Force Microscopy, and Infrared Spectroscopy from Grafted Films. *J. Phys. Chem. C* **2016**,

120 (14), 7543–7552.

(31) Saby, C.; Ortiz, B.; Champagne, G. Y.; Bélanger, D. Electrochemical Modification of Glassy Carbon Electrode Using Aromatic Diazonium Salts. 1. Blocking Effect of 4-Nitrophenyl and 4-Carboxyphenyl Groups. *Langmuir* **1997**, *13* (14), 6805–6813.

(32) Chockalingam, M.; Magenau, A.; Parker, S. G.; Parviz, M.; Vivekchand, S. R. C.; Gaus, K.; Gooding, J. J. Biointerfaces on Indium-Tin Oxide Prepared from Organophosphonic Acid Self-Assembled Monolayers. *Langmuir* **2014**, *30* (28), 8509–8515.

(33) Mirkhalaf, F.; Mason, T. J.; Morgan, D. J.; Saez, V. Frequency Effects on the Surface Coverage of Nitrophenyl Films Ultrasonically Grafted onto Indium Tin Oxide. *Langmuir* **2011**, *27* (5), 1853–1858.

(34) La, Y.; Jung, Y. J.; Kang, T.; Ihm, K.; Kim, K.; Kim, B. NEXAFS Studies on the Soft X-Ray Induced Chemical Transformation of a 4-Nitrobenzaldimine Monolayer *Langmuir* **2003**, *19*, 9984–9987.

(35) Ivashenko, O.; Van Herpt, J. T.; Feringa, B. L.; Browne, W. R.; Rudolf, P. Rapid Reduction of Self-Assembled Monolayers of a Disulfide Terminated Para-Nitrophenyl Alkyl Ester on Roughened Au Surfaces during XPS Measurements. *Chem. Phys. Lett.* **2013**, *559*, 76–81.

(36) Mendes, P.; Belloni, M.; Ashworth, M.; Hardy, C.; Nikitin, K.; Fitzmaurice, D.; Critchley, K.; Evans, S.; Preece, J. A Novel Example of X-Ray-Radiation-Induced Chemical Reduction of an Aromatic Nitro-Group-Containing Thin Film on SiO_2 to an Aromatic Amine Film. *ChemPhysChem* **2003**, *4* (8), 884–889.

(37) Eck, W.; Stadler, V.; Geyer, W.; Zharnikov, M.; Gölzhäuser, A.; Grunze, M. Generation of Surface Amino Groups on Aromatic Self-Assembled Monolayers by Low Energy Electron Beams. *Adv. Mater.* **2000**, *12* (11), 805–808.

(38) Geyer, W.; Stadler, V.; Eck, W.; Gölzhäuser, A.; Grunze, M.; Sauer, M.; Weimann, T.; Hinze, P. Electron Induced Chemical Nanolithography with Self-Assembled Monolayers. *J. Vac. Sci. Technol. B* **2001**, *19* (6), 2732.

(39) Geyer, W.; Stadler, V.; Eck, W.; Zharnikov, M.; Gölzhäuser, A.; Grunze, M. Electron-Induced Crosslinking of Aromatic Self-Assembled Monolayers: Negative Resists for Nanolithography. *Appl. Phys. Lett.* **1999**, *75* (16), 2401–2403.

(40) Sun, R.-D.; Nakajima, A.; Fujishima, A.; Watanabe, T.; Hashimoto, K. Photoinduced Surface Wettability Conversion of ZnO and TiO_2 Thin Films. *J. Phys. Chem. B* **2001**, *105* (10), 1984–1990.

(41) English, C. R.; Hamers, R. J. Molecular Electronic Effects on the Thermal Grafting of Aryl Iodides to TiO_2 Surfaces. *J. Phys. Chem. C* **2015**, *119* (50), 27972–27981.

(42) Hanwell, M. D.; Curtis, D. E.; Lonie, D. C.; Vandermeersch, T.; Zurek, E.; Hutchison, G. R. Avogadro: An Advanced Semantic Chemical Editor, Visualisation, and Analysis Platform. *J. Chem. Informatics* **2012**, *4.17*, 1–17.

(43) Heinhold, R.; Williams, G. T.; Cooil, S. P.; Evans, D. A.; Allen, M. W. Influence of Polarity and Hydroxyl Termination on the Band Bending at ZnO Surfaces. *Phys. Rev. B: Condens. Matter* **2013**, *88* (23), 235315.

(44) Morkoç, H.; Özgür, Ü. *Zinc Oxide: Fundamentals, Materials and Device Technology*; Wiley-VCH: Weinheim, 2009.

(45) Paulik, M. G.; Brooksby, P. A.; Abell, A. D.; Downard, A. J. Grafting Aryl Diazonium Cations to Polycrystalline Gold: Insights into Film Structure Using Gold Oxide Reduction, Redox Probe Electrochemistry, and Contact Angle Behavior. *J. Phys. Chem. C* **2007**, *111* (21), 7808–7815.

(46) Hurley, B. L.; McCreery, R. L. Covalent Bonding of Organic Molecules to Cu and Al Alloy 2024 T3 Surfaces via Diazonium Ion Reduction. *J. Electrochem. Soc.* **2004**, *151* (5), B252.

(47) Dicke, C.; Morstein, M.; Hähner, G. Surface Inorganic Chemistry: The Reaction of Hydroxyl-Terminated Thiols on Gold with a Zirconium Coordination Compound. *Langmuir* **2002**, *18* (2), 336–344.

(48) Samanta, S.; Bakas, I.; Singh, A.; Aswal, D. K.; Chehimi, M. M. In Situ Diazonium-Modified Flexible ITO-Coated PEN Substrates for the Deposition of Adherent Silver-Polypyrrole Nanocomposite Films. *Langmuir* **2014**, *30*, 9397–9406.

(49) Gao, F.; Aminane, S.; Bai, S.; Teplyakov, A. V. Chemical Protection of Material Morphology: Robust and Gentle Gas-Phase Surface Functionalization of ZnO with Propiolic Acid. *Chem. Mater.* **2017**, *29* (9), 4063–4071.

(50) Berisha, A.; Hazimeh, H.; Galtayries, A.; Decorse, P.; Kanoufi, F.; Combellas, C.; Pinson, J.; Podvorica, F. I. Grafting of an Aluminium Surface with Organic Layers. *RSC Adv.* **2016**, *6* (82), 78369–78377.

(51) de Villeneuve, C. H.; Pinson, J.; Bernard, M. C.; Allongue, P. Electrochemical Formation of Close-Packed Phenyl Layers on Si(111). *J. Phys. Chem. B* **1997**, *101* (14), 2415–2420.

(52) Hartig, P.; Dittrich, T.; Rappich, J. Surface Dipole Formation and Non-Radiative Recombination at *p*-Si(111) Surfaces during Electrochemical Deposition of Organic Layers. *J. Electroanal. Chem.* **2002**, *524–525*, 120–126.

(53) Vasheghani Farahani, S. K.; Veal, T. D.; Mudd, J. J.; Scanlon, D. O.; Watson, G. W.; Bierwagen, O.; White, M. E.; Speck, J. S.; McConville, C. F. Valence-Band Density of States and Surface Electron Accumulation in Epitaxial SnO_2 Films. *Phys. Rev. B: Condens. Matter* **2014**, *90* (15), 1–9.

(54) Richard, W.; Evrard, D.; Busson, B.; Humbert, C.; Dalstein, L.; Tadjeddine, A.; Gros, P. The Reduction of 4-Nitrobenzene Diazonium Electrografted Layer: An Electrochemical Study Coupled to In Situ Sum-Frequency Generation Spectroscopy. *Electrochim. Acta* **2018**, *283*, 1640–1648.

(55) Love, J. C.; Wolfe, D. B.; Haasch, R.; L, M.; Paul, K. E.; Whitesides, G. M.; Nuzzo, R. G.; Chabinyc, M. L. Formation and Structure of Self-Assembled Monolayers of Alkanethiolates on Palladium. **2003**, 2597–2609.

(56) Chen, J.; Ruther, R. E.; Tan, Y.; Bishop, L. M.; Hamers, R. J. Molecular Adsorption on ZnO$(10\bar{1}0)$ Single-Crystal Surfaces: Morphology and Charge Transfer. *Langmuir* **2012**, *28* (28), 10437–10445.

(57) Heinhold, R.; Allen, M. W. Polarity-Dependent Photoemission of In Situ Cleaved Zinc Oxide Single Crystals. *J. Mater. Res.* **2012**, *27* (17), 2214–2219.

(58) Ozawa, K.; Munakata, S.; Edamoto, K.; Mase, K. Electron Donor Molecule on the Oxide Surface: Influence of Surface Termination of ZnO on Adsorption of Tetrathiafulvalene. *J. Phys. Chem. C* **2011**, *115* (44), 21843–21851.

(59) Petrovykh, D.; Yang, M.; Whitman, L. Chemical and Electronic Properties of Sulfur-Passivated InAs Surfaces. *Surf. Sci.* **2002**, *523*, 231–240.

(60) Besser, R. S.; Helms, C. R. Effect of Sodium Sulfide Treatment on Band Bending in GaAs. *Appl. Phys. Lett.* **1988**, *52* (20), 1707–1709.

(61) Besser, R. S.; Helms, C. R. Comparison of Surface Properties of Sodium Sulfide and Ammonium

Sulfide Passivation of GaAs. *J. Appl. Phys.* **1989**, *65* (11), 4306–4310.

(62) Chen, X.; Xia, N.; Yang, Z.; Gong, F.; Wei, Z.; Wang, D.; Tang, J.; Fang, X.; Fang, D.; Liao, L. Analysis of the Influence and Mechanism of Sulfur Passivation on the Dark Current of a Single GaAs Nanowire Photodetector. *Nanotechnology* **2018**, *29* (9), 95201.

(63) Kittel, C. *Introduction to Solid State Physics*, 6th ed.; New York, 1986.

(64) Sosa, V.; Rack, P. D.; Holloway, P. H. X-Ray Photoelectron Spectroscopy Valence Band Data for ZnS, SrS, and $Sr_{0.45}Ca_{0.55}Ga_2S_4$ Luminescent Thin Films **2011**, *393* (1998), 1–5.

(65) Parmar, N. S.; Lynn, K. G. Sodium Doping in ZnO Crystals. *Appl. Phys. Lett.* **2015**, *106* (2), 1–4.

(66) Valtiner, M.; Borodin, S.; Grundmeier, G. Stabilization and Acidic Dissolution Mechanism of Single-Crystalline ZnO(0001) Surfaces in Electrolytes Studied by In-Situ AFM Imaging and Ex-Situ LEED. *Langmuir* **2008**, *24* (10), 5350–5358.

6 Aryldiazonium Ion Chemistry at MBE-Grown ZnO Thin Films

6.1 Introduction and Aims

Aryldiazonium ions can be reduced at single crystal ZnO surfaces via electrochemistry to produce disordered multi-layered aryl films, as shown in Chapter 5 with nitrobenzene diazonium (NBD). However, results indicated that the polarity and carrier concentration of the substrate influence the reproducibility and thickness of these electrografted aryl layers, with thinner layers at the m-plane face than the two polar faces. The O-polar face appeared to give the most reproducible cyclic voltammograms (CVs). In this chapter, further studies of surface modification of O-polar ZnO using aryldiazonium ions is described. Sb-doped ZnO was used because the increased carrier concentration was expected to give improved electrochemical responses.[1] Thin-film O-polar-type Sb-doped ZnO was grown via plasma-assisted molecular beam epitaxy (MBE) on sapphire substrates and used for these studies. They will be referred to in this chapter as 'MBE-ZnO'.

In the previous chapter, nitrophenyl (NP) films were shown to decrease downwards band bending on single crystal ZnO, and it was seen that electrochemical reduction of the nitro functional groups did not significantly change the band bending. In this chapter, another method for reduction of nitro groups using synchrotron XPS photoelectrons is investigated. A second aryldiazonium salt, trifluoromethylbenzene diazonium tetrafluoroborate (TFMBD), is also examined to compare the effect on the band bending with that of NBD. Both NBD and TFMBD have electron-withdrawing functional groups and aromatic rings; NBD has a dipole moment of 4.22 ± 0.08 D while that of TFMBD is 2.86 ± 0.08 D; as such, the latter is expected to have a smaller effect on the band bending.[2] Furthermore, fixed-energy XPS used in Chapter 5 was unable to reveal the binding mode of NP groups on the ZnO surface; in this Chapter, surface-sensitive synchrotron XPS is used to obtain detailed surface characterisation.

A third section of work in this chapter examines the stability of the modifying layers on ZnO. The samples were exposed to heat, UV light, acidic conditions, or stored in the dark for ≥ 60 days to

determine if the aryl layers can withstand conditions typically of concern for potential device applications. Changes in the films were monitored using XPS measurements. The effect of NP modification layers on persistent photoconductivity (PPC) of MBE-ZnO was also examined and compared to the effect of ODPA layers (Section 3.3.8).

The MBE-ZnO electrodes used for the work in this chapter had two different formats. Either the area of the working electrode was defined by use of an O-ring as described in Section 2.3.1.1, or a 5 × 10 cm^2 sample was immersed into the grafting solution as described in Section 6.2.1. The O-ring method has the advantage of giving a known electrochemical surface area whereas the dipping method results in a modifying layer over the whole ZnO surface as required for PPC measurements and modifier stability investigations.

6.2 Methods

6.2.1 Electrochemical Grafting on MBE-ZnO

Grafting on MBE-ZnO was carried out using cyclic voltammetry with either the O-ring (Section 2.3.1.1) or dipping format in ACN-$[Bu_4N]BF_4$. A scan rate of 200 mV s^{-1} was used, and each potential range was scanned twice.

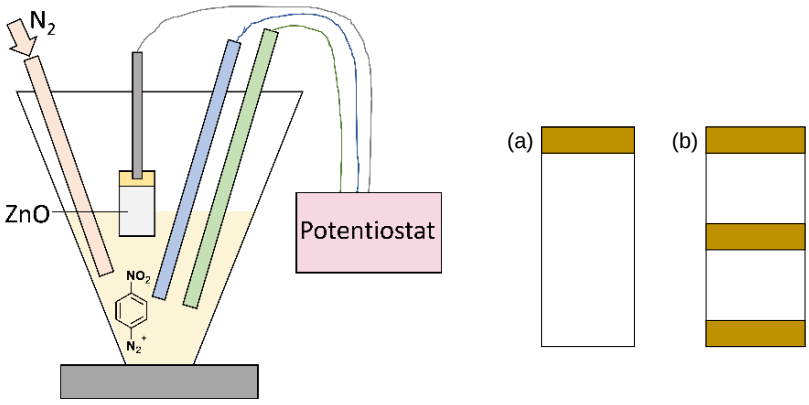

Figure 6.1. Electrochemical cell setup for the dipping method, including reference and counter electrodes (SCE and Pt, respectively). (a) and (b) show enlarged views of the ZnO samples used in the stability tests and PPC measurements, respectively. Each sample measures 5 × 10 mm^2.

Figure 6.1 shows the cell set-up for the dipping method for electrografting. The 5 × 10 mm^2 ZnO working electrode was contacted with a crocodile clip at an evaporated Ti/Au contact strip on the upper edge of the sample (Section 2.1.1). It was suspended above the solution during 15 min of nitrogen purging and was then lowered into solution. While care was taken to minimise contact between the clip and solution, wicking of the solution was unavoidable; a control sample determined that the contribution of this to the resulting CV was ~40% of total signal (see below).

Two types of samples were prepared for the dipping method: for use in stability tests, a single Ti/Au contact was applied to the ZnO (

Figure 6.1a); for PPC measurements, where a square sample area was needed for use with the Hall effect measurement setup, three Ti/Au strips were applied (

Figure 6.1b). The top strip gave a contact for electrochemistry, whereas the lower strips acted as contacts for PPC measurements.

6.2.2 Stability of Phenyl Films on MBE-ZnO

To probe the stability of phenyl films on ZnO, NP- and TFMP-modified MBE-grown ZnO samples were subjected to a range of conditions. The effect of each treatment was assessed by fixed-energy XPS analysis of samples before and after treatment. After each treatment (below), and prior to XPS analysis, samples were rinsed briefly in acetone, methanol, and IPA before being dried with nitrogen.

Heat treatment: Samples were heated at 160 °C for 40 min on a hotplate, in air.

UV treatment: Samples were exposed to 365 nm, 9.9 mW cm^{-2} light for 5 min (corresponding to 2970 mJ cm^{-2}).

Acid treatment: Samples were immersed in 5 mM aqueous NH_4Cl (pH 5.6) for 40 min. NH_4Cl is a mildly acidic solution capable of controllably etching ZnO.[3,4]

*Storage in the air in the dar*k: Samples were stored in closed containers for 80 d (NP-modified MBE-ZnO) or 60 d (TFMP-modified MBE-ZnO) at 22 ± 2°C.

6.3 Results and Discussion

6.3.1 Preparation and Characterisation of NP- and TFMP-Modified MBE-ZnO for Synchrotron XPS Measurements

For all electrografting of samples in Sections 6.3.1 and 6.3.2, the O-ring method was used.

6.3.1.1 Cyclic Voltammetry

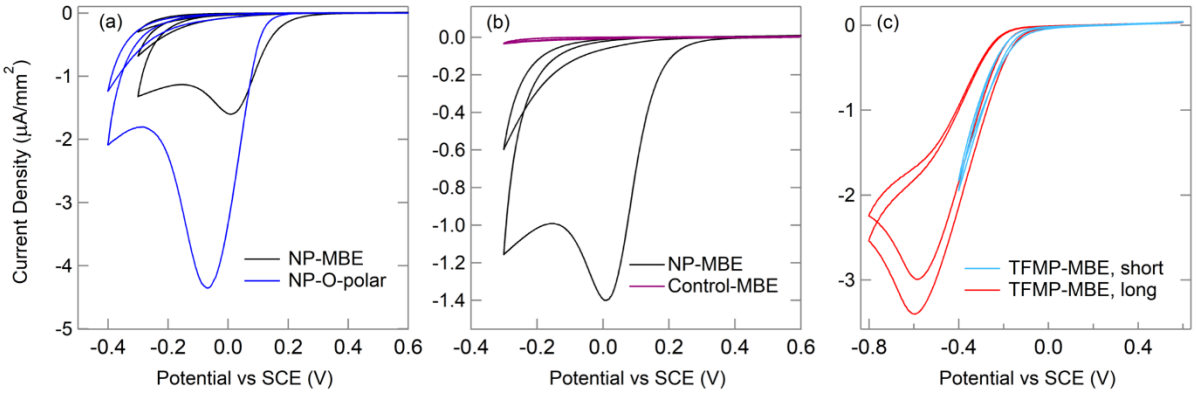

Figure 6.2. (a) Repeat CVs obtained at CrysTec single crystal O-polar ZnO and MBE-ZnO; (b) enlarged view of CVs obtained at MBE-ZnO in the presence (black) and the absence (purple) of NBD ('control'); (c) repeat CVs obtained at MBE-ZnO in TFMBD solution over a short and long potential range. Repeat scans are indicated by CVs of the same colour with the current density decreasing with scan number. The concentration of aryldiazonium salt for MBE-ZnO electrografting was 10 mM, and 2 mM for single crystal ZnO.

The features of the NP-grafting CV shown in Figure 6.2a for MBE-ZnO are similar to that for single crystal ZnO. However, two main differences are seen. Firstly, the reduction onset potential and the position of the reduction peak potential are more positive at MBE-ZnO than at single crystal O-polar ZnO. This observation can be attributed to the higher carrier concentration of Sb-doped MBE-ZnO (9.1 ± 0.5 × 10^{18} cm^{-3}) than CrysTec single crystals (~5.0 × 10^{13} cm^{-3}). It is also possible that the different peak potentials at the two substrates correspond to different reduction processes as proposed for carbon surfaces.[5] However, the difference in carrier concentration seems a more likely explanation.

The second clear difference between the CVs in Figure 6.2a is the peak current densities. The MBE-ZnO CV is expected to have a higher peak current density due to having a higher NBD concentration than that used for modifying single crystal ZnO (10 mM compared to 2 mM), but the opposite is observed. This observation was not investigated further but it is reasonable to propose that doped MBE-ZnO may be able to spontaneously reduce NBD while in contact with the electrografting solution during 15 min of solution degassing in the O-ring format cell. When electrografting is subsequently initiated, only a small current for reduction of NBD would be expected because the surface already bears a partially blocking film. Such behaviour has been clearly demonstrated on carbon electrodes.[5] While work described in Section 5.3.1 determined that spontaneous grafting does not occur on single crystal Zn-polar, O-polar, or m-plane ZnO, the ability of NBD to graft spontaneously to doped MBE-ZnO was not investigated. Figure 6.2b confirms that the reduction peak is due to NBD, as negligible current is seen for an identical CV carried out in electrolyte solution that did not contain NBD ('control').

TFMP grafting on MBE-ZnO was also investigated (Figure 6.2c). An identical potential range as for NP grafting was used initially, based on NBD and TFMBD having similar reduction peak potentials on carbon.[6] However, on MBE-ZnO the TFMBD reduction peak occurred at −0.6 V vs SCE, a significantly more negative potential than that seen for NBD (0 vs SCE). Nevertheless, preliminary XPS results showed that a modifying layer was present on MBE-ZnO samples which had not been exposed to the wider potential range, so the shorter range was used in further experiments. The peak current at −0.6 V is similar to that seen for NP-grafting at single crystal O-polar ZnO (Figure 6.2a), suggesting that spontaneous grafting did not occur. This is consistent with reduction of TFMBD occurring at more negative potentials than does NBD at ZnO.

6.3.1.2 AFM Analysis of Nitrophenyl and Trifluoromethylphenyl on Films MBE-ZnO

Tapping-mode AFM was used to determine the surface morphology and thickness of the organic modification layers grown on MBE-ZnO. Figure 6.3 shows topographical AFM images and averaged

line-profiles of as-received, control, NP-modified, and TFMP-modified ZnO after a 1 × 1 μm^2 area of each surface was deliberately removed by the AFM tip in contact mode.

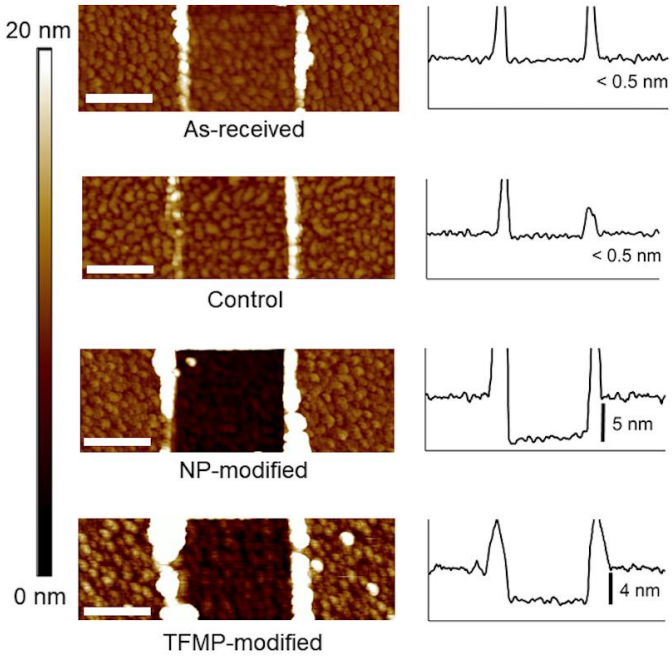

Figure 6.3. Typical AFM images and line profiles of as-received, control, and NP- and TFMP-modified MBE-ZnO samples after a 1 × 1 μm^2 area of the surface was removed using the AFM tip. All x scale bars are 800 nm. [NBD] = 10 mM, [TFMBD] = 10 mM; potential range +0.6 to –0.4 V vs SCE.

A modification layer is clearly present after electrografting, with globular features appearing to follow the morphology of the MBE-ZnO substrate. The average scratch depth was corrected against that on the as-received ZnO surface, giving thicknesses of 5 ± 1 nm and 4 ± 1 nm for NP and TFMP layers, respectively. Given the height of vertically-aligned NP and TFMP groups (0.6 nm and 0.5 nm,[7] respectively), this suggests that in both cases the modification has resulted in multilayers. This is typical for films grafted electrochemically from aryldiazonium ions with small para substitutents,[8,9] and is more than double the thickness of the NP film on single crystal O-polar ZnO grafted under similar conditions in the previous Chapter (~2 nm). The greater thickness of the film prepared on MBE-ZnO can be attributed to the higher carrier concentration of Sb-doped MBE-ZnO compared to single crystal ZnO, as well as the higher NBD concentration used to modify the MBE-ZnO (10 mM) compared to

single crystal ZnO (2 mM). The MBE-ZnO surface roughness increases after modification, giving values of 1.6 nm and 1.9 nm for the NP and TMFP film, respectively, compared with 1.4 nm and 1.3 nm for the reference and control surfaces, respectively. Again, this confirms that a layer has been deposited on the surface during electrografting, presumably following a similar mechanism to that proposed at other conducting substrates (Figure 1.18).[10]

6.3.2 Synchrotron XPS Characterisation of NP and TFMP Layers on MBE-ZnO

6.3.2.1 Elemental XPS Results

Synchrotron XPS measurements were carried out to characterise the nature of NP- and TFMP- films on MBE-ZnO and to compare their effects on surface band bending. Figure 6.4 shows the survey scans collected at *hv* = 835 eV or 680 eV. The peaks are quantified in Table 6.1 with respect to the Zn 3p intensity; this signal was used as it was obtained for all samples.

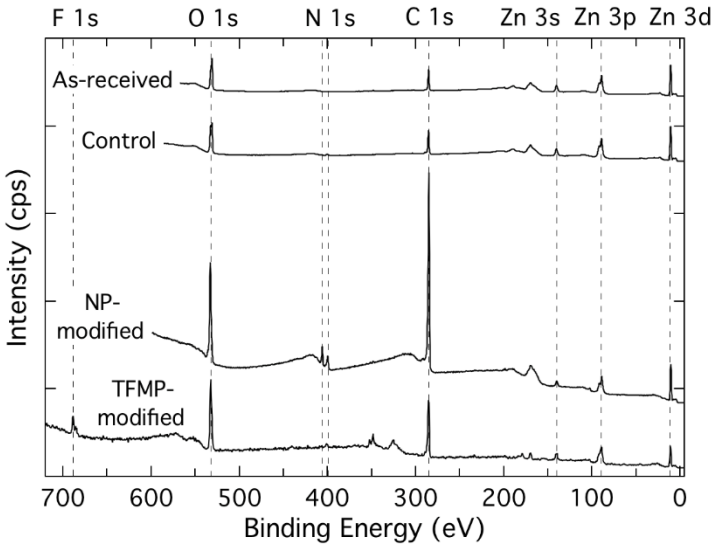

Figure 6.4. Synchrotron XPS survey spectra of as-received, control, and NP- and TFMP-modified MBE-ZnO (O-ring method). All spectra were measured at hv = 680 eV, except for the TFMP-modified spectrum which was measured at hv = 835 eV. All spectra are normalised to the same Zn 3p intensity.

There is a small C 1s signal on the as-received and control samples due to adventitious carbon, however the C 1s peak increases significantly upon modification with NP and TFMP groups. Similarly,

an increase in the O 1s signal is seen, and a F 1s signal is present for TFMP-modified ZnO. There is a substantial increase in N 1s signal for both modified samples, with the NP-modified sample giving the strongest signal. The same trend is seen with C, which is greatest on the NP-modified sample. The control sample spectrum is very similar to that of the as-received sample, indicating that the changes seen on the modified samples are due to the reaction of NBD or TFMBD with ZnO, rather than reaction of the electrolyte solution with the substrate.

Table 6.1. Ratios from synchrotron XPS survey spectra for as-received, control, and NP- and TFMP-modified MBE-ZnO.

Modification	**O : Zn**	**N : Zn**	**C : Zn**	**F : Zn**
As-received	0.50 : 1	0.01 : 1	0.35 : 1	-
Control	0.52 : 1	0.02 : 1	0.40 : 1	-
NP-modified	1.79 : 1	0.58 : 1	5.07 : 1	-
TFMP-modified	1.49 : 1	0.10 : 1	1.43 : 1	0.38 : 1

Figure 6.5 shows the core level XPS spectra for each element, which are discussed below.

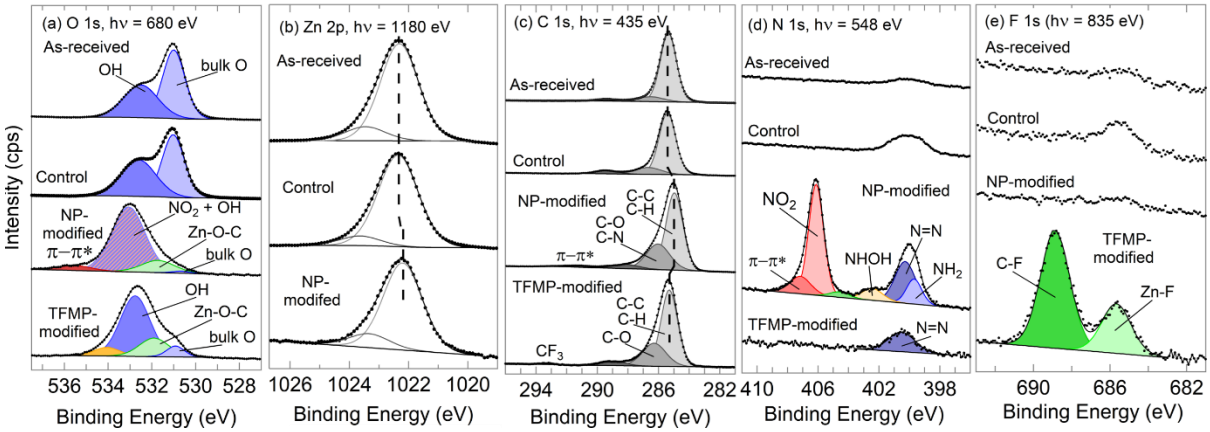

Figure 6.5. Synchrotron XPS core level spectra for as-received, control, and NP- and TFMP-modified MBE-ZnO. (a) O 1s (hv = 680 eV); (b) Zn 2p (hv = 1180 eV); (c) C 1s (hv = 435 eV); (d) N 1s (hv = 548 eV); (e) F 1s (hv = 835 eV). Spectra have been normalised to the same Zn 3p peak area.

O 1s and Zn 2p

Core level synchrotron XPS O 1s results are shown in Figure 6.5a and listed in Table 6.2. As seen in previous chapters, two main peaks are observed in the O 1s spectrum of as-received ZnO. The lower BE peak, located at 531.4 eV, is assigned to bulk O, while the higher BE peak at ~533 eV is associated with surface O.[11] The spectrum of the control sample is essentially the same as that for the as-received sample. Upon modification with NP and TFMP layers, the ratio of the intensity of the peak at ~533 eV increases significantly. In the case of NP films, the increase in this signal can be partially attributed to the oxygen-containing $N\underline{O_2}$ groups, however the TFMP-modified sample also shows a large ~533 eV peak relative to the bulk O peak. For both modified samples it is assumed that unreacted surface OH groups contribute to this signal (or are the sole contributor, for the TFMP-modified sample). Aryldiazonium ion grafting typically gives loosely-packed disordered multilayers,[12] with studies at carbon and gold electrodes indicating that $2.5 – 4 \times 10^{-10}$ mol cm^{-2} of aryl groups are directly bound to the surface. This is 20 – 30% of an ideal close-packed monolayer of aryl groups (~1.3×10^{-9} mol cm^{-2}). An O-polar ZnO surface has an OH surface concentration of ~1.8×10^{-9} mol cm^{-2}, therefore at least ~30% of OH groups cannot have reacted with aryl groups due to steric effects. These unreacted OH groups account for the surface O emission peak around 533 eV. The increase in the intensity of the surface O peak after grafting NP and TFMP layers is attributed to the presence of the surface film which decreases the depth of ZnO sampled during XPS measurements, thereby increasing the measured surface O:bulk O ratio. Other workers have also noted an increase in surface O signal after modification with species not containing oxygen. Polydorou et al. noted an increase in surface O 1s signal on F-passivated ZnO,[13] but did not offer an explanation. Li et al. used in situ formation and reduction of pentafluorobenzene diazonium to modify microporous carbon surfaces.[14] They saw an increase in surface O after modification and suggested that the diazotisation reagent, nitrite, may have directly reacted with the carbon surface. This explanation is not relevant in the present work as no nitrite is present during grafting.

Table 6.2. Synchrotron XPS O 1s core-level components of as-received, control, and NP- and TFMP-modified MBE-ZnO.

BE (eV)	Assignment	As-received [Control] (%)	NP-modified (%)	TFMP-modified (%)
530.7 – 531.0	Bulk O	57.9 [52.5]	3.5	9.4
532.5	Surface OH	42.1 [57.5]	-	-
531.8	Zn-O-C	-	10.3	-
533.0	NO_2 / OH	-	81.4	-
535.6	π–π* (NO_2)	-	4.7	-
532.6	Zn-O-C / OH	-	-	83.7
534.0	O_2	-	-	6.9

The proposed binding mode of aryl radicals on hydroxylated surfaces is through metal–O–C bonds to the pre-existing OH groups.[15] The peaks at 531.8 eV and 532.6 eV in the O 1s spectra of the NP- and TFMP- modified samples, respectively, are assigned to O in Zn-O-C bonds. This assignment is supported by data for other metal oxide surfaces: O in M-O-C bonds appears in the O 1s spectrum at 533, 532, ~533, 531.5, and 531.5 eV for M = Cu,[16] Zr,[17] Mn,[18] and In and Sn,[19] respectively. In contrast, Charlton et al. proposed that for NP-modified ITO, the In-O-C emission appears at the same BE as the NO_2 signal (~533 eV) while unreacted OH groups appear at 531.8 eV.[20] This interpretation requires that the peak for unreacted surface OH on modified samples shifts −0.7 eV compared to the as-received sample; such a BE shift for surface OH groups has not been reported by other workers under any conditions and thus is unlikely to be relevant here.

Supporting the assignment of Zn-O-C species, only a very small BE shift for the Zn 2p peak is observed after NP-modification (Figure 6.5b), suggesting that Zn-C binding is unlikely to be significant. Direct Zn-C bonds would be expected to change the chemical environment of the Zn atoms and thus the XPS Zn 2p spectrum.

In the spectrum of the NP-modified sample, there is a small high-BE O 1s peak which is attributed to the π-π* $C_6H_5NO_2$ shakeup (~535 eV) as seen in Chapter 5, Figure 5.14.[21] As expected, this peak is not visible on the as-received, control, or TFMP-modified samples. This further confirms the presence of NP groups on the surface.

The O 1s spectrum of the TFMP-modified sample shows an additional small peak with BE = 534 eV. It is likely due to molecular oxygen, which has been reported at BE = 534.7 eV.[22] Preliminary reports have observed that fluorinated metal-organic frameworks have a higher affinity for O_2 than non-fluorinated analogues; this could be a reason for why O_2 is retained in the TFMP-modified samples but not detected in the NP-modified MBE-ZnO.[23,24]

C 1s

Further evidence for aryl modification lies in the C 1s spectra (Figure 6.5c) which, in addition to adventitious carbon at ~286 eV, show a significantly strong peak at ~286.1 eV, associated with C-O and C-N bonds, on the modified samples.[25] Additionally, a satellite peak at high BE on NP-modified ZnO is due to π-π* transitions within aromatic carbon rings. This is absent for TFMP-modified ZnO, possibly due to the thinner film of this modifier. An emission peak at ~293 eV in the spectrum of TFMP-modified ZnO is attributed to the CF_3 group and thus confirms the presence of the intact modifier. Table 6.1 shows that the amount of C on the NP-modified surface is 5 times greater than that on TFMP-modified MBE-ZnO, despite the NP film being only 1.25 times thicker than the TFMP film. There are two possible reasons for this. Firstly, it was seen in Chapter 3 that surfaces with fluorinated modifiers have less adventitious carbon on the surface, presumably due to the hydro- and lipophobicity of F groups. The second possibility is that the density of NP groups within the modification layer is greater than the TFMP density, giving a disproportionately higher C 1s signal relative to the vertical thickness of the film.

N 1s

The N 1s spectrum of NP-modified ZnO (Figure 6.5d) has six components relating to different oxidation states of N on the surface; these are the same as those found for NP-modified single crystal ZnO (Chapter 5, Figure 5.12) and are quantified in Table 6.3.

Table 6.3. Synchrotron XPS N 1s core-level components of NP-modified MBE-ZnO before and after X-ray induced reduction at hv = 548 eV.

Binding Energy (eV)	Assignment	Ref.	Before (%)	After (%)
407.1 – 407.2	π–π* (NO_2)	[21]	9.9	1.4
406.1	NO_2	[21]	45.4	11.5
404.2 – 404.6	nitroso (NO)	[21]	2.9	3.6
402.2 – 402.4	NHOH, NH^+	[21]	6.8	7.1
400.1 – 400.3	N=N	[26]	24.3	23.4
399.5 – 399.7	NH_2	[27]	10.8	53.1

The largest peak, positioned at 406.1 eV, is attributed to the NO_2 group of NP, while the smaller shakeup peak at 407.2 eV is indicative of π-π* NO_2 transitions.[21,26] A peak at 400.3 eV is attributed to azo linkages (N=N) which are widely accepted to be present in modifying layers formed via aryldiazonium salts.[6] This assignment is supported by the TFMP-modified sample having a N 1s signal at the same BE (Figure 6.5d). A small amount of N contamination is present on the as-received and control samples (Table 6.1) and is assigned to trace amounts of ACN.[28] As seen in Table 6.3, approximately 24% of the total N on the NP-modified sample is azo-related. Assuming that the remaining N 1s signal is due to NO_2 or reduced NO_2, this suggests that there is one azo linkage for every 6 NP groups. This is the same as found on NP-modified single crystal ZnO (Chapter 5), and is similar to Yu et al., who reported one azo linkage for every 4 NP groups on carbon.[29] The presence of azo groups in the films is due to the operation of at least 2 grafting pathways as discussed in Chapter 5 and shown in Figure 1.18. The signals at 399.7, 402.4, and 404.5 eV in the N 1s spectrum of NP-

modified ZnO can be assigned to reduced species: NH_2, NHOH, and NO, respectively.[21,28,30–32] Reduction of NP groups during XPS measurements is discussed in section 6.3.2.2.

F 1s

Figure 6.5e shows the F 1s spectrum for each sample. As expected, on TFMP-modified ZnO there is a large peak at 688.9 eV arising from the CF_3 group.[33,34] This confirms the presence of TFMP groups on the surface. For all samples there is also a peak at a BE consistent with Zn-F species. On the as-received, control, and NP-modified samples, this signal is very small and is attributed to a small degree of hydrolysis of residual BF_4^- (or cross-sample contamination of the as-received sample).[13] For the TFMP-modified sample, the inorganic F signal is significantly larger than on the other samples and is attributed to F from CF_3 groups liberated by photoelectrons during XPS analysis and interacting with the ZnO surface. This is discussed in the following section.

6.3.2.2 Decomposition of Nitrophenyl and Trifluoromethyl Groups

X-rays have been shown to reduce the nitro groups of NP films,[54,67,35] and decompose fluorinated species.[34,36] Roodenko et al. determined that on Si(111), reduction is caused by secondary photoelectrons interacting with the NP film.[21] In this work, care was taken to use a low XPS photon flux to minimise unintended reduction of NP films or decomposition of TFMP films. After core level and VB spectra were obtained, the photon slit was widened on a 'fresh' area of the modified samples to purposely provide a high photon flux ($h\nu$ = 548 eV for NP films and 835 eV for TFMP films). Repeat scans of either the N 1s (NP) or F 1s (TFMP) region allowed the resulting degradation to be followed over 540 s. Figure 6.6a shows NP-modified ZnO before and after this treatment as well as during treatment, and Figure 6.6b shows the spectra from all scans. During the repeat scans, the NO_2 signal decreases significantly while the 'reduced N 1s region' signal increases, with < 5% loss of total N (Figure 6.6c) suggesting that few aryl groups have desorbed from the surface. In contrast, Roodenko et al.[21] observed that 25% of NO_2 groups desorbed from NP-modified Si(111) when exposed to X-ray irradiation ($h\nu$ = 650 eV), while Mendes et al.[27] reported an 18% loss of N 1s signal from 3-(4-

nitrophenoxy)propyltrimethoxysilane on Si/SiO_2 during irradiation ($h\nu$ = 1253.6 eV). Aromatic NO_2-functionalised imine monolayers on Si(100) prepared by La et al.[37] exhibited selective cleavage of > 80% of NO_2 groups when exposed to ($h\nu$ = 550 eV) X-rays. The variability of these studies and differences with the present study are attributed to variations in X-ray flux, energy, and irradiation time, as well as the chemical nature of the substrate and the modifier. A similar conclusion was drawn by La et al.[37]

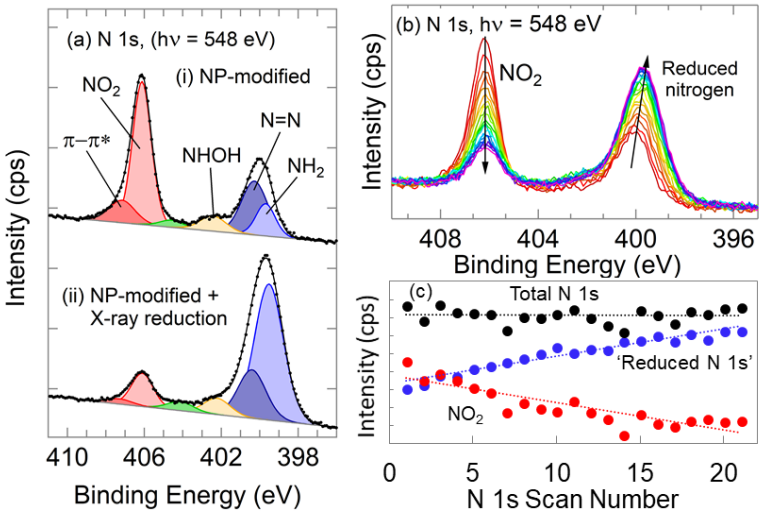

Figure 6.6. (a) N 1s spectra for NP-modified MBE-ZnO before and after X-ray-induced NO_2 reduction. Spectrum (i) was taken using a photon slit size of 5.7 × 10 µm², while spectrum (ii) was taken after irradiation for 540 s using a slit of 5.7 × 20 µm² and scaled by 0.5 to account for the difference in photon flux; (b) N 1s spectra for NP-modified MBE-ZnO during 21 scans over 540 s with 5.7 × 20 µm² photon slit size (initial scan is red, final scan is purple); (c) NO_2 component (red), reduced N 1s component (blue) and total N 1s signal (black) showing intensities during the scans shown in (b).

As discussed in Chapter 5, in protic conditions the reduction of NP films is well-known to give aminophenyl and hydroxyaminophenyl groups (Equations 5.1 and 5.2). As noted by others, the BEs of the reduced N species produced during XPS measurement of NP films strongly suggest formation of aminophenyl groups, however the mechanism for this is unclear. In Figure 6.6b, the BE peak near 400 eV appears to broaden and shift to a lower BE; this supports the interpretation that the amino component is increasing. The possibility of N being cleaved from the aryl groups and directly

interacting with ZnO was ruled out as such interaction gives a significantly lower N 1s BE than that found here (~396 eV).[38]

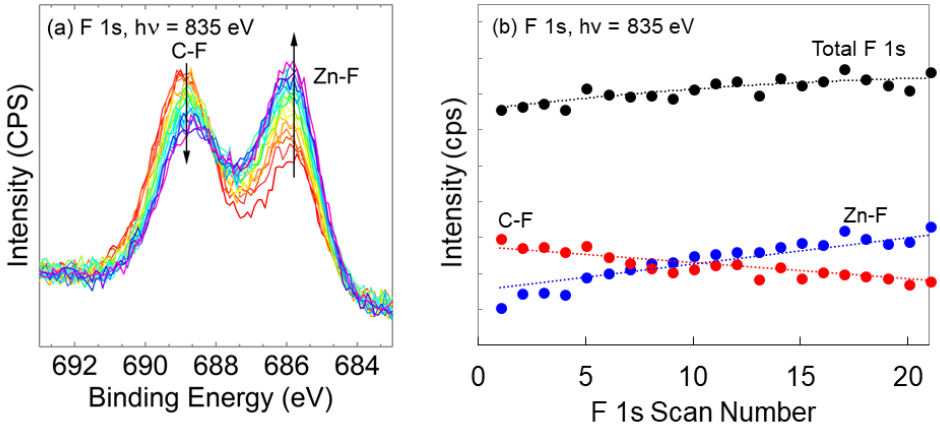

Figure 6.7. (a) F 1s spectra for TFMP-modified MBE-ZnO during continuous single scans at hν = 835 eV with a photon slit size of 5.7 × 20 μm² (the initial scan is red; final scan is purple); (b) C-F (red), Zn-F (blue), and their sum (black) showing the intensity of each component during the scans of (a).

Figure 6.7a shows the F 1s region for TFMP-modified MBE-ZnO during 540 s of continuous scans (*hν* = 835 eV). As the number of scans increases, the organic F peak (~689 eV) decreases in intensity and broadens in BE. This is attributed to CF_3 groups being decomposed to CF_2 and CF groups. Concomitant with this, the peak at lower BE (686 eV), which is consistent with F interacting with Zn, increases and broadens. No loss of F was observed (

Figure 6.7b); it appears that F liberated via CF_3 decomposition interacts with the ZnO substrate, as also noted for PAs (Chapter 3). Surprisingly, despite the high vacuum environment, it appears that the expected loose packing of aryl groups in the grafted film allows F to reach the substrate surface.

6.3.2.3 Effect of Phenyl Films on Surface Band Bending

VB spectra were collected at *hν* = 150 eV for as-received, control, TFMP-modified, and NP-modified MBE-ZnO samples, and NP-modified samples subjected to 540 s of high X-ray photon flux ('reduced NP-modified'). Spectra are shown in Figure 6.8a alongside values for ζ ($E_F - E_V$) and V_{bb}, which are listed in Table 6.4 and illustrated in Figure 6.8e. A schematic of the band bending is shown in Figure 6.9. Due

to the differences in substrates, results cannot be compared with those for NP-modified single crystals (Chapter 5).

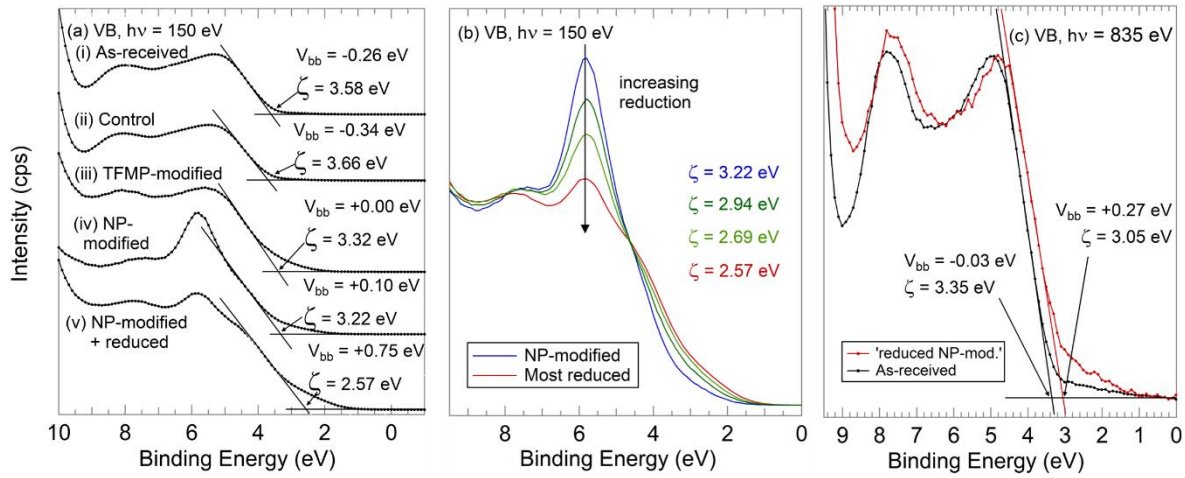

Figure 6.8. (a) Normalised synchrotron XPS VB spectra (hv = 150 eV) with ζ and V_{bb} values for as-received, control, TFMP-modified, NP-modified, and 'reduced NP-modified' MBE-ZnO samples; (b) VB spectra (hv = 150 eV) during irradiation-induced reduction of NP-modified ZnO; (c) VB spectra of as-received (black) and 'reduced NP-modified' (red) ZnO at less-surface-sensitive photon energy (hv = 835 eV).

As-received MBE-ZnO shows V_{bb} = −0.26 eV, indicating downwards band bending and an electron accumulation layer consistent with previous work on intrinsic ZnO.[41,26] The control sample has a slightly lower value of V_{bb} = −0.34 eV corresponding to increased downwards band bending. This effect may arise from the F interactions with Zn, seen on the F 1s spectrum for the control sample (Figure 6.5e) and attributed to physisorption of hydrolysed BF_4^-. In Chapter 3, it was seen that F interactions with Zn can give increased negative band bending on ZnO, thought to arise from F acting as shallow donors when incorporated into ZnO oxygen vacancies (V_o).[42,43] (This was shown by Polydorou et al. when a F plasma treatment, designed to passivate V_o on ZnO, produced a downwards shift in surface bands.[17])

TFMP-modification of ZnO results in an upwards shift of the band bending, with ΔV_{bb} = +0.26 eV (Table 6.4) giving flat surface bands of V_{bb} = 0.00 eV. The upwards shift is attributed to the strong electron withdrawing nature of the CF_3 substituent on the phenyl ring. However, the F 1s spectrum (Figure 6.5e) showed that TFMP-modified ZnO has a significant inorganic F peak (30%), assigned to F-Zn interactions, alongside the expected organic CF_3 peak (70%). If inorganic F acts as substitutional shallow donors, there may be competition between the electron-donating nature of this F and the electron-withdrawing effect of the CF_3 group within the TFMP modification layer. From flat band VB evidence, it appears that the TFMP groups have the dominant effect.

Table 6.4. Synchrotron XPS VB data for TFMP- and NP-modified ZnO.

MBE-ZnO Surface	**ζ (eV)**	**V_{bb} (eV)**	**ΔV_{bb} (eV)**
As-received	3.58	−0.26	-
Control	3.66	−0.34	−0.08
TFMP-modified	3.32	+0.00	+0.26
NP-modified	3.22	+0.10	+0.36
'Reduced NP-modified'	2.57	+0.75	+1.01

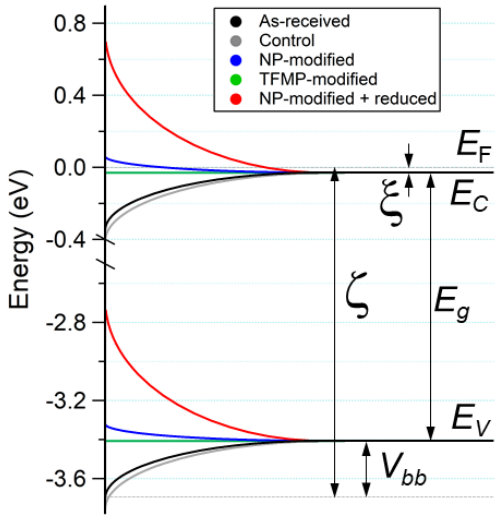

Figure 6.9. Schematic energy level diagram for as-received, control, TFMP-modified, NP-modified, and 'reduced NP-modified' MBE-ZnO derived from the ζ and V_{bb} values in Figure 6.8, where the zero of the energy scale is the Fermi level, E_F.

Modification of MBE-ZnO with NP groups also produces significant changes in the VB spectrum, in particular the appearance of a high-intensity peak around 5.7 eV. This is assigned to lone-pair-like orbitals in the NO_2 group, as determined by Hunger et al. for NP-modified *p*-Si(111) ($h\nu$ = 40.82 eV).[9] Here, the attenuation of the peak during intentional reduction by X-ray exposure supports this assignment (Figure 6.8b). After NP modification, V_{bb} shifts in the positive direction by +0.36 eV compared to as-received ZnO, replacing the downwards V_{bb} with upwards V_{bb} = +0.10 eV. The effect is expected due to the electron-withdrawing nature of NP groups, and is very similar to the ΔV_{bb} of +0.38 eV reported by Hunger et al. for NP-modified Si(111) surfaces compared to as-received Si(111).[21] Work in Chapter 5 determined that ΔV_{bb} for NP-modified single crystal O-polar ZnO, determined by fixed-energy XPS, is +0.23 eV, which is 0.13 eV less than that observed for NP-modified MBE-ZnO with synchrotron XPS. This is consistent with the higher photon energy used for the former, which probes further into the bulk relative to the surface where band bending is less pronounced. As opposed to the upwards band bending of NP-modified MBE-ZnO, the direction of band bending at NP-modified

O-polar ZnO was still downwards; this difference is mainly attributed to the lack of calibration to an external reference.

Upon X-ray-induced reduction of NP-modified ZnO, the positive band bending increases significantly to give V_{bb} = +0.75 and a total ΔV_{bb} = +1.01 eV, the largest reported upward band bending produced by chemical modification of ZnO. This was an unexpected result, as amine groups are electron-donating and were expected to reverse the effect of the electron-withdrawing NO_2 groups. The intensity of the azo peak appeared to remain constant during X-ray irradiation so was ruled out as a contributor to the changes in band bending.

The possibility that the apparent shift in VB edge of NP-modified ZnO is not due to changes in the ZnO itself, but rather due to contributions to the VB spectrum from NO_2 and π-bonding orbitals of the phenyl layer, was considered.[21] In order to rule out this possibility, the two spectra were remeasured with a less-surface-sensitive photon energy (*hv* = 835 eV, Figure 6.8c) where the photoelectrons have an inelastic mean free path λ = ~17.2 Å compared to ~6.2 Å for X-rays with *hv* = 150 eV. The shapes of the two VB spectra obtained at *hv* = 835 eV are the same, but a shift to lower BE of the VB edge is still seen for the modified sample, meaning the upwards band bending caused by reduced NP-modifiers is real and extends partially into the bulk of ZnO (V_{bb} = +0.30 eV).

Upward band bending on Schottky contacts and organic-semiconductor junctions is associated with an insulating, electron-depleted region as opposed to a SEAL, or 2DEG, which is typical for ZnO surfaces.[39] The upwards band bending on NP-modified ZnO is consistent with the electron-withdrawing substituents, and is promising for applications requiring an insulating layer. The result for reduced NP-modified ZnO, however, is unexpected and highlights subtleties in the photoelectron-induced reduction process. As noted earlier, NO_2 groups can be reduced during XPS measurements by secondary electrons travelling through the organic layers.[21] It is possible that near-surface secondary electrons from ZnO can participate in this process. The transfer of electrons away from the surface would explain the large upwards band bending observed on 'reduced NP-modified' ZnO.

Reduction of NP groups to aminophenyl groups in wet chemical or electrochemical conditions requires not only 6 electrons but also 6 protons (Eq 5.1, 5.2). In UHV conditions, it is unlikely that these protons are provided from external sources. Roodenko et al. proposed that H is supplied from the phenyl rings during electron-induced polymerisation of NP layers, giving polyaniline-like layers as shown in Figure 6.10.[21]

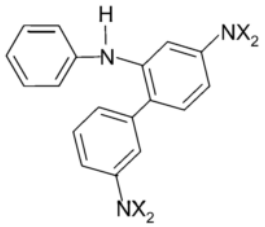

Figure 6.10. Proposed polymerisation product of reduced NP films. X = O or H. From Roodenko et al.[21]

Others have suggested that residual water or solvents trapped within the NP layers can provide H, although Roodenko et al. did not observe any evidence of this.[21,35] ZnO itself also contains significant amounts of H in different forms: interstitial H (H_i), substitutional H in O vacancies (H_O), and so-called 'hidden' H_2 molecules (invisible to infrared spectroscopy) have all been characterised.[40–42] van de Walle[43] showed that H_i and H_O are shallow donors in ZnO, and Traeger et al.[44] found that there is significantly higher H concentration in near-surface regions of ZnO compared to the bulk. Importantly, they found that some of this H was less-strongly bound and was more mobile within ZnO, making it another potential source of protons required for the nitro-to-amino conversion. Since H occurs exclusively as a donor in ZnO,[1,43] transfer of sub-surface H to the NP layer would decrease electron density at ZnO and thus decrease downwards V_{bb}. H is also present in *p*-type Si, suggesting that this same process might have been operative for the reduction of NP films on Si as reported by Roodenko et al. The effect of NP reduction during XPS measurements on band bending was not investigated by those researchers.[46]

The large changes in band bending seen here are fundamentally interesting and deserve to be studied in future work to determine if they are stable when removed from the UHV XPS chamber. Reduction

of NP layers on ZnO to aminophenyl layers is a desirable outcome for sensor applications, as the amino groups can be used to attach recognition agents via amide bonds for use in field effect transistor-based sensors. However, such applications rely on the stability of the modification layers. This was investigated in experiments described in the following sections.

6.3.3 Preparation and Characterisation of NP-Modified MBE-ZnO for PPC and Stability Investigations

For all electrografting of samples in Sections 6.3.3, 6.3.5, and 6.3.4, the dipping method was used as described in Section 6.2.1 and

Figure 6.1.

6.3.3.1 Nitrophenyl Modification of MBE-ZnO

Figure 6.11 shows CVs obtained at four separate MBE-ZnO samples (single Ti/Au strip) in 2 mM NBD solution, using the dipping method. Due to the uncertainty of the electrode area exposed to solution, the current, not current density, is shown, with a maximum peak current of ~250 µA. The approximate surface area of the dipped samples is ~50 mm^2, meaning that the estimated average maximum current density is similar to that seen on single-crystal O-polar ZnO with the same NBD concentration (~4.5 $\mu A/mm^2$). The shape of the response is similar to those seen previously, with an NBD reduction peak close to −0.15 V; at more positive potentials, an oxidation process can be observed. No oxidation current was recorded at the same potential using either single crystal ZnO or MBE-ZnO with the O-ring method, a consequence of using an *n*-type semiconductor as the working electrode. Hence it is assumed that the oxidation response seen in Figure 6.11 was due to the presence of the Au strip, which might be wetted by wicking of the solution, allowing reduction and oxidation reactions to occur at the gold surface. A control sample consisting of non-conducting sapphire with an Au strip in the same position as for ZnO samples was immersed in the solution in the same position as for the ZnO electrodes. The CV, shown in Figure 6.11, has a similar oxidation current to that recorded at the ZnO electrode and has a maximum current of ~100 µA. Hence for the dipping method, ~40% of the

reduction peak current and all of the oxidation current can be attributed to electrochemistry at the Au strip.

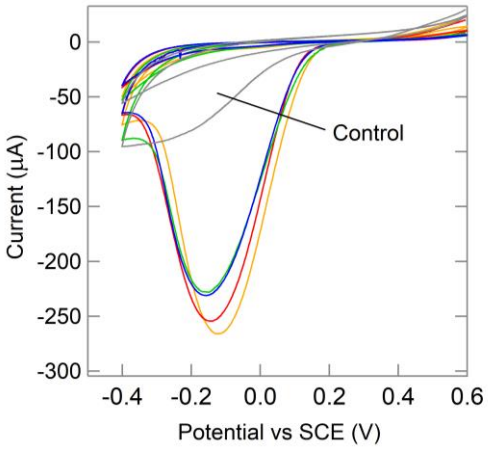

Figure 6.11. Repeat CVs obtained in NBD solution of four MBE-ZnO samples using the dipping method and at a sapphire control sample (grey). All samples had a Ti/Au contact strip. [NBD] = 2 mM.

6.3.3.2 Trifluoromethylphenyl Modification of MBE-ZnO

CVs obtained during TFMP modification of four separate MBE-ZnO samples are shown in Figure 6.12. The main reduction peak for TFMBD lies at a more negative potential than that shown here, as discussed in Section 6.3.1.1. However, there is a small reduction peak visible on Sample 4 (blue) close to −0.05 V which is similar to that seen by Menanteau et al. – although they also saw a larger reduction peak at a position 200 mV more negative.[6] Samples 1, 2, and 4 have similar maximum currents, while Sample 3 is significantly lower.

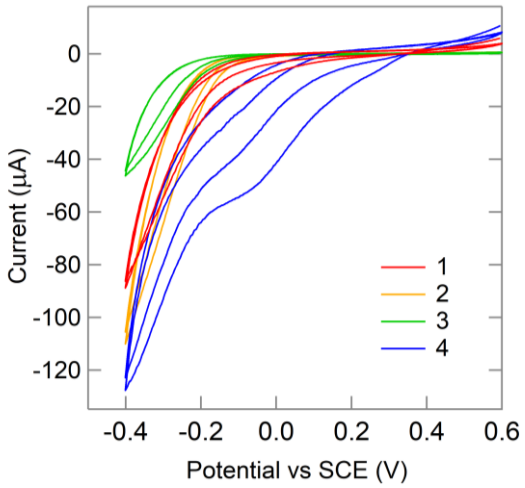

Figure 6.12. Repeat CVs for TFMP modification of four MBE-ZnO samples via dipping method. Scan rate is 200 mV s^{-1}; [TFMBD] = 2 mM.

As noted with NBD reduction via the dipping method (Figure 6.11), oxidation current can be seen at higher potentials in Figure 6.12. This is not seen on CVs of TFMBD obtained using an O-ring (Figure 6.2) and is attributed to the gold being wetted, confirming that wicking occurred.

6.3.3.3 AFM Analysis of Nitrophenyl Films on MBE-ZnO

Figure 6.13a shows the topography of MBE-ZnO modified with a NP film using the dipping method. The surface roughness R_a is 1.7 nm, similar to that for the film prepared using the O-ring method (1.6 nm). The film thickness was measured by AFM depth-profiling, giving a blank-corrected value of 2 ± 1 nm (Figure 6.13b and c). This is less than half the thickness of the NP films grafted using the O-ring method (~5 nm) and suggests that the film consists of ~3 layers of NP groups. The difference in film thickness is attributed to different NBD concentrations used in each method (2 mM for the dipping method and 10 mM for the O-ring method).

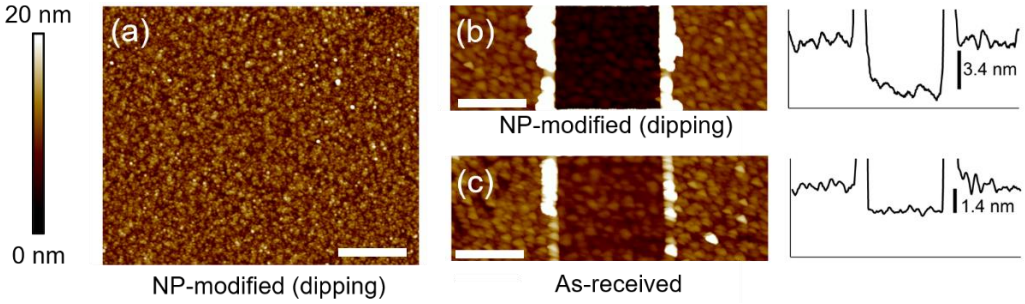

Figure 6.13. (a) AFM image of dipping method NP-modified MBE-ZnO; (b) depth profile AFM image and line profile for dipping method NP-modified MBE-ZnO, (c) depth profile AFM image and line profile for as-received MBE-ZnO. Scale bar is 800 nm.

6.3.4 Stability of Nitrophenyl- and Trifluoromethylphenyl-Modified MBE-ZnO

As described in Section 6.3.2.2, synchrotron XPS irradiation was shown to change the chemical nature of NP- and TFMP- films. The ability of these films to withstand heat, UV light, acid, and storage conditions was investigated in the current Section: four NP films and four TFMP films were grafted under identical conditions using the dipping method to ensure a complete coverage of the organic layers on the MBE-ZnO substrate. Each sample was analysed with AFM and XPS before and after treatment with heat, UV light, acid, or prolonged storage.

6.3.4.1 Surface Morphology Changes of Nitrophenyl and Trifluoromethylphenyl Films with Heat, UV Light, Acid, and Storage Treatments

Tapping-mode AFM images in Figure 6.14 show the topographical differences seen on as-received and modified ZnO after treatment with heat, UV light, acid, or storage. The as-received surfaces (Figure 6.14a – d) are very similar to the modified samples, where globular formations appear to reflect the morphology of the bare surfaces. The effects of each treatment on the film morphology is discussed alongside XPS data below.

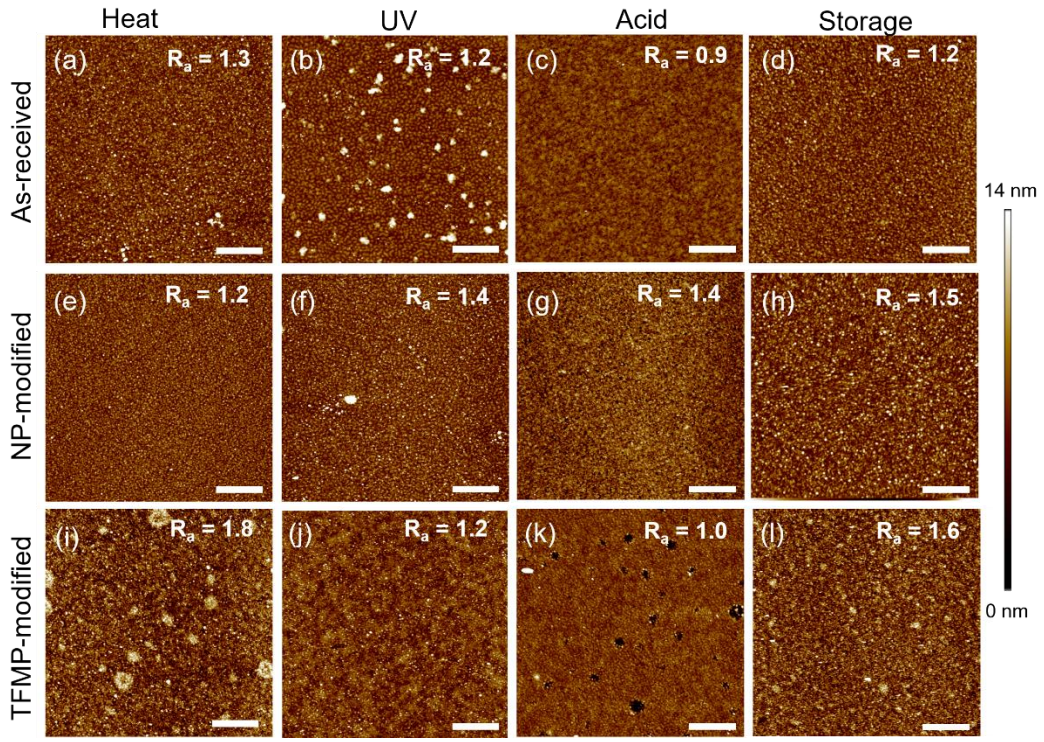

Figure 6.14. Tapping-mode AFM images of (a – d) as-received, (e – h) NP-modified, and (i – l) TFMP-modified MBE-ZnO subjected to chemical or physical treatments: heated to 160 °C, irradiated with 365 nm UV light, immersed in 5 mM $NH_4Cl_{(aq)}$, or stored in the dark for ≥ 60 days. All samples were rinsed with solvent after treatment. The horizontal scale bar is 1 µm.

6.3.4.2 XPS Characterisation of Nitrophenyl Films with Heat, UV, Acid, or Storage Treatments

Fixed-energy XPS survey spectra were analysed to determine the elemental composition of modified ZnO; peak quantifications are listed in Table 6.5. As expected, fresh NP-modified MBE-ZnO samples show attenuation of signals from the ZnO substrate (Zn, O) and an increase in N and C signals. The percentages of C, N, O, and Zn show that the 4 freshly-modified samples are very similar and have excellent reproducibility. The average modification layer thickness with the dipping method is 1.3 nm, which is thinner than the ~5 nm for O-ring NP-modified MBE-ZnO (Section 6.3.1.2) due to the lower NBD concentration used for grafting.

Table 6.5. Elemental percentages and film thicknesses from XPS survey spectra, and core level N 1s ratios for NP-modified MBE-ZnO grafted via dipping method, before and after various treatments.

NP-modified ZnO	% C	% N	% O	% Zn	NP Thickness (nm)
1 Before heat	44	4	35	17	1.4 ± 0.3
After heat	51	5	33	11	2.0 ± 0.4
2 Before UV	43	4	35	18	1.2 ± 0.2
After UV	31	2	41	26	0.7 ± 0.1
3 Before acid	42	4	36	17	1.0 ± 0.2
After acid	43	4	36	16	1.3 ± 0.3
4 Before storage	46	5	34	14	1.6 ± 0.3
After storage	50	4	33	12	2.3 ± 0.5
As-received	18	0	46	36	-

Core level XPS spectra for N 1s, C 1s, and O 1s are shown in Figure 6.15, Figure 6.16, and Figure 6.17, respectively. Analysis of the spectra of freshly-prepared NP films is discussed below; the effects of each stability treatment on the elemental percentages are discussed alongside the core level XPS results in the following sections.

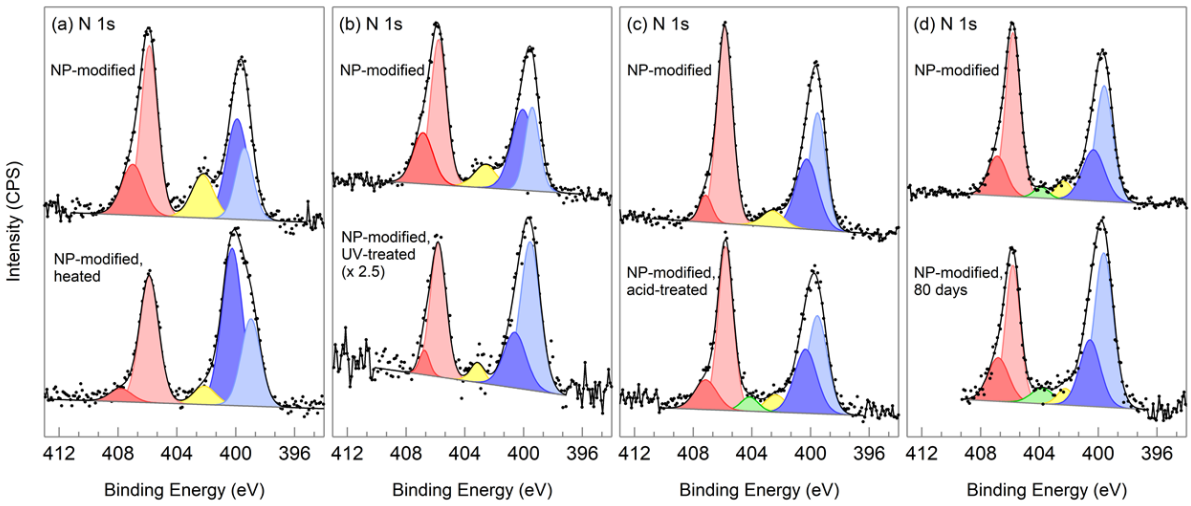

Figure 6.15. Fixed-energy N 1s spectra for dipping-method NP-modified MBE-ZnO, treated with (a) heat, (b) UV light, (c) acidic solution, and (d) storage for 80 days in the dark. Spectra have been offset for clarity and enlarged where noted.

Peaks in the N 1s spectra (Figure 6.15) were assigned as discussed in Section 6.3.2.1, and tabulated in Table 6.6 for ease of comparison. On average, the N=N signal accounts for 23% of the N 1s signal for freshly-prepared NP-modified MBE-ZnO, representative of one azo linkage for every ~6 grafted NP groups. This is the same as seen for other N in this work (Chapter 5 and Section 6.3.2.1) and by Menanteau et al. on carbon surfaces.[6] Although the survey spectra (Table 6.5) show that all freshly-prepared samples have 4 – 5% surface N, the relative amounts of N=N and NH_2 varies between samples (Table 6.6). The N 1s intensities are weaker than those seen on single-crystal ZnO, which decreases the signal:noise ratio. As such, the reliability of fitting the very close azo and amine peaks is poor. However, 'total reduced N' (that is, all N signal except NO_2 and its satellite) can be reliably quantified and accounts for 51 – 53% of N on freshly-prepared NP-modified samples.

Table 6.6. Fixed-energy XPS N 1s peak assignments and percentages for NP-modified MBE-ZnO, before and after treatment with heat, UV light, acid, and storage.

Sample	NO_2 π - π* (%)	NO_2 (%)	NO, NHOH (%)	N=N (%)	NH_2 (%)
1 Before heat	15	34	11	27	13
After heat	4	30	4	46	16
2 Before UV light	15	34	8	26	18
After UV light	4	31	4	23	38
3 Before acid	5	43	5	22	26
After acid	9	35	8	20	27
4 Before storage	4	36	6	17	30
After storage	12	25	7	17	38

O 1s spectra for NP-modified MBE-ZnO are shown in Figure 6.16. When freshly prepared, all four NP-modified MBE-ZnO samples have similar features. As seen previously, the bulk oxygen peak is assigned at 530.2 – 530.4 eV, while the NO_2 peak, shown in pink around 532.3 eV, and the OH + Zn-O-C peak (531.3 – 531.7 eV) were assigned as discussed earlier and in Chapter 5. The spectra of the freshly-prepared NP-modified samples bear resemblance to the O 1s spectra of 'thin' NP films on single crystal samples analysed with fixed-energy XPS (Figure 5.12) and are unlike the 'thick' NP films in the same

Figure, which showed a very intense high-BE peak for NO_2 and its corresponding satellite peak. This difference is consistent with the thinness of the NP films shown in Table 6.5, and the relatively small NO_2 signal compared to that for reduced N (Table 6.6). Synchrotron-analysed NP-modified samples showed a large decrease in the low-energy bulk O signal, which is not seen here due the decreased surface sensitivity of fixed-energy XPS (*hv* = 1486 eV) compared to tuneable soft X-rays (*hv* = 680 eV for O 1s).

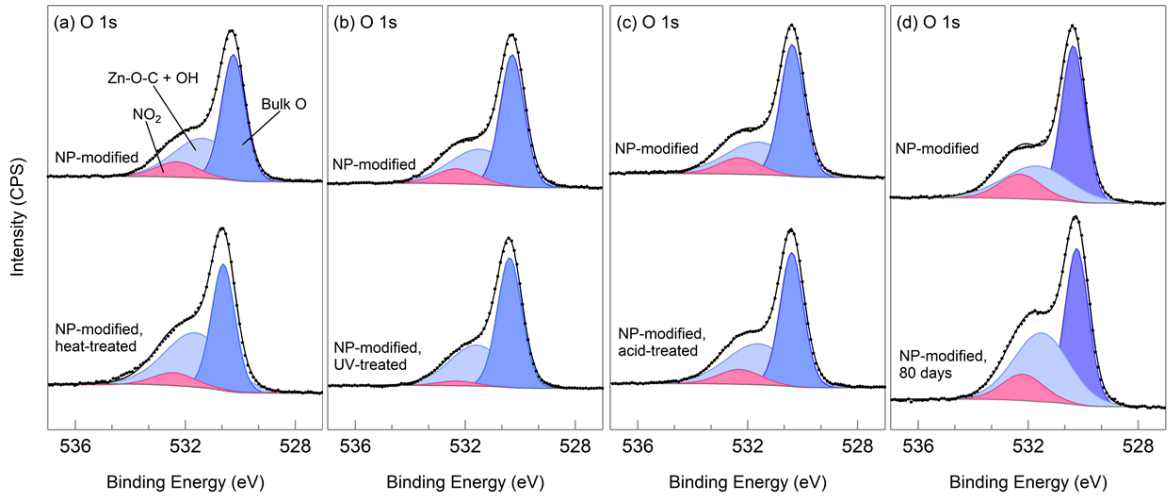

Figure 6.16. Fixed-energy XPS O 1s spectra for NP-modified MBE-ZnO, treated with (a) heat, (b) UV light, (c) acidic solution, and (d) storage for 80 d in the dark. Spectra have been normalised to bulk oxygen (530.2 – 530.4 eV).

Figure 6.17 shows the C 1s spectra for NP-modified MBE-ZnO before and after each treatment. Three C 1s peaks typical of adventitious carbon are present on each of the freshly-prepared samples, masking the signal expected from the aromatic carbon rings on the surface (284 eV), and C-N bonds (286 eV). There is a small π–π* satellite peak visible on 3 of the NP-modified samples (~292 eV), indicating that phenyl groups are present on the surface.

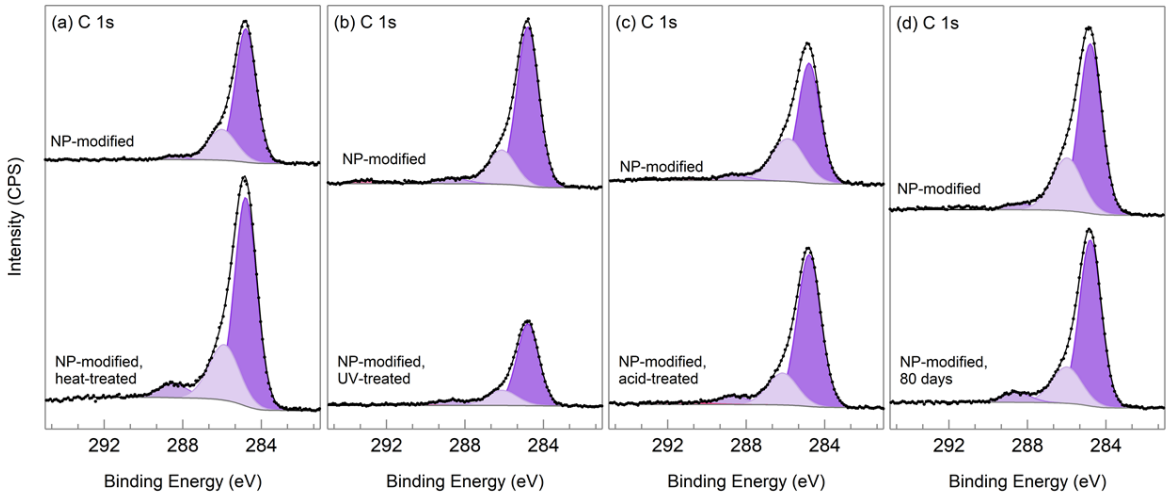

Figure 6.17. Fixed-energy XPS C 1s spectra for NP-modified MBE-ZnO, treated with (a) heat, (b) UV light, (c) acidic solution, and (d) storage for 80 d in the dark. Spectra have been normalised to Zn 2p and offset for clarity.

6.3.4.2.1 Heat Treatment of Nitrophenyl Films on MBE-ZnO

Figure 6.15a shows the N 1s spectra for NP-modified MBE-ZnO before and after heat treatment. No loss of C, N, or O is observed upon heating (Table 6.5), but the $\underline{N}O_2$ signal decreases from 49% to 34%. Correspondingly, there is a distinct change in the shape of the reduced N signal consistent with an increase in the azo component (Table 6.1). The reason for this is not known – it could be the product of coupling of nitrosophenyl and aminophenyl groups – but due to the uncertainty in fitting the 'reduced' components in the N 1s spectrum, it was not investigated further. However, it appears that heating of the NP film may have induced NO_2 reduction. This is consistent with the O 1s spectra in Figure 6.16a, which show a small decrease in the $N\underline{O}_2$ signal, but no significant change to the bulk or surface O after heating at 160 °C. No significant change was seen in the C 1s spectra for NP-modified MBE-ZnO after heating (Figure 6.17a): the freshly-modified sample does not have a significant π-π* satellite peak (~292 eV) so it cannot be compared to the heat-treated sample. However, the surface showed an increase in C-N signal (286 eV), which may stem from adventitious carbon or heat-induced polymerisation of the NP groups via N-H linkages.[21] It appears that heat treatment was able to induce

some reduction of NP groups without affecting the overall elemental composition, or surface morphology or roughness as determined by AFM (Figure 6.14a and e).

Gross and Downard reported that heating NP-modified pyrolysed photoresist films (PPF) in an inert atmosphere at ~545 °C for 25 min removed almost all N signal.[47] Similarly, NO_2 groups were removed from NP-modified carbon black during heating in air to 300 °C, with the nitro signal disappearing completely after heating to 500 °C, leaving only a small azo nitrogen peak around 400 eV.[48] It is thus not surprising that heat-treated NP films on MBE-ZnO show only minor evidence of degradation at 160 °C.

6.3.4.2.2 UV Light Treatment of Nitrophenyl Films on MBE-ZnO

The total amounts of N and C on the surface halved after UV light treatment of NP-modified MBE-ZnO (Table 6.5), giving a calculated decrease in thickness from 1.2 nm to 0.7 nm. This is consistent with a loss of aryl groups from the modification layer. As seen in Table 6.6, as a percentage of total N, $\underline{N}O_2$ decreased from 49% to 35% upon UV irradiation, while the percentage of $\underline{N}H_2$ increased from 18% to 38%. Hence, UV light converted NO_2 groups to amino groups and in addition, NP and/or aminophenyl groups were lost from the surface. Figure 6.16b shows a corresponding decrease in O 1s $N\underline{O}_2$ signal with no other significant changes, while Figure 6.17b further shows the dramatic decrease in C 1s signal. After UV treatment, the satellite at 293 eV disappears, further suggesting a loss of aromatic rings.

While AFM images of the UV-treated control sample shows clumps on the surface (Figure 6.14b), this is attributed to contamination. The NP-modified sample shown in Figure 6.14f has no significant morphology or surface roughness changes after UV irradiation, despite XPS evidence of loss of film.

UV light appears to heavily damage NP-modified samples, which is consistent with the instability of many polymers under UV irradiation.[49–51] Photolysis products of nitrobenzene include nitrosobenzene and phenol.[52] Additionally, ZnO has photocatalytic properties: electron-hole pairs are created when ZnO is exposed to above-band-gap energy photons (3.3 eV or ~365 nm). Adsorbed atmospheric

species such as O_2 can trap the photoelectrons to form superoxide anion radicals $\cdot O_2^-$, while OH^- can trap the photogenerated holes to form hydroxy radicals (·OH). These are known to be highly reactive and capable of oxidising organic compounds.[53]

The amount of solar radiation at 365 nm at sea level equates to about 1×10^{-4} J s^{-1} or 0.03 J cm^{-2} in 5 min.[54] The energy used in this experiment was 2970 mJ cm^{-2}, which is the equivalent of 8.25 h of 365 nm solar radiation at sea level. This is only for one wavelength and hence care would need to be taken if modified ZnO is used in applications involving UV light exposure.

6.3.4.2.3 Acid Treatment of Nitrophenyl Films on MBE-ZnO

The total surface N, C, and O remained constant after NP-modified MBE-ZnO was immersed in acidic solution (Table 6.5). Similarly, the percentages of reduced and unreduced N do not change significantly, suggesting that the NP film was not chemically modified (Figure 6.15, Table 6.6).

As expected, as-received MBE-ZnO immersed in weak acidic solution has a noticeably changed topography (Figure 6.14c), with the addition of small pits and a significant decrease in surface roughness to 0.9 nm. In contrast, the roughness of NP-modified ZnO decreases by only 0.2 nm (1.4 nm from 1.6 nm) after acid treatment (Figure 6.13a, Figure 6.14g). From this evidence, it appears that NP films are stable in weakly acidic conditions and able to protect the MBE-ZnO substrate from etching.

6.3.4.2.4 Storage of Nitrophenyl Films on MBE-ZnO

Very little change in N, C, or O percentages are seen for NP-modified MBE-ZnO upon storage in the dark for 80 days (Table 6.5). A small increase in NH_2 groups from 30% to 38% may suggest that some NO_2 groups were reduced during this time (Figure 6.15, Table 6.6), but further experiments would be required to establish the significance of this observation.

After storage, little topographical difference is seen for the as-received MBE-ZnO (Figure 6.14d). Similarly, the stored NP-modified surface (Figure 6.14h) appears very similar to a freshly-prepared film (Figure 6.13a), suggesting that the NP film does not undergo significant morphology changes when

stored in the dark, although a small decrease in surface roughness, from 1.7 nm to 1.5 nm, is observed, likely due to surface contamination. Overall, it appears that NP-modified MBE-ZnO is stable when stored for > 2 months in the dark.

6.3.4.3 XPS Characterisation of Trifluoromethylphenyl Films with Heat, UV Light, Acid, or Storage Treatments

The stability of TFMP modification layers on MBE-ZnO was tested against heat, UV light, acid, or storage, as above; Table 6.7 shows the fixed-energy XPS core level spectra results. Core level XPS spectra collected for TFMP-modified MBE-ZnO can be seen in Appendix 8.4. Like NP-modified MBE-ZnO, the TFMP film thicknesses (~2.5 nm) are less than those seen in Section 6.3.1.2 (~4 nm) due to the difference in aryldiazonium salt concentration during grafting. In general, thicknesses obtained through TFMP grafting are slightly greater than NP films obtained via the same method. From the reduction peak currents in the CVs shown in Figure 6.12, Sample 3 might be expected to have the lowest surface coverage and Sample 4 the highest. However, modification layer thicknesses show that Sample 1 was thinnest, with Samples 3 and 4 having similar thicker layers. This indicates that dipping mode CVs are not a reliable predictor of film thickness on ZnO.

Table 6.7. Atomic percentages and film thicknesses from fixed-energy XPS survey spectra, and core level N 1s ratios for TFMP-modified MBE-ZnO grafted via dipping method, before and after various treatments. The thickness of the stored sample is unknown due to problems with its as-received reference sample. TFMP/azo values were calculated to account for 3 F in TFM groups and 2 N in azo linkages.

Sample	C (%)	O (%)	N (%)	F (%)	Zn (%)	TFMP/Azo	Thickness (nm)
1 Before heat	30	36	1	7	25	2.0	0.5 ± 0.1
After heat	30	38	1	4	28	2.2	< 0.5
2 Before UV	51	31	1	6	11	1.9	2.0 ± 0.4
After UV	49	30	1	5	15	1.5	1.5 ± 0.3
3 Before acid	59	27	1	6	7	1.9	2.7 ± 0.5
After acid	40	35	1	3	21	1.3	0.7 ± 0.1
4 Before storage	61	26	1	6	6	1.7	2.7 ± 0.5
After storage	64	25	1	5	6	1.6	-
As-received	21	46	0	1	32	0	-

On average, samples freshly modified with TFMP have ~6 F per N, corresponding to ~1 azo linkage for every 4 TFMP groups. This is compared with NP-modified samples, which had an average of one azo linkage for every 6 NP groups on both MBE-ZnO (Section 6.3.2.1 and 6.3.4.2) and single-crystal O-polar ZnO (Chapter 5). Azo bonds form when unreduced diazonium species participate in electrophilic aromatic substitution with already-grafted phenyl groups. Electron-withdrawing groups such as NO_2 and CF_3 should be deactivating to this grafting mechanism and multilayer formation is expected to occur mainly via radicals, without azo formation. However, TFM groups are less electron-withdrawing than nitro groups and hence less deactivating to azo bond formation, possibly explaining why TFMP-modified samples have more azo linkages per aryl group compared to NP-modified samples. Surprisingly, Menanteau et al. observed one azo linkage for every 35 TFMP electrografted groups on carbon, and one azo linkage for every 6 NP groups.[6] They confirmed that azo bonds were present

between the modification layer and the substrate, and thus the possibility of direct bonding to ZnO through azo groups cannot be discounted here.

For convenience, Figure 6.18 summarises the core level N 1s and F 1s results listed in Table 6.7.

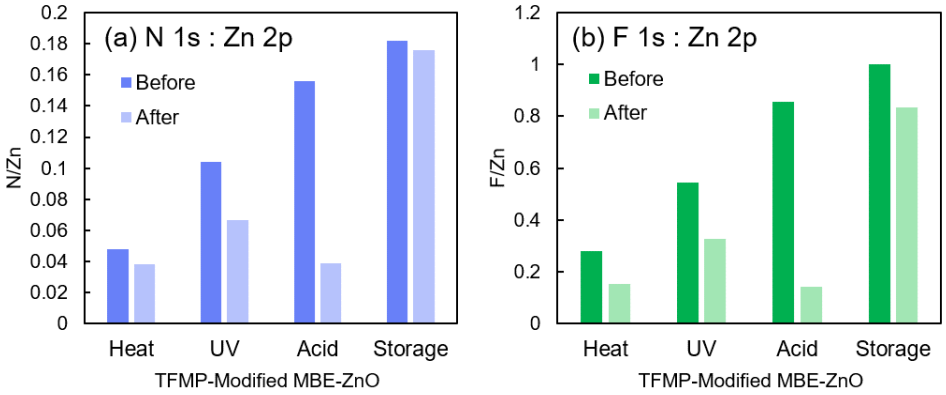

Figure 6.18. (a) N 1s : Zn 2p and (b) F 1s : Zn 2p ratios for TFMP-modified MBE-ZnO before and after treatment with heat, UV light, acid, and storage. From core level spectra.

6.3.4.3.1 Heat Treatment of Trifluoromethylphenyl Films on MBE-ZnO

As seen in Figure 6.18, the N signal on TFMP-modified MBE-ZnO decreases only slightly after heat treatment while the amount of carbon on the surface remains constant (Table 6.7). These data indicate that the TFMP film has reasonable stability at 160 °C. AFM images (Figure 6.2e) show large raised circular areas with height ~5 nm on heated TFMP films. These may be due to aromatic groups clumping together as water is removed from the surface. The O 1s spectrum (Appendix 8.6) showed the disappearance of water (533 eV) upon heating, which supports this hypothesis.

6.3.4.3.2 UV Light Treatment of Trifluoromethylphenyl Films on MBE-ZnO

Significant decreases in the N 1s:Zn and F 1s:Zn ratios are seen after UV treatment of TFMP-modified MBE-ZnO (Figure 6.18), suggesting that the film is not stable to these conditions. However, the percentages of N, C, and F on the surface remain reasonably constant (Table 6.7), indicating that whole TFMP groups are cleaved from the film. The AFM image of UV-treated TFMP-modified MBE-ZnO shows clumping or patterning on the surface and a large decrease in roughness to 1.2 nm from 1.9 nm (Figure

6.3). This could indicate photo-induced polymerisation occurring on the surface, although no evidence of this was seen in either the C 1s or N 1s spectra (Appendix 8.6).

The loss of F from TFMP films upon UV irradiation is not unexpected since F was lost from PFBPA-modified ZnO after UV irradiation as shown in Chapter 3, and C-F bonds in pentafluorobenzoic acid have been shown to cleave via ZnO nanoparticle photocatalysis.[55] However, Ravichandran et al. noted that a wavelength of 254 nm was more effective at C-F bond cleavage than 365 nm; this highlights the need for a more systematic study of the UV wavelengths at which TFMP-modified ZnO is degraded.

6.3.4.3.3 Acid Treatment of Trifluoromethylphenyl Films on MBE-ZnO

On TFMP-modified MBE-ZnO, F 1s signal decreases dramatically after acid treatment, as does N 1s signal and the percentage of C on the surface (Figure 6.18 and Table 6.7). The calculated TFMP film thickness decreases from 2.7 nm (Table 6.7) to 0.7 nm. This shows that a significant amount of the modification layer was removed from the surface. This is consistent with AFM results (Figure 6.14k): the acid-treated TFMP-modified sample has numerous large pits ~10 nm deep and up to 250 nm wide. The pits are much larger than on the as-received surface, and the calculated roughness is larger. This suggests that while the as-received sample was etched uniformly by the NH_4Cl solution, the TFMP-modified sample was etched preferentially in places where the TFMP modification layer was more porous or thinner.

The instability of the TFMP-modified samples contrasts with NP-modified MBE-ZnO, which appeared to be stable in the same acidic conditions. As CF_3 groups are not likely to be affected by weak acid, it is proposed that the TFMP modification layer is more porous than NP layers and allows acid to diffuse through it and etch the ZnO substrate. As the ZnO dissolves, TFMP groups are lost from the surface. This explains the pits seen by AFM, and the decrease in average film thickness observed from XPS results.

While it is difficult to quantify the density of TFMP and NP films, an estimation can be made by comparing $\underline{N}O_2$:$\underline{C}$=C and $C\underline{F}_3$:$\underline{C}$=C ratios on freshly-modified samples. On NP-modified samples in

Section 6.3.3.1, the average $\underline{N}O_2$:C=C ratio is 0.038. The average $C\underline{F}_3$:C=C ratio for the TFMP-modified samples in this section is 20% smaller (0.032), which suggests that TFMP films are less dense than NP films. Furthermore, TFMP films in this section are ~50% (~1 nm) thicker than NP films in Section 6.3.3.1, which adds weight to this argument. However, due to the uncertainties of these values, and the unknown amounts of adventitious carbon, further investigation into the quantification of aryl groups in grafted films is required to confirm this hypothesis.

6.3.4.3.4 Storage of Trifluoromethylphenyl Films on MBE-ZnO

The N 1s and F 1s signals on TFMP-modified MBE-ZnO do not significantly change after 60 days of storage (Figure 6.18), nor does the TFMP:azo ratio (Table 6.7). While the percentage of C on the surface increases, this is attributed to contamination on top of the TFMP layer. The thickness of the TFMP film could not be calculated due to a lack of a reliable reference sample, but from the other evidence listed here, it is likely that TFMP films are stable when stored in dark conditions. No morphology change was seen using AFM (Figure 6.14l).

6.3.4.4 Band Bending Changes with Heat, UV Light, Acid, or Storage Treatments

Band bending was measured via fixed-energy XPS on NP- and TFMP-modified MBE-ZnO before and after treatment or storage. Unlike synchrotron XPS VB spectra in Section 6.3.2.3, VB spectra in this section were not calibrated to Au, so the magnitudes of band bending should not be directly compared. However, ΔV_{bb} values are directly comparable for ZnO samples of the same type, measured using the same XPS photon energy.

6.3.4.4.1 Nitrophenyl-Modified MBE-ZnO

Upon modification with NP groups, the 4 samples of MBE-ZnO showed a decrease in downwards band bending by 0.12 eV – 0.24 eV, with a mean ΔV_{bb} value of +0.16 eV (Figure 6.19 and Table 6.8). This is smaller than ΔV_{bb} observed via fixed-energy XPS for single-crystal O-polar ZnO modified with a thin NP film (+0.21 eV, Table 5.5). This is expected because of the high Sb-doping of MBE-ZnO, which increases the charge carrier concentration by more than 5 orders of magnitude relative to bulk CrysTec O-polar

ZnO (Table 2.1). This has two effects. Firstly, there are now more electrons present at the surface, meaning that the overall effect of electron-withdrawing substituents will not be as large as for the same substituents on a less-electron-dense surface. Secondly, as reported by Vasheghani et al. for SnO_2, increasing the Sb dopant concentration increases the energy of the Fermi level, resulting in a decrease in the width of the SEAL.[56] The band bending of Sb-doped MBE-ZnO, then, is more 'steep' than for unintentionally-doped single crystal ZnO, and the difference between surface V_{bb} and near-surface V_{bb} will be large. For unintentionally-doped ZnO, which has 'shallower' band bending that extends further into the bulk, the difference between surface V_{bb} and near-surface V_{bb} will be smaller. This also means that the difference in band bending of undoped and Sb-doped ZnO is larger when observed with high-energy XPS than when observed with low-energy XPS. NP-modified films grafted with the O-ring method showed upwards band bending ($\zeta < 3.315$ eV) when analysed with synchrotron XPS, but the ζ values in Table 6.8 reflect downwards band bending. This difference is attributed to the lack of external calibration of the fixed-energy XPS ζ values; ΔV_{bb} values are more reliable.

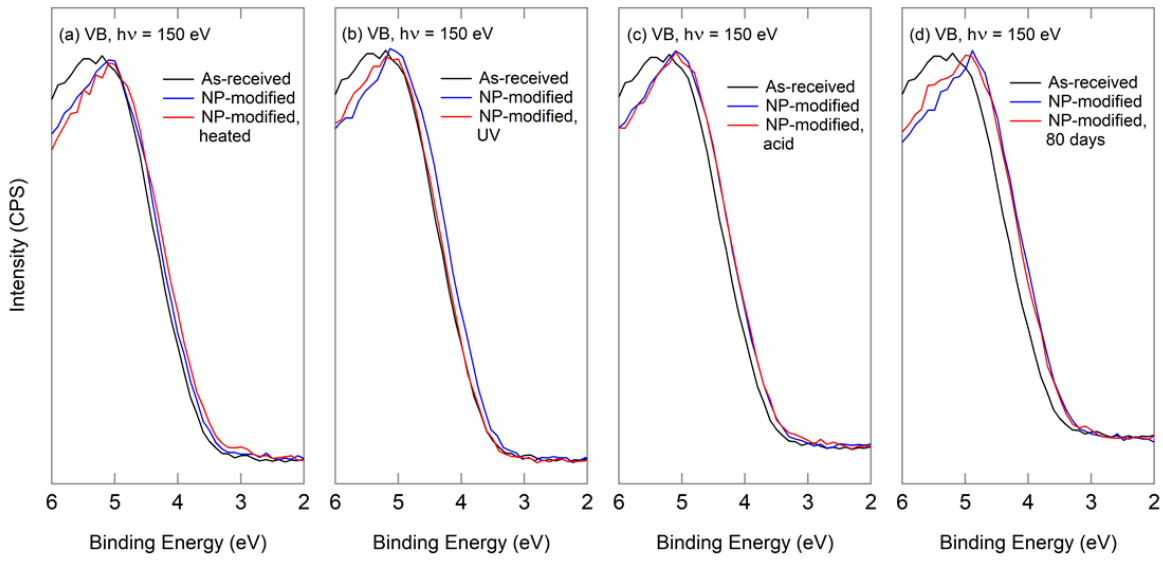

Figure 6.19. XPS valence band spectra for as-received MBE-ZnO and NP-modified MBE-ZnO before (blue) and after (red) treatment in (a) heat, (b) UV light, (c) acid, (d) ambient storage for 80 days.

Table 6.8. Band bending data from XPS valence band spectra for NP-modified MBE-ZnO before and after treatment with heat, UV light, acid, or long-term exposure to dark ambient conditions. ΔV_{bb} = change in band bending relative to as-received MBE-ZnO. $\Delta(\Delta V_{bb})$ = change in band bending after treatment relative to the freshly-prepared sample.

	ζ, before (eV)	ζ, after (eV)	ΔV_{bb}, before (eV)	ΔV_{bb}, after (eV)	$\Delta(\Delta V_{bb})$ (eV)	Initial NP Thickness (nm)	Final NP Thickness (nm)
As-received	3.76	3.76	-	-	-	-	-
1 Heat	3.64	3.52	+0.12	+0.24	+0.12	1.4 ± 0.3	2.0 ± 0.4
2 UV	3.61	3.67	+0.15	+0.09	-0.06	1.2 ± 0.2	0.5 ± 0.1
3 Acid	3.62	3.59	+0.14	+0.17	+0.03	1.0 ± 0.2	1.4 ± 0.3
4 Storage	3.52	3.55	+0.24	+0.21	-0.03	1.6 ± 0.3	2.4 ± 0.5

Figure 6.19 shows the VB spectra for as-received MBE-ZnO and NP-modified samples before and after treatment. Table 6.8 lists all relevant data. After heat treatment, NP-modified MBE-ZnO had smaller downwards band bending than when freshly-modified. It is possible that the increased number of azo bonds observed in the N 1s spectrum of the heat-treated NP-modified MBE-ZnO, compared to the freshly-modified MBE-ZnO, contribute an increased electron-withdrawing nature to the film, but this requires further investigation.

After UV light treatment of NP-modified MBE-ZnO, there was an increase in downwards V_{bb}, that is, a shift of 0.06 eV towards the original V_{bb} of as-received MBE-ZnO. This shift is attributed to the removal of a significant percentage of the electron-withdrawing NP modifying groups, as seen in the core level spectra (Section 6.3.4.2). However, V_{bb} did not return to that of as-received MBE-ZnO; this is thought to be because approximately a monolayer of electron-withdrawing NP groups was still present on the surface.

No significant change in band bending occurred after acid treatment or prolonged storage of NP-modified MBE-ZnO. This is consistent with both samples retaining their original makeup after

treatment, as determined by core level spectra (Section 6.3.4.2). Overall, all band bending data are consistent with the effects of each treatment on the NP-modified samples.

6.3.4.4.2 Trifluoromethylphenyl-Modified MBE-ZnO

Figure 6.20 shows the change in band bending upon TFMP modification of MBE-grown ZnO, and the changes when modified samples are exposed to heat, UV light, or acid. These are quantified in Table 6.9. The VB spectrum for the stored sample was not collected.

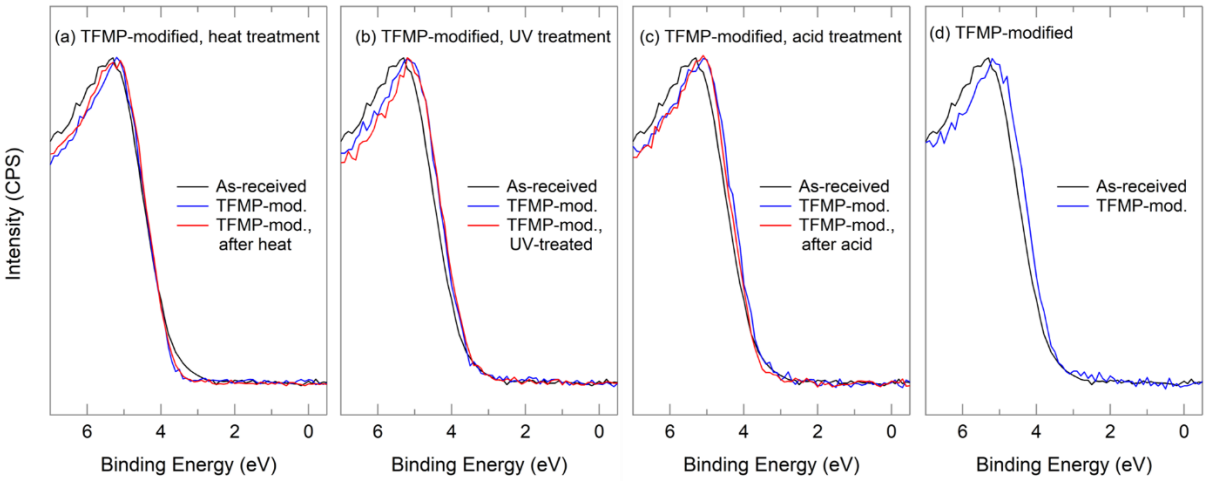

Figure 6.20. XPS VB spectra for as-received MBE-ZnO and 4 separate TFMP-modified MBE-ZnO samples before (blue) and after (red) treatment in (a) heat, (b) UV light, (c) acid, and (d) storage. The VB spectrum was not collected for the sample stored for 60 days.

Freshly TFMP-modified MBE-ZnO samples 2, 3, and 4 show a reproducible decrease in band bending by ~0.12 eV compared to as-received MBE-ZnO, which is similar to the changes seen after NP modification of MBE-ZnO. While synchrotron XPS determined that NP films decrease the band bending more than TFMP modification (Section 6.3.2.3), fixed-energy XPS is not as surface-sensitive and as such this difference between modifiers is not seen here. Sample 1, with sub-monolayer TFMP modification, had no significant change in V_{bb} compared to the as-received surface. Given that this TFMP film thickness is significantly thinner than the other samples, this is evidence that ΔV_{bb} is related to the amount of TFMP groups on the surface (see Section 6.3.4.4.3). After heat treatment, V_{bb}

remained the same, further indicating that the thin TFMP modification had had minimal influence on the band bending.

Table 6.9. Band bending information from XPS valence band spectra for TFMP-modified MBE-ZnO before and after treatment in heat, UV light, and acid. ΔV_{bb} = change in band bending relative to as-received MBE-ZnO. $\Delta(\Delta V_{bb})$ = change in band bending after treatment relative to the freshly-prepared sample.

	ζ, before (eV)	ζ, after (eV)	ΔV_{bb}, before (eV)	ΔV_{bb}, after (eV)	$\Delta(\Delta V_{bb})$ (eV)	Initial TFMP Thickness (nm)	Final TFMP Thickness (nm)
As-received	3.70	3.70	-	-	-	-	-
1 Heat	3.72	3.73	-0.02	-0.03	-0.01	0.5 ± 0.1	< 0.5
2 UV	3.58	3.60	+0.12	+0.10	-0.02	2.0 ± 0.4	1.5 ± 0.3
3 Acid	3.58	3.64	+0.12	+0.06	-0.06	2.7 ± 0.5	0.7 ± 0.1
4 (Storage)	3.57	-	+0.13	-	-	2.7 ± 0.5	-

UV-treated TFMP-modified MBE-ZnO had only a −0.02 eV change in ζ relative to the freshly-prepared sample, indicating that the loss of F and N, the decrease in film thickness to 1.5 nm, or morphology changes seen via AFM did not significantly affect the band banding. This contrasts with the acid-treated TFMP-modified sample, where V_{bb} was shifted 0.06 eV closer to the original downwards V_{bb} alongside a decrease in film thickness to 0.7 nm. This reversion to as-received V_{bb} is consistent with the core level XPS results, which showed a significant loss of F and C from the surface after treatment in acid. While the N:Zn and F:Zn ratios for acid-treated and UV-treated TFMP films are very similar (Figure 6.18), the samples have a −0.04 eV difference in ζ and a > 0.4 nm difference in average film thickness. This suggests that the pitted morphology of the acid-treated TFMP-modified sample has affected V_{bb} more than the non-pitted UV-treated TFMP film.

VB spectra were not collected for the stored TFMP-modified MBE-ZnO sample.

6.3.4.4.3 Effect of NP and TFMP Modification Layer Thickness on Band Bending

Data collected regarding V_{bb}, film thicknesses, and NO_2:Zn 2p or CF_3:Zn 2p ratio for NP- and TFMP-modified MBE-ZnO, respectively, in the previous sections are shown in Figure 6.21. Figure 6.21a shows the change in band bending compared to the thickness of NP and TFMP films on MBE-ZnO. However, Section 6.3.4 showed that the nature of these films, in particular NO_2 and CF_3 groups, can change independently of film thickness after stability treatments. As such, Figure 6.21b shows the changes in V_{bb} observed for different concentrations of NO_2 and CF_3 on NP- and TFMP-modified MBE-ZnO, respectively.

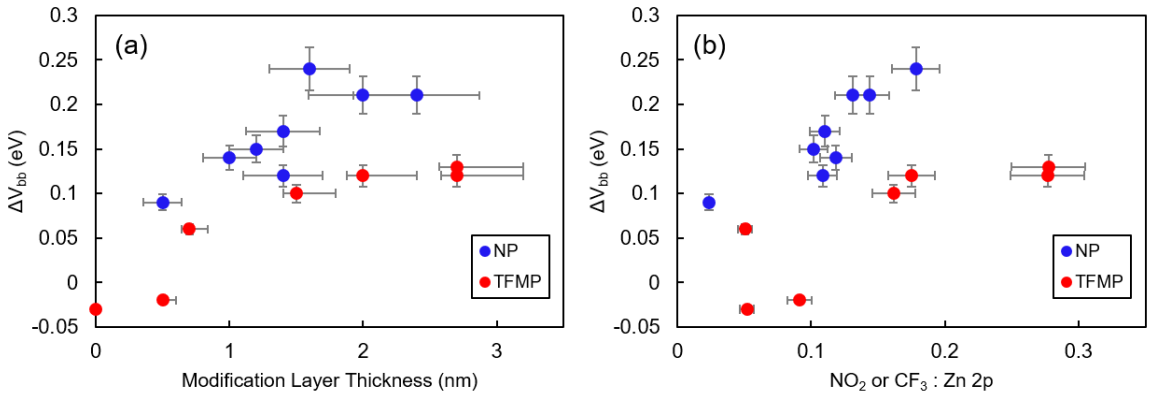

Figure 6.21. Changes in band bending (ΔV_{bb}) relative to as-received MBE-ZnO for (a) different thicknesses and (b) different NO_2:Zn or CF_3:Zn ratios of NP and TFMP modification layers on MBE-ZnO, collated from Sections 6.3.4.4.1 and 6.3.4.4.2. Band bending information was collected using fixed-energy XPS (hv = 1486 eV).

From Figure 6.21a, it appears that the effect of a TFMP modification layer on ΔV_{bb} reaches a maximum when the TFMP film has a thickness of ~1.5 ± 0.3 nm and/or a CF_3:Zn ratio of 0.17 (Figure 6.21b). This decreases downwards V_{bb} relative to as-received MBE-ZnO by +0.13 eV, while thicker films have no further effect on V_{bb}. Similarly, the maximum ΔV_{bb} for NP-modified MBE-ZnO is seen when the NP layer is ~1.6 ± 0.3 eV thick or has a NO_2:Zn ratio of ~0.18; NP layers of this thickness and thicker give ΔV_{bb} = +0.24 eV. These ΔV_{bb} values are smaller than observed using synchrotron XPS (Section 6.3.2.3), as expected due to the differences in photon energy and therefore probing depth.

Two conclusions can be drawn from Figure 6.21. Firstly, NP groups have a greater effect on the band bending of MBE-ZnO than TFMP, as expected from their larger electron withdrawing ability. Secondly, to have maximum effect on ΔV_{bb} of MBE-ZnO using NP or TFMP groups, the modification layer should be at least 3 phenyl layers thick, based on the heights of NP and TFMP.[7] Monolayer and sub-monolayer coverage gives smaller ΔV_{bb}, most likely due to the small number of electron-withdrawing groups present. Meanwhile, multilayers thicker than ~1.5 nm have no further effect on the band bending despite increased numbers of functional groups. It does not appear that having 'extra' groups on the surface is detrimental to the band bending effect. This suggests that grafting thicker films for increased protection of the ZnO substrate can be performed while still having the largest effect on MBE-ZnO band bending.

A direct comparison cannot be made between thin NP and TFMP films on MBE-ZnO analysed with fixed-energy XPS ($h\nu$ = 1486 eV) and thick NP and TFMP films on MBE-ZnO analysed with synchrotron XPS ($h\nu$ = 150 eV, Section 6.3.2.3) due to calibration and photon energy differences. However, it is worth noting that V_{bb} changes observed via synchrotron XPS for 4 – 5 nm thick TFMP and NP films (+0.26 eV, +0.36 eV) are larger than those observed for thinner films via fixed-energy XPS (+0.15 eV, +0.25 eV). This is consistent with band bending being greater at the surface of MBE-ZnO than in the bulk, and the lower photon energy of synchrotron XPS being more surface sensitive compared to fixed-energy XPS. While the direction of the band bending on NP-modified MBE-ZnO differs for samples analysed with synchrotron XPS and fixed-energy XPS, this is attributed a lack of calibration to an external reference sample for the latter. This means that the values for ζ determined from fixed-energy XPS are not absolute values. However, in both cases NP films have a larger effect on V_{bb} than TFMP films, by ~0.1 eV, which confirms that both types of XPS instrument give reliable ΔV_{bb} data.

6.3.5 Persistent Photoconductivity of NP-Modified ZnO

PPC measurements were carried out by Dr Rodrigo Martinez Gazoni on as-received and NP-modified MBE-ZnO. Samples were consecutively exposed to UV light ($h\nu$ = 365 nm) in air and stored in dark

ambient conditions while their photocurrent was monitored, as seen in Figure 6.22. Upon the initial UV irradiation, the NP-modified sample shows an increase in current due to the desorption of atmospheric species and the release of electrons back to the SEAL (Section 1.1.3). This suggests that the NP film is porous and allows the adsorbates to leave the ZnO surface. The rate of decay to the conductivity baseline decreased on each subsequent UV exposure. Considering that adsorbates desorb from the ZnO surface upon UV illumination and re-adsorb after irradiation (Section 1.3),[57] a longer photocurrent decay time might indicate that a change has happened within the modifying film that makes it more difficult for this re-adsorption to occur. However, because the same effect was seen on as-received ZnO (not shown), it is not inherent to the modified surface; this phenomenon was not investigated further.

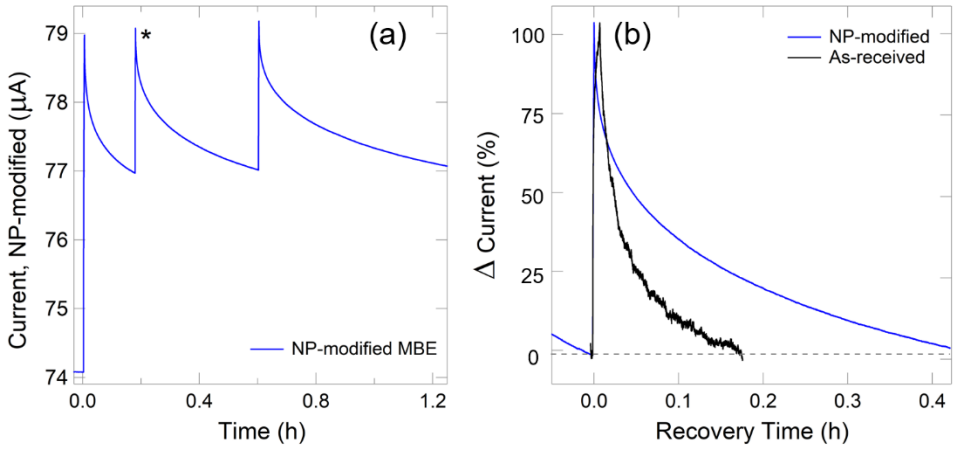

*Figure 6.22. (a) Current measured for NP-modified MBE-ZnO upon 3 illuminations with 365 nm UV light (1.5 mW cm^{-2}). Between these times, the sample was in darkness in air. (b) Change in current measured on as-received and NP-modified MBE-ZnO after 2 UV illuminations, shown with * in (a) for NP-modified MBE-ZnO. After illumination, samples were in darkness in air.*

Figure 6.22b shows the time taken for the current of NP-modified MBE-ZnO to return to a baseline (~60% of the maximum PPC value) compared to as-received MBE-ZnO, after 2 successive UV illuminations on each surface to ensure steady-state conditions. PPC data was not collected in a way that allowed the direct comparison of current on as-received MBE ZnO to NP-modified MBE-ZnO. However, Figure 6.22b shows that the time taken for the current on as-received MBE-ZnO to reach

60% of the original current is ~0.17 h. On NP-modified MBE-ZnO, the time taken for the photocurrent to return to two-thirds of the original value is ~0.42 h, which is approximately 2.5 times longer than for as-received MBE-ZnO.

It appears that NP-modified ZnO can prolong the effects of PPC but not indefinitely. The NP-modification serves to decrease the rate at which the conductivity returns to the original value, as also seen in Chapter 3 with ODPA on ZnO (Figure 3.18). However, the NP film appears to be less effective at increasing PPC than ODPA, which increased the recovery time of ZnO by 8 times relative to as-received ZnO. This is likely due to the well-ordered structure of ODPA monolayers (~2.2 nm thick)[7] as compared to ~1.3 nm of loosely-packed NP groups (Table 6.6). Furthermore, as seen in Section 6.3.4.2.2, NP films do not appear to be stable to intense UV light, while ODPA-modified surfaces are more robust.

6.4 Conclusions

Sb-doped MBE-ZnO samples were electrochemically grafted with NP and TFMP films. The straight-forward modification method was more reproducible on these samples than single-crystal ZnO sample with lower charge carrier concentrations. Surface-sensitive synchrotron XPS was used to fully assign the O 1s spectrum and determine the presence of Zn-O-C bonds on the surface. While no Zn-C evidence was seen in the C 1s or Zn 2p spectra, direct Zn-C binding cannot be ruled out. However, it is most likely that binding occurs via surface O groups as seen for other metal oxides.

Synchrotron XPS also showed that NP and TFMP modification layers of 4 and 5 nm thick, respectively, decreased downwards band bending on ZnO, with TFMP removing it completely and NP producing upwards band bending and an insulating surface. Upon deliberate synchrotron XPS reduction of NP groups to amine-like groups, upwards band bending increased to ~+1 eV. This is a very large but unexpected change and is promising for FET-based devices which require the surface to be non-conducting. The change is proposed to be due to photoelectrons from ZnO participating in the reduction of NP groups. Further analysis of the reduced films is warranted to fully characterise the

reduced NO_2 groups. If NO_2 groups are involved in XPS-induced polymerisation via N-H bonds, this could make the layers more stable. On the other hand, NH_2-type functional groups offer the potential of coupling with sensing molecules via amide bond formation.

The dipping method provided a more flexible method of modification compared to the O-ring method but resulted in thinner films as determined by XPS due to the use of lower concentrations of NBD and TFMBD. To graft thicker films, a higher aryldiazonium salt concentration should be used, or multiple CV scans could be performed to graft more aryl radicals to the surface. Furthermore, protecting the metallic contact from the aryldiazonium ion solution would mean that more precise current densities could be determined, aiding the correlation of CVs to the characteristics of the produced film.

Thin NP layers on ZnO proved to be stable to long-term storage and treatment in weakly acidic aqueous conditions, but chemically changed to a small extent when heated, and were significantly degraded on exposure to intense UV light. TFMP films were stable to heat and storage in the dark, but the surfaces degraded under UV and acidic conditions. The apparent chemical and electronic stability of NP-modified MBE-ZnO to acidic conditions (pH 5) suggests that NP-modified ZnO could be used in aqueous conditions with pH values of biological interest. This means that NP films could be a promising protective layer for ZnO-based biological sensors, especially as they are also stable to long-term storage. Furthermore, controllable reduction of NP groups to amino groups is expected to provide a pathway to functionalisation of ZnO with biosensing groups. TFMP films appear more porous than NP films and would be more suited to use in dry devices. Neither NP- nor TFMP-modified ZnO appear to be suitable for UV-based devices.

Fixed-energy XPS analysis, also as expected, showed that NP and TFMP layers on MBE-ZnO decrease downwards band bending on MBE-ZnO. The band bending effect is controllable by the film thickness: NP and TFMP films thinner than 1.5 ± 0.3 nm and 1.6 ± 0.3 nm, respectively, have less effect on the band bending than thicker films. This shows that thicker films can be deliberately grafted for stability purposes while maintaining the maximum effect on the band bending.

PPC measurements showed that atmospheric species can diffuse through thin NP modifying films, which are unable to prevent photoinduced conductivity changes on MBE-ZnO. However, PPC was lengthened on the modified sample, showing that aryldiazonium-derived films, although porous to gaseous species, influence the rates of adsorption and desorption on ZnO. Thicker aryl films may be able to further prolong PPC, and again could be grafted via repeated CVs. However, long-term effects of UV light are expected to degrade NP films on MBE-ZnO.

6.5 References

(1) Sadananda Kumar, N.; Bangera, K. V.; Shivakumar, G. K. Properties of Antimony Doped ZnO Thin Films Deposited by Spray Pyrolysis Technique. *Semiconductors* **2015**, *49* (7), 899–904.

(2) Hayes, W. M. *CRC Handbook of Chemistry and Physics (96th Edition)*; CRC Press: Boca Raton, FL, USA.

(3) Sun, J.; Bian, J.; Liang, H.; Zhao, J.; Hu, L.; Zhao, Z.; Liu, W.; Du, G. Realization of Controllable Etching for ZnO Film by NH_4Cl Aqueous Solution and Its Influence on Optical and Electrical Properties. *Appl. Surf. Sci.* **2007**, *253* (11), 5161–5165.

(4) Perkins, C. L. Molecular Anchors for Self-Assembled Monolayers on ZnO: A Direct Comparison of the Thiol and Phosphonic Acid Moieties. *J. Phys. Chem. C* **2009**, *113* (42), 18276–18286.

(5) Lee, L.; Brooksby, P. A.; Hapiot, P.; Downard, A. J. Electrografting of 4-Nitrobenzenediazonium Ion at Carbon Electrodes: Catalyzed and Uncatalyzed Reduction Processes. *Langmuir* **2016**, *32* (2), 468–476.

(6) Menanteau, T.; Dias, M.; Levillain, E.; Downard, A. J.; Breton, T. Electrografting via Diazonium Chemistry: The Key Role of the Aryl Substituent in the Layer Growth Mechanism. *J. Phys. Chem. C* **2016**, *120* (8), 4423–4429.

(7) Hanwell, M. D.; Curtis, D. E.; Lonie, D. C.; Vandermeersch, T.; Zurek, E.; Hutchison, G. R. Avogadro: An Advanced Semantic Chemical Editor, Visualisation, and Analysis Platform. *J. Chem. Informatics* **2012**, *4.17*, 1–17.

(8) Stewart, M. P.; Maya, F.; Kosynkin, D. V; Dirk, S. M.; Stapleton, J. J.; McGuiness, C. L.; Allara, D. L.; Tour, J. M. Direct Covalent Grafting of Conjugated Molecules onto Si, GaAs, and Pd Surfaces from Aryidiazonium Salts. *J. Am. Chem. Soc.* **2004**, *126* (1), 370–378.

(9) Hunger, R.; Jaegermann, W.; Merson, A.; Shapira, Y.; Pettenkofer, C.; Rappich, J. Electronic Structure of Methoxy-, Bromo-, and Nitrobenzene Grafted onto Si(111). *J. Phys. Chem. B* **2006**, *110* (31), 15432–15441.

(10) Doppelt, P.; Hallais, G.; Pinson, J.; Podvorica, F.; Verneyre, S. Surface Modification of Conducting Substrates. Existence of Azo Bonds in the Structure of Organic Layers Obtained from Diazonium Salts. *Chem. Mater.* **2007**, *19* (18), 4570–4575.

(11) Heinhold, R.; Allen, M. W. Polarity-Dependent Photoemission of In Situ Cleaved Zinc Oxide Single Crystals. *J. Mater. Res.* **2012**, *27* (17), 2214–2219.

(12) Brooksby, P. A.; Downard, A. J. Electrochemical and Atomic Force Microscopy Study of Carbon

Surface Modification via Diazonium Reduction in Aqueous and Acetonitrile Solutions. *Langmuir* **2004**, *20* (12), 5038–5045.

(13) Polydorou, E.; Zeniou, A.; Tsikritzis, D.; Soultati, A.; Sakellis, I.; Gardelis, S.; Papadopoulos, T. A.; Briscoe, J.; Palilis, L. C.; Kennou, S.; Gogolides, E.; Argitis, P.; Davazoglou, D.; Vasilopoulou, M. Surface Passivation Effect by Fluorine Plasma Treatment on ZnO for Efficiency and Lifetime Improvement of Inverted Polymer Solar Cells. *J. Mater. Chem. A* **2016**, *4* (30), 11844–11858.

(14) Li, X.; Forouzandeh, F.; Kakanat, A. J.; Feng, F.; Banham, D. W. H.; Ye, S.; Kwok, D. Y.; Birss, V. Surface Characteristics of Microporous and Mesoporous Carbons Functionalized with Pentafluorophenyl Groups. *ACS Appl. Mater. Interfaces* **2018**, *10* (2), 2130–2142.

(15) Lund, T.; Nguyen, P. T.; Ruhland, T. Electrochemical Grafting of TiO_2-Based Photo-Anodes and Its Effect in Dye-Sensitized Solar Cells. *J. Electroanal. Chem.* **2015**, *758*, 85–92.

(16) Hurley, B. L.; McCreery, R. L. Covalent Bonding of Organic Molecules to Cu and Al Alloy 2024 T3 Surfaces via Diazonium Ion Reduction. *J. Electrochem. Soc.* **2004**, *151* (5), B252–B259.

(17) Dicke, C.; Morstein, M.; Hähner, G. Surface Inorganic Chemistry: The Reaction of Hydroxyl-Terminated Thiols on Gold with a Zirconium Coordination Compound. *Langmuir* **2002**, *18* (2), 336–344.

(18) Bell, K. J.; Brooksby, P. A.; Polson, M. I. J.; Downard, A. J. Evidence for Covalent Bonding of Aryl Groups to MnO_2 Nanorods from Diazonium-Based Grafting. *Chem. Commun.* **2014**, *50* (89), 13687–13690.

(19) Samanta, S.; Bakas, I.; Singh, A.; Aswal, D. K.; Chehimi, M. M. In Situ Diazonium-Modified Flexible ITO-Coated PEN Substrates for the Deposition of Adherent Silver-Polypyrrole Nanocomposite Films. *Langmuir* **2014**, *30*, 9397–9406.

(20) Charlton, M. R.; Suhr, K. J.; Holliday, B. J.; Stevenson, K. J. Electrochemical Modification of Indium Tin Oxide Using Di(4-Nitrophenyl) Iodonium Tetrafluoroborate. *Langmuir* **2015**, *31* (2), 695–702.

(21) Roodenko, K.; Gensch, M.; Rappich, J.; Hinrichs, K.; Esser, N.; Hunger, R. Time-Resolved Synchrotron XPS Monitoring of Irradiation-Induced Nitrobenzene Reduction for Chemical Lithography. *J. Phys. Chem. B* **2007**, *111* (26), 7541–7549.

(22) Kim, C. M.; Jeong, H. S.; Kim, E. H. NEXAFS and XPS Characterization of Molecular Oxygen Adsorbed on Ni(100) at 80 K. *Surf. Sci. Lett.* **2000**, *459*, 457–461.

(23) Piscopo, C. G.; Trapani, F.; Polyzoidis, A.; Schwarzer, M.; Pace, A.; Loebbecke, S. Positive Effect of the Fluorine Moiety on the Oxygen Storage Capacity of UiO-66 Metal–Organic Frameworks. *New J. Chem.* **2016**, *40* (10), 8220–8224.

(24) Yang, C.; Wang, X.; Omary, M. A. Fluorous Metal-Organic Frameworks for High-Density Gas Adsorption. *J. Am. Chem. Soc.* **2007**, *129* (50), 15454–15455.

(25) Chehimi, M. M. *Aryl Diazonium Salts: New Coupling Agents and Surface Science*; Chehimi, M. M., Ed.; Wiley-VCH: Weinheim, 2012.

(26) Saby, C.; Ortiz, B.; Champagne, G. Y.; Bélanger, D. Electrochemical Modification of Glassy Carbon Electrode Using Aromatic Diazonium Salts. 1. Blocking Effect of 4-Nitrophenyl and 4-Carboxyphenyl Groups. *Langmuir* **1997**, *13* (14), 6805–6813.

(27) Mendes, P.; Belloni, M.; Ashworth, M.; Hardy, C.; Nikitin, K.; Fitzmaurice, D.; Critchley, K.; Evans, S.; Preece, J. A Novel Example of X-Ray-Radiation-Induced Chemical Reduction of an Aromatic Nitro-Group-Containing Thin Film on SiO_2 to an Aromatic Amine Film. *ChemPhysChem*

2003, *4* (8), 884–889.

(28) Adenier, A.; Cabet-Deliry, E.; Chaussé, A.; Griveau, S.; Mercier, F.; Pinson, J.; Vautrin-Ul, C. Grafting of Nitrophenyl Groups on Carbon and Metallic Surfaces Without Electrochemical Induction. *Chem. Mater.* **2005**, *17* (3), 491–501.

(29) Yu, S. S. C.; Tan, E. S. Q.; Jane, R. T.; Downard, A. J. An Electrochemical and XPS Study of Reduction of Nitrophenyl Films Covalently Grafted to Planar Carbon Surfaces. *Langmuir* **2007**, *23* (22), 11074–11082.

(30) Cottineau, T.; Morin, M.; Bélanger, D. Surface Band Structure of Aryl-Diazonium Modified *p*-Si Electrodes Determined by X-Ray Photoelectron Spectroscopy and Electrochemical Measurements. *RSC Adv.* **2013**, *3* (45), 23649.

(31) Richard, W.; Evrard, D.; Gros, P. New Insight into 4-Nitrobenzene Diazonium Reduction Process: Evidence for a Grafting Step Distinct from NO_2 Electrochemical Reactivity. *J. Electroanal. Chem.* **2012**, *685*, 109–115.

(32) Brooksby, P. A.; Shields, J. D.; Farquhar, A. K.; Downard, A. J. Reduction of Nitrophenyl Films in Aqueous Solutions: How Many Electrons? *ChemElectroChem* **2016**, *3* (12), 2021–2026.

(33) Nansé, G.; Papirer, E.; Fioux, P.; Moguet, F.; Tressaud, A. Fluorination of Carbon Blacks: An X-Ray Photoelectron Spectroscopy Study: I. A Literature Review of XPS Studies of Fluorinated Carbons. XPS Investigation of Some Reference Compounds. *Carbon* **1997**, *35*, 175–194.

(34) Ferraria, A. M.; Lopes da Silva, J. D.; Botelho do Rego, A. M. XPS Studies of Directly Fluorinated HDPE: Problems and Solutions. *Polymer* **2003**, *44* (23), 7241–7249.

(35) Eck, W.; Stadler, V.; Geyer, W.; Zharnikov, M.; Gölzhäuser, A.; Grunze, M. Generation of Surface Amino Groups on Aromatic Self-Assembled Monolayers by Low Energy Electron Beams. *Adv. Mater.* **2000**, *12* (11), 805–808.

(36) Timpel, M.; Nardi, M. V.; Krause, S.; Ligorio, G.; Christodoulou, C.; Pasquali, L.; Giglia, A.; Frisch, J.; Wegner, B.; Moras, P.; Koch, N. Surface Modification of ZnO(0001)-Zn with Phosphonate-Based Self-Assembled Monolayers: Binding Modes, Orientation, and Work Function. *Chem. Mater.* **2014**, *26* (17), 5042–5050.

(37) La, Y. H.; Kim, H. J.; Maeng, I. S.; Jung, Y. J.; Park, J. W.; Kim, K. J.; Kang, T. H.; Kim, B. Selective Cleavage of Nitro Groups in Nitro-Substituted Aromatic Monolayers by Synchrotron Soft X-Rays: Effect of Molecular Structure on Cleavage Rates. *Langmuir* **2002**, *18* (6), 2430–2433.

(38) Perkins, C. L.; Lee, S. H.; Li, X.; Asher, S. E.; Coutts, T. J. Identification of Nitrogen Chemical States in n-Doped ZnO via X-Ray Photoelectron Spectroscopy. *J. Appl. Phys.* **2005**, *97* (3).

(39) Takshi, A.; Dimopoulos, A.; Madden, J. D. Depletion Width Measurement in an Organic Schottky Contact Using a Metal-Semiconductor Field-Effect Transistor. *Appl. Phys. Lett.* **2007**, *91*, 083513.

(40) Lavrov, E. V.; Herklotz, F.; Weber, J. Identification of Two Hydrogen Donors in ZnO. *Phys. Rev. B: Condens. Matter* **2009**, *79*, 165210.

(41) Du, M. H.; Biswas, K. Anionic and Hidden Hydrogen in ZnO. *Phys. Rev. Lett.* **2011**, *106* (11), 1–4.

(42) Heinhold, R.; Neiman, A.; Kennedy, J. V.; Markwitz, A.; Reeves, R. J.; Allen, M. W. Hydrogen-Related Excitons and Their Excited-State Transitions in ZnO. *Phys. Rev. B: Condens. Matter* **2017**, *95*, 054120.

(43) Walle, C. G. Van De. Hydrogen as a Cause of Doping in Zinc Oxide. **2000**, *85* (1), 0–3.

(44) Traeger, F.; Kauer, M.; Wöll, C.; Rogalla, D.; Becker, H.-W. Analysis of Surface, Subsurface, and Bulk Hydrogen in ZnO Using Nuclear Reaction Analysis. *Phys. Rev. B: Condens. Matter* **2011**, *84*, 075462.

(45) Janotti, A.; Van de Walle, C. G. Fundamentals of Zinc Oxide as a Semiconductor. *Reports Prog. Phys.* **2009**, *72* (12), 126501.

(46) Rizk, R.; Mierry, P. De; Ballutaud, D.; Aucouturier, M.; Mathiot, D. Hydrogen Diffusion and Passivation Processes in *p*- and *n*-Type Crystalline Silicon. *Phys. Rev. B: Condens. Matter* **1991**, *44* (12), 6141–6151.

(47) Gross, A. J.; Downard, A. J. Regeneration of Pyrolyzed Photoresist Film by Heat Treatment. *Anal. Chem.* **2011**, *83* (6), 2397–2402.

(48) Toupin, M.; Bélanger, D. Thermal Stability Study of Aryl Modified Carbon Black by In Situ Generated Diazonium Salt. *J. Phys. Chem. C* **2007**, *111* (14), 5394–5401.

(49) Achhammer, B. G.; Reiney, M. J.; Reinhart, F. W. Study of Degradation of Polystyrene, Using Infrared Spectrophotometry. *J. Res. Natl. Bur. Stand.* **1951**, *47* (2), 116.

(50) Rasmussen, K.; Grampp, G.; Eesbeek, M. Van; Rohr, T. Thermal and UV Degradation of Polymer Films Studied In Situ with ESR Spectroscopy. *ACS Appl. Mater. Interfaces* **2010**, *2* (7), 1879–1883.

(51) Nikafshar, S.; Zabihi, O.; Ahmadi, M.; Mirmohseni, A.; Taseidifar, M.; Naebe, M. The Effects of UV Light on the Chemical and Mechanical Properties of a Transparent Epoxy-Diamine System in the Presence of an Organic UV Absorber. *Materials* **2017**, *10* (2), 1–18.

(52) Jameson, C. W.; Lunn, R. M.; Jeter, S.; Sabella, S. *Report on Carcinogens Background Document for Nitrobenzene*; 2002.

(53) Visnapuu, M.; Rosenberg, M.; Truska, E.; Nõmmiste, E.; Šutka, A.; Kahru, A.; Rähn, M.; Vija, H.; Orupõld, K.; Kisand, V.; Ivask, A. UVA-Induced Antimicrobial Activity of ZnO/Ag Nanocomposite Covered Surfaces. *Colloids Surf. B* **2018**, *169*, 222–232.

(54) *ASTM G173-03(2012), Standard Tables for Reference Solar Spectral Irradiances: Direct Normal and Hemispherical on 37° Tilted Surface*; ASTM International: West Conshohocken, PA, 2012.

(55) Ravichandran, L.; Selvam, K.; Swaminathan, M. Effect of Oxidants and Metal Ions on Photodefluoridation of Pentafluorobenzoic Acid with ZnO. *Sep. Purif. Technol.* **2007**, *56* (2), 192–198.

(56) Vasheghani Farahani, S. K.; Veal, T. D.; Mudd, J. J.; Scanlon, D. O.; Watson, G. W.; Bierwagen, O.; White, M. E.; Speck, J. S.; McConville, C. F. Valence-Band Density of States and Surface Electron Accumulation in Epitaxial SnO_2 Films. *Phys. Rev. B: Condens. Matter* **2014**, *90* (15), 1–9.

(57) Li, Y.; Della Valle, F.; Simonnet, M.; Yamada, I.; Delaunay, J.-J. Competitive Surface Effects of Oxygen and Water on UV Photoresponse of ZnO Nanowires. *Appl. Phys. Lett.* **2009**, *94* (2).

7 Conclusions and Future Work

ZnO is a transparent metal oxide semiconductor with a range of electronic device applications including solar cell electrodes, biosensors, and UV detectors. Unusually, it has significant downwards band bending and a 2-dimensional electron gas at the surface due to OH termination, which gives surface metallicity. The aim of this thesis work was to determine surface modifiers and methods suitable for tuning this band bending, with the overall aim of permanently removing it. Robust and straight-forward attachment of organic modifiers is useful for the development of efficient and stable electronic devices, such as sensors, on metal oxides. In this work, phosphonic acids (PA), thiols, and aryldiazonium ions were investigated as precursors to covalently-bonded organic modification layers on ZnO. Furthermore, the effects of these modification methods on each of the three main crystal faces of ZnO was explored.

7.1 Conclusions

Figure 7.1 shows the change in band bending achieved on different ZnO surfaces with covalently-bound modifiers (a table of these values, obtained from XPS valence band measurements, can be seen in Appendix 8.5). Because different photon energies were used for analysis, the magnitudes are not directly comparable as they are probed at different sample depths: smaller photon energies probe closer to the surface, where band bending is greatest. Thus, for a particular sample, the band bending will be bigger when measured by surface-sensitive synchrotron XPS than fixed-energy XPS. It is difficult to extract a trend with confidence given the small number of samples, different crystal types, and different photon energies used. Unfortunately, single crystal ZnO samples and XPS analysis are both expensive, which limited modification and analysis of duplicate samples. However, Figure 7.1 shows that downwards band bending on ZnO can be either increased or decreased, depending on the modifier choice.

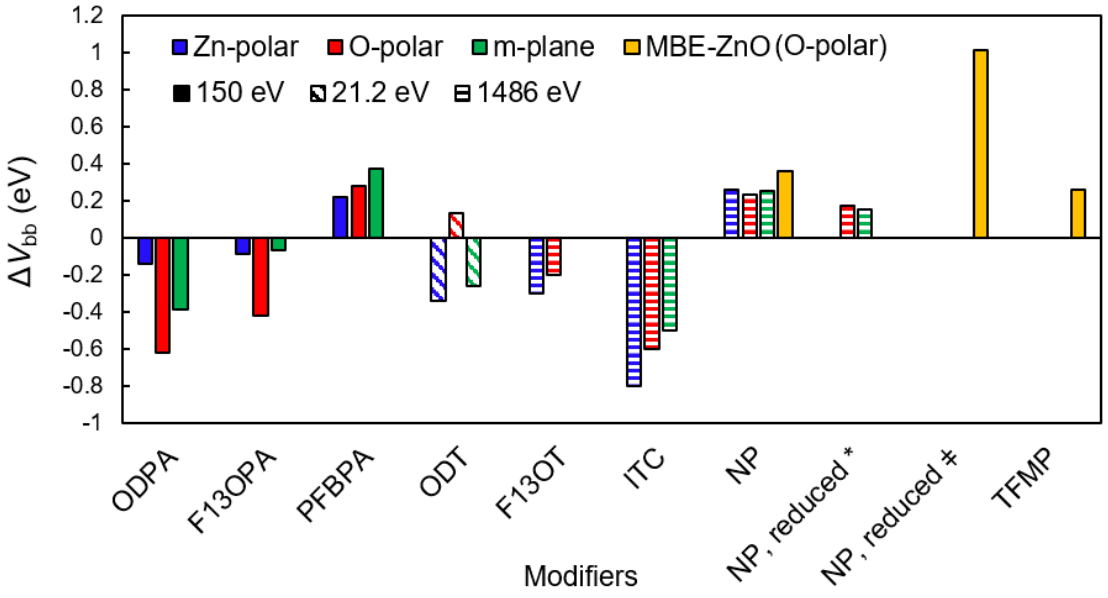

*Figure 7.1. Changes in surface band bending relative to as-received ZnO as determined from XPS and UPS valence band spectra for surface-modified Zn-polar, O-polar, m-plane, and Sb-doped MBE-grown ZnO. Photon energies used were 150 eV (ODPA-, F_{13}OPA-, and PFBPA-modified single crystals; NP- and TFMP-modified MBE-ZnO), 21.2 eV (ODT-modified single crystals), and 1486 eV (F_{13}OT-, ITC-, and NP-modified single crystals). For duplicate samples, the largest change in band bending is reported. *Successfully electrochemically reduced in ethanolic KOH (as determined by core level XPS N 1s spectra). ǂReduced using synchrotron XPS.*

Surface modification with PA was investigated because of the wealth of previous work on PA modification of metal oxides. Through water contact angle and XPS measurements, the surface coverage could be estimated. Of the three ZnO faces examined, O-polar and m-plane ZnO typically gave the largest molecular surface concentrations. The m-plane has the highest surface OH concentration of the three ZnO faces (2.2×10^{-9} mol cm $^{-2}$ compared to 1.8×10^{-9} mol cm^{-2}) and the spatial arrangement of OH groups is different to that of Zn-polar and O-polar faces. However, the uncertainties of the calculated surface modifier concentrations do not allow the effect (if any) of surface OH concentration or spatial arrangement to be discerned. PA binding modes on ZnO were determined by examining XPS data. While there were differences in binding modes between modifiers, there was little difference between different ZnO faces modified with the same PA,

suggesting that the modifiers themselves have a larger effect on binding than do the differences in the ZnO face reactivities. F_{13}OPA molecules on Zn-polar, O-polar, and m-plane ZnO were unambiguously determined to bind in a tridentate mode. PFBPA on all ZnO faces was also observed to have significant tridentate character, although bidentate PAs were most likely also present. ODPA was found to bind with a mixture of bi- and tridentate modes. Additionally, it appeared that both PFBPA- and ODPA-modified ZnO were likely to have physisorbed multilayers which were stable to sonication.

Synchrotron XPS showed that modifications with ODPA and F_{13}OPA resulted in increased downwards band bending on all three ZnO faces. While this was expected for ODPA, the F_{13}OPA result was surprising because of the strong electron-withdrawing properties of F. However, analysis of the effects of modification was complicated by decomposition of the molecules during XPS analysis, which liberated a significant amount of F from the organic modifier. The F appeared to interact with Zn atoms to give donor-like effects. PFBPA was also analysed with synchrotron XPS using a lower photon flux to decrease decomposition. The modifier decreased the downwards band bending on all three faces, suggesting that the modifier was effective at removing electron density from the ZnO surface despite having a non-conjugated CH_2 group between the PA headgroup and the fluorinated functional group. When XPS irradiation was used to deliberately decompose PFBPA molecules leading to some loss of F, an insignificant difference in band bending was seen. This indicates that the electronic effects of the PFBPA modification are stable to small changes in the fluorination of the modification layer. Importantly, this result may suggest that changes can be made to an initial modifying layer through further coupling reactions with functional molecules, without significantly changing the electronic properties.

XPS experiments showed that PFBPA modifiers on ZnO were stable to storage in the dark for 2 months but degraded when irradiated with intense UV light. The effect of UV light on F_{13}OPA-modified ZnO (all faces) was analysed by water contact angle measurements and showed a loss of surface

hydrophobicity after relatively short term (2 h) exposure to UV light. Similar results were seen for ODPA-modified Zn-polar ZnO. In contrast, ODPA-modified O-polar and m-plane ZnO appeared stable to UV light; this difference was attributed to increased surface coverage on the O-polar and m-plane faces, as well as Zn-polar ZnO having the highest catalytic activity of the three faces. Furthermore, ODPA modification on O-polar ZnO was able to extend the duration of persistent photoconductivity from 2 days to 2 weeks.

Thiol attachment to ZnO was investigated because of seemingly inconsistent reports of the binding mode and stability; however, reproducible modification proved challenging. O-polar ZnO was modified with ODT to give significant 'thiolate' XPS signals. However, when rinsed with a solvent in which the thiol is soluble, a significant proportion of these molecules were removed, leading to the conclusion that they were unreacted, non-oxidised, physisorbed thiols, not bound to ZnO. When exposed to short periods of air (< 1 day), thiols were further removed or were oxidised to sulfonate-like head groups, resulting in approximately a monolayer of sulfonate-type modifiers on Zn-polar and m-plane ZnO. Non-oxidised thiols remained on O-polar ZnO and this difference was attributed to the relative catalytic activities of O-polar, Zn-polar, and m-plane ZnO: at the more active Zn-polar and m-plane faces, all thiols are oxidised to sulfonates. F_{13}OT was shown to desorb from ZnO within several days, while after 40 days, ODT-modified ZnO surface concentrations halved for Zn-polar and m-plane ZnO and remained constant for O-polar ZnO. None of the layers formed by modification of ZnO with thiols gave significant band bending. The nature of the modifying layer formed when ITC was reacted with ZnO is unclear, but it significantly increased the downwards band bending, measured with a high photon energy ($h\nu$ = 1486 eV), relative to as-received ZnO. This effect is interesting, but it was reversed within 5 days along with desorption of the modifier. This suggests the modifier would have no practical application.

This work showed that it is difficult to obtain well-defined modifying layers on ZnO using thiol derivatives. The catalytic activity of the substrate appears to have a significant effect on the layer and

this factor, plus the sensitivity to oxidation and variable conditions used for reacting and rinsing ZnO, leads to variability in literature reports. For practical applications, however, it is recommended that thiols are not further pursued as a modifier for ZnO, as PAs and films grafted from aryldiazonium ions are better-understood and are more robust to atmospheric conditions than thiols. If thiol modification was pursued, the O-polar face would be recommended over the more catalytic Zn-polar and m-plane faces.

Very little previous work has been reported concerning the use of aryldiazonium ions to modify ZnO and there were no reports of systematic studies of the different ZnO faces or the effect of modification on electronic properties. Electrochemical grafting on single-crystal ZnO from nitrobenzenediazonium ions gave nitrophenyl (NP) multilayers of 1 – 7 nm, although spontaneous grafting was not successful. The solubility of ZnO in acid precluded use of that grafting medium, so all modification experiments with aryldiazonium ions used ACN as the solvent. The NP layer thicknesses appeared to be influenced by the relative charge carrier concentrations of the ZnO faces, with the low carrier concentration of the m-plane face giving the thinnest NP layers under similar electrochemical conditions to O-polar ZnO modification. As found for other substrates, the layer thicknesses depended strongly on the negative potential limit of the grafting cyclic voltammogram. The proposed grafting mechanism is the same as that suggested for other metal oxides, resulting in an estimated ~30% of surface OH groups reacting to give direct Zn-O-C bonds, and approximately 1 azo linkage for every ~6 phenyl groups. To further explore the electrochemistry of aryldiazonium ions, Sb-doped O-polar ZnO thin films, prepared by MBE, were also grafted with NP and trifluoromethylphenyl (TFMP) multilayers, and similar XPS results to those obtained on single crystal ZnO were observed. Additionally, electrochemical grafting of both NP and TFMP layers on this surface appeared to be very reproducible, a result attributed to the higher charge carrier concentration of MBE-ZnO.

When measured with fixed-energy XPS ($h\nu$ = 1486 eV), NP films showed a decrease in downwards band bending on Zn-polar, O-polar, and m-plane faces by a maximum of +0.26 eV, +0.23 eV, and +0.25

eV, respectively. These were similar to values observed on PFBPA-modified ZnO analysed with the more surface-sensitive photon energy of *hv* = 150 eV, which indicates that the absolute change in band bending was greater on NP-modified ZnO than PFBPA-modified ZnO. These values were obtained when the NP film thickness was > 1 nm; thinner films did not have a large effect on the band bending. Synchrotron XPS showed that 5 nm thick NP films and 4 nm thick TFMP films on MBE-ZnO changed the downwards band bending by +0.36 eV and +0.26 eV, respectively. This resulted in upwards band bending on NP-modified MBE-ZnO (+0.10 eV) and flat bands on TFMP-modified MBE-ZnO (+0.00 eV). Thinner films on MBE-ZnO (~1.5 nm for NP, ~1.6 nm for TFMP) were investigated with fixed-energy XPS (*hv* = 1486 eV) and found to decrease downwards band bending by +0.16 eV and +0.13 eV, respectively. The band bending changes were attributed to the electron-withdrawing nature of NP and TFMP groups, but surprisingly, electrochemical reduction of grafted NP groups on single crystal ZnO in basic medium slightly increased the downwards band bending relative to that of the NP-modified surface. This is a surprising find because XPS analysis supported the formation of aminophenyl groups (as expected), and amino substituents are known to be electron donating. However, when synchrotron XPS was used to induce reduction of NP groups on MBE-ZnO to aminophenyl groups, upwards band bending increased to +0.75 eV, a total change in band bending of +1.0 eV. Again, this result was unexpected as it appeared from core level N 1s spectra that NP group had been reduced to amine groups. It is proposed that ZnO valence band photoelectrons generated during XPS measurements participate in NP reduction, leaving behind an electron depletion region at the substrate surface. It may be that a similar mechanism occurs to a lesser degree during electrochemical reduction of NP groups. The magnitude of the upwards band bending is greater than has been reported with any other covalently-bound chemical modifier and provides promise for FET-based devices which require an electron-depleted surface. It also offers a starting point for further functionalisation of ZnO.

An attempt to chemically reduce NP films with ethanolic Na_2S removed the modifying films, but S- and Na-containing species remained on the surface, with S 2p binding energies indicative of Zn-S

interactions. The VB spectra showed a very reproducible shift in band bending for Na_2S-treated single crystal O-polar ZnO. The resulting change in band bending, measured with fixed-energy XPS (*hv* = 1486 eV), was +1.95 eV relative to as-received O-polar ZnO. This very significant shift was also observed on MBE-ZnO and suggests that the ZnO surfaces were insulating well into the bulk of the material. Such a modification could be excellent in FET applications where a dielectric termination layer is required on the metal oxide. However, similar reports concerning Na_2S treatment of GaAs suggest that the band bending effect may be short-lived (~3 days) so the importance of this result is unclear.

Through XPS and AFM measurements, NP films grafted to MBE-ZnO were shown to be unaffected by storage in the dark for ~3 months or immersion in acidic conditions (pH ~5). Conversely, the chemical composition of the film was affected by heat, and UV irradiation was shown to degrade the film and decrease its thickness by 50%. On the other hand, TFMP-modified MBE-ZnO was stable to both heating and storage in the dark for 2 months but was affected by UV irradiation and acidic solution. The degradation under UV was expected, and the differences between the modifiers in acidic conditions were likely due to the relative density of aryl groups on the surface.

NP layers were shown to prolong the effect of PPC on MBE-ZnO surfaces but were less effective than ODPA; this was attributed to the film being thinner and more disordered than the ODPA layer. Additionally, the hydrophobicity of ODPA compared to NP may influence the rate of re-adsorption of atmospheric species. Moreover, NP layers were shown to desorb under UV light while ODPA appeared stable. It was seen that consecutive UV irradiation periods increased the PPC recovery time, as also seen for as-received ZnO. This is an interesting phenomenon that could affect the ability of ZnO to perform reliably in UV conditions and thus should be investigated to determine the cause of this change and whether ODPA or other organic layers are able to prevent it occurring.

In summary, this thesis work showed that the native downwards band bending on ZnO surfaces can be tuned up to ~1.0 eV in the positive direction and at least ~0.8 eV in the negative direction (*hv* = 150 eV) using covalently-bound organic modifiers which have varying stabilities on the surface in different

conditions. This establishes the potential for surface-modified ZnO to be used in a variety of transparent devices which require a non-conducting semiconductor surface for efficient performance. It was shown that aryldiazonium ions can be electrografted to single crystal ZnO and MBE-ZnO and for the first time, the binding mode was characterised. This work showed that modifications via phosphonic acids and aryldiazonium ions are promising for removing downwards band bending from ZnO, using either fluorinated modifiers or molecules functionalised with NO_2 groups. This gives some flexibility in modifier choice for future ZnO-based devices. Because there is little difference between the modification of different crystallographic faces, the approaches outlined here would be suitable for chemically modifying the surfaces of nanostructures comprising mostly of m-plane ZnO, such as nanowires.

7.2 Future Work

In this work, there were several intriguing observations regarding the fundamental behaviour of ZnO during and after surface modification which were not followed up. Additionally, this work showed that changes in band bending upon the addition of covalently-attached modifiers can be observed using XPS in UHV conditions, but it now needs to be determined how these changes affect the behaviour of ZnO in practical applications in ambient conditions.

Firstly, thiol modification is not recommended for practical applications, but because oxidised sulfonate-type ODT on ZnO appeared to be relatively stable during storage in air and darkness, it may be worth investigating the ability of an already-oxidised sulfonate group, for example a long-chain sulfonic acid, to bind to ZnO, and to compare its stability to that formed by an analogous phosphonic acid. However, its effect on band bending is expected to be similar to those of phosphonic acids due to the oxidised headgroup.

Na_2S treatment of O-polar ZnO (both single crystal and MBE thin films) resulted in a very large decrease in downwards band bending. Based on previous reports on different semiconductor materials, the long-term stability of this effect should be investigated. The effect of Na_2S on the other

main faces of ZnO should also be determined, in case it is specific to the O-polar face. Angle-resolved XPS may be useful for determining whether S and Na are on the surface of ZnO, or whether they have become incorporated into the lattice. In the case of the latter, further surface modification could be attempted to potentially provide a protective layer for the Na_2S-treated ZnO and retain the electron-depleted surface for longer than a few days: even a modification layer which increases downwards band bending would be unlikely to completely reverse the very large upwards band bending caused by the Na_2S treatment.

Both PFBPA and NP modifications decreased the downwards band bending at single crystal ZnO, but their chemical differences mean that the modified surfaces would be suited to different applications. The fluorinated nature of PFBPA is most suited for simply passivating the SEAL of ZnO and protecting the surface from atmospheric species, without any further functionalisation. Meanwhile, NP groups on ZnO can be reduced to aminophenyl groups that can be coupled with recognition species for chemical and biosensing transistors with a reactive surface, while retaining an insulating surface. However, the exact nature of the 'amino' groups at the surface needs to be determined to fully understand their effect on band bending. Furthermore, XPS is not an efficient method for chemically modifying NP films for application purposes due to the micron-sized analysis area, large cost, and time constraints. It would be interesting to observe the effect on band bending if NP groups were reduced by direct electron beams from a flood gun or scanning electron microscope. This experiment could help determine the cause of the upwards band bending as well as potentially provide a larger area of NP reduction. There are reports of NP reduction via electron beams, but no investigation into the resulting band bending has yet been performed. Further investigation into electrochemical reduction of NP films at ZnO and other semiconductors should be carried out, as it should be a straightforward process. In this work, only one electrolyte was used, but other non-acidic electrolytes could be pursued, such as ethanol and water. These may allow successful reduction of NP groups on Zn-polar ZnO, and more complete reduction of NP groups on O-polar and m-plane ZnO.

It appears from this work that an electron-donating aryldiazonium ion substituent, such as an amino group, cannot be assumed to increase downwards band bending on ZnO. Similarly, the band bending of PFBPA-modified ZnO showed little change when F was liberated from the modifying molecules. Electron-donating aryl substituents such as methoxy or methyl groups should be investigated to clarify the role of aryl substituents in the ZnO band bending. Other modifier substituents such as azides and ethynyls may decrease the downwards band bending of ZnO while being able to react with sensing molecules. A broad range of aryldiazonium ion precursors are available for relatively low cost compared to phosphonic acid derivatives and would thus be a practical route to obtaining a wide range of ZnO modifiers. Computational models of these modifiers on ZnO surfaces could also help with understanding the electron transfer processes within a film, as it appears that comparing dipole moments of substituted benzene rings is not sufficient to predict the direction of ZnO band bending. The multilayer nature of the aryl films is a complicated system to investigate computationally, especially due to the presence of azo linkages. However, this work showed that aryl rings attach to ZnO via Zn-O-C bonds, which gives a valuable starting point for the structure of the multilayer and thus the electron density calculations. This work also gives an indication of the number of azo groups in the film per aryl substituent. From computational and practical experiments, a database of modifiers that tune band bending on ZnO and other metal oxides with native downwards band bending (SnO_2, CdO, In_2O_3, InN) could be collated to allow rational choice of modifier to achieve the desired surface band bending. Also, there exist transparent metal oxides such as Ga_2O_3 that have native upwards band bending and a surface electron depletion layer. Preliminary work on tuning the band bending of this material has already begun. The effect of electron withdrawing and donating aryl substituents on these surfaces may also help in determining the role of surface electrons in the band bending of covalently-modified materials.

Preliminary stability tests suggest that NP modification layers are best suited to aqueous biosensing applications, while TFMP layers may be more suited to dry conditions. Neither film is stable when exposed to 365 nm UV light, but further investigation into the relationship between film stability,

wavelength, and intensity of UV light is necessary. Likewise, further tests should be carried out to determine the full pH range in which NP- and TFMP-modified ZnO is stable. This was not done here due to the limited availability of MBE-ZnO samples but will be necessary for aqueous solution-based applications involving aryl layers on ZnO. Furthermore, aryl groups with different substituents may prove to give denser, more protective layers on ZnO, or be inherently less susceptible to UV light and acidic conditions, while still decreasing downwards band bending.

Similarly, the disordered multilayer nature of NP films appears to allow the adsorption and desorption of atmospheric species, the process of which causes PPC. By applying more negative potentials during grafting, it should be possible to graft thicker, more blocking films. Hydrophobic films may be more successful in prolonging PPC, so hydrophobic aryl substituents, including trifluoromethyl groups, should be investigated in relation to PPC. There are also methods for controlling the grafting of aryl layers at carbon and metal surfaces which could be applied to ZnO to form a more ordered, denser modification layer with more bonds to the surface. In this work, it appeared that many OH groups on MBE-ZnO did not react with aryl radicals to give Zn-O-C bonds. If a greater fraction of OH groups undergo reaction with aryl radicals, the multilayer is expected to be denser and more protecting, and the effect on band bending might also increase, as the aryl layers would have more direct bonds with the surface. The density of the molecules may be difficult to analyse by electrochemistry if there is no redox-active substituent, but relative densities could be determined by comparing the effects of differently-modified samples on PPC. Pre-modification treatment of the bare ZnO could also be investigated: UV irradiation prior to electrochemical grafting would remove adsorbates and may prevent PPC from occurring on the modified surface. The surface would also become more hydrophilic, which may hinder or help the electrochemical grafting process.

Clearly, electrochemistry at single crystal ZnO surfaces is far from straightforward and it should be further investigated to achieve fundamental understanding of the grafting process at the different faces. While thicker aryl films can be grafted by using a more negative potential than for thinner films,

and larger reduction currents generally result in thicker films, questions about the mechanisms remain. In general, it appeared that there were no obvious trends in reactivity of different ZnO faces towards aryldiazonium ion grafting, and the role of surface topography, defects, and catalytical properties is unclear. Factors such as scan rate, aryldiazonium salt concentration, and potential range also control the rate of growth and can be further optimised for ZnO faces. Furthermore, the modification methods outlined in this work could be extended to other metal oxide substrates. While electrochemical grafting on ITO and SnO_2 has been performed previously, the effects of band bending have not been reported, and removal of downwards band bending could increase the efficiency and reproducibility of devices based on these materials.

8 Appendices

8.1 Phosphonic Acid Modifiers on Single Crystal ZnO

8.1.1 AFM Images of Phosphonic Acid-Modified ZnO

Figure 8.1 shows topographical AFM images obtained on ODPA-, F_{13}OPA- and PFBPA-modified Zn-polar, O-polar, and m-plane ZnO after synchrotron XPS analysis. Table 8.1 shows the corresponding root mean square roughnesses.

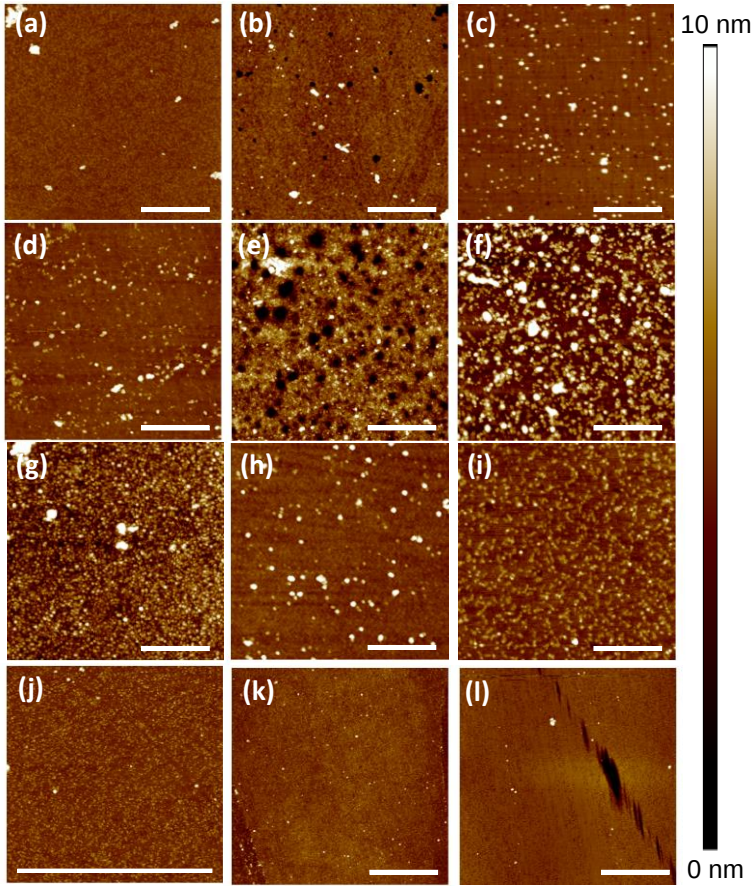

Figure 8.1: AFM images for (a, d, g, j) Zn-polar, (b, e, h, k) O-polar, and (c, f, i, l) m-plane ZnO, modified with (a, b, c) ODPA, (d, e, f) F_{13}OPA, and (g, h, i) PFBPA. (j, k, l) are as-received samples. The horizontal scale bar is 1 µm.

Table 8.1. AFM root mean square roughness values for ODPA-, F_{13}OPA-, and PFBPA-modified Zn-polar, O-polar, and m-plane ZnO.

Sample	**R_a (nm)**		
	Zn-polar	O-polar	m-plane
ODPA	0.3	0.5	0.9
F_{13}OPA	0.4	1.3	1.5
PFBPA	1.1	0.5	0.6
As-received (after Synchrotron)	0.5	0.5	0.4

AFM depth profile experiments, as outlined in Chapter 2, were attempted on PA-modified samples to determine the thickness of the film. However, these proved to be inconclusive. Bare ZnO is a relatively soft material, and as such is easily scratched during contact mode AFM, even at very low setpoint voltages (Figure 8.2). Typically, the bare ZnO is scratched a known amount *x* at a specific voltage setpoint (Figure 8.2), and a modified sample scratched under the same conditions would be expected to have a scratch height of *x* + *y*, where *y* is the height of the modification layer. However, PA layers proved to be mechanically strong, requiring a high setpoint voltage (> 0.6 V) for the tip to break through: for very long or fluorinated molecules, the tip was still unable to scratch through the modifier. At this high voltage, the scratch height on bare ZnO is ≥ 1 nm. This is a similar scale to the height of the aromatic PA modifiers used, making the error in calculation too large to be meaningful. As such, the scratching method for PAs and thiols was ignored, and only the native topography of modified images could be analysed by AFM.

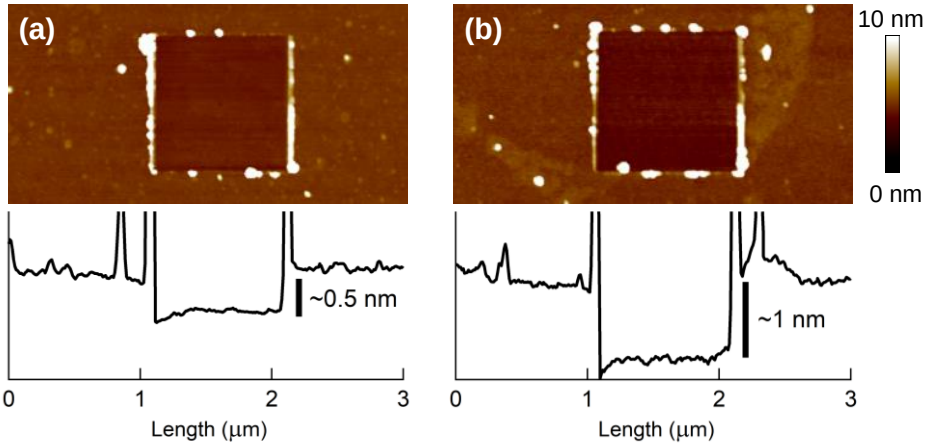

Figure 8.2: Tapping-mode AFM images of as-received (a) Zn-polar and (b) O-polar ZnO samples after a 1 µm x 1 µm square was scratched into the surface using contact-mode AFM with a setpoint voltage of 0.2 V. Line profiles indicate the depth of each scratch.

8.1.2 Comparison of Fixed-Energy XPS Results for Phosphonic Acid Modifiers on ZnO

XPS was carried out to quantitatively determine differences between PA modifiers on Zn-polar, O-polar, and m-plane ZnO. Figure 8.3 shows a survey XPS spectrum for unmodified ZnO and the typical elements present.

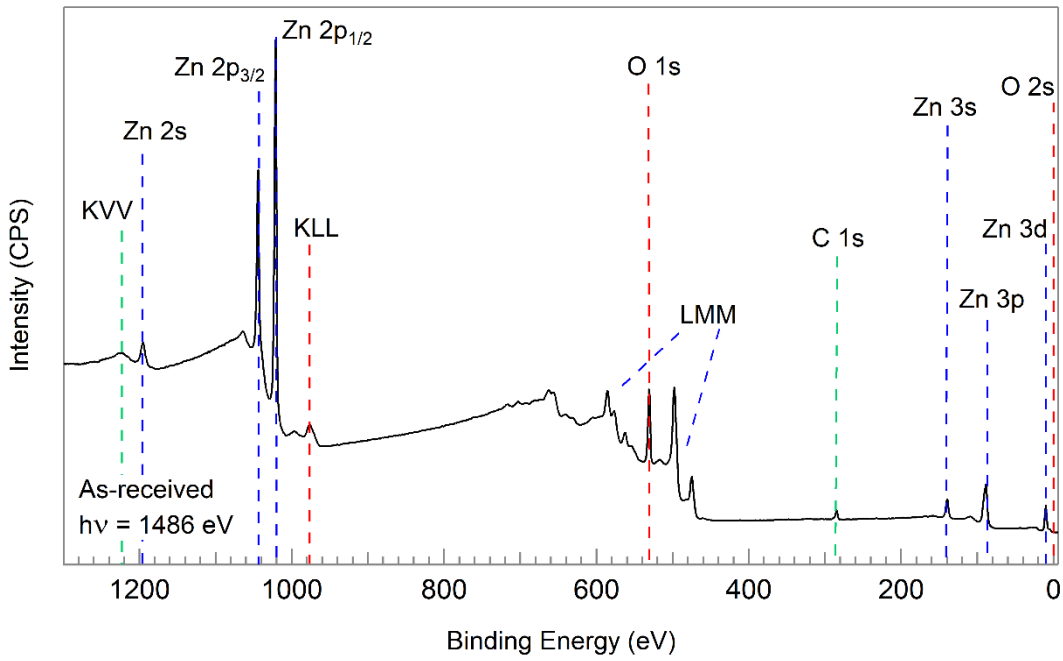

Figure 8.3. Fixed-energy XPS survey spectrum and peak assignments for as-received Zn-polar ZnO.

A selection of fluorinated and non-fluorinated alkyl chains and aromatic groups were chosen as the tail groups of the phosphonic acids. The atomic percentages of each modified sample are shown in Table 3.3, and the fixed-energy XPS spectra are shown in Figure 8.4. Further elemental ratios are shown in Table 8.3.

Table 8.2. Fixed-energy XPS atomic percentages for as-received and PA-modified ZnO faces (ASF-corrected). VBPA = (4-vinylbenzyl)phosphonic acid.

Face	**Modifier**	**Zn %**	**O %**	**C %**	**P %**	**F %**
Zn-polar	As-received	23	45	32	0	0
	F_{13}OPA	17	37	17	2	26
	ODPA	8	30	59	3	0
	PFBPA	33	43	15	2	8
	VBPA	9	40	48	3	0
O-polar	As-received	21	43	36	0	0
	F_{13}OPA	17	36	18	2	27
	ODPA	14	35	49	2	0
	PFBPA	29	47	16	3	6
	VBPA	13	37	46	4	0
m-plane	As-received	27	41	33	0	0
	F_{13}OPA	16	29	20	2	33
	ODPA	9	28	60	3	0
	PFBPA	23	36	23	3	14
	VBPA	12	39	46	3	0

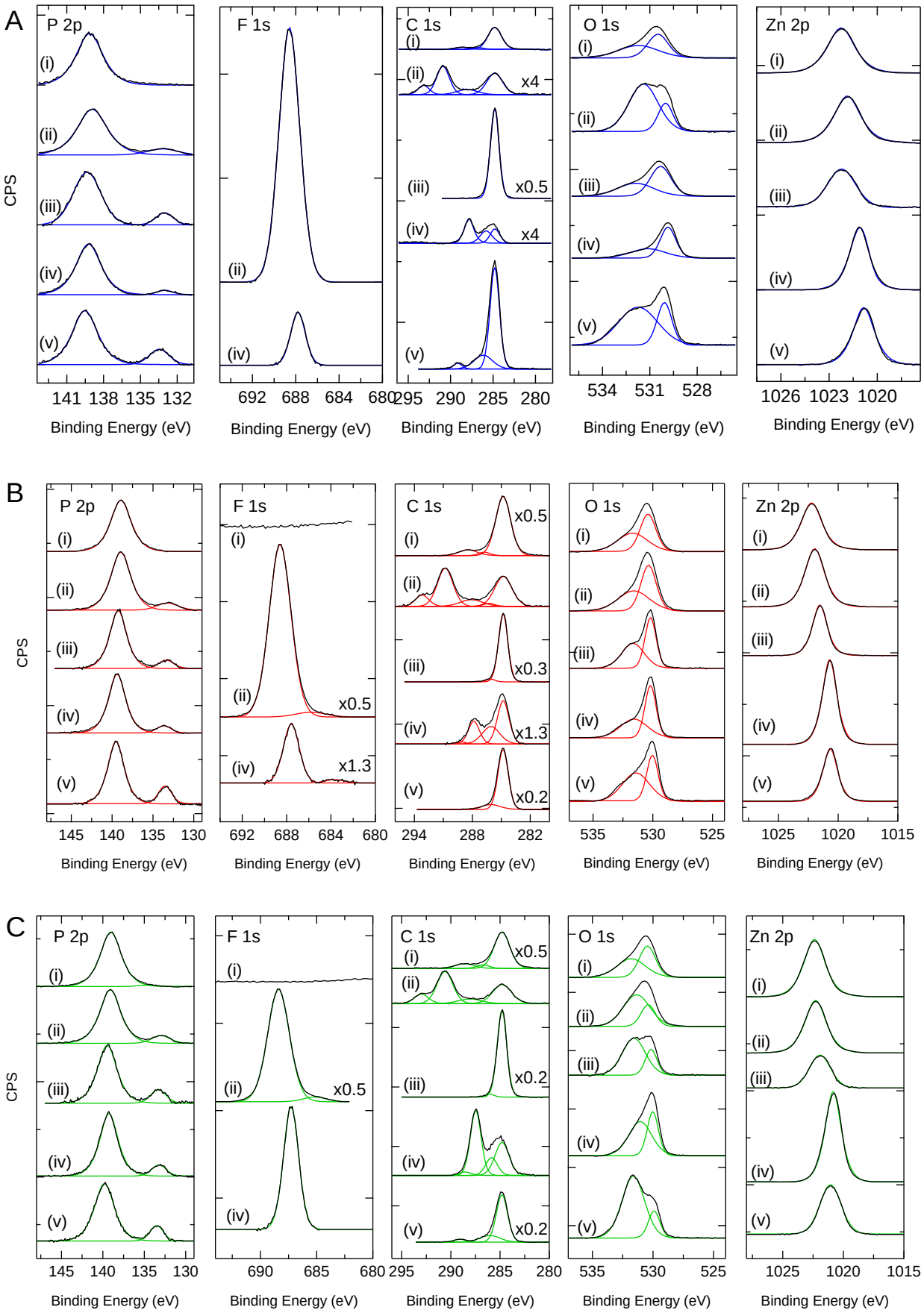
A
P 2p
F 1s
C 1s
O 1s
Zn 2p
CPS
(i)
(ii)
(iii)
(iv)
(v)
x4
x0.5
141 138 135 132
692 688 684 680
295 290 285 280
534 531 528
1026 1023 1020
Binding Energy (eV)
B
x0.5
x1.3
x0.3
x0.2
145 140 135 130
535 530 525
1025 1020 1015
C
690 685 680

Figure 8.4: P 2p, F 1s, C 1s, O 1s, and Zn 2p fixed-energy XPS spectra for (A) Zn-polar, (B) O-polar, and (C) m-plane ZnO, modified with (ii) F_{13}OPA, (iii) ODPA, (iv) PFBPA, (v) VBPA. Spectra (i) are of the solvent-cleaned reference samples. All spectra have been offset for clarity, and area-normalised to the Zn 3s peak area (binding energy = 140 eV) except where rescaled and noted.

Table 8.3: ASF-corrected elemental ratios obtained from the UW XPS spectra for Zn-polar, O-polar, and m-plane ZnO modified with an assortment of phosphonic acids and their as-received (as-rec.) samples.

Face	*Modifier*	*P 2p:Zn 3s**	*P 2p:Zn 2p*	*F-C:F-Zn*	*C:Zn*	*CF_x:P*	*F:P*	*O:Zn*	*% $O_{surf.}$*
Zn-polar	As-rec.	0	0		1.4			1.9	51
	F_{13}OPA	0.12	0.15	27	1.0	3.4	7.6	2.2	43
	ODPA	0.17	0.32		7.2			3.6	77
	PFBPA	0.08	0.06		0.4	0.19	0.38	1.3	41
	VBPA	0.21	0.36		5.2			4.3	67
O-polar	As-rec.	0	0		1.7			2.1	49
	F_{13}OPA	0.12	0.14	26	1.0	3.8	8.4	2.1	47
	ODPA	0.11	0.17		3.6			2.5	50
	PFBPA	0.10	0.09	17	0.53	0.11	0.22	1.6	47
	VBPA	0.21	0.32		3.6			3.0	60
m-plane	As-rec.	0	0		1.2			1.5	51
	F_{13}OPA	0.12	0.14	23	1.2	4.9	11	1.9	73
	ODPA	0.17	0.35		6.9			3.2	74
	PFBPA	0.13	0.12	86	1.0	0.24	0.48	1.6	62
	VBPA	0.17	0.23		3.7			3.1	82

* denotes ratios that are not ASF-corrected

Figure 8.5 displays the differences in PA concentrations on ZnO faces by way of comparing the P 2p and Zn 2p peak areas for each modified sample.

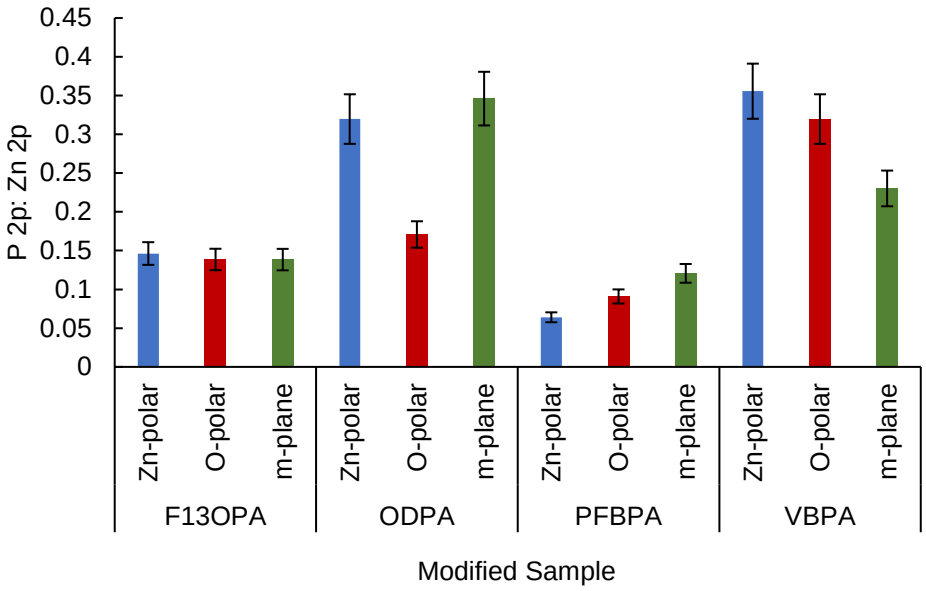

Figure 8.5: Fixed-energy XPS peak area ratios for P 2p and Zn 2p signals arising from F_{13}OPA-, ODPA-, PFBPA-, and VBPA-modified Zn-polar, O-polar, and m-plane ZnO.

8.1.3 Water Contact Angles for ODPA-, F_{13}OPA-, and PFBPA-modified ZnO

Table 8.4 shows the water CA and surface concentrations for as-received and ODPA-, F_{13}OPA-, and PFBPA-modified Zn-polar, O-polar, and m-plane ZnO.

Table 8.4. Water contact angles and molecular surface concentration, estimated from synchrotron XPS, for single-crystal Zn-polar, O-polar, and m-plane ZnO samples modified with F_{13}OPA, ODPA, and PFBPA.

Face	Modifier	Water CA (°)	Image	Molecules nm^{-2} (Synchrotron XPS)
Zn-polar	As-received	64 ± 4	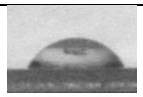	-
	F_{13}OPA	89 ± 18		1.7
	ODPA	77 ± 5		4.3
	PFBPA	76 ± 11	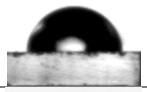	3.9
O-polar	As-received	56 ± 2		-
	F_{13}OPA	86 ± 2		1.3
	ODPA	106 ± 4		5.6
	PFBPA	85 ± 3		4.3
m-plane	As-received	48 ± 2	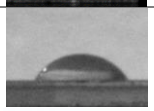	-
	F_{13}OPA	93 ± 8		2.0
	ODPA	97 ± 4		7.0
	PFBPA	83 ± 6		3.8

8.1.4 Comparison of Synchrotron XPS Results for Phosphonic Acid Modifiers on ZnO

Table 8.5 compares synchrotron XPS results for ODPA, F_{13}OPA, and PFBPA modifiers on ZnO.

*Table 8.5: Synchrotron XPS data for ODPA-, F_{13}OPA-, and PFBPA-modified single crystal ZnO. Those marked with * are CrysTec, while all others were Tokyo Denpa samples.*

Face	Modifier	Zn 3s : P 2p	F-Zn:F-C	Zn:C	P:F	Δ_{surf} (eV)	% Surface O
Zn-polar	As-received	1:0.05	-	1:3.2	-	1.17	57
	OPDA	1:4.0	-	1:7.9	-	1.12	82
	F_{13}OPA	1:1.6	1:1	1:1.6	1:0.8	1.00	64
	PFBPA*	1:3.7	1:101	1:15.7	1:2.2	1.17	80
	As-received*	1:0.3	-	1:11.5	-	1.50	64
O-polar	As-received	1:0.2	-	1:4.4	-	1.66	61
	OPDA	1:5.3	-	1:14.0	-	1.07	95
	F_{13}OPA	1:2.1	1:2	1:2.0	1:1.2	0.96	71
	PFBPA*	1:4.0	1:52	1:17.1	1:2.4	1.10	83
	As-received*	1:0.3	-	1:13.1	-	1.26	67
m-plane	As-received	1:0.3	-	1:3.0	-	1.39	61
	OPDA	1:6.6	-	1:19.9	-	1.17	97
	F_{13}OPA	1:2.0	1:1	1:2.4	1:0.9	1.01	79
	PFBPA*	1:3.6	1:30	1:14.2	1:2.0	1.12	78
	As-received*	1:0.2	-	1:21.0	-	1.49	57

8.2 Thiol and Sulfur-Containing Modifiers on Single Crystal ZnO

8.2.1 NMR Spectrum of Octadecanethiol

Figure 8.6 shows a calculated and experimental ^{13}C NMR spectrum for the octadecanethiol used in this work.

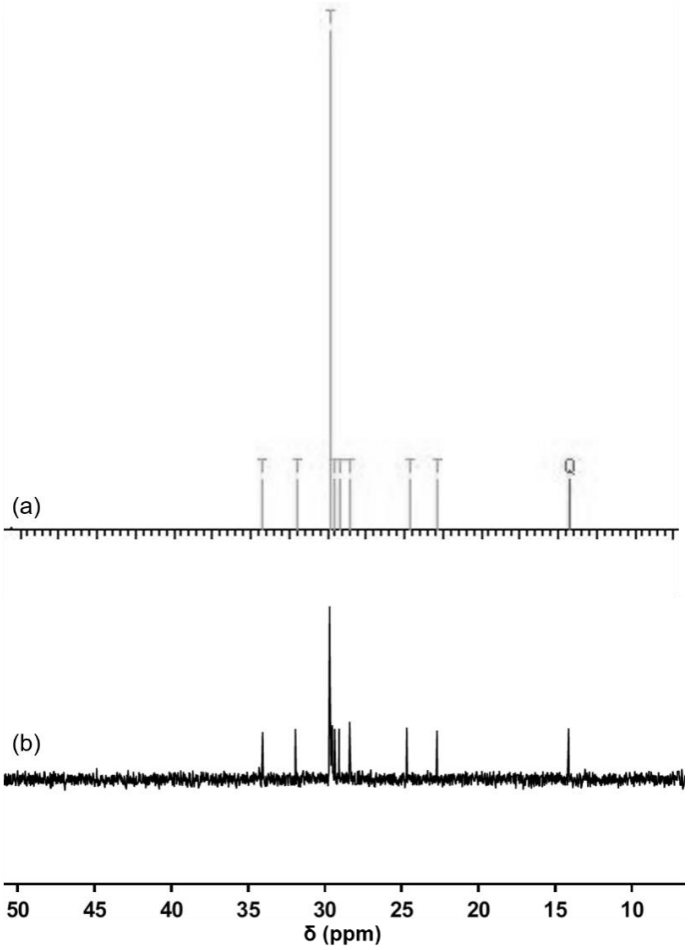

Figure 8.6: ^{13}C NMR spectrum for ODT; (a) calculated and (b) obtained from ODT used in this work. Spectrum collected by Sarah Guillot, UW-Madison.

8.2.2 Fixed-Energy XPS Comparison of Thiol-Like Modifiers on Single Crystal ZnO

Table 8.6 shows the atomic percentages obtained from fixed-energy XPS for ODT-, F_{13}OT-, 4TFMBM-, and ITC-modified Zn-polar, O-polar, and m-plane ZnO.

Table 8.6. Atomic percentages from fixed-energy XPS analysis of ODT-, F_{13}OT-, 4TFMBM-, and ITC-modified Zn-polar, O-polar, and m-plane ZnO.

	Zn %	O %	F %	S %	C %	N %
Zn-polar						
ODT	29	43	0	0.2	27	-
F_{13}OT	31	47	2	0.4	19	-
4TFMBM	29	45	0	0.4	26	-
ITC	28	41	5	0.3	25	0.4
O-polar						
ODT	18	36	0	1.2	45	-
F_{13}OT	30	46	4	0.4	20	-
4TFMBM	29	43	1	0.5	26	-
ITC	27	47	4	0.4	22	0.4
m-plane						
ODT	15	48	0	0.1	36	-
F_{13}OT	26	41	15	1.2	16	-
4TFMBM	32	47	0	0.5	20	-
ITC	29	44	6	0.4	20	0.9

8.2.3 ITC Modification of Zn-polar ZnO

Figure 8.7 shows fixed-energy XPS spectra for ITC-modified Zn-polar ZnO when analysed 1, 3, and 5 days after modification. A decrease in S and F is seen. Figure 8.7c shows the valence band spectrum for 5-day-old ITC-modified Zn-polar ZnO alongside an as-received sample.

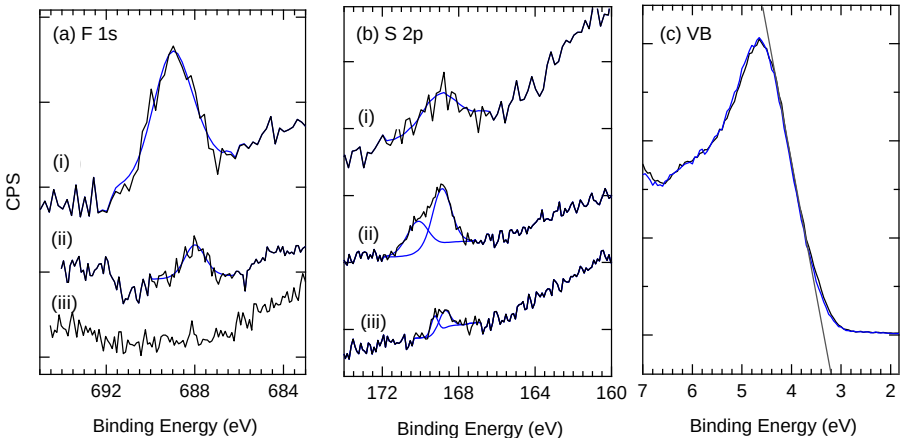

Figure 8.7. Fixed-energy XPS spectra (a) F 1s and (b) S 2p for Zn-polar ZnO modified with ITC, analysed (i) 1 day, (ii) 2 days, and (iii) 5 days after modification. Samples labelled with (i) were analysed with a pass energy of 93.3 eV, while all others were analysed with a pass energy of 29.93 eV. (c) Shows the valence band spectra for as-received (black) and ITC-modified ZnO (blue) 5 days after modification. Spectra have been offset and normalised to the Zn 2p peak area for clarity.

8.3 Nitrobenzenediazonium-Treated Single Crystal ZnO

Figure 8.8 shows the fixed-energy XPS spectra obtained on m-plane ZnO treated with NBD under different 'spontaneous' conditions. Figure 8.9 shows synchrotron XPS spectra Zn-polar, O-polar, and m-plane ZnO treated with 1 mM NBD in ACN for 6 h.

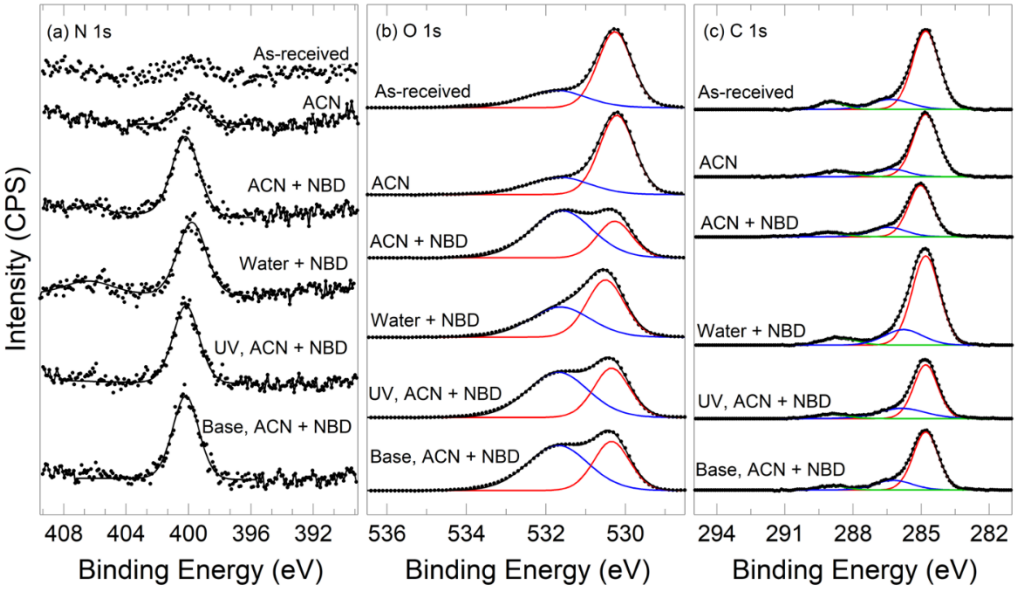

Figure 8.8: XPS spectra for (a) N 1s, (b) O 1s, and (c) C 1s regions of m-plane ZnO immersed in a range of NBD solutions: ACN, ACN and NBD, or water and NBD. All samples were solvent-cleaned prior to treatment, and where noted, were also pre-treated with either UV light or NaOH. Spectra have been normalised to the same Zn 2p peak area and vertically offset for clarity.

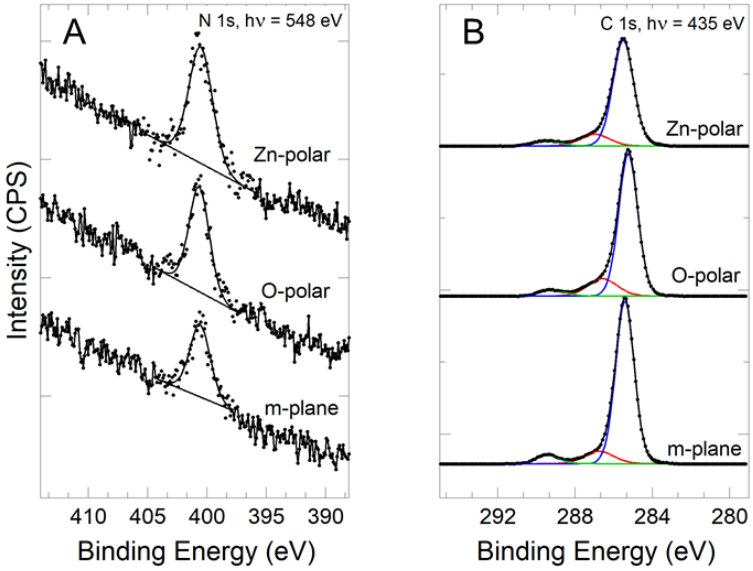

Figure 8.9: (A) N 1s and (B) C 1s synchrotron XPS spectra for NP-modified Zn-polar, O-polar, and m-plane faces. Spectra have been normalised to the same Zn 2p peak area and vertically offset for clarity.

8.4 Trifluoromethyl-Modified MBE-ZnO

Figured 8.10 to 8.13 show core level, fixed-energy XPS spectra for TFMP-modified MBE-ZnO used in Section 6.3.4.3 to monitor the effects of various stability treatments.

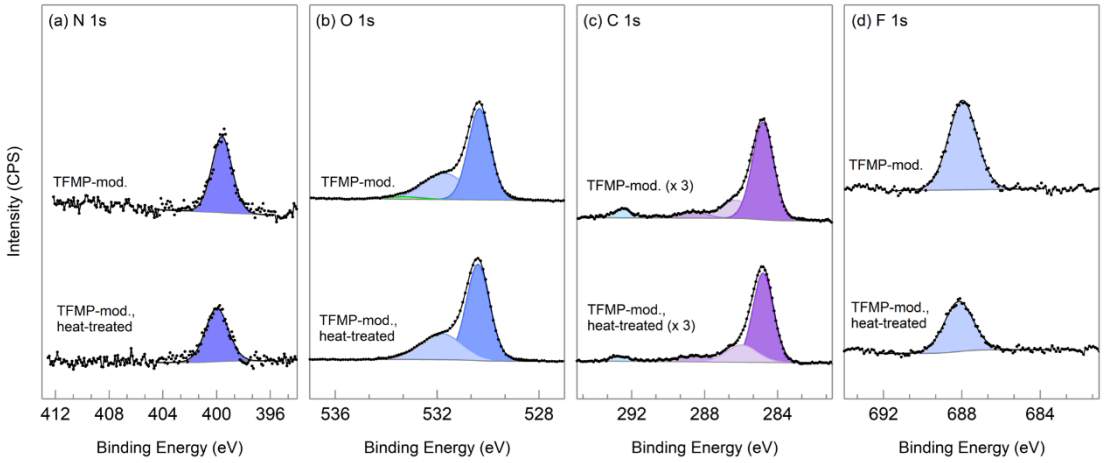

Figure 8.10. Fixed-energy XPS N 1s spectra for TFMP-modified MBE-grown MBE-ZnO before and after treatment with heat. (a) N 1s, (b) O 1s, (c) C 1s, (d) F 1s. Spectra have been normalised to the same Zn 2p peak area and vertically offset for clarity.

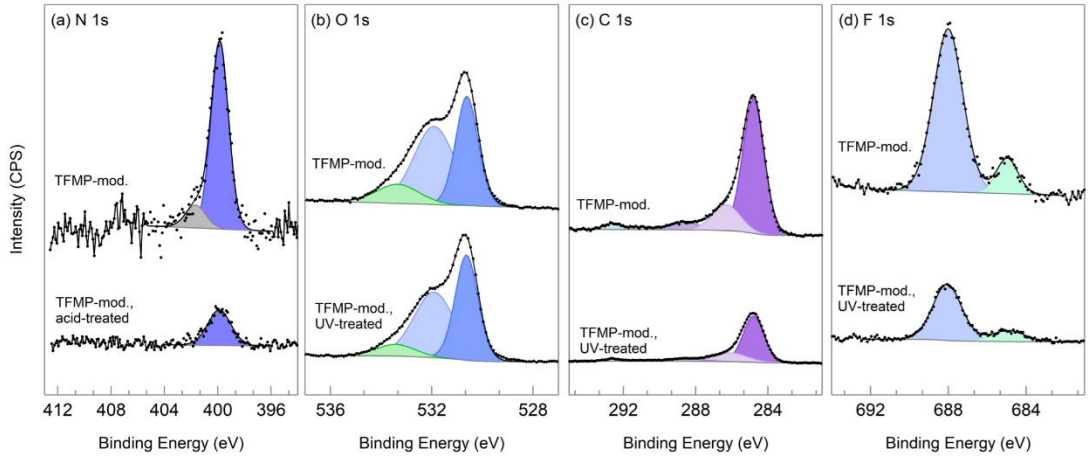

Figure 8.11. Fixed-energy XPS F 1s spectra for TFMP-modified MBE-grown MBE-ZnO before and after treatment with UV light. (a) N 1s, (b) O 1s, (c) C 1s, (d) F 1s. Spectra have been normalised to the same Zn 2p peak area and vertically offset for clarity.

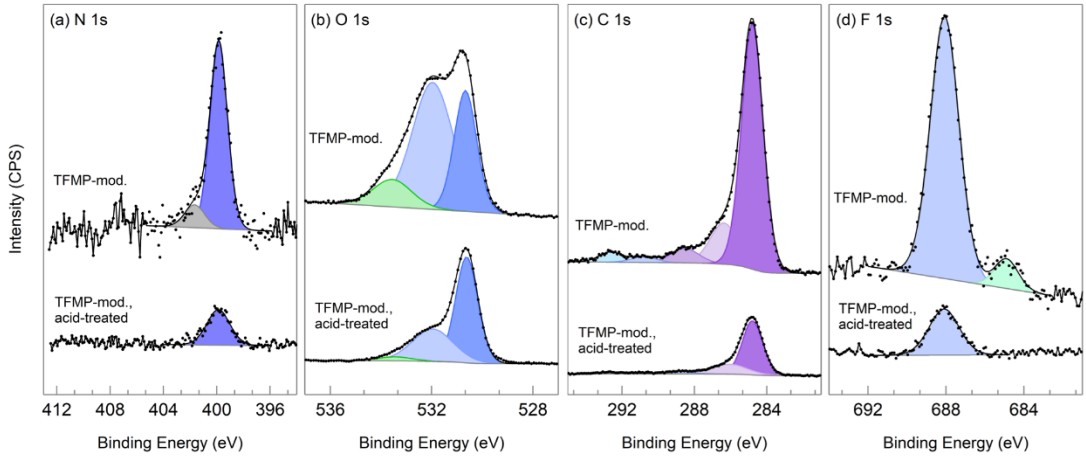

Figure 8.12. Fixed-energy XPS O 1s spectra for TFMP-modified MBE-grown MBE-ZnO before and after treatment with acid. (a) N 1s, (b) O 1s, (c) C 1s, (d) F 1s. have been normalised to the same Zn 2p peak area and vertically offset for clarity.

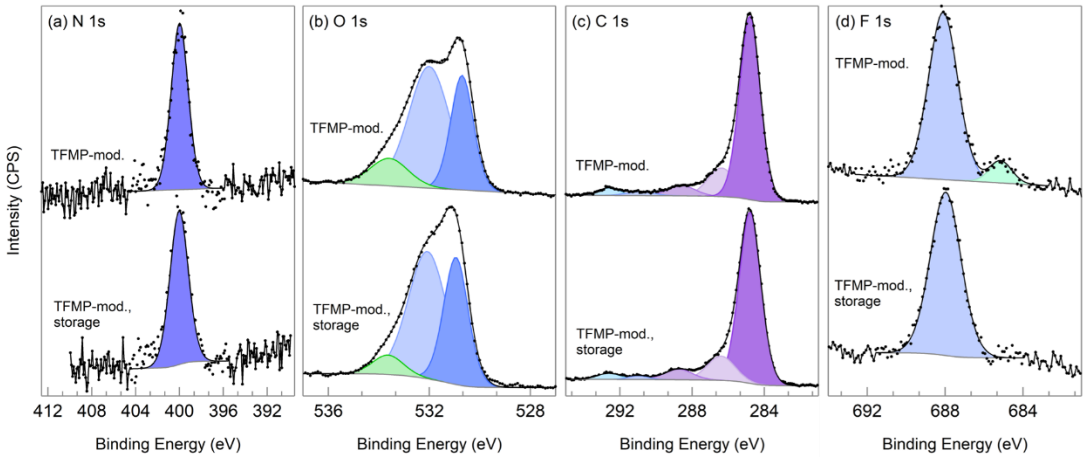

Figure 8.13. XPS C 1s spectra for TFMP-modified MBE-grown MBE-ZnO before and after stored in dark conditions for 60 days. (a) N 1s, (b) O 1s, (c) C 1s, (d) F 1s. Spectra have been normalised to the same Zn 2p peak area and vertically offset for clarity.

8.5 Summary of Band Bending Changes Achieved on ZnO Surfaces

Table 8.7 shows a summary of the band bending changes achieved in this work using a variety of covalently-bound organic modifiers.

Table 8.7. Summary of band bending changes relative to as-received ZnO for Zn-polar, O-polar, and m-plane ZnO modified with phosphonic acids (ODPA, F_{13}OPA, PFBPA; hv = 150 eV), thiols and S-containing molecules (ODT, hv = 21.2 eV; F_{13}OT, ITC; hv = 1486 eV), and electrochemically-grafted aryl layers (NP, TFMP; hv = 150 eV). For duplicate samples, the largest change in band bending is reported.

Modifier	**Substrate**	***hv* (eV)**	**Zn-polar ZnO ΔV_{bb} (eV)**	**O-polar ZnO ΔV_{bb} (eV)**	**m-plane ZnO ΔV_{bb} (eV)**
ODPA	Tokyo Denpa	150	–0.14	–0.62	–0.39
F_{13}OPA	Tokyo Denpa	150	–0.09	–0.42	–0.07
PFBPA	Tokyo Denpa	150	+0.22	+0.28	+0.37
ODT	CrysTec	21.2	–0.34	+0.13	–0.26
F_{13}OT	CrysTec	1486	–0.3	–0.2	–0.0
ITC	CrysTec	1486	–0.8	–0.6	–0.5
NP	CrysTec	1486	+0.26	+0.23	+0.25
NP	MBE-ZnO	1486	-	–0.24	-
NP	MBE-ZnO	150	-	+0.36	-
NP, reduced	MBE-ZnO	150	-	+1.01	-
TFMP	MBE-ZnO	1486	-	–0.13	-
TFMP	MBE-ZnO	150	-	+0.26	-